

**A study on understanding the modulation in MAPK/ERK and
PI3KCA/Akt signaling during acquirement of drug resistance**

By

Aniketh Bishnu

LIFE09201504006

**Tata Memorial Center
Mumbai**

*A thesis submitted to the
Board of Studies in Life Sciences*

*In partial fulfillment of requirements
for the Degree of*

DOCTOR OF PHILOSOPHY

of

HOMI BHABHA NATIONAL INSTITUTE



August, 2021

Homi Bhabha National Institute

Recommendations of the Viva Voce Committee

As members of the Viva Voce Committee, we certify that we have read the dissertation prepared by Mr. Aniketh Bishnu entitled "A study on understanding the modulation in MAPK/ERK and PI3KCA/Akt signaling during acquirement of drug resistance" and recommend that it may be accepted as fulfilling the thesis requirement for the award of Degree of Doctor of Philosophy.

S. N. Dalal

27/8/2021

Chairperson – Dr. Sorab Dalal

Date:

Pritha Ray

27/8/2021

Guide/Convener – Dr. Pritha Ray

Date:

Sandhya

External Examiner – Prof. Sandhya S. Visweswariah

Date: 11th August 2021

Prasanna

Member- Dr. Prasanna Venkatraman

Date: *27/08/2021*

Sanjay

Member- Dr. Sanjay Gupta

Date:

27/08/2021

Abhijit De

Technical Advisor- Dr. Abhijit De

Date: *27/08/2021*

Final approval and acceptance of this thesis is contingent upon the candidate's submission of the final copies of the thesis to HBNI.

I hereby certify that I have read this thesis prepared under my direction and recommend that it may be accepted as fulfilling the thesis requirement.

Date:

Place: Navi Mumbai

Dr.

Dr. *Pritha Ray*

27/08/2021

Guide

STATEMENT BY AUTHOR

This dissertation has been submitted in partial fulfillment of requirements for an advanced degree at Homi Bhabha National Institute (HBNI) and is deposited in the Library to be made available to borrowers under rules of the HBNI.

Brief quotations from this dissertation are allowable without special permission, provided that accurate acknowledgement of source is made. Requests for permission for extended quotation from or reproduction of this manuscript in whole or in part may be granted by the Competent Authority of HBNI when in his or her judgment the proposed use of the material is in the interests of scholarship. In all other instances, however, permission must be obtained from the author.

Aniketh Bishnu

Aniketh Bishnu

DECLARATION

I, hereby declare that the investigation presented in the thesis has been carried out by me.
The work is original and has not been submitted earlier as a whole or in part for a degree /
diploma at this or any other Institution / University.

Aniketh Bishnu

Aniketh Bishnu

List of Publications arising from the thesis

Journals

1. Aniketh Bishnu, Pratham Phadte., Ajit Dhadve, Asmita Sakpal, Bharat Rekhi, Pritha Ray*; Molecular imaging of the kinetics of hyperactivated ERK1/2-mediated autophagy during acquirement of chemoresistance; Cell Death Diseases; 12, 161 (2021).
2. Aniketh Bishnu, Asmita Sakpal, Nilanjana Ghosh, Priyanka Choudhury, Koel Chaudhury, Pritha Ray*; Long term treatment of metformin impedes development of chemoresistance by regulating cancer stem cell differentiation through taurine generation in ovarian cancer cells; The International Journal of Biochemistry & Cell Biology, 107,116-127 (2019)
3. Aniketh Bishnu, Megha Mehrotra, Ajit Dhadve, Shalini Dimri, Abhijit De and Pritha Ray*; Predicting response to platinum and non-platinum drugs through Bioluminescence Resonance Energy Transfer (BRET) based bio-molecular interactions in platinum resistant Epithelial Ovarian Cancer; Translational Oncology, 14,11 (2021)

Patent

1. India Patent No. TEMP/E-1/10868/2019-MUM “A method for detection of protein activation using phosphor-BRET imaging sensor and methods thereof” by Abhijit De, Pritha Ray, Shalini Dimri and Aniketh Bishnu

Conference Awards

1. V.C. Shaw award for “Hyper activated ERK1/2 kinase drives autophagy to promote survival of ovarian cancer cells at the onset of chemoresistance” at AICBC 2019
2. CCMB best poster award for “BRET based monitoring of the dynamic nature of RTK/PI3K/AKT signalling Pathway” at ICCB 2018, Hyderabad
3. Best poster award for “ERK1/2 activation paves the way for onset of chemoresistance in ovarian cancer cells through sustenance of autophagic flux” at stem cell conference 2018, Somaiya college, Mumbai
4. Best poster award for presenting the work entitled “Maintenance of autophagic flux through MAPK/ERK signalling leads to initiation of chemoresistance in ovarian cancer cells” in NRSM 2017, ACTREC, Navi Mumbai

International conference: Non-invasive bioluminescence imaging elucidates the role of ERK1/2 kinase in sustenance of autophagic flux during acquirement of chemoresistance in 5th EACR: A Matter of Life or Death: Mechanisms, Models and Therapeutic Opportunities, Bergamo, Italy, 2020.

Others

Journals

Selectivity Enhancement of paclitaxel liposome towards folate receptor positive tumor cells by ligand number optimization approach. Prajapati M.K., Bishnu A., Ray P. and Vavia P.R.* ;AAPS PharmSciTech;2019

Book chapters

Bishnu A., Deo A., Dhadve A, Thakur B, Mukherjee S, Ray P. Non Invasive Imaging in Clinical Oncology: A Testimony of Current Modalities and a Glimpse into the Future.” *Molecular Medicines for Cancer: Concepts and Applications of Nanotechnology*, CRC Press, Taylor & Francis Group, 2018, pp. 217–262.

Review articles

Dhadve, A., Deo, A, **Bishnu, A.**, Mukherjee, S. and Ray, P., 2017. MOLECULAR IMAGING IN CANCER: HOW THE HALLMARKS AID IN HUNTING. *International Journal of Drug Research and Technology*, 7(1), p.1.

Aniketh Bishnu

Aniketh Bishnu

DEDICATIONS

To the passionately curious global scientific community

ACKNOWLEDGEMENTS

I would like to sincerely thank my mentor Dr. Pritha Ray for teaching me how to pursue scientific research. Her resounding advice and critical appreciation have enabled me to acquire the skill set and scientific inquisitiveness. Furthermore, I want to thank her for helping me realize my potential not just technically but in scientific communications. Despite her busy schedule, she has always been involved in the work and open for discussion. She has always been a critic of my work and proponent of my success. Finally, if it was not for her support, this work would not have been possible. I am grateful to be a part of her research team.

I thank Dr. Sudeep Gupta (Director, ACTREC), Dr. Prasanna Venkatraman (Deputy Director, CRI, ACTREC), and ACTREC for providing me with an excellent research atmosphere, infrastructure, and fellowship. I would also like to thank the members of my doctoral committee, Dr. Sorab Dalal, Dr. Prasanna Venkatraman, Dr. Sanjay Gupta and Dr. Abhijit De for their guidance and suggestions. I like to especially thank Dr. Abhijit De for being closely involved in the project and providing me immense moral and scientific support. I extend my gratitude to the Molecular Imaging Facility (Dr. Abhijit De and Snehal), Animal House Facility (Dr. Ingale and staff), Digital Imaging Facility (Dr. Dibendu Bhattacharya and Vaishali ma'am), FACS Facility (Dr. Sanjeev Waghmare and Shamal ma'am), Common Instrumentation Facility (Mr. Uday Dandekar), Library, SCOPE cell, steno pool and administration. I would like to thank HBNI and Sam Mistry for providing travel support to attend all the conferences. I would also like to thank all scientists I have met in several conferences for the scientific discussions and motivation.

I would like to thank all present and past members of the lab, Ram, Bhushan, Snehal, Lata Di, Ajit, Abhilash, Souvik, Megha, Pratham, Priti, Sourav and Arun ji for all the scientific as well as non-scientific discussions, arguments, coffee breaks and memories. I would especially thank Pratham for his help with immunohistochemical analysis of tumour tissues and Lata di for helping me in all my projects. Also, I like to thank Ajit for helping me with animal work. I like to thank all the trainees I have been involved with especially Irfan, Rucha and Aashi. I would also like to thank all the De lab members especially Maitrayi, Pranay and Snehal for the wonderful memories and scientific discussions. The memories that I have made over the course of time is something that I will truly cherish for the rest of my life. I would also like to thank all my batch mates and friends here in ACTREC.

Whatever I have achieved till now, would have not been possible without my family. My parents Mr. Premalendu Bishnu and Mrs. Rina Bishnu, who have always let me explore all the avenues in my life and provided me with everything I needed. I would like to thank my brother Mr. Prabirendu Bishnu and sister in law Dr. Amrita Mitra for always motivating me to achieve my goals and encouraging me to dream bigger. I would like to thank my 8 year old nephew, Bishwarup for asking me very difficult scientific questions, which makes me revisit basic scientific principles. I would like to thank Purbasha, for teaching me never to give up in life, no matter what it throws at you. They have always been my life support.

I would also like to thank my close friends who have embarked on the journey since my bachelors in St. Xaviers College, Arijit, Rohit, Disha, Arijit Bhowmick, Sambita, Snigdha and Shuboshree. They have been part of many exciting memories.

Aniketh Bishnu
Aniketh Bishnu

Contents

SYNOPSIS OF Ph. D. THESIS	15
Chapter 1: Introduction and review of literature	37
1.1 Cellular signaling: the central processing unit of cellular system	38
1.1.1 Monitoring of signaling events	39
1.1.2 Methods to monitor molecular interaction	40
1.1.2.1 Yeast two Hybrid (Y2H) assay	41
1.1.2.2 Spilt Reporter system	42
1.1.2.3 Resonance energy transfer (RET) based assays	43
1.1.2.3.1 Fluorescence resonance energy transfer (FRET)	45
1.1.2.3.2 Bioluminescence resonance energy transfer (BRET)	48
1.1.3 Understanding the implication of signaling pathway modulation	52
1.2 Chemoresistance	54
1.2.1 The role of Extracellular Regulated Kinase 1/2 (ERK1/2) in chemoresistance ..	56
1.2.2 The role of AKT in chemoresistance	60
1.2.3 Autophagy in chemoresistance	65
1.2.3.1 Real time monitoring of autophagy during therapy:	70
1.2.4 Cancer stem cell in chemoresistance	72
1.3 Multi drug resistance:	76
1.4 Ovarian cancer	78
1.4.1 Subtypes of ovarian cancer	79
1.4.2 Disease management and treatment	80
1.4.3 Acquirement of therapy resistance to platinum-taxol in EOC	82
Aim:	85
Key questions:	85
Objectives:	85
Chapter 2: Hyper activated ERK1/2 kinase drives autophagy to promote survival of ovarian cancer cells at the onset of chemoresistance	86
2.1 Introduction	87
2.2 Methodology	92
2.2.1 Development of chemoresistant model	92
2.2.2 Immunoblotting	93
2.2.3 Transmission electron microscopy	94

2.2.4 Confocal and immunofluorescence microscopy	94
2.2.5 Generation of firefly luciferase/mutant thermostable firefly luciferase-p62 fusion construct (Fl-p62/ mtFL-p62)	94
2.2.6 ERK1 silencing by lentiviral mediated sh-RNA constructs	95
2.2.7 Apoptosis detection with Annexin/PI	95
2.2.8 Real-time cell death assessment using CellTox™	95
2.2.9 Cell viability assay	95
2.2.10 Generation of stable clones expressing	96
2.2.11 Luciferase assay	96
2.2.12 Live-cell imaging	96
2.2.13 <i>In-vivo</i> imaging	96
2.2.14 Statistical analysis	97
2.3 Results:	97
2.3.1 ERK1/2 activation predominates in the onset of therapy resistance.....	97
2.3.2 Autophagic flux remains upregulated at the early stage of platinum-taxol dual resistance	101
2.3.3 Activated ERK1/2 promotes autophagic flux at onset of platinum-taxol resistance	105
2.3.4 Activated ERK 1/2 kinase regulates autophagosome–lysosome fusion.....	112
2.3.5 ERK1/2 inhibition promotes platinum-taxol induced apoptosis in early stage of resistance	119
2.3.6 mtFL-p62 sensor captures inducer/inhibitor induced differential autophagic flux	121
2.3.7 mTFL-p62 reveals differential autophagic flux at different stages of chemoresistance	124
2.3.8 mtFL-p62 sensor tracks real time autophagy kinetics in live cells and mouse model	126
2.4 Discussion	132
Chapter 3: Repurposing metabolic drug to impede development of platinum-taxol resistance in ovarian cancer	142
3.1 Introduction	143
3.2 Materials and Methods:.....	146
3.2.1 Development of cisplatin-paclitaxel dual resistant model in presence of metformin:	146
3.2.2 MTT assay	147

3.2.3 Trypan blue exclusion assay for cell proliferation	147
3.2.4 Clonogenic assay	147
3.2.5 Immunoblotting	148
3.2.6 Quantitative real-time PCR	148
3.2.7 Side population assay	148
3.2.8 Surface biomarker based CSC quantification	148
3.2.9 Cell Metabolome Quenching and Metabolites Extraction for NMR Analysis .	149
3.2.10 NMR experimentation and metabolite identification	149
3.2.11 Statistical analysis	149
3.3 Results:	149
3.3.1 Metformin intervention during acquirement of platinum-taxol resistance promotes proliferation	149
3.3.2 Long term metformin treatment impedes development of chemoresistance and reduce CSCs	152
3.3.3 Metformin treatment alters the level of semi-essential amino acids	156
3.3.4 Taurine regulates CSC differentiation and sensitizes cells to therapy	158
3.4 Discussion:	159
Chapter 4: Development of BRET based bio-molecular interaction platform to predict response of non-platinum drugs	166
4.1 Introduction:	167
4.2 Methodology	170
4.2.1 Development of chemoresistant model	170
4.2.2 Enrichment of tumour cells from ascitic fluid	170
4.2.3 Development of PIP3/AKT BRET construct (NAT)	171
4.2.4 Development of BRET sensor for monitoring ERK1/2 activation (NEO)	171
4.2.5 Side directed mutagenesis	171
4.2.6 Immunoblotting:	172
4.2.7 Confocal microscopy	172
4.2.8 Cell viability assay	172
4.2.9 BRET imaging and analysis	172
4.3 Results:	173
4.3.1 PIP3 BRET biosensor NAT accurately predicts PIP3/AKT activation:	173
4.3.2 BRET based ERK activity reporter (NEO) accurately predicts ERK1/2 activation:	177

4.3.3 Dynamic modulation of ERK and AKT activation in sensitive and chemoresistant ovarian cancer ascites and cell lines	180
4.3.4 ERK1/2 activation predicts cross-resistance to second line of ovarian cancer therapy	183
4.3.5 ERK1/2 promotes survival and anti-apoptotic signature in platinum-taxol resistant cells	186
4.4 Discussion:	188
Chapter 5: Summary	193
Chapter 6: Materials and methods	199
6.1 Bacterial culture	200
6.2 Molecular Cloning	204
6.3 Cell culture	209
6.4 Cell viability assay	212
6.5. Immunoblotting	215
6.6 Transmission Electron Microscopy	221
6.7 Confocal and Immuno-fluorescence microscopy	222
6.8 Flow cytometry	224
6.9 Luciferase assay	226
6.10 Live cell imaging of autophagic flux	228
6.11 Quantitative Real-time PCR	229
6.12 Lentiviral mediated genetic knock down	232
6.13 Side population assay	234
6.14 Metabolite extraction and NMR	235
6.15 BRET	237
6.16 In-Vivo imaging	241
6.17 Statistics	244



Homi Bhabha National Institute

SYNOPSIS OF Ph. D. THESIS

- 1. Name of the Student:** Aniketh Bishnu
- 2. Name of the Constituent Institution:** Tata Memorial Centre – Advanced Centre for Treatment Research and Education in Cancer
- 3. Enrolment No. :** LIFE09201504006
- 4. Title of the Thesis:** A study on understanding the modulation in MAPK/ERK and PI3KCA/Akt signaling during acquirement of drug resistance
- 5. Board of Studies:** Life science

SYNOPSIS

Introduction

Acquirement of resistance to various modes of therapy (chemo/targeted/radio) is the major impediment in management of several cancers including epithelial ovarian cancer (EOC). Though majority of EOC patients respond well initially to classical platinum-taxol combination, nearly 10-20% of the cases relapse within 6 months of therapy completion and does not respond to platinum again, thus termed as platinum-resistant relapse while cases which relapses after 6-12 months are categorized as partially platinum-sensitive and disease recurrence after 1 year is classified as platinum-sensitive relapse (1). Platinum resistant relapse cases are generally confronted with second line of non-platinum agents like doxorubicin, gemcitabine, irinotecan and etoposide while the platinum sensitive relapse patients are again treated with platinum agents followed by non-platinum agents once they become non-responsive to platinum (2). In either scenario, these platinum or non-platinum based cytotoxic agents do not cease further relapse of the disease leading to high mortality (3, 4). Thus it is critical to identify molecular processes or targets that would allow 1) the

platinum-resistant tumor cells be sensitized to targeted therapy or 2) delay in acquisition of platinum-resistance or 3) predict response of non-platinum drugs to identify the right choice and avoid excessive side-effects. All these three or any one of them is beneficial for improved treatment response and better health of the resistant relapse patients.

Acquired chemoresistance, a multi-step process developed through series of molecular and biochemical changes resulting from modulation in several key signaling components. Evolution of a cancer cell to a highly resistant disease can be categorized in different stages based on the degree of resistance which can be manipulated for therapeutic purpose. *Utilizing indigenously built platinum-taxol resistant A2780 and OAW42 dynamic cellular models developed using pulse method of chemotherapy, we aim to identify and target key molecular components capable of 1) preventing promotion of resistance or 2) delaying the development of a highly chemoresistant disease or 3) predicting response for alternate non-platinum agents to identify the optimal choice.*

Previous reports from our lab suggested that an upregulated IGF1R expression promotes development of resistance at an early stage while increased AKT activation but low IGF1R level maintains a highly resistant phenotype in our cellular chemoresistant models (5). PI3K/AKT and MAPK/ERK are the two key downstream signaling pathway of IGF1R implicated in regulation of chemoresistance in several cancer including EOC (6-9). *Though there are several studies which shows activation of these signaling pathways in chemo resistant ovarian cancer cells there are no reports on how these signaling pathways are modulated as ovarian cancer cells gradually become more and more resistant to platinum-taxol treatment.* Among several cellular and molecular pathways associated with chemoresistance, multiple reports correlate activation of autophagic flux with chemoresistant phenotype in several cancers including EOC (9-12). Alterations in key kinases and signalling pathways can fine tune autophagic flux to promote development of chemoresistance (10, 13, 14). An active AKT signaling is reported to inhibit autophagic flux

while ERK activation regulates autophagy in a context dependent manner (11, 15, 16). Thus investigating the association of autophagy during gradual acquirement of chemoresistance and its regulation through key signaling intermediates may help in developing novel therapeutic strategy against chemoresistant ovarian cancer.

Identifying molecular processes or targets that could impede development of therapy resistance is the need of the hour for EOC. Repurposing of FDA approved drug for one pathological condition to another disease significantly reduces the cost and time of approving a promising drug. Vast clinical and basic studies support the idea of repurposing of metformin, a first line drug for treating type-2 Diabetes, against EOC. Administration of metformin was associated with better survival in 73 EOC patients. A reduced incidence of EOC was also reported in diabetic patients who received metformin (17-19). Combinatorial treatment of metformin along with paclitaxel was reported to reduce tumor volume in LSL-KrasG12D/+PtenloxP/loxP mice (20). High dose of metformin treatment was reported to inhibit cell proliferation in a panel EOC cell lines (21). Although, multiple reports suggests various role of metformin in regulation of proliferation, sensitization and tumor development, the role of metformin as an adjuvant to cisplatin-paclitaxel during the attainment of therapy resistance is yet to explored.

Development of highly platinum resistant phenotype compels the use of second line non-platinum agents like doxorubicin, gemcitabine, irino/topotecan and etoposide. A prior subject specific assessment of the effectivity of these drugs can guide the choice of second or third line chemotherapeutics to improve response rate. Classically, cytotoxicity based approaches are used to determine effectivity of chemotherapeutic drugs which though provides a gross estimation drug sensitivity but fails to monitor molecular response to therapy, which may impart cross-resistance. The complexity in molecular response to an external chemotherapeutic stimuli is governed by multitude of differential protein-protein interaction (PPI) involving few key signaling hubs. In recent years, Bioluminescence

Resonance Energy Transfer (BRET) has emerged as a powerful technique for studying Protein-protein (PPI) and lipid-protein (PLI) interactions (22, 23). BRET works on the principle of non-radiative energy transfer between a donor luciferase and a acceptor fluorophore within a permissible distance (1-10nm). Thus real time monitoring of PPI and PLI using -BRET may provide a better understanding of the drug response which may ultimately predict therapy outcome.

In the quest for deep understanding of the contributory role of MAPK/ERK and PI3KCA/AKT signaling in acquired platinum-resistance and develop remedial strategies, the following questions were framed.

Key questions

1. Whether MAPK/ERK and PI3K/AKT signaling are modulated during the gradual acquirement of chemo resistance in ovarian cancer cells?
2. Is it possible to target and pause promotion of resistance at the onset of cisplatin-paclitaxel dual resistance in ovarian cancer cells?
3. Is it possible to impede development of a highly chemoresistant phenotype?
4. Is it possible to utilize the dynamic modulation in MAPK/ERK and PI3K/AKT signaling to predict therapeutic efficacy of second line non-platinum agents in platinum-taxol resistant cells?

Based on these key questions, the following specific objectives were designed:

Objective 1: Understanding the biological relevance of MAPK/ERK and PI3K/AKT signaling in dual chemo resistant ovarian cancer model

Results:

1. A. Evaluating the role of MAPK/ERK and PI3K/AKT in regulation of chemotherapy induced autophagic flux during acquirement of resistance

To understand the modulation of MAPK/ERK and PI3K/AKT signaling during the course of acquired chemoresistance, we utilized indigenously developed cisplatin–paclitaxel dual resistant model in A2780 and OAW42 cell lines. These models were developed by

successive and incremental treatment of cisplatin-paclitaxel over six months and were classified into sensitive, early (A2780/OAW42Dual^{ER}) and late (A2780/OAW42Dual^{LR}) resistant cells depending on their resistant indices (5). Basal level of ERK1/2 phosphorylation and phosphorylation of its downstream target p90^{RSK1/2} and Fra-1 were significantly higher in Dual^{ER} cells of both models, inhibition of which with U0126 (a MEK1/2 inhibitor) along with cisplatin-paclitaxel (CisPac) induced an additive cytotoxic effect specifically in Dual^{ER} cells (26.15% and 23.28% respectively) of both A2780 and OAW42 models compared to only CisPac or U0126 indicating the dependency of Dual^{ER} cells upon activated ERK1/2 signaling.

Among the several molecular phenotypes regulated by ERK1/2, we were interested in understanding the role of ERK1/2 in regulation of chemotherapy induced autophagic flux. CisPac treatment to both sensitive and Dual^{ER} cells showed increased LC3 I-II conversion at 12 and 24 hrs for both the models. Surprisingly, p62 degradation which denotes completion of autophagy was only evident in Dual^{ER} cells. CisPac treatment of A2780Dual^{LR} and OAW42Dual^{LR} cells induced minimal LC3 I-II conversion and p62 degradation. Assessment of autophagic flux in presence of chloroquine (CQ, an autophagy inhibitor) revealed highest change in LC3 conversion specifically in A2780Dual^{ER} cells post CisPac+CQ treatment in comparison to only CisPac, indicating an increased chemotherapy induced autophagy flux while blocked/ reduced autophagic flux was observed in A2780 and A2780Dual^{LR} cells. Transmission electron microscopy also revealed a distinct surge in numbers of autophagosomes (2.1 fold and 3.4 fold) as well as autophagolysosomes (3.4 fold and 3.2 fold) in drug treated A2780Dual^{ER} and OAW42Dual^{ER} cells while increased formation of autophagosomes without any change in autophagolysosome number was observed in sensitive cells, indicating a blockade in completion of autophagic flux. A

minimal increase in the number of autophagic bodies was observed in Dual^{LR} cells of both models, suggestive of a low level of autophagy.

Exclusive presence of drug induced autophagic flux at the onset of resistance prompted us to investigate the molecular crosstalk between autophagic flux and activated ERK1/2 signaling. Estimation of autophagic flux revealed a significantly increased LC3 conversion and p62 level post treatment with CisPac+CQ compared to only CisPac while addition of chloroquine along with CisPac and U0126 did not lead to further increase in LC3 and p62 accumulation in comparison to CisPac+U0126, indicating a blockade in late stage of autophagy upon ERK1/2 inhibition. Similar results were observed when Trametinib (a clinically approved MEK inhibitor) was used in the same conditions. Genetic knock-down of ERK1 increased LC3II and p62 accumulation compared to parental A2780Dual^{ER} cells post CisPac treatment. Combinatorial treatment of U0126 and CisPac increased phagophores and autophagosomes with a concomitant reduction in autophagolysosomes in Dual^{ER} cells indicating the role of ERK1/2 in completion of autophagic flux during the onset of therapy resistance. Reduced initiation of autophagy flux in the Dual^{LR} was attributed to the hyperactive AKT signaling, inhibition of which induced higher LC3I-II conversion and p62 degradation.

In order to understand whether ERK1/2 regulates completion of autophagy via maturation and subsequent fusion of autophagosome with lysosome we utilized the classical mCherry-EGFP-LC3 reporter. Combinatorial treatment of CisPac along with U0126 in A2780Dual^{ER} cells reduced mcherry/EGFP ratio (1.91) with an accumulation of yellow puncta (co-localization coefficient: 0.70 ± 0.04) in the perinuclear region, compared to only drug treated cells, which predominantly displayed red puncta (mcherry/GFP ratio 4.11) with fewer co-localization (co-localization coefficient: 0.48 ± 0.06). Dual immuno-staining with LC3 (autophagosome marker) and LAMPI (lysosomal marker) revealed enhanced

LC3^{+ve}LAMP^{+ve} puncta specifically in CisPac treated Dual^{ER} cells than untreated cells (27.16±2.71 vs. 6.89±0.78 puncta/cell) which again reduced by 5-fold (5.3±0.59 puncta/cell) after combinatorial treatment of U0126 and CisPac. Autophagosome-lysosome fusion involve a large number of molecular players of which UV radiation resistance-associated (UVRAG) and Rubicon (RUBCN) are involved in endocytic transport, autophagosome maturation and/or autophagosome–lysosome fusion through Rab7 (24, 25). Both pharmacological and genetic inhibition of ERK1/2 along CisPac reduced level of UVRAG and Rab7, implying a molecular link between ERK1/2 activation and autophagosome-lysosome fusion. Inhibition of ERK1/2 activation (Trametinib) in Dual^{ER} cells increased apoptosis indicated by increased dead cell population, PARP cleavage and annexin^{+ve}/PI^{+ve} population.

The above results suggested a promising role of ERK inhibitor to combat chemoresistance at an early stage through inhibition of drug induced autophagic flux. However, to evaluate the therapeutic efficacy at preclinical stage, an appropriate autophagy sensor is required. Since the currently available sensors fails to monitor real-time autophagic flux in-vivo, we developed a luciferase based novel autophagy sensor, mtFL-p62 which showed enhanced luciferase signal due to accumulation of p62 upon blockade of autophagic flux and reduced luciferase signal due to degradation of p62 upon induction of autophagy. After initial validation of the sensor using different known modulators of autophagy we utilized the sensor to monitor chemotherapy induced autophagic flux in A2780 and OAW42 chemoresistant model from cell lysate as well as live-cell assay. In agreement to our previous data, chemotherapeutic treatment in A2780 and A2780Dual^{LR} cells increased luciferase signal (1.48±0.06 and 1.62±0.04 fold at 12 and 24 hour) and (0.62±0.03 and 2.07±0.16 fold at 12 and 24 hour) compared to their untreated group. Contrarily, a reduced luciferase signal was observed upon drug treatment in A2780Dual^{ER} cells which enhanced

after combinatorial treatments of U0126 and CisPac. Chloroquine treatment along with CisPac also increased signal output at all the stages.

Next tumour xenografts of A2780Dual^{ER} cells stably expressing mtFL-p62 fusion reporter were developed in nude mice and therapy induced autophagic flux was monitored for 14 days. CisPac treatment (day 1) resulted in 0.62 fold reduction in luminescence signal on day 2 which reduced further over subsequent treatment till 0.32-fold on day 14, indicating ongoing p62 degradation and an active autophagic flux. While combinatorial treatment of Trametinib with CisPac induced a 3.12 fold increase in luminescence signal on day-2 which remain steady till day 4 and then dropped on day 6. A 3.80 and 3.78 fold gain in luminescence signal was observed post administration of second and third dose on day 8 and day 14 respectively indicating the role of Trametinib in inhibition of CisPac induced autophagic flux. Combinatorial treatment of CisPac along with CQ showed a similar kinetics while change in luciferase signal upon treatment with only Trametinib or chloroquine did not change significantly. Further, combinatorial treatment of Trametinib along with CisPac significantly reduced tumor growth with respect to only CisPac, only Trametinib and untreated group respectively. Altogether our data suggests that a hyper-activated ERK1/2 drives autophagic flux to withstand therapeutic stress at the onset of chemoresistance inhibition of which sensitizes these cells to therapy and prevent development of highly chemoresistant phenotype.

1.B. Understanding the role of metformin in acquirement of chemoresistance

To determine the role of metformin on acquirement of chemoresistance, two different strategies for administration of metformin treatment were adopted: i) Sequential treatment of metformin and then cisplatin-paclitaxel [referred as MSLR (A2780^{MSLR} or

OAW42^{MSLR}], and ii) Combinatorial treatment of metformin along with platinum-taxol [referred as MCLR (A2780^{MCLR} or OAW42^{MCLR})]. A low (IC₂₀) dosage of metformin (2mM) was used to avoid cytotoxicity. The proliferation rate of MCLR and MSLR cells was significantly higher than Dual^{LR} in both A2780 and OAW42 model. Dual^{LR} exhibited longest doubling time of (39±0.93 and 84.25±11.42 hours) while MSLR and MCLR showed a doubling time 28.05±0.60 hours and 24.18±0.14 hours respectively in A2780 model and 43.59±1.02 hours and 36.66±0.11 hours respectively in OAW42 model. MSLR and MCLR cells of both A2780 and OAW42 cell lines, showed reduced AKT phosphorylation in comparison to Dual^{LR} cells while ERK activation was higher in metformin treated groups. To assess the tolerance of MCLR and MSLR cells towards cisplatin and paclitaxel, cell viability was measured post CisPac treatment. A combined dosage of cisplatin and paclitaxel induced only 4.5±2 % and 6.2±4.2% cell death in A2780Dual^{LR} and OAW42Dual^{LR} cells respectively while 33±2.73% and 18.51±2.4 % cell death was observed in A2780^{MSLR} and OAW42^{MSLR} cells. Similarly, a 32.26±2.9% and 39±0.46 % cell death was observed A2780^{MCLR} and OAW42^{MCLR} cells respectively. Next, we estimated the long term survival of these cells with increasing concentrations of cisplatin and paclitaxel through clonogenic assay. A2780Dual^{LR} cells showed significantly increased number of colonies (~90% and 65% surviving fraction) compared to A2780MSLR (~66% and 18%), and A2780MCLR (~19% and 17%) in both the drug concentrations tested (100ng cisplatin+13ng paclitaxel/ml and 100ng cisplatin+42.5ng paclitaxel/ml). OAW42^{MSLR} and OAW42^{MCLR} cells also showed reduced number of colony in comparison to OAW42Dual^{LR} cells.

Since, multiple reports suggest the role of metformin in stemness regulation, we quantified the percentage of CSC population based on their innate drug efflux property by Side Population assay. Highest percentage of CSC population (28.6 % and 22.1% respectively)

was observed in A2780Dual^{LR} and OAW42Dual^{LR} cells while MSLR (15.1% and 4.13%) and MCLR (9.70% and 6.79%) showed reduced percentage of CSC population in both A2780 and OAW42 respectively. Dual^{LR} cells also showed highest percentage of CD133^{+ve} population compared to MSLR and MCLR cells of both models. A significantly higher relative expression of pluripotent genes like Sox2, Oct 4, and Nanog was also observed in Dual^{LR} cells in comparison to MSLR and MCLR cells of both models. These results indicated that metformin attenuates development of CisPac resistance by targeting CSC in EOC cells.

Since metformin is known to affect cellular metabolism, we performed 1D 1H-NMR spectroscopy to identify the altered metabolites in presence and absence of metformin. Taurine and histidine were found to be the most significantly altered metabolites between the groups. Presence of metformin upregulated taurine level in A2780^{MSLR} (~2 fold) and A2780^{MCLR} (~1.7 fold) as compared to A2780 cells while A2780Dual^{LR} (~1.2 fold) cells showed similar level of taurine as compared to sensitive cells.

Since taurine is reported to promote stem cell differentiation (26, 27) and we also had observed a decrease in the percent CSC population in MCLR and MSLR cells, we evaluated the effect of taurine directly on CSC population of Dual^{LR} cells. Taurine reduced the CSC population by 5.7% and 10.6% respectively in comparison to untreated cells (30.5% SP population). Combinatorial treatment of taurine and CisPac also sensitized Dual^{LR} cells to therapy, indicating the role of taurine in maintenance of CSC and therapy resistance.

Objective 2: Development of BRET based sensors to monitor PI3K/AKT signaling and MAPK/ERK signaling during the acquirement of chemoresistance

Targeting specific molecular pathways in late or highly resistant cells may improve therapeutic outcome. However, it's also important to assess the molecular changes (PPI or PLI) during therapy for optimization of the currently available therapeutic options.

Membrane translocation of AKT via its Pleckstrin Homology (PH) domain upon conversion of PIP2 to PIP3 by phosphoinositol-3-kinase is a crucial and initial step of AKT activation. In this report, we developed an improved BRET based PIP3 sensor (NAT) utilizing the already available Luc-PH-AKT/YFP-Mem BRET biosensor by replacing Rluc with nanoluciferase (NLuc, BRET donor), and a red-shifted TurboFP fluorescent (BRET acceptor) protein instead of YFP. Real-time live cell imaging of A2780 cells expressing NAT revealed a dose dependent increase in AKT activation, which peaked at 5 min (0.95 ± 0.01) compared to untreated (0.13 ± 0.02) cells and then remained fairly constant till 15 min. A similar dose dependent AKT activation kinetics was also observed in MCF7 cells post insulin treatment. Increase in NAT BRET ratio was also observed post 15 min of IGF-1 (0.98 ± 0.03) or EGF (1 ± 0.02) treatment while pre-treatment of cells with wortmannin (PI3KCA inhibitor) and picropodophyllin (IGF1R inhibitor) reduced BRET ratio. In corroboration with the BRET data, a similar trend in AKT phosphorylation was observed in A2780 cells post treatment with different growth factors and inhibitors by immunoblotting, indicating the accuracy of the BRET sensor, NAT in portraying AKT activation dynamics. Next, we developed ERK based BRET reporter by replacing the FRET compatible fluorophores of FRET based Extracellular signal-regulated Kinase Activity Reporter (EKAR_{cyto} and EKAR_{nucleus}) with NanoLuc and mOrange (Nluc-EKAR-mOrange, NEO). Briefly, the sensor consists of consensus ERK target phosphorylation sequence of cdc25 (PRTP), phospho ERK binding domain (FQFP), a flexible linker of 72 glycine residue and a proline directed phospho binding domain. Phosphorylation by ERK1/2 triggers a conformational change which brings the donor and acceptor proteins in close proximity and induce resonance energy transfer between them. To monitor the total ERK activity (Cytoplasmic+Nuclear) both the constructs were transfected together in all the experiments. Live cell monitoring of ERK activation revealed a dose and time dependent increase in BRET ratio (27.44 ± 0.19 and 48.21 ± 0.51 mBu at 15 min respectively) post 100nM and 200

nM IGF-1 treatment in comparison unstimulated A2780 cells (13.34 ± 0.41 mBu). Similar increase in BRET ratio indicating gradual ERK activation was observed in IGF-1 stimulated MCF7 cells. Insulin and EGF stimulation induced increased BRET ratio (58.55 ± 0.68 and 54.64 ± 1.89 mBu respectively) while pre-treatment with U0126 (21.07 ± 0.99 mBu) or picropodophyllin (26.72 ± 0.97 mBu) reduced BRET in A2780 cells. A similar trend of ERK phosphorylation was observed post treatment with different growth factors and inhibitors by immunoblotting indicating the efficiency of NEO in accurately portraying autophagy flux.

Next we utilized our NAT and NEO sensor to monitor platinum-taxol induced ERK1/2 and AKT activation in our Dual^{LR} and SKOV3 (an intrinsically platinum resistant cell-line) cells in comparison to sensitive A2780 and OAW42 cells. Interestingly, platinum-taxol treatment increased in NEO BRET signal in A2780Dual^{LR} (86.10 ± 1.37 and 117.29 ± 4.39 mBu) and OAW42Dual^{LR} (85.59 ± 4.63 and 93.12 ± 4.14 mBu) cells post 12 and 24 hours, while no significant change in BRET ratio was observed in parental cells. A similar increase in BRET signal was observed in SKOV3 cells post 12 and 24 hours of platinum-taxol treatment. No significant increase in NAT BRET signal was observed post cisplatin-paclitaxel treatment in both sensitive and chemoresistant cells, however an increased basal BRET ratio was observed in A2780Dual^{LR}, OAW42Dual^{LR} and SKOV3 cells in comparison to sensitive A2780 and OAW42 cells. These results indicated a therapy induced ERK1/2 activation but not AKT activation in cisplatin-paclitaxel dual resistant cells. Till date, ERK and AKT activation are never measured in real time using BRET strategy in patient derived primary tumor cells. We attempted live cell imaging of BRET phenomenon in ovarian cancer cells (CD90^{-ve}EPCAM^{+ve}) derived from malignant ascites from chemo naïve, platinum resistant relapse and platinum sensitive relapse patients. Interestingly, an increased NEO (4.72 fold) and NAT BRET (10.11 fold) ratio was observed in cells derived from platinum-resistant patient while no significant change in BRET ratio was observed in ascites derived from

chemo-naive and platinum-sensitive relapse patient post platinum treatment. Cells derived from platinum-resistant patient also showed higher tolerance to cisplatin compared to chemo-naïve and platinum-sensitive cases. Collectively this data suggests the importance of ERK1/2 and AKT activation in predicting effectivity of a platinum-taxol therapy.

Disease recurrence within six months of initial therapy followed by non-responsiveness to reintroduction of platinum drugs necessitates the use of second line of therapy with non-platinum agents. The most commonly chosen second line of non-platinum drugs include doxorubicin, gemcitabine, irinotecan and etoposide. It is important to understand whether and which of these second line non-platinum agents will be appropriate in platinum-taxol resistant cells by assessing the ERK1/2 and AKT signalling arms. Doxorubicin treatment increased NEO BRET signal by 2.3 fold in A2780Dual^{LR} cells, by 3.5 fold in OAW42Dual^{LR} cell and by 2.6 fold in SKOV3 cells post 24 hours of treatment, while no significant change in BRET signal was observed in A2780 and OAW42 cells. Increased NEO BRET signal was also observed post 24 hours of gemcitabine and etoposide treatment specifically in A2780Dual^{LR}, OAW42Dual^{LR} and SKOV3 cells but not in sensitive A2780 and OAW42 cells. Intriguingly, Irinotecan treatment did not result any significant change in NEO BRET ratio in chemoresistant or chemosensitive cells. In comparison to the NEO BRET, NAT BRET ratio did not get significantly altered significantly post treatment with any of the second line therapeutic agents in both chemoresistant and sensitive cells. A2780Dual^{LR}, OAW42Dual^{LR} and SKOV3 cells showed increased tolerance to doxorubicin, gemcitabine and etoposide but not Irinotecan, which sensitize these dual resistant cells to therapy. Doxorubicin induced ERK1/2 activation led to increased activation of its downstream target p90^{RSK}, a growth promoting survival signal, while inhibiting pro-apoptotic BAD protein specifically in Dual^{LR} and SKOV3 cells. However non-significant alteration in phospho p90RSK and pBAD was observed post irinotecan treatment in both sensitive as well as chemoresistant cells. Altogether our data suggests that chemotherapy induced ERK1/2

activation may support development of cross-resistance to non-platinum agent and may lead to poorer therapeutic outcome.

Conclusion:

Our data suggests that inhibition of ERK1/2 activation blocks chemotherapy induced autophagic flux to prevent development of highly chemoresistant phenotype in the onset of cisplatin-paclitaxel dual resistance. Repurposing metformin, an anti-diabetic drug, as an adjuvant to platinum-taxol could impede the development of highly chemoresistant phenotype. However, complete development of chemoresistance necessitate the administration of currently available second line therapy, the choice of which can be guided by prior evaluation of therapeutic effectivity by real-time BRET based monitoring of ERK1/2 and AKT activation.

Reference:

1. Colombo, P.E., et al., *Sensitivity and resistance to treatment in the primary management of epithelial ovarian cancer*. Crit Rev Oncol Hematol, 2014. **89**(2): p. 207-16.
2. Markman, M. and M.A. Bookman, *Second-Line Treatment of Ovarian Cancer*. The Oncologist, 2000. **5**(1): p. 26-35.
3. Pujade-Lauraine, E. and P. Combe, *Recurrent ovarian cancer*. Ann Oncol, 2016. **27 Suppl 1**: p. i63-i65.
4. Pujade-Lauraine, E., S. Banerjee, and S. Pignata, *Management of Platinum-Resistant, Relapsed Epithelial Ovarian Cancer and New Drug Perspectives*. J Clin Oncol, 2019. **37**(27): p. 2437-2448.
5. Singh, R.K., et al., *IGF-1R inhibition potentiates cytotoxic effects of chemotherapeutic agents in early stages of chemoresistant ovarian cancer cells*. Cancer Lett, 2014. **354**(2): p. 254-62.
6. Peng, D.J., et al., *Role of the Akt/mTOR survival pathway in cisplatin resistance in ovarian cancer cells*. Biochem Biophys Res Commun, 2010. **394**(3): p. 600-5.
7. Abedini, M.R., et al., *Akt promotes chemoresistance in human ovarian cancer cells by modulating cisplatin-induced, p53-dependent ubiquitination of FLICE-like inhibitory protein*. Oncogene, 2010. **29**(1): p. 11-25.
8. Koti, M., et al., *Identification of the IGF1/PI3K/NF kappaB/ERK gene signalling networks associated with chemotherapy resistance and treatment response in high-grade serous epithelial ovarian cancer*. BMC Cancer, 2013. **13**: p. 549.
9. Wang, J. and G.S. Wu, *Role of autophagy in cisplatin resistance in ovarian cancer cells*. J Biol Chem, 2014. **289**(24): p. 17163-73.
10. Wu, T., et al., *Autophagy facilitates lung adenocarcinoma resistance to cisplatin treatment by activation of AMPK/mTOR signaling pathway*. Drug Des Devel Ther, 2015. **9**: p. 6421-31.
11. Zhang, X.Y., et al., *Hexokinase 2 confers resistance to cisplatin in ovarian cancer cells by enhancing cisplatin-induced autophagy*. Int J Biochem Cell Biol, 2018. **95**: p. 9-16.
12. Lin, Q., et al., *Cisplatin regulates cell autophagy in endometrial cancer cells via the PI3K/AKT/mTOR signalling pathway*. Oncol Lett, 2017. **13**(5): p. 3567-3571.

13. Che, L., et al., *Loss of BRUCE reduces cellular energy level and induces autophagy by driving activation of the AMPK-ULK1 autophagic initiating axis*. PLoS One, 2019. **14**(5): p. e0216553.
14. Pei, G., et al., *Autophagy Facilitates Metadherin-Induced Chemotherapy Resistance Through the AMPK/ATG5 Pathway in Gastric Cancer*. Cell Physiol Biochem, 2018. **46**(2): p. 847-859.
15. Peng, H., et al., *Orlistat induces apoptosis and protective autophagy in ovarian cancer cells: involvement of Akt-mTOR-mediated signaling pathway*. Arch Gynecol Obstet, 2018. **298**(3): p. 597-605.
16. Pattingre, S., C. Bauvy, and P. Codogno, *Amino acids interfere with the ERK1/2-dependent control of macroautophagy by controlling the activation of Raf-1 in human colon cancer HT-29 cells*. J Biol Chem, 2003. **278**(19): p. 16667-74.
17. Kumar, S., et al., *Metformin intake is associated with better survival in ovarian cancer: a case-control study*. Cancer, 2013. **119**(3): p. 555-62.
18. Xu, S., et al., *Metformin Suppresses Tumor Progression by Inactivating Stromal Fibroblasts in Ovarian Cancer*. Molecular Cancer Therapeutics, 2018. **17**(6): p. 1291-1302.
19. Chan, D.K. and W.K. Miskimins, *Metformin and phenethyl isothiocyanate combined treatment in vitro is cytotoxic to ovarian cancer cultures*. J Ovarian Res, 2012. **5**(1): p. 19.
20. Lengyel, E., et al., *Metformin inhibits ovarian cancer growth and increases sensitivity to paclitaxel in mouse models*. Am J Obstet Gynecol, 2015. **212**(4): p. 479 e1-479 e10.
21. Rattan, R., et al., *Metformin suppresses ovarian cancer growth and metastasis with enhancement of cisplatin cytotoxicity in vivo*. Neoplasia, 2011. **13**(5): p. 483-91.
22. Dragulescu-Andrasi, A., et al., *Bioluminescence resonance energy transfer (BRET) imaging of protein-protein interactions within deep tissues of living subjects*. Proc Natl Acad Sci U S A, 2011. **108**(29): p. 12060-5.
23. Dimri, S., et al., *Dynamic monitoring of STAT3 activation in live cells using a novel STAT3 Phospho-BRET sensor*. Am J Nucl Med Mol Imaging, 2019. **9**(6): p. 321-334.
24. Matsunaga, K., et al., *Two Beclin 1-binding proteins, Atg14L and Rubicon, reciprocally regulate autophagy at different stages*. Nat Cell Biol, 2009. **11**(4): p. 385-96.
25. Sun, Q., et al., *Rubicon controls endosome maturation as a Rab7 effector*. Proc Natl Acad Sci U S A, 2010. **107**(45): p. 19338-43.
26. Li, X.W., H.Y. Gao, and J. Liu, *The role of taurine in improving neural stem cells proliferation and differentiation*. Nutr Neurosci, 2017. **20**(7): p. 409-415.
27. Zhou, C., et al., *Taurine promotes human mesenchymal stem cells to differentiate into osteoblast through the ERK pathway*. Amino Acids, 2014. **46**(7): p. 1673-80.

Publications in Refereed Journal:

a) **Published:** 1. Long term treatment of metformin impedes development of chemoresistance by regulating cancer stem cell differentiation through taurine generation in ovarian cancer cells.

Bishnu A¹., Sakpal A¹., Ghosh N., Choudhury P., Chaudhury K., Ray P.*; Int J Biochem Cell Bio; 2019 (from thesis)

2. Selectivity Enhancement of paclitaxel liposome towards folate receptor positive tumor cells by ligand number optimization approach. Prajapati M.K., **Bishnu A.**, Ray P. and Vavia P.R.* ;AAPS PharmSciTech;2019

b) **Accepted:** not applicable

c) **Communicated:** 1. Molecular Imaging of the kinetics of hyper activated ERK1/2 mediated autophagy during acquirement of chemoresistance. **Bishnu A.**, Phadte P., Dhadve A., Sakpal A., Rekhi B. and Ray P.*; Cell death dis. (Under review, from thesis).

2. BRET-based live cell detection of biomolecular interaction predicting response to second line therapy in platinum-taxol resistant ovarian cancer. **Bishnu A.**, Mehrotra M., Dhadve A., Dimri S., De A. and Ray P.*; Cancer Lett (Submitted, from thesis).

Patent: India Patent No. TEMP/E-1/10868/2019-MUM “A method for detection of protein activation using phosphor-BRET imaging sensor and methods thereof” by Abhijit De, Pritha Ray, Shalini Dimri and Aniketh Bishnu

Other Publications:

a) **Book Chapter 1. Bishnu A.**, Deo A., Dhadve A, Thakur B, Mukherjee S, Ray P. Non Invasive Imaging in Clinical Oncology: A Testimony of Current Modalities and a Glimpse into the Future.” *Molecular Medicines for Cancer: Concepts and Applications of Nanotechnology*, CRC Press, Taylor & Francis Group, 2018, pp. 217–262.

b) **Review articles:** 1. Dhadve, A., Deo, A, **Bishnu, A.**, Mukherjee, S. and Ray, P., 2017. MOLECULAR IMAGING IN CANCER: HOW THE HALLMARKS AID IN HUNTING. *International Journal of Drug Research and Technology*, 7(1), p.1.

c) **Conference/Symposium Awards:** 1. V.C. Shaw award for “Hyper activated ERK1/2 kinase drives autophagy to promote survival of ovarian cancer cells at the onset of chemoresistance” at AICBC 2019

2. CCMB best poster award for “BRET based monitoring of the dynamic nature of RTK/PI3K/AKT signalling Pathway” at ICCB 2018, Hyderabad

3. Best poster award for “ERK1/2 activation paves the way for onset of chemoresistance in ovarian cancer cells through sustenance of autophagic flux” at stem cell conference 2018, Somaiya college, Mumbai

4. Best poster award for presenting the work entitled "Maintenance of autophagic flux through MAPK/ERK signalling leads to initiation of chemoresistance in ovarian cancer cells" in NRSM 2017, ACTREC, Navi Mumbai

International conference: Non-invasive bioluminescence imaging elucidates the role of ERK1/2 kinase in sustenance of autophagic flux during acquirement of chemoresistance in 5th EACR: A Matter of Life or Death: Mechanisms, Models and Therapeutic Opportunities, Bergamo, Italy, 2020.

Aniketh Bishnu

Signature of Student:

Date:

Doctoral Committee:

S. No.	Name	Designation	Signature	Date
1.	Dr. Sorab Dalal	Chairperson	<i>S. N. Dalal</i>	15/1/2021
2.	Dr. Pritha Ray	Guide/ Convener	<i>Pritha Ray</i>	14/1/2021
3.	Dr. Prasanna Venkatraman	Member	<i>Prasanna</i>	18/1/2021
4.	Dr. Sanjay Gupta	Member	<i>Sanjay</i>	15/1/2021
5.	Dr. Abhijit De	Technical advisor	<i>Abhijit De</i>	15/01/2021

Forwarded Through:

S. N. Dalal

Dr. Sorab N. Dalal, 15/1/2021
Chairperson, Academic &
Training Programme, ACTREC
(Dr. Sorab N. Dalal)
Chairperson, Academic & Training Programme
Tata Memorial Center, ACTREC,
Kharghar, Navi Mumbai - 410210

S. D. Banavali
19/1/21

Prof. S. D. Banavali,
Dean (Academics)
T.M.C

PROF. S. D. BANAVALI, MD
DEAN (ACADEMICS)
TATA MEMORIAL CENTRE
MUMBAI - 400 012.

List of abbreviations

Y2H	Yeast two Hybrid
RET	Resonance Energy Transfer
FRET	Fluorescence Resonance Energy Transfer
BRET	Bioluminescence Resonance Energy Transfer
RLuc	Renilla Luciferase
EGFP	Enhanced Green Fluorescent Protein
CFP	Cyan Fluorescent Protein
YFP	Yellow Fluorescent Protein
ERK1/2	Extracellular signal Regulated Kinase 1/2
RTK	Receptor Tyrosine Kinase
EGFR	Epidermal Growth Factor Receptor
IGF1R	Insulin like Growth Factor Receptor 1
CSC	Cancer Stem Cells
MDR	Multi Drug Resistance
EOC	Epithelial Ovarian Cancer
HGSOC	High Grade Serous Ovarian Cancer
CQ	Chloroquine
HCQ	Hydroxychloroquine
CisPac	Cisplatin-Paclitaxel
5-FU	5-FluoroUracil
BCRP	Breast Cancer Resistant Protein
MRP1	M
EMT	Epithelial-Mesenchymal Transition

ABC	ATP Binding Cassette
ALDH	Aldehyde Dehydrogenase
CDK	Cyclin Dependent Kinase
IGF1	Insulin Growth Factor 1
SP	Side Population
EGF	Epidermal growth factor
FL2	Firefly Luciferase
mtFL	mutant Thermostable Firefly Luciferase
Dox	Doxorubicin
Gem	Gemcitabine
Irino	Irinotecan
Etopo	Etoposide

List of figures

- Figure 1: Strategies to explore signaling pathway modulation **38**
- Figure 2: Schematic representation of Resonance energy transfer (RET) **43**
- Figure 3: Basic working principle of BRET based protein-protein interaction **48**
- Figure 4: Alterations in key signaling axis **51**
- Figure 5: Modes of chemoresistance **53**
- Figure 6: Mechanisms regulating chemoresistance **54**
- Figure 7: MAPK/ERK signaling cascade **56**
- Figure 8: Role of PI3K/AKT and MAPK/ERK in chemoresistance **57**
- Figure 9: AKT protein domains and isoforms **60**
- Figure 10: PI3K/AKT signalling pathway **61**
- Figure 11: The process of macroautophagy **64**
- Figure 12: The dual role of autophagy in cancer **65**
- Figure 13: Dual role of autophagy in cancer therapy **66**
- Figure 14: Role of cancer stem cells in disease relapse **72**
- Figure 15: Cancer stem cells and therapy resistance **74**
- Figure 16: Classification of ovarian cancer based on histology **78**
- Figure 17: Treatment modalities and clinical classification of therapy resistance **81**
- Figure 18: Development of chemoresistant models **92**
- Figure 19: Basal ERK1/2 activation peaks during the onset of platinum-taxol dual resistance **98**
- Figure 20: Densitometric quantification of phospho ERK1/2 and phospho AKT in comparison to total protein **99**
- Figure 21: platinum-taxol induced autophagic flux remains high at the early stage of resistance **101**
- Figure 22: platinum-taxol induced increased autophagosome and autophagolysosome formation in the early stage of resistance **103**
- Figure 23: Hyperactive ERK1/2 drives autophagic flux specifically at the early stage of resistance **105**
- Figure 24: Densitometric quantification of LC3II conversion and p62 degradation **106**
- Figure 25: Inhibition of ERK1/2 activation regulates chemotherapy induced autophagic flux specifically in the early stage of resistance **107**
- Figure 26: Densitometric quantification of LC3II conversion and p62 degradation **108**

Figure 27: ERK1/2 inhibition along with chemotherapy induces autophagosome accumulation **109**

Figure 28: Hyper activated AKT signalling negatively regulates therapy induced autophagic in the late stage of resistance **110**

Figure 29: ERK1/2 inhibition abrogates autophagolysosome formation in the early stage of resistance development **112**

Figure 30: ERK1/2 activation regulates autophagosome morphology **115**

Figure 31: ERK1/2 regulates multiple components of autophagosome-lysosome fusion **116**

Figure 32: Densitometric quantification of UVRAG and Rab7 in DualER cells **117**

Figure 33: ERK1/2 inhibition sensitize DualER cells to platinum-taxol induced apoptosis **119**

Figure 34: Monitoring of autophagy flux based p62 kinetics using mtFL-p62 construct **122**

Figure 35: mtFL-p62 portrays differential autophagic flux depending on the stage of platinum-taxol resistance **124**

Figure 36: Monitoring of therapy induced autophagy dynamics in live cell **126**

Figure 37: Non-invasive bioluminescence imaging of therapy induced autophagy flux in live animals **128**

Figure 38: Inhibition of ERK1/2 or autophagy sensitizes DualER tumour xenografts to therapy **130**

Figure 39: Proposed model of the role of ERK1/2 driven autophagic flux during acquirement of therapy resistance **139**

Figure 40: Schematic representation of cisplatin-paclitaxel dual resistant model developed in presence or absence of metformin **145**

Figure 41: Presence of metformin during acquirement of resistance promotes a proliferative phenotype **150**

Figure 42: Presence of metformin reduces tolerance of resistance cells to therapy **152**

Figure 43: Presence of metformin reduces stemness properties **154**

Figure 44: Continuous presence of metformin during development of resistance alters amino acid metabolism **156**

Figure 45: Taurine promotes CSC differentiation and sensitizes cells to therapy **158**

Figure 46: Proposed role of metformin in development of therapy resistance **164**

Figure 47: Validation of NAT BRET sensor **173**

Figure 48: NAT accurately predicts AKT activation dynamics **175**

Figure 49: Validation of NEO BRET sensor **177**

Figure 50: Platinum-taxol induces increased ERK1/2 activation specifically in late stage of resistance **179**

Figure 51: Platinum specifically induces ERK1/2 and AKT activation in platinum resistant patients **181**

Figure 52: Non-platinum therapy induced modulation in ERK1/2 and AKT activation in sensitive and platinum-taxol resistant ovarian cancer cells **183**

Figure 53: Densitometric quantification of phospho/total ERK1/2 and phospho/total AKT post chemotherapeutic challenge **184**

Figure 54: Activation of ERK1/2 signalling negatively correlates with sensitivity of platinum-taxol resistant cells to non-platinum agents **186**

Figure 55: BRET based platform accurately predicts therapeutic efficacy of non-platinum agents **191**

List of tables

Table 1: Commonly used FRET pairs with examples of their application in monitoring signal transduction events **45**

Table 2: Commonly used BRET pair for monitoring biomolecular interactions **49**

Chapter 1: Introduction and review of literature

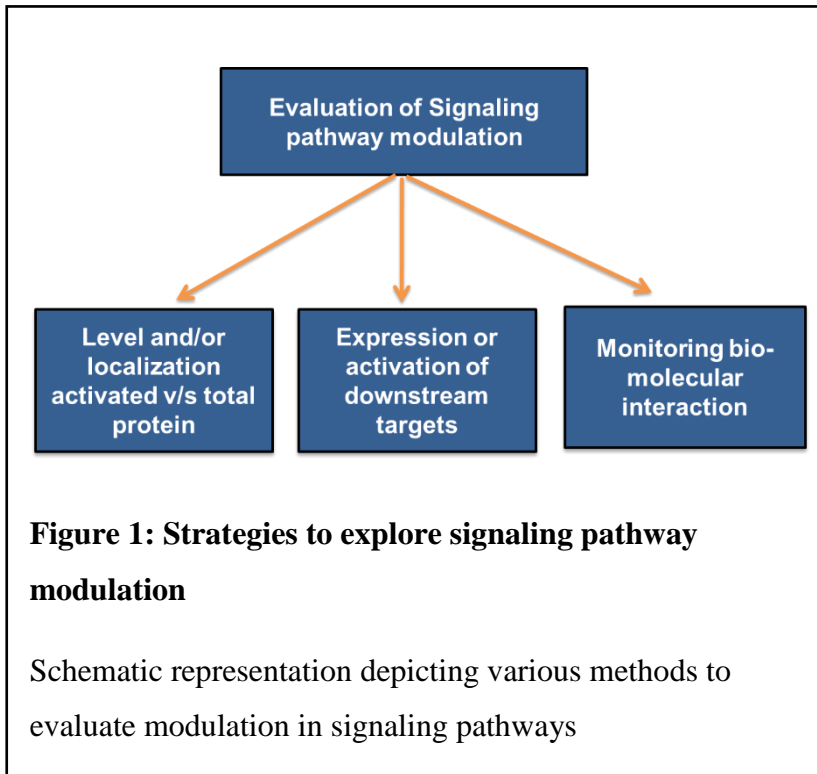
1.1 Cellular signaling: the central processing unit of cellular system

A vast array of signaling networks governs the ability of a cell to sense, respond and adapt to diverse external stimuli. The interpretation of this external cues depend on the downstream signaling network which shapes the behavior of a cell. Cells generally respond to extracellular environment via its membrane receptors, which then transduces the information to downstream signaling messengers, which in turn activates key effector molecules. In a cellular system, signaling networks maintain normal physiological function and homeostasis, however its perturbation leads to diseased states like cancer, diabetes and neuro-degenerative diseases etc. (28). Alteration in amyloid β cleavage and degradation, APOE-cholesterol pathways are the hallmarks of Alzheimer's (29). A recent proteomic study reported that survival promoting signaling pathways and signaling associated with homologous recombination to be significantly altered between ovarian cancer and normal tissue (30). Interestingly, cells responds to a vast array of stimulus with a fairly limited number of signaling hubs with different temporal and spatial dynamics. Further the amplitude of the signaling pathway i.e., the extent to which a pathway becomes active also modulates the nature of response and a differential activation level of signaling pathways are often observed in cancer. Though cancer is considered to be a genomic disease, the post genomic era identifies the altered signaling pathways as the functional component of a cancer cell that ultimately dictates the disease biology (31). Alteration in signaling pathways are generally governed by either the expression of signaling intermediates or activation of its components. Activation of signaling components are generally regulated by protein-protein or protein-lipid interaction which may lead to formation of active protein complex or post-translational modifications (32). Thus monitoring the modulation of key signaling pathways and understanding the implication of such modulation in diseased state is crucial

for a deeper understanding of the disease biology and provides a scope for new therapeutic strategies.

1.1.1 Monitoring of signaling events

Modulation in signaling pathways can generally be studied by (i) **Evaluating the level and/or localization of the molecule/s of interest:** Activation of a signaling pathway is



generally associated with increased levels of key signaling components. In the context of signaling pathways relayed through kinases, pathway activation is usually associated with phosphorylation of multiple kinases and their substrates leading to

activation or degradation of these proteins. Additionally, pathway activation can also be studied with respect to the change in cellular localization of the participating proteins.

ii) **Evaluating the expression level of downstream targets:** Activation of signaling pathways ultimately leads to activation of transcriptional modulators resulting in transcriptional activation followed by enhanced expression of specific set of target genes. The net effect of this activation kinetics gets reflected in altered functional and structural properties of the cancer cells.

(iii) **Monitoring of key molecular interactions:** Physical interaction amongst the signaling components is pivotal for activation of signaling pathways. Thus modulation in signaling arms is often evaluated through dynamic monitoring of key bio-molecular interactions, such as protein-lipid interaction (PLI) and protein-protein interactions (PPI). Physical interactions between membrane lipids and Ras or AKT oncoprotein is crucial for the activation of respective signaling arms. PPI between two Her-2 monomers leading to Her-2 dimerization marks the initiation of Her-2 signaling (Figure 1). A large number of PLI and PPI events have been identified in cancer manifestation, progression and resistance development (33, 34). Monitoring dynamics and strength of PPI or PLI among the components of a signalling cascade is critical to develop therapeutics and therapeutic strategies. Since these molecular interactions can be monitored from live cells in real time, they offer a deeper understanding of temporal signaling kinetics in comparison to the two other methods. On the contrary, monitoring of biomolecular interactions in live cells requires introduction of exogenous reporter proteins in cells, which is difficult in many circumstances. In the context of fusion reporter (protein of interest fused with a reporter protein) proteins, the expression level of the protein of interest and the reporter needs to be carefully regulated. Thus all these methods are complimentary and need to be evaluated simultaneously. Differential modulation in PPI or PLI in normal and diseased cells may help in shedding light towards understanding of disease biology and to design pharmacological strategies to modulate the same (35).

1.1.2 Methods to monitor molecular interaction

PPI and PLI govern all aspects of cellular functioning which include signaling, metabolism, replication and death. Thus understanding the real-time dynamics of these interaction is crucial for interpretation of any biological phenomenon. Classically, biochemical assays

like co-immunoprecipitation, ELISA, isothermal calorimetry and Surface Plasmon Resonance (SPR) are used for studying PPI and PLI. Though additional modifications to standardized protocols are required to study PLI. Prior labelling of cells with photoactivable lipid probes in dilapidate media is generally performed to immunoprecipitate protein-lipid complexes from live cells (36). These protein-lipid complexes are generally visualized by autoradiography instead of immunoblots which are used to detect PPI. Depending on the PLI of interest, choice of competitive or indirect Eliza methods are decided in plates pre-coated with lipids of interest (37). SPR protocols are modified to eliminate nonspecific binding of lipid to the sensor (38). These assays provide critical thermodynamic and biochemical information about biomolecular interactions. However, majority of these techniques require purified proteins/lipids or cell lysates thereby not reflecting the real-time biomolecular interaction dynamics *in-vivo* (39). In the context of this present work we will majorly focus on molecular assays capable of evaluating molecular interaction noninvasively from live cell or living subjects.

1.1.2.1 Yeast two Hybrid (Y2H) assay

The Yeast two Hybrid (Y2H) was the first *in-vivo* assay system to evaluate molecular interactions between proteins. However this system has yet not been explored to study PLI in live cells. The Y2H system is based on the reconstitution of a functional transcription factor (TF) which is split into DNA binding domain (DNB) and activation domain (AB) and thereby generating a signature. Each of these domains are genetically fused to proteins of interest assumed to be interacting partners. Upon their interaction, the two domains are brought together to reconstitute a functional transcription factor which then transcribes a reporter gene or selection marker to generate molecular signature (40). Numerous PPIs had been identified and validated using Y2H system and were instrumental for identifying many

molecular inhibitors (41). The Y2H system has also been adapted in mammalian systems. The TNF- α induced Y2H system (IY2H) was successfully utilized to monitor ID-MyoD protein interaction in HEK293 cells and in tumor xenografts. This IY2H system consisted of DNB of Gal4 fused to ID protein and activation domain of VP16 fused to MyoD protein as the two interacting partners and a Gal4 response element driven firefly luciferase as the reporter gene (42). Upon induction, MyoD and ID physically interact resulting in formation of active Gal4-VP16 transcriptional complex that binds to Gal4 response elements driving luciferase gene expression. Following a similar strategy, the interaction of P53-SV40 was monitored in HeLa cells and tumor xenograft utilizing GFP or thymidine kinase as reporter genes (43). Despite several advantages, the Y2H assay can only take place in the nuclear compartment of the cell, which may result in false-positive interactions between proteins (belonging to other cellular compartments) artificially expressed in the nucleus. Moreover, the Y2H system lacks temporal resolution and because of the multi-component (AD, DBD, reporter gene and its promoter element) nature of the assay system and adaptation of Y2H in bacterial and mammalian system requires multiple modification (40).

1.1.2.2 Split Reporter system

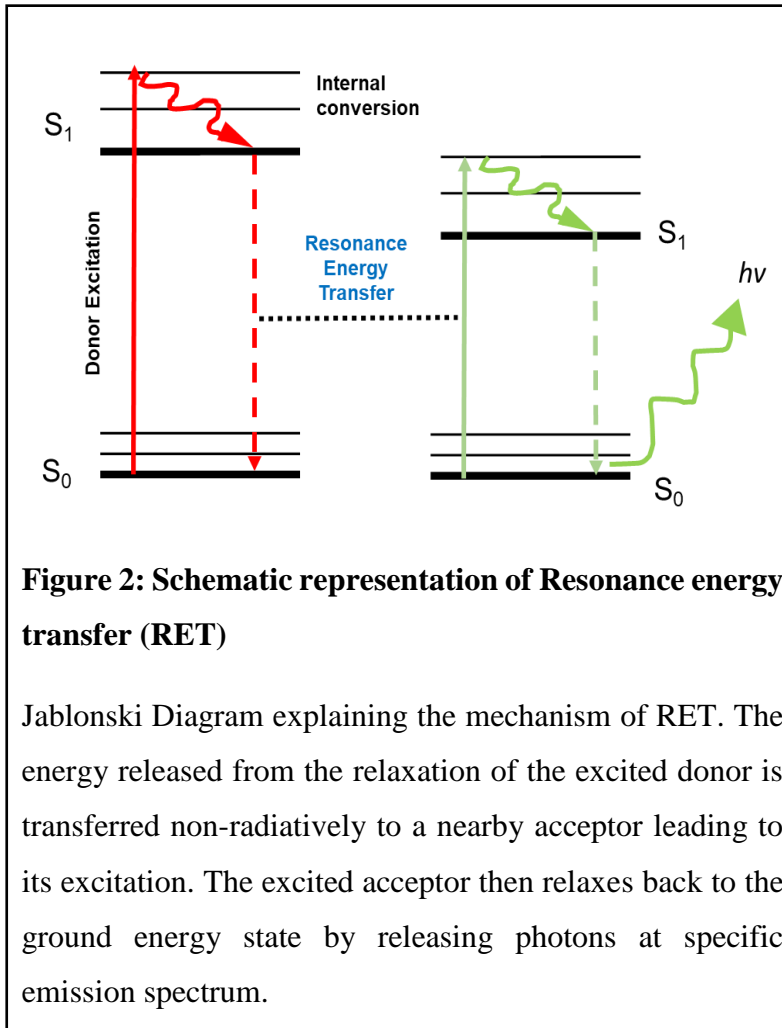
The introduction of fluorescent and luciferase probes along with gene fusion and protein labelling technology has revolutionized the field of PPI measurement. Split protein completion is a powerful technique to study PPI where, a reporter protein (fluorescent or luciferase) is genetically split into two non-functional peptides and fused with two interacting protein components. Under appropriate condition and through interaction of the component partner proteins, the non-functional halves of the reporter protein come in close proximity and produce an active functional reporter to generate the signal (44). The first split fluorescent reporter assay, also known as bimolecular fluorescence complementation

(BiFC) assays, demonstrated complementation of two split GFP subunit in presence of antiparallel leucine zipper domain in E.coli cells (45). Subsequently, complementation of YFP was utilized to study interaction between NF κ B and basic leucine zipper domain proteins in mammalian cells (46). Currently, there are several fluorescent proteins utilized in BiFC for monitoring PPI and their subcellular localization in bacteria, mammalian and plant cells (40, 44, 47). However, due to the irreversible nature of fluorescent complementation and inherent delay in chromophore maturation, the BiFC assay suffers from low temporal resolution. Moreover, overexpression of split fluorescent protein fragment leads to protein accumulation and complementation which often generate false positive results (44, 48). In parallel, split luciferase complementation assay has also been adapted to monitor PPI in live cells. The first split luciferase system utilized beetle luciferase to study interaction between ID1-MyoD (49). Split firefly luciferase system was also utilized to study rapamycin induced interaction between FK506-binding proteins (FKBP12) and FRB proteins (50). Interaction between insulin receptor substrate (IRS-1) and SH2 domain of phosphatidylinositol 3-kinase (PI3K) was demonstrated utilizing split Renilla luciferase system (51). Currently there are several split luciferase systems available utilizing Renilla as well as secretory gaussia luciferase (52, 53). However, split luciferase reporters suffer from significant loss in quantum yield of the reconstituted luciferase thereby lowering sensitivity of the assay. However, both the split reporter system has yet not been explored to study protein-lipid interaction in live cells.

1.1.2.3 Resonance energy transfer (RET) based assays

RET is the physical phenomenon describing the non-radiative energy transfer between two transient dipoles separated by distance exceeding the sum of their van der Waals radii via dipole-dipole coupling mechanism (54, 55). Upon excitation, donor electrons reach a higher energy state and then rapidly relax to a lower singlet energy state by internal conversion. In

presence of an acceptor molecule in close proximity, RET takes place, and the donor



molecule returns back to the ground energy state by non-radiative transfer of energy to the acceptor molecule (Figure 2). The efficiency of RET is inversely proportional to sixth power of intermolecular distance, making the RET based assay highly sensitive for monitoring PPI/PLI (56). There are several factors that affects the efficiency of RET (22,

57): (i) **Intermolecular distance:** The physical distance between the donor and acceptor is inversely related to energy transfer efficiency. The optimal distance between two interacting molecules is in the range of 1-10nm. (ii) **Spectral overlap:** The overlap between the emission spectra of the donor and the excitation spectra of the acceptor is directly proportional with the efficiency of the energy transfer. (iii) **Spectral Resolution:** The extent of overlap between the donor emission wavelengths and acceptor emission wavelengths increases bleed through signal in the acceptor channel (Filter) leading to increased non-specific signal. Thus larger spectral resolution increases the specificity of RET (iv) **Dipole orientation:** As the RET occurs via dipole-dipole coupling, the relative orientation of donor and acceptor also effects RET efficiency. (V) **Quantum yield of donor:** A part of total

energy from donor is generally lost as non-radiative decay before being transferred to the acceptor moiety. Thus donors with high quantum efficiency or high photon output are generally more efficient in exciting nearby acceptor molecule.

Based on the nature of the donor molecule, there are currently two types of RET based assays for real-time monitoring of PPI/PLI dynamics: (i) Fluorescence resonance energy transfer (FRET) and (ii) Bioluminescence resonance energy transfer (BRET).

1.1.2.3.1 Fluorescence resonance energy transfer (FRET)

Fluorescence resonance energy transfer (FRET) is a non-radiative energy transfer process between an excited donor fluorophore and a nearby fluorescent acceptor protein via a long-range dipole-dipole coupling (58). FRET efficiency is calculated based on the formula:

$$E = 1 / (1 + r^6/r_0^6)$$

Where r refers to the distance between acceptor and donor dipole and r_0 refers to foster radius, which implies to the distance where FRET efficiency is 50%. The r_0 value depends on the interdipole orientation, refractive index of the surrounding environment, quantum yield of the donor, extinction coefficient of the acceptor and the spectral overlap between the donor and acceptor fluorescent proteins (54). In FRET based PPI/PLI assays, the change in FRET efficiency is generally calculated rather than static FRET efficiency. There are several variation of FRET microscopy depending on procedure of estimation of PPI/PLI, for example, fluorescence lifetime imaging FRET (FLIM-FRET) evaluates reduction in fluorescence life time of the donor in presence of the acceptor. On the other hand sensitized emission FRET (seFRET) directly correlates changes in fluorescence intensity and

polarization with FRET changes (59, 60). Depending on the types of fluorophores, several efficient FRET pairs have been developed and has been summarized in table 1.

FRET pairs	Ex/Em (Donor,nm)	Ex/Em (Acceptor, nm)	Examples of Biological application	Ref
ECFP-EYFP	433/475	513/527	Activation of Src Kinase	(61)
ECFP-Venus	433/475	515/528	Caspase 8/9 cleavage	(62)
ECFP-Ypet	433/475	517/530	Activation of AKT	(63)
mTurquoise- mVenus	434/474	515/528	Activation of PKA	(64)
mCerulean- Ypet	433/475	517/530	Cyclin B-Cdk1 interaction	(65)
mCerulean- Venus	433/475	515/528	ERK activation	(66)
EGFP- mCherry	488/507	587/610	RhoA activation	(67)
mNeonGreen- mRuby	506/517	558/600	CaMKII α reporter	(67)
mClover- mRuby	506/518	587/610	Polarization of transmembrane volatage domain	(67)

mOrange2- mCherry	437/572	587/610	MMP1 cleavage	(68)
EGFP- ShadowG	488/507	486/510	Activation of HRas	(69)

Table 1: Commonly used FRET pairs with examples of their application in monitoring signal transduction events.

One of major advantages of FRET based sensors is that, they not only allow real-time detection of PPI/PLI from live cells but also provide spatial information of the interacting proteins. FRET based sensors have been extensively used to study calcium signaling, cellular localization and level of Rac signaling, kinase signaling, secondary messenger probes and many more (70). FRET based monitoring of ERK and AKT activation downstream of PDGF in malignant mesothelioma cells revealed significant crosstalk between the signaling arms (71). Recently, FRET based ERK and AKT sensors have been utilized to screen kinase inhibitor library against TNBC cells (72). FRET has also been used to study PLI in live cells following two distinct strategies. The first strategy involves tagging the lipid-protein pair directly with the FRET fluorescent pair. In 2002, Hughes et al., reported the interaction between GFP tagged phospholipase D and BODIPY labelled phosphocholine (PC) in Hela cells using FLIM-FRET microscopy (73). Alternatively, lipid assisted protein-protein interactions can be used as a measure of protein-lipid interactions. In order to study this, the interaction between PIP3 and AKT was measured using an intramolecular FRET sensor consisting of PIP3 interacting PH-AKT domain flanked between CFP and YFP. PIP3-PH-AKT interactions induce significant conformational changes leading to induction of FRET between CFP and YFP (74). However, requirement of an external light source, photo bleaching, photo-toxicity, low signal to noise ratio and

non-specific activation of acceptor fluorophore by the external light source limit application of FRET to single cell level, measured only microscopically. The use of fluorescent protein as energy donor, significantly limits the application of FRET in tumor tissues due to signal attenuation, low signal to noise ratio and auto-fluorescence. To circumvent these issues and adapt RET technology for measuring molecular interaction in small animals or group of live cells, bioluminescence reporter proteins have emerged as the preferred choice for donor protein.

1.1.2.3.2 Bioluminescence resonance energy transfer (BRET)

Bioluminescence resonance energy transfer (BRET) is a natural phenomenon observed in marine plankton like jellyfish *Aequorea victoria* and sea pansy like *Renilla reniformis*. The calcium dependent photoprotein, aequorin synthesized by *Aequora victoria* oxidizes coelenterazine to emit blue light, which excites GFP protein in close proximity to emit green light (75). The basic principle of this natural phenomenon involves luciferase mediated oxidation of its substrate luciferin thereby, exciting it to a high energy state. After internal conversion to low energy state by dissipating some amount of energy as heat due to random collisions, the remaining electronic relaxation energy is transferred as non-radiative dipole-dipole coupling to adjacent acceptor fluorophore, which then emits photon at characteristic wavelengths (Figure 3) (35, 76). Utilizing this underlying principle, various BRET pairs have been developed using either native or genetically modified luciferase enzymes coupled with various florescent proteins or fluorophores or synthetic dyes and are summarized in table 2. The use of luciferase enzyme as the energy donor eliminates the need of external light source thus avoiding photo bleaching or phototoxic effects. Furthermore, the enzymatic nature of luciferase-luciferin system offers high signal to noise ratio and increased sensitivity. Several BRET pairs have been genetically coupled with proteins of

interest to study their interaction directly from live cells in their natural cellular milieu and are quantified in terms of BRET ratio which is calculated using the formula (35, 77)

$$\text{milliBRET unit (mBU)} = \frac{\text{Avg.Rad(Acceptor filter)} - Cf * \text{Avg.Rad (Donor filter)}}{\text{Avg.Rad (Donor filter)}} * 1000$$

$$Cf = \frac{\text{Avg.Rad(Acceptor filter)donor only}}{\text{Avg.Rad(donor filter)donor only}}$$

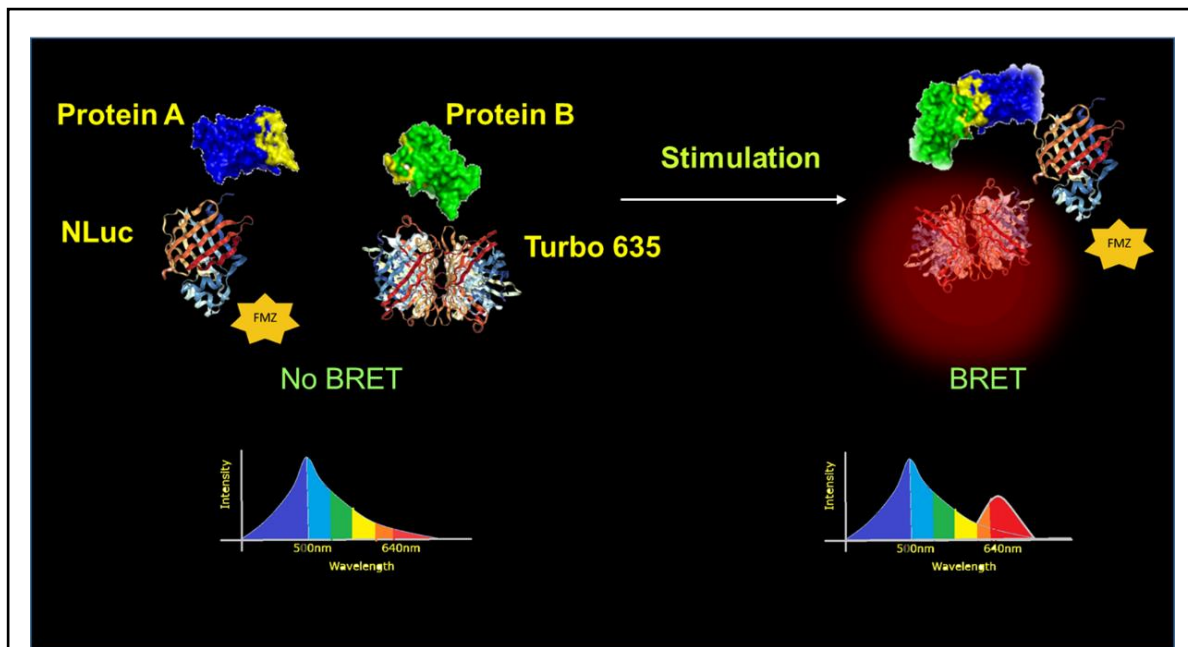


Figure 2: Basic working principle of BRET based protein-protein interaction

Interaction between protein A and B brings the donor luciferase (example: Nanoluciferase, Nluc) and acceptor luciferase (example: TurboFP 635) within a permissible distance (<10 nm), the energy from donor upon catalysis of its substrate is transferred to acceptor molecule resulting in acceptor emission at respective wavelength. In BRET upon positive interaction, two resultant peaks are obtained, donor emission and acceptor emission

Assay	BRET-Pairs	Em (donor, nm)	Ex/Em (Acceptor,nm)	Ref	
BRET ¹	Rluc480-EYFP	480	513/527	(78)	
BRET2	Rluc-EGFP (with modified coelenterazine)	400	488/507	(79)	
BRET 3	Rluc8-mOrange	480	548/560	(22)	
BRET4	Rluc8-Tag RFP	480	555/584		
BRET 5	Rluc8-Tag RFP (with coelenterazine-V)	515	555/584		
BRET 6	Rluc8.6-TagRFP	535	555/584		
BRET 7	Rluc8-TurboFP635	480	588/635		
BRET 8	Rluc8.6-TurboFP635	535	588/635		
nanoBRET with fluorescent proteins	Nluc-Ypet	480	517/530		(80)
	Nluc-EGFP	480	488/507		(81)
	Nluc-Venus	480	515/528	(82)	
	Nluc-mNeonGreen	480	506/517	(83)	
	Nluc-cyOFP1	480	497/589	(84)	
	Nluc-mOrange	480	548/560	(23)	
	Nluc-TagRFP	480	555/584		
	Nluc-TurboFP635	480	588/635		
nanoBRET- with fluorescent dyes	Nluc-HaloTag TMR	480	552/578	(85)	
	Nluc-HaloTag NCT	480	595/635		
	Nluc-HaloTag OG	480	492/520		
	Nluc-CGP 12177	480	543/560	(86)	

Table 3: Commonly used BRET pair for monitoring biomolecular interactions

One of the major consideration for designing BRET sensors is the choice of luciferase as BRET donor. The quantum yield of the donor luciferase is directly proportional to the amount of energy transferred to the fluorescent acceptor protein. Several BRET sensors have been initially developed using *Renilla luciferase* (Rluc) which emits light at 480 nm and thus can pair with proteins of excitation range of 500-520 nm. The Rluc-EYFP BRET pair was used to study growth factor induced conformational changes in IGF1R receptor and modulation in IGF1R activation in presence of various antibodies (78, 87). Rluc based BRET reporters had also been successfully adapted to monitor activation of key kinases, like PI3K in MCF7 breast cancer cell line and ERK1/2 in the primary hippocampal neurons isolated from mice embryos (88, 89). The Rluc-EYFP BRET system was later improved by replacing the Rluc with brighter Rluc 8 and EYFP with red shifted TurboFP635 (BRET^{6.1}) fluorescent protein. The Rluc8-TurboFP635 was the first BRET pair employed to detect protein-protein interaction from live animals (22). Recently, development of Nanoluciferase (Nluc) by random mutagenesis of the 19kDa subunit of a heteromeric luciferase produced naturally by deep sea shrimp *O.gracilirostris* along with substrate optimization has revolutionized the field of BRET (nanoBRET) technology (90). Nluc offers three major benefits in comparison to its predecessors (i) Nluc is an extremely bright luciferase which produces 150 times greater light output than Renilla and Firefly luciferase thus increasing the sensitivity of the BRET platform (ii) Nluc exhibits substantial brightness even at longer wavelengths thus could be coupled with red-shifted fluorophores to increase the spectral resolution and specificity of the BRET system (iii) Nluc can readily be exploited to generate fusion protein with various partners since the smaller size excludes the possibility of structural alteration of target protein (91-93). The nanoBRET system has been successfully utilized to monitor ligand-receptor interaction, caspase activation, various intercellular protein-protein interaction like p53-MDM2, YAP-14-3-3 ζ etc. (80, 91, 94-96). All these

highly sophisticated techniques allow us to assess the dynamics of molecular interactions (Protein-Protein or Protein-Lipid) occurring in altered signaling pathways due to pathogenesis or changes in external cues.

1.1.3 Understanding the implication of signaling pathway modulation

Perturbation in the signaling networks due to genetic or extracellular environmental factors may govern the nature and behavior of all diseased phenotype. In context of cancers, which

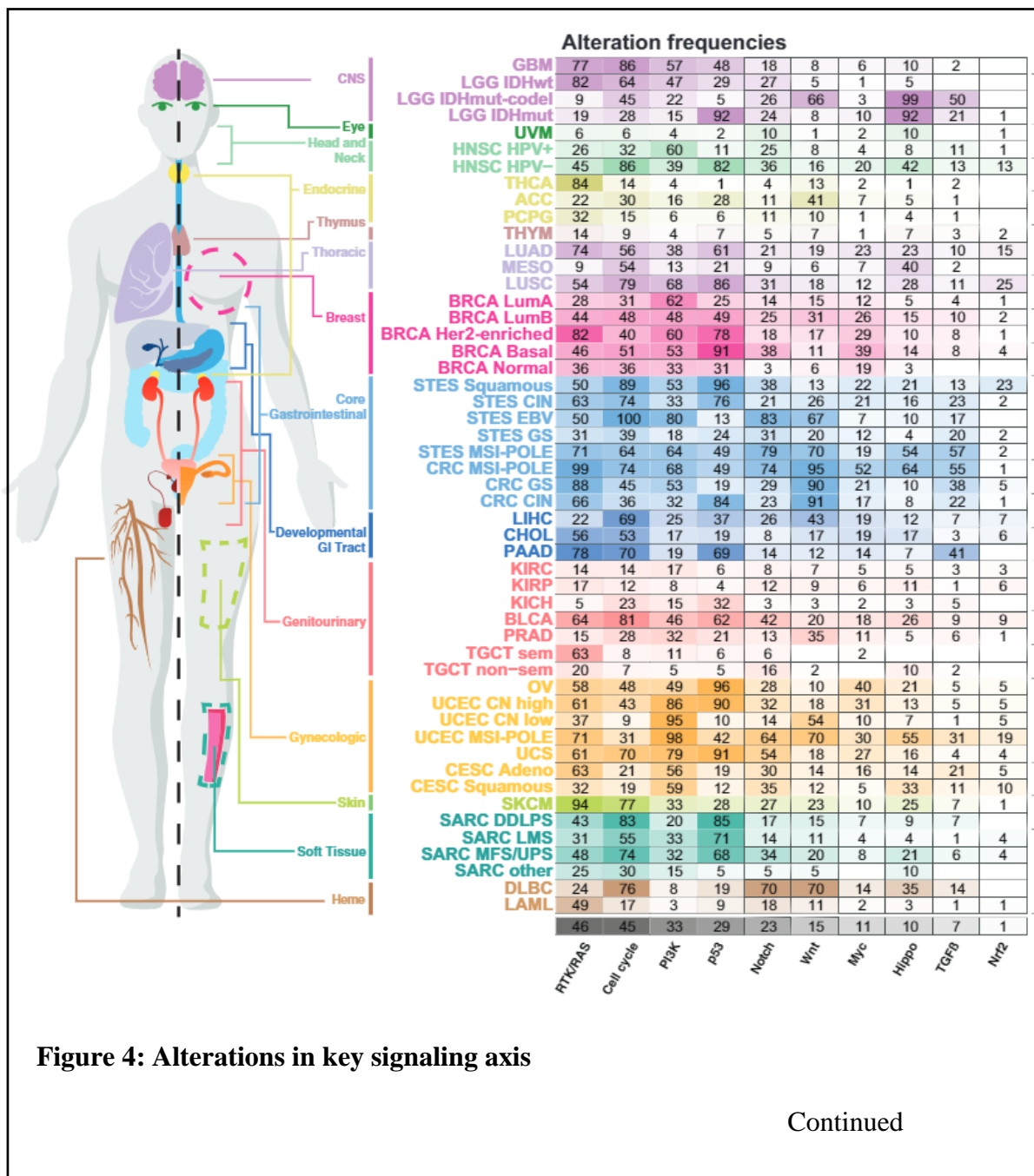


Figure 4: Alterations in key signaling axis

Continued

Schematic representation of alteration in 10 key signaling pathways in a cohort of 9125 cancer cases of various types. The numbers represents the fraction of altered samples in each pathways. The pathways are ranked on the basis of median alteration frequencies. (Adapted from Sanchez-Vega F. *et al*; Oncogenic Signaling Pathways in The Cancer Genome Atlas; Cell; 2018)

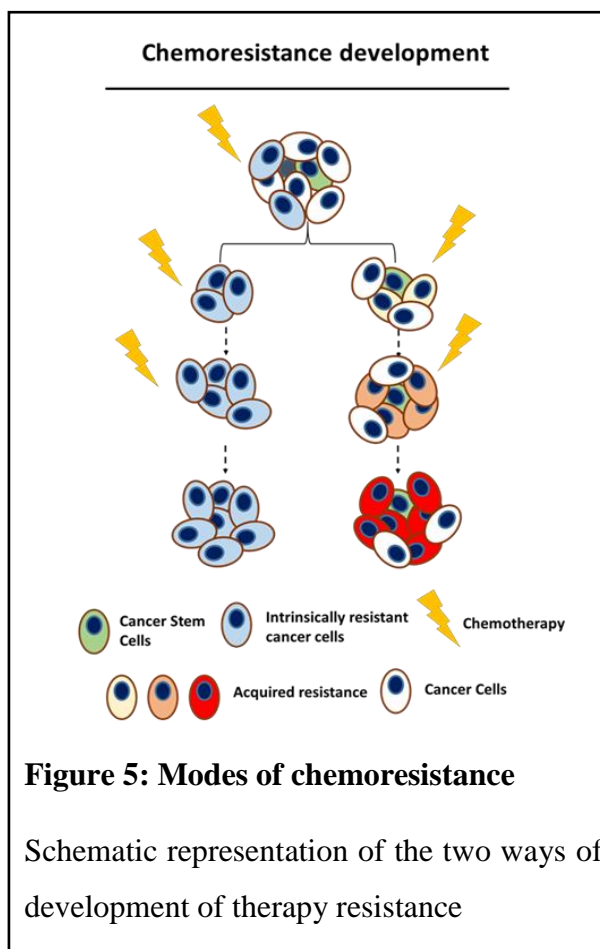
are characterized by uncontrolled cellular division and proliferation, increased activation of growth promoting signaling pathways along with suppression of cell death pathways are frequently observed. These differential activation in signaling pathways are often governed by oncogenic mutations or overexpression of key signaling intermediates (97). Several key signaling pathways have been identified as the driver for various cancers and have been extensively studied (Figure 4). It is difficult to mention all those reports and therefore most relevant ones are summarized below. Details regarding other key signaling pathways are described in other reviews (98-100). Alteration in RTK-Ras signaling pathways is frequently observed in 94% of melanoma, 88% of genomically-stable subtype of colorectal cancer, 82% of Her2 positive breast cancer, 78% of pancreatic cancer, 74% of lung adenocarcinoma and 58% of ovarian cancer. Alteration in PI3K-AKT signaling is observed in 68% of lung squamous cell carcinoma. 80% of esophagogastric cancer and 49% of ovarian cancer (100). Several strategies have been approved by the FDA to therapeutically challenge these signaling axes in various cancer types. Use of Gefitinib and Erlotinib for targeting the EGFR have been approved for lung cancers, Lapatinib for targeting Her2 in breast cancer, Imatinib targeting the BCL-ABL activation in leukemia, Trametinib targeting MEK in melanomas, etc. (101, 102).

However, the success of administering these drugs alone or along with traditional chemotherapeutics have been significantly curtailed due to therapy induced rewiring of signaling networks, which confers cancers cells the ability to withstand cytotoxic effect of these therapies. Often the success of chemotherapeutic regimen is significantly

compromised due to differential modulation in key signaling pathways leading to the development of chemoresistance. Thus it is important to understand these modulations in response to chemotherapeutic stress to identify the possible mechanisms of chemoresistance.

1.2 Chemoresistance

Chemoresistance implies to the molecular conundrum that bestows cancer cells the ability



to tolerate the toxic effect of chemotherapeutics to evade cell death. Certain cancers have the intrinsic ability to resist chemotherapeutic drugs due to their genetic makeup. However, in most of the cases chemoresistance is generally acquired over time in multiple steps involving alteration in many molecular pathways or signaling hubs (Figure 5). Globally several mechanisms contribute to the generation of chemoresistant phenotype which include, but not limited to, increased expression of drug efflux

pumps (MDR1, MRP1 and MRP 6), altered drug metabolism, increased DNA repair, increased stemness properties, altered cell-cycle checkpoints, increased activation of survival promoting pathways with concomitant reduction in apoptosis, increased cytoprotective autophagic flux, etc. (Figure 6) (103, 104). Underlying these mechanisms are

aberrant gene regulatory networks and intricate signaling pathways that are activated by membrane receptors (growth factor receptors, G-protein-linked receptors, chemokine receptors and integrins) and are often deregulated in chemoresistant cancer cells (105-109).

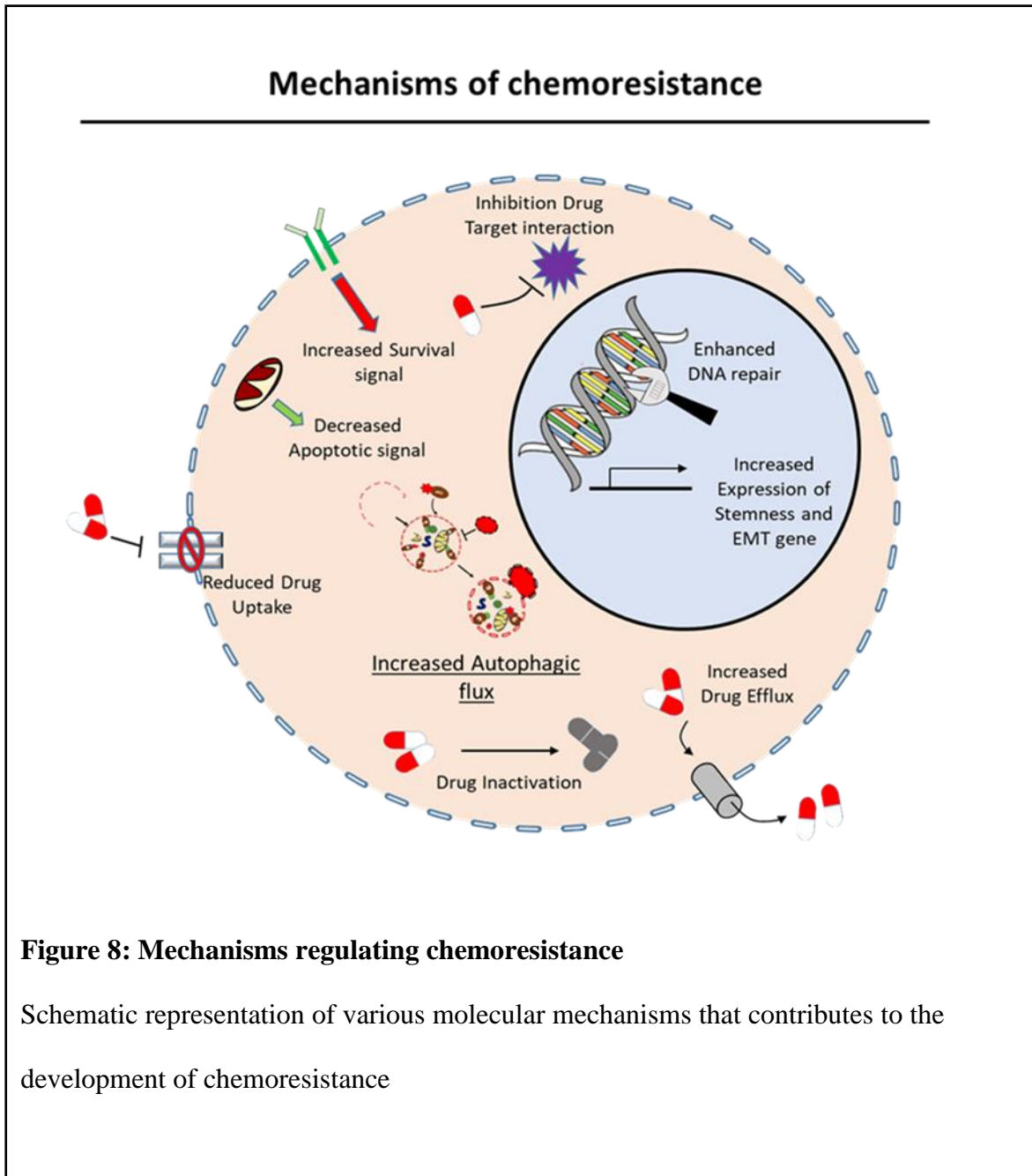


Figure 8: Mechanisms regulating chemoresistance

Schematic representation of various molecular mechanisms that contributes to the development of chemoresistance

Therapy induced rewiring of signaling networks contributes to the development of therapy resistance in most if not all the cancers and has been extensively researched and reviewed

(110-112). In context of chemoresistant ovarian cancer, several reports demonstrate the role of receptor/non-receptor tyrosine kinases in therapy resistance. Increased activation of EGFR via amphiregulin was reported to promote docetaxel and carboplatin resistance by promoting cancer stem cell phenotype in patient derived ovarian cancer line (113). Resistance to CDK inhibitors were attributed to activation of Her2-Ras signalling in a panel of ovarian cancer cell lines (114). Increased activation of non-receptor tyrosine kinase, Src was reported to promote stemness via MAPK/ERK1/2 pathway (115). Promotion of paclitaxel resistance in SKOV3 cells was shown to be modulated by expression of TAM receptor tyrosine kinases (Tyro3) (116). We previously showed that an up regulated IGF1R expression was beneficial for the cancer cells to survive the therapeutic stress at the onset of resistance but was dispensable when they attained a highly resistant phenotype with high levels of hyperactivated AKT signaling (5, 117). We also report the role of IGF1R as prognostic marker of in a cohort 19 high grade serous ovarian cancer patients (118). Additionally, in a cohort of 28 ovarian cancer cases, increased activation of IGF1R/AKT/ERK signaling axis was specifically observed in platinum-resistant ovarian cancer patients (8). The involvement of the two major signaling arms - MAPK/ERK1/2 and PI3K/AKT signalling, downstream of RTKs, are well established in the regulation of therapy resistance in several cancers.

1.2.1 The role of Extracellular Regulated Kinase 1/2 (ERK1/2) in chemoresistance

ERK1/2 is the one of most well studied effector kinase belonging to mitogen activated protein kinase (MAPK) family. Activated ERK1/2 integrates various extracellular signaling cues with an array of effector kinases and transcription factors to regulate cellular growth, proliferation, differentiation, apoptosis, autophagy and cellular migration (119-121). Activation of various receptors like RTKs, G-protein coupled receptors, T-cell receptors,

etc., lead to activation of Ras through conversion of Ras-GDP to Ras-GTP which induces membrane translocation and activation of Raf, which in turn activates its downstream kinases MEK1/2. Upon activation, MEK1/2 phosphorylates ERK1/2 leading to its activation (120). ERK1/2 is one of the key effector kinases in the MAPK pathway, that regulates a plethora of downstream targets in both cytoplasm as well as the nucleus (Figure 7) (122). Till now, around 497 ERK1/2 targets have been identified utilizing recombinant protein, mass-spectrometry, kinase assay and immunoprecipitation based assays (123). This list of ERK1/2 target genes is increasing every day indicating the importance of this effector kinase in regulation of various diseases including cancer.

The MAPK/ERK1/2 pathway is extremely complex due to several feedback and

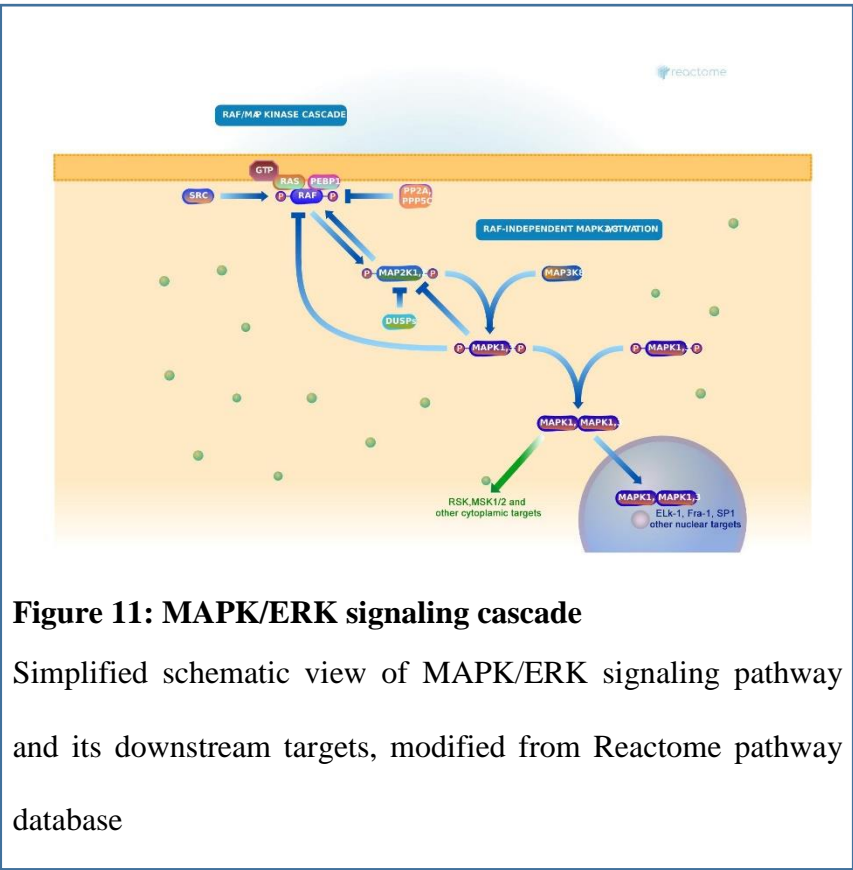


Figure 11: MAPK/ERK signaling cascade

Simplified schematic view of MAPK/ERK signaling pathway and its downstream targets, modified from Reactome pathway database

feedforward loops within the core cascade, and the complexity is further elevated by non-canonical activation of ERK1/2 and cross-talk with other pathways like PI3K/AKT. Deregulation in multiple components of this pathway had

been associated with cancer progression and therapy resistance. RAS, a designated oncogene, remains hyper activated due to mutation in approximately 30% of cancers. 90% of pancreatic, 30% of lung and 50% of colon cancers are characterized by somatic KRAS

mutation which leads into its constitutive activation (124, 125). An increased percentage (41%, 45% and 33%) of BRAF mutation (most prevalent point mutation V600E) was reported in melanoma, thyroid and low grade serous ovarian carcinoma (126). Mutations in MEK1/2 and ERK1/2 are less frequent but they remain activated in majority of human cancers.

The MAPK/ERK activation regulates several molecular process like apoptosis, evasion of cell cycle checkpoints, drug efflux, stemness etc., which in turn confers resistance to multiple drugs (Figure 8).

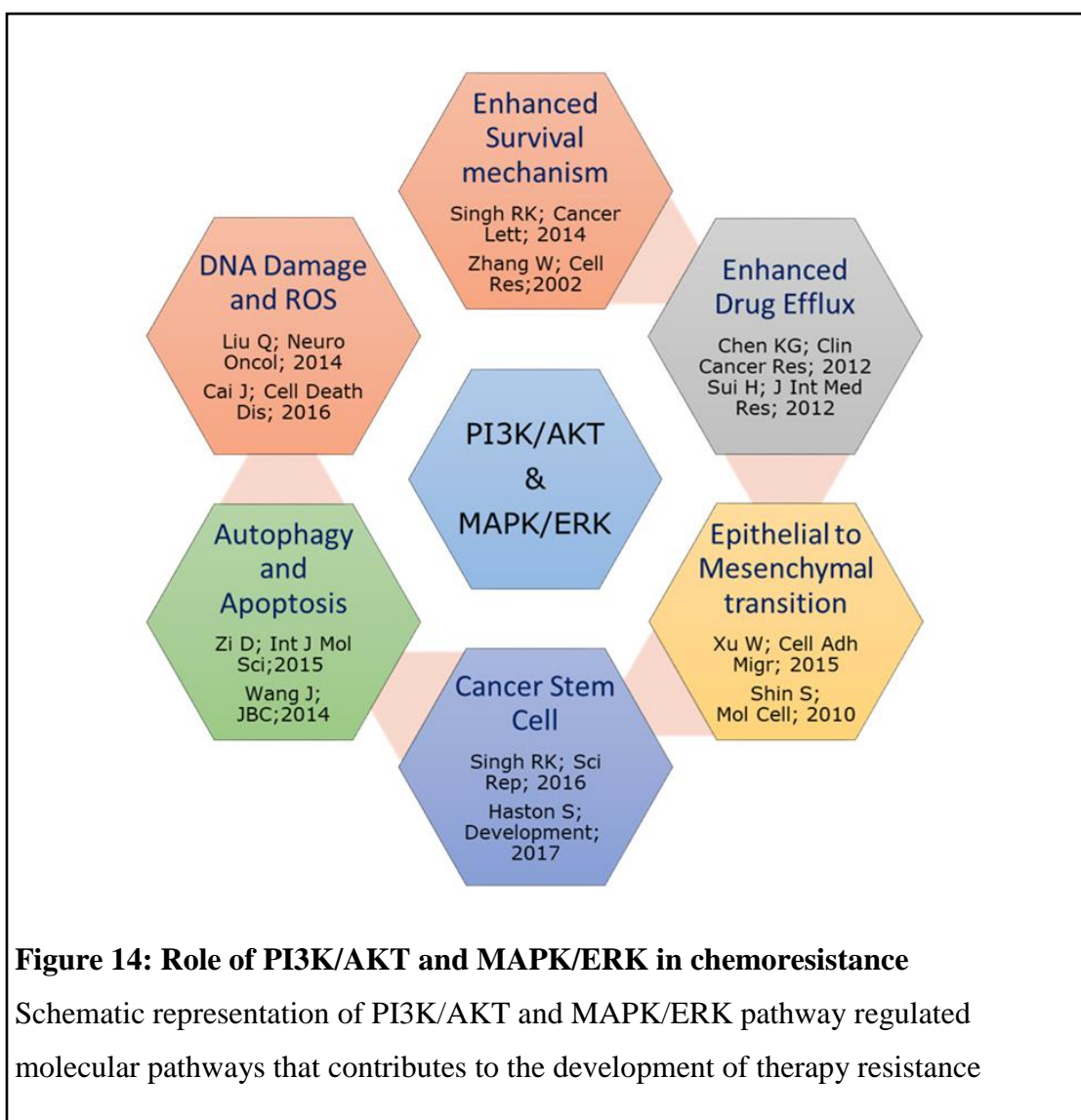


Figure 14: Role of PI3K/AKT and MAPK/ERK in chemoresistance

Schematic representation of PI3K/AKT and MAPK/ERK pathway regulated molecular pathways that contributes to the development of therapy resistance

Increased activation of MEK/ERK1/2 was reported to activate anti-apoptotic proteins of Bcl-2 family in response to 5-fluoro-uracil treatment in colon and gastric cancer cells (127, 128). ERK1/2 promoted anti-apoptotic phenotype via increased expression of survivins also conferred resistance to paclitaxel in breast cancer cells (128). Upregulation of cyclin D1/E1 through increased ERK1/2 activation conferred resistance to cisplatin in osteosarcoma (129). Increased stabilization of c-Myc as a consequence of phosphorylation by ERK1/2 promoted G1-S phase transition (130). ERK1/2 mediated alteration in cancer cell metabolism was also reported to promote a resistant phenotype in breast, ovarian and colon cancer cells. FGFR4 mediated activation of ERK1/2 and anaerobic glucose metabolism conferred doxorubicin resistance in breast cancer cells and combinatorial treatment with 2-deoxy glucose and MEK inhibitor U0126 was reported to sensitize these cells to doxorubicin (131). Increased activation of ERK1/2 also support stemness phenotype, which is a crucial determinant of therapeutic outcome. An increased percentage of cells expressing CD133, which is a marker for pancreatic cancer stem cells, directly correlates with ERK1/2 activation conferring gemcitabine resistance (132). ERK1/2 activation through EGFR was reported to regulate maintenance of stemness properties in ovarian cancer cells to mediate docetaxel and carboplatin resistance (113). Cancer-ECM interaction play a crucial role in determining therapy resistance. Collagen-I and fibronectin mediated ERK1/2 activation was demonstrated to promote resistance to cisplatin, 5-FU and epirubicin in esophageal cancer (133). Similarly, integrin- β 1 and laminin 5 mediated ERK1/2 activation regulated trastuzumab resistance in metastatic breast carcinoma cell lines (134). Nidogen 1 (NID1) mediated activation of ERK1/2 was reported to promote both epithelial-mesenchymal transition and platinum resistance in ovarian cancer (135). Increased ERK1/2 activation in response to cisplatin conferred resistance in a panel of ovarian cancer cell lines by promoting cytoprotective autophagy. Over expression of metabolic enzymes like Hexokinase 2 was

established to enhance ERK1/2 activation and autophagic flux in platinum resistant ovarian cancer cells (11).

The highly complex but crucial role of MAPK/ERK pathway in multiple aspect of therapy resistance has attracted a vast number of clinical trials aimed to target various members of this pathway in several cancer and reviewed extensively by Yang *et al.* Currently, 131 different combinations of MAPK pathway inhibitors either alone or in combination with other therapies are being assessed in clinical trials. Out of which, majority are MEK inhibitors (58%), while rest are either RAF inhibitors or combination of MEK and RAF inhibitors (136). Presently, there are four clinically approved RAF inhibitors for cancer management. Use of Sorafenib has been approved for treatment of advanced renal cell carcinoma and advanced hepatocellular carcinoma. All of the other three approved Raf inhibitors, Vemrafenib, Dabrafenib and Encorafenib are used in management of late-stage metastatic melanoma (137). Trametinib, Cobimetinib and Binimetinib are currently the approved MEK inhibitors for treatment of advanced metastatic melanoma (138).

1.2.2 The role of AKT in chemoresistance

The serine/threonine kinase, AKT belongs to the AGC family of kinases which are activated by various RTKs, G-protein coupled receptors, integrin receptors etc. AKT regulates several cellular process like survival, growth, metabolism and metastasis (139). The three isoforms of AKT (AKT1, AKT2 and AKT3) share structural and some amount of functional activity (Figure 9). Isoform specific AKT knockout mice were utilized to identify the unique and overlapping functions of the AKT isoforms. AKT1 knockout was reported to significantly increase apoptosis in mice. AKT2 knockout is known to be associated with glucose metabolism deficiency while impaired brain development was reported in AKT3 knock out

mice. Interestingly, double knockout of AKT1 and AKT2 or AKT 1 and AKT3 is

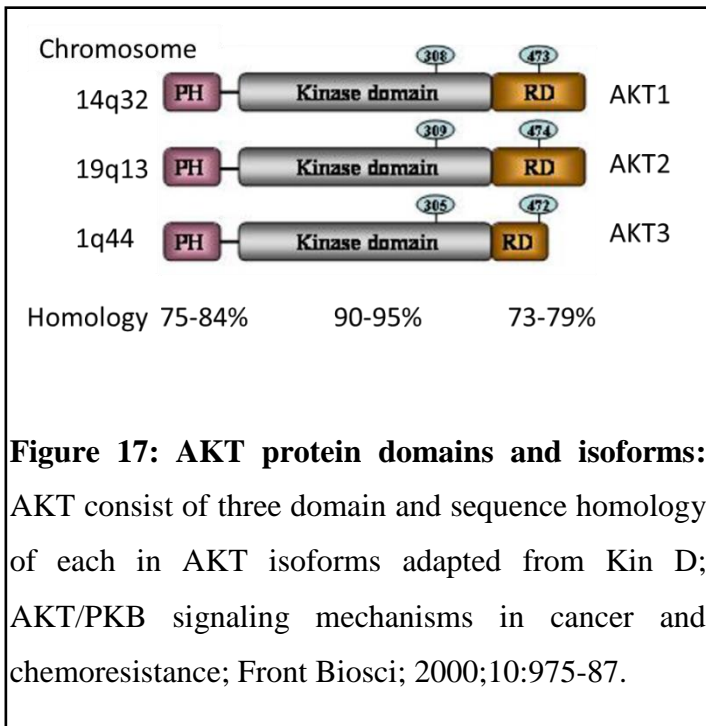


Figure 17: AKT protein domains and isoforms: AKT consist of three domain and sequence homology of each in AKT isoforms adapted from Kin D; AKT/PKB signaling mechanisms in cancer and chemoresistance; Front Biosci; 2000;10:975-87.

embryonically lethal and phenotypic analysis of these dual knockout models show overlapping functions of AKT isoforms (140). Structurally AKT has three distinct domain, the N-terminal Pleckstrin homology (PH domain), the catalytic domain and the C-terminal regulatory domain (141). Upon

activation of the upstream receptor tyrosine kinase, the catalytic domain of phosphatidylinositol 3-kinases translocates to the membrane where it phosphorylates Phosphatidylinositol Biphosphate (PIP₂) to Phosphatidylinositol trisphosphate (PIP₃). PIP₃ induces membrane translocation of AKT via its PH domain. In the membrane AKT is phosphorylated at the threonine 308 residue by Phosphoinositide-dependent kinase-1 (PDK) and translocates back to the cytoplasm where it is phosphorylated by mTORC2 at the serine 473 for complete activation. The functional AKT can further activate a plethora of downstream targets including mTOR, GSK3 β , NF κ B and FOXO3A (Figure 10) (142). Upregulation of AKT activation regulates several molecular phenomenon that contribute to the development of therapy resistance in multiple cancers (Figure 8). Increased AKT activation was reported to enhance DNA repair via upregulation of ribonucleotide reductase M2 (RRM2) in tamoxifen resistant breast cancer cells (143). AKT mediated phosphorylation of protein phosphatase magnesium-dependent 1 D (PPM1D) prevents its

degradation, which in turn dephosphorylates p53, checkpoint kinase 2 (Chk2) and ATM to prevent cell death in response to platinum treatment

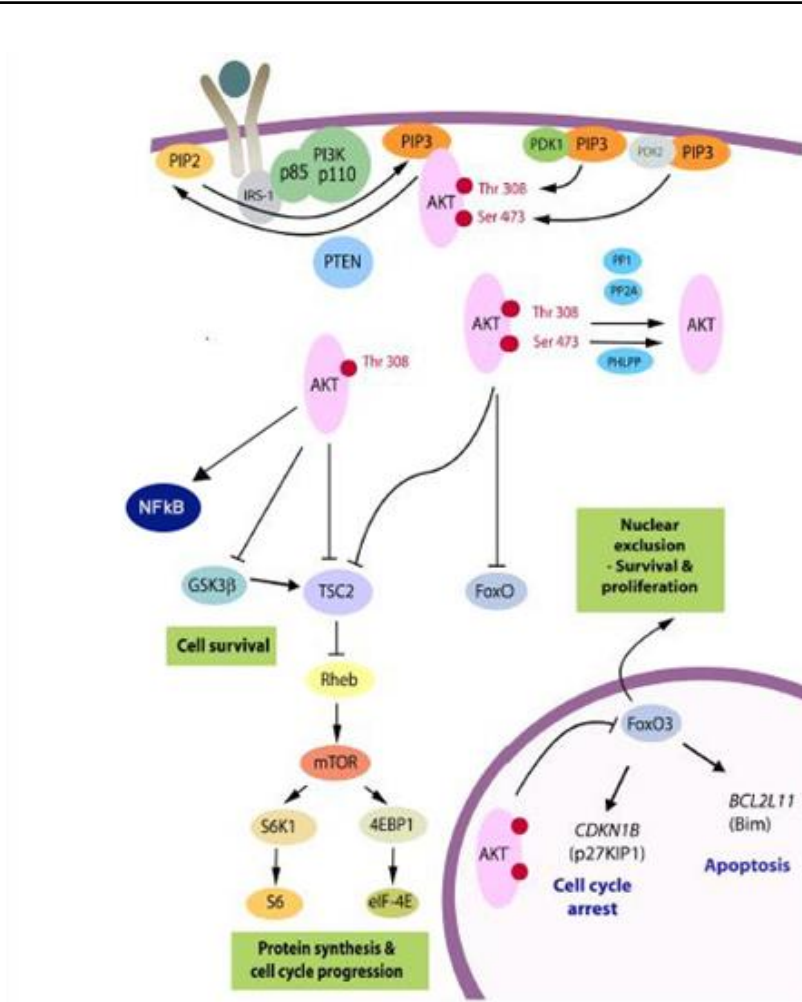


Figure 20: PI3K/AKT signalling pathway

Simplistic representation of PI3K/AKT signalling pathway and downstream target adapted from Robbins HL and Hague A; The PI3K/Akt Pathway in Tumours of Endocrine Tissues; Front Endocrinol (Lausanne); 2016; 6:188.

in ovarian and cervical cancer cell lines (144). The cytotoxic effect of majority of the chemotherapeutics converge upon activation of apoptotic pathway. AKT mediated enhancement of Bcl-2 and XIAP (anti-apoptotic proteins) expression with concomitant reduction in Bax (pro-apoptotic) contributed to the resistant phenotype in non-small cell lung cancer cell line (145). AKT activation was also reported to promote anti-apoptotic phenotype by inducing inhibitory phosphorylation of Bad (Serine 112) thereby preventing its interaction with Bcl-xl in A549 lung carcinoma cell line (146). Cisplatin treatment was reported to activate PI3K/AKT signaling in chemoresistant ovarian cancer cells, inhibition of which sensitized these cells to chemotherapeutic drugs. AKT signaling had also been demonstrated to abrogate cisplatin induced apoptosis in ovarian cancer cells (6). Elevated levels of activated AKT was also reported to promote stemness through increased level of Nanog in HT1080 fibrosarcoma, SK-LMS-1 leiomyosarcoma, and DDLS8817 dedifferentiated liposarcoma cell lines (147). A strong correlation between AKT mediated mTOR activation and increased stemness phenotype was reported in U251 (glioblastoma) and SH-SY5Y (neuroblastoma) human cell lines which was reversed in presence of rapamycin (148). Previously, we have also reported the role of AKT in enrichment of cancer stem cell population in highly platinum-taxol resistant ovarian cancer cells (149). AKT mediated increase in hypoxia inducible factor (HIF-1 α) expression can also promote stemness phenotype. Under hypoxic condition activated AKT was also reported to increase transcription and translation of HIF-1 α via activation of P300 and eukaryotic initiation factor-4E in U87MG, glioma and MCF-7 breast cancer cell line (148). Activation of HIF-1 α increased expression of Oct-4 and Nanog to promote a cancer stem like phenotype and therapy resistance in breast cancer cells (150). MDM2 mediated p53 ubiquitination and its subsequent degradation contributes to development of chemoresistance in multiple carcinomas. AKT activation was reported to enhance this process by activating MDM2 by

phosphorylating at Ser-166 and Ser-186 (151). AKT activation also regulates several cell cycle regulators to promote cellular proliferation (139). Phosphorylation of p21^{Cip1} by AKT stimulates DNA synthesis and CDK activity to enhance proliferation. Inhibition of AKT activation in ovarian carcinoma cell lines reduces the level of p21^{Cip1} and sensitizes cells to platinum and taxol (152). Activated AKT also prevents degradation of Cyclin D1 by inducing a negative phosphorylation on GSK3 β to regulate cell cycle (139). Increased level of AKT was reported to negatively regulate cytotoxic autophagy in ER⁺ breast cancer cells whereas inhibition of AKT sensitized these cells to tamoxifen and fulvestrant by inducing autophagic cell death (153). All these reports altogether indicate the role of AKT in regulation of several molecular phenotypes to promote chemoresistance.

Considerable efforts have been made for therapeutically targeting AKT to reverse therapy resistance. However, a majority of AKT inhibitors have failed in clinical settings. Among several inhibitors, Perifosine has moved furthest in clinical trials. It is a 3rd generation alkylphospholipid which inhibits the localization of PH domain to the membrane. However administration of Perifosine in combination with capecitabine and bortezomib lacked efficacy in treatment of multiple myeloma (154). Another phase II trial of Perifosine against recurrent malignant gliomas is currently underway. Various kinase domain inhibitors like AZD5363, GSK2110183, and LY2780301 etc are in multiple phase II clinical trials (155). Interestingly, PI3K, the upstream activator of AKT, was successfully targeted using alpelisib. Combinatorial treatment of alpelisib along with fulvestrant was reported to prolong progression-free survival in advanced breast cancer patients harboring PI3K mutation (156).

Amongst a deluge of molecular mechanisms regulated by the PI3K/AKT and MAPK/ERK signaling pathways, autophagy and cancer stem cells are of paramount importance as they are two crucial determinants of therapy resistance. Thus in context of this present work, we majorly focus on these two aspects.

1.2.3 Autophagy in chemoresistance

The ability of chemoresistant cells to endure cytotoxic effect of chemotherapeutic drug also depends upon its ability to respond and adapt to therapy induced intracellular and micro environmental stress. One of the key adaptive phenomenon against various extracellular or intracellular stress responses is autophagy, which remains active in both normal and disease states. It is a highly dynamic, lysosomal degradative catabolic process, which is evolutionarily conserved across species. The autophagic pathway starts with the formation of a double membraneous structure called phagophore, which extends to form a double membrane vacuole called autophagosome by sequestering damaged organelles and proteins. Autophagosome loaded with damaged cargo ultimately fuse with lysosome leading to its degradation (Figure 11). The pioneering discovery of ATG genes in yeast initiated the understanding of the process and currently the role of autophagy is evident in all major physiological process and diseases. (157).

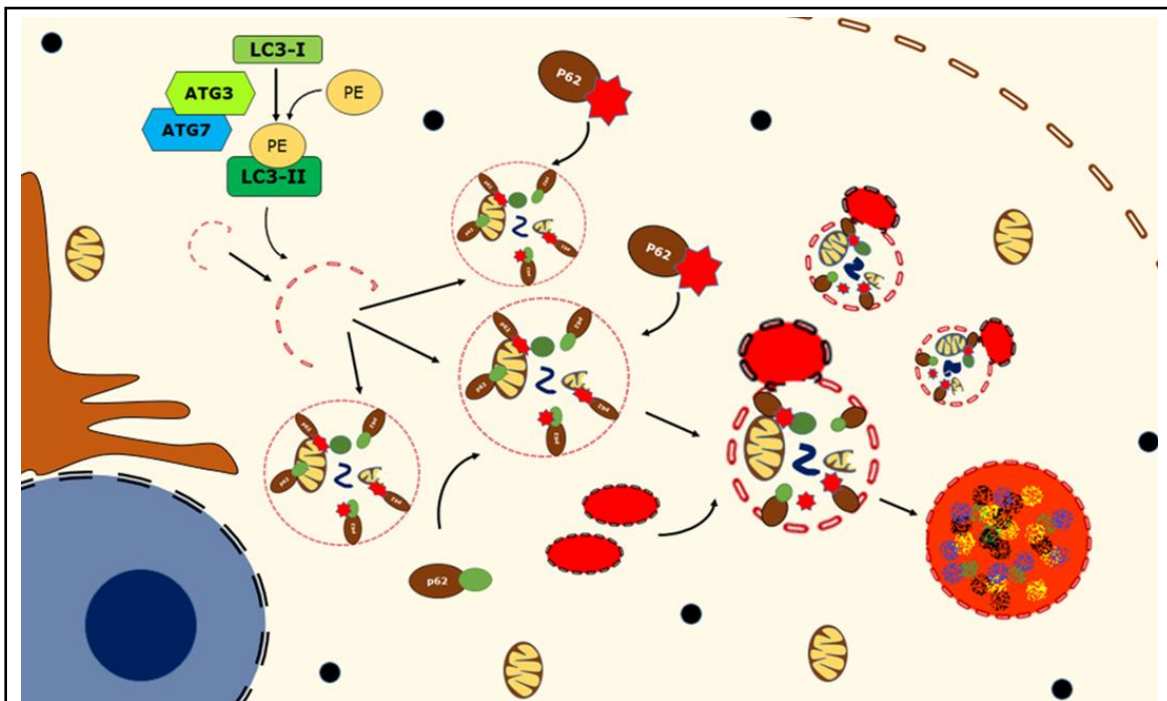
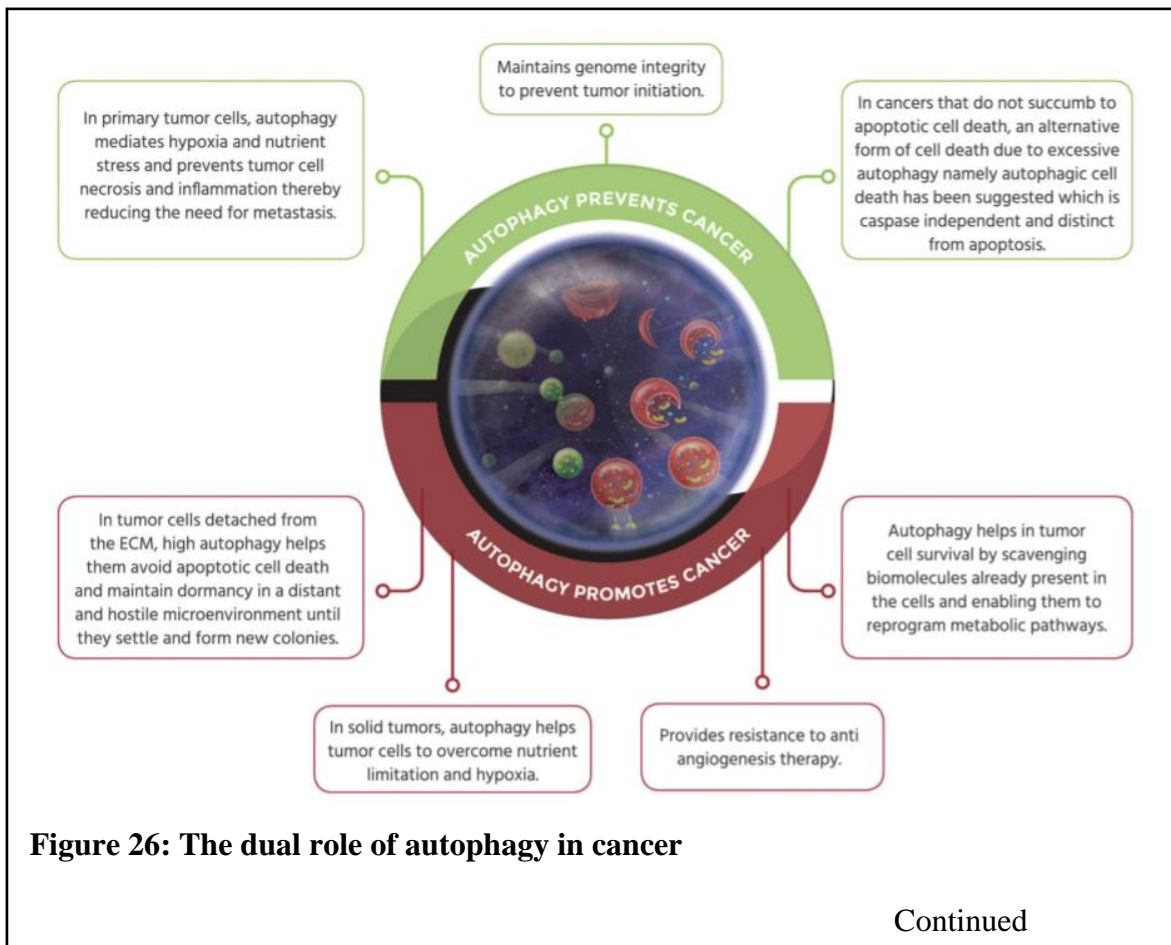


Figure 23: The process of macroautophagy

Continued

Pictorial representation of macroautophagy which initiates with sequestering of cytoplasm along with its damaged content of organelles directly or through adaptor proteins like p62 within double membrane structure called phagophore or isolation membrane, which eventually closes to form an autophagosome. The outer autophagosomal membrane then subsequently fuses with lysosomes (red coloured vesicles) leading to degradation of internal materials

Depending on the cargo being degraded, autophagy has been divided into several types, herein we discuss about macroautophagy, which is characterized by non-selective bulk degradation of damaged cargo. Autophagy plays a contextual role in carcinogenesis. Increased autophagic flux is reported to prevent cancer initiation by maintaining homeostatic balance (158, 159). On the contrary, autophagy is also reported to impart a protective function in advanced tumor exposed to various stresses like starvation, nutrient or growth factor deprivation and hypoxia (Figure 12) (160-162).



Autophagy prevents tumour initiation by maintaining genomic integrity and tissue homeostasis however it promotes tumour progression by inhibiting necrotic cell death in nutrient or oxygen starved micro environment and promotes metastasis by preventing anoikis; adapted from Singh S.S et al; Dual role of autophagy in hallmarks of cancer; Oncogene; 2018;37(9):1142-1158.

The role of chemotherapy induced autophagy is highly context-dependent. Increasing evidence on the role of cytoprotective autophagy in ameliorating chemotherapeutic stress in

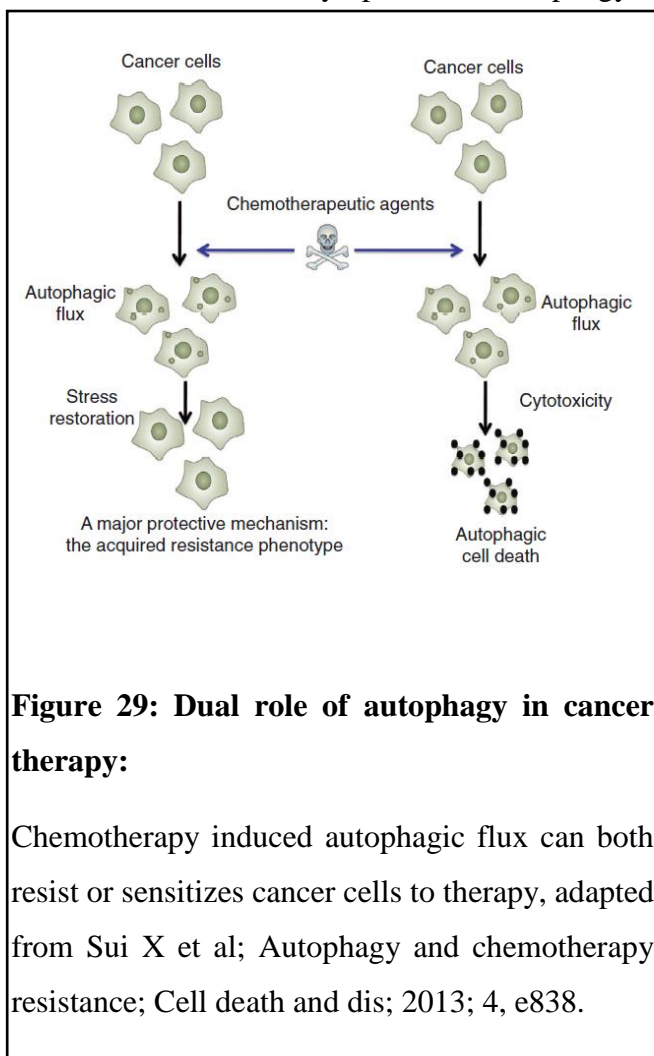


Figure 29: Dual role of autophagy in cancer therapy:

Chemotherapy induced autophagic flux can both resist or sensitizes cancer cells to therapy, adapted from Sui X et al; Autophagy and chemotherapy resistance; Cell death and dis; 2013; 4, e838.

various chemoresistant cancer cells is well studied. However, hyper activation of therapy induced autophagic flux is also reported to induce cell death (Figure 13) (163). Epirubicin induced autophagic flux was reported to promote resistance in MCF7 breast cancer cells. Emergence of antiestrogen resistance in breast cancer cells was found to be regulated by increased autophagic flux (164). The anti-cancer effect of 5-FU along with other drugs such as oxaliplatin was reported to be significantly

augmented in the presence of autophagy inhibitors in colorectal cancer for both in-vitro as well as *in-vivo* settings and resistance to these drugs were significantly attributed to the increased autophagic flux via p38 α (165-167). Resistance to anti-angiogenic therapy of

bevacizumab was attributed to hypoxia induced autophagic flux in GBM xenografts, targeting which with chloroquine inhibited tumor growth (168). Activation of therapy induced autophagy was also reported in HCC cell line post oxaliplatin treatment. Combination treatment of resistant HCC cell line with bevacizumab or sorafenib along with chloroquine was reported to significantly induce cell death both in *in-vitro* and *in-vivo* (169). Similarly, combinatorial treatment of hydroxychloroquine, HCQ was also reported to be more effective against therapy resistant B-chronic lymphocytic leukemia and mantle cell lymphoma (MCL) (170, 171). Several components of autophagic pathway also contribute to the development of therapy resistance. SQSTM1 or P62 is an autophagic adaptor protein that binds to ubiquitinated proteins and organelles and delivers them to autophagosome for degradation. Interestingly, p62 also regulates process such as inflammation, anti-oxidant response and apoptosis (172). Upregulation of NRF-2 mediated anti-oxidant response via p62 imparts resistance against cisplatin in ovarian, breast and colon cancer cells (173).

Though chemotherapy induced autophagy can enhance cancer cell survival, induction of excessive autophagy can lead to cancer cell death. Suberoylanilide hydroxamic acid (SAHA), a newly developed HDAC inhibitor is reported to induce autophagic cell death in breast cancer cells resistant to tamoxifen (174). Tanshinone IIA, a functional compounds of *Salvia miltiorrhiza*, was reported to induce beclin1 dependent autophagic cell death in squamous cell carcinoma cell line (175). Gemcitabine induced autophagic flux was reported to play cytoprotective function in oestrogen receptor negative MDMB-231 cells while promoting cell death in oestrogen receptor positive MCF-7 cells by activation of excessive autophagic flux through ER α -ERK1/2-p62 axis. Inhibition of ERK1/2 impaired autophagic flux and promoted “autophagic switch” from cytotoxic to cytoprotective (176). The PI3K/mTOR dual inhibitor NVP-BEZ235 was reported to induce autophagic cell death and

cell cycle arrest in cisplatin resistant urothelial cells (177). Thus induction of excessive autophagy may augment chemotherapy induced cell killing.

Several clinical trials are already underway to test the efficacy of autophagy inhibitor either alone or in combination with other therapies against various malignancies. HCQ is the FDA approved autophagic inhibitor in clinical practice (178). However, the available clinical data regarding HCQ is inconsistent. Administration of HCQ as a monotherapy against metastatic pancreatic cancer was found to be well tolerated in a cohort of 20 patients, however no significant increase therapeutic efficacy was observed (179). Combinatorial treatment of HCQ along with proteasome inhibitor Bortezomib in a phase-I clinical trial of 25 patients with relapsed or refractory myeloma showed good response in 3 (14%) patients and disease stabilization in 10 patients (180). Combination of HCQ with radiotherapy along with successive or concurrent temozolamide failed to improve overall survival rate in a cohort of 76 GBM patients (181). Two clinical trials are currently ongoing to test the safety and maximum tolerated dose of HCQ in refractory and relapsed advanced stage high grade serous ovarian carcinoma (NCT03081702, NCT01634893). Till now, clinical data regarding inhibition of autophagy as a therapeutic option is in its early days and requires thorough and rigorous investigation and such studies are partly hindered because of lack of *in-vivo* assay systems capable of monitoring therapy induced autophagic flux in real time.

Currently, transgenic animal models stably expressing fluorescent autophagy sensor are used to monitor autophagy induction or inhibition in response to stress or treatments on the tissue cryosections of interest using fluorescent microscopy (182). Such assays tend to provide valuable information but they fail to monitor the dynamic nature of autophagic flux. Thus development of novel autophagy reporter system to test the efficacy of FDA approved HCQ and other experimental autophagy inhibitors in combination with chemo or radiotherapy for various malignancies is a necessity at present time.

1.2.3.1 Real time monitoring of autophagy during therapy:

Two types of molecular probes comprised of reporter proteins have been generated to monitor autophagic flux in real time i) Fluorescent based probes and ii) Luciferase based probes.

Fluorescent based probes:

EGFP-LC3 was the first autophagic sensor to be developed, which was used extensively for real time monitoring of autophagy kinetics. Besides deciphering the intricate biology associated autophagy, scientists have employed this reporter to screen chemical libraries to identify novel autophagic inducers/blockers. This sensor was used to screen bioactive compounds that are capable for induction of autophagy in glioblastoma cells (183). A similar screen identified four FDA approved drug perhexiline, niclosamide, amiodarone and rottlerin as autophagy inducer in MCF7 cells (184). Microscopic analysis of tissue cryosections from transgenic mice ubiquitously expressing GFP-LC3 under cag promoter was utilized to monitor autophagic flux (185). However, the EGFP-LC3 sensor does not provide a complete picture since an increase in LC3 puncta can result from both increased induction of autophagy or blocked autophagic degradation. Development of mRFP-GFP-LC3 sensor (tfLC3) led to a more accurate estimate of autophagy induction and inhibition by measuring both autophagosome and autophagolysosome formation (186). Subsequently, this probe was utilized to identify novel/alternate drugs for autophagy modulation. The potential of flubendazole, an antihelminthic drug as an autophagy inducer was described in HeLa cell line (187). Pampaloni et al., (2017) identified six potent autophagy inducers and four inhibitors from a natural compound library in U343 glioma 3D tumor spheroids by time lapse fluorescence imaging (188). Mice model expressing mCherry-EGFP LC3 construct was used to study autophagic flux in peripheral and central nervous system of new born animals and ischemia-reperfusion injury in mice. The principle of which has been explained in detail

in section 2.3.4 (189, 190). Kaizuka et al., (2016) reported a novel autophagy sensor GFP-LC3-RFP-LC3ΔG which when cleaved by endogenous ATG4 proteases generated equimolar amounts of GFP-LC3 and RFP-LC3ΔG. GFP-LC3 is degraded by autophagy, while RFP-LC3ΔG remains in the cytosol, serving as an internal control and producing a quantitative method to evaluate autophagic flux in cultured cells and whole organisms such as zebrafish and mouse embryo. This sensor was further used to screen more than 1000 FDA approved drugs in HeLa cells and 13 novel autophagy inducers and 18 novel inhibitors were identified (191). A potential drawback of this sensor is rapid decrease in GFP signal within 30 minutes of autophagy induction which limits the longitudinal kinetic measurement (182).

Luciferase based probes:

LC3-Rluc^{C124A} luciferase system was developed to estimate the autophagic flux based on the reduction of luciferase signal due to degradation of the fusion protein in the autophagolysosome upon induction of autophagy. In this system, mutated Renilla luciferase with increased half-life was used as a reporter probe to avoid any reduction of luciferase signal due to autophagy independent degradation. The mutated form of LC3^{G120A}, which does not undergo degradation upon induction of autophagy was used for normalization. Autophagic flux was estimated as the ratio of luciferase signal of wild type LC3 fusion protein to LC3^{G120A} fusion protein from cell lysates. This sensor system was utilized to screen small molecule library in cell lines to identify various inhibitors and activators of autophagic process (192). Apart from the inherent limitation of LC3 degradation as an estimate of autophagic flux, the need for ratio metric quantification of luciferase readout for estimating autophagic flux makes the system suboptimal for in vivo application by bioluminescence imaging.

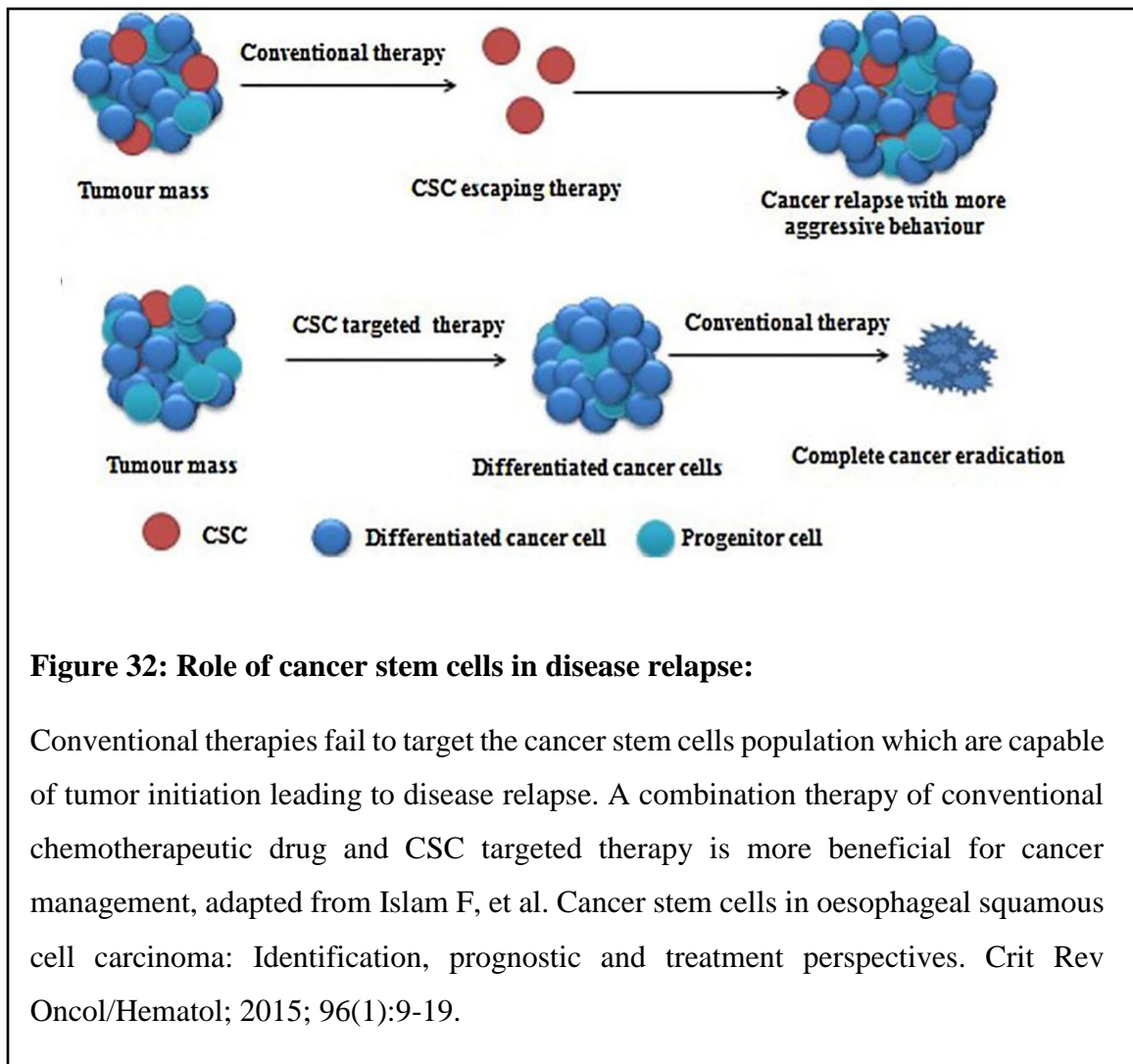
Next utilizing the degradation of p62 as an estimate for studying autophagy, Luc2p-p62 reporter sensor was developed. An ubiquitination defective p62 Δ U mutant was used for normalization as it does not undergo autophagic degradation. The ratio of luciferase readout of Luc2p-p62 Δ U to Luc2p-p62 was used to estimate autophagic flux (an increase ratio suggestive of increased autophagic flux). This sensor was used to ratio metrically quantify autophagic flux in glioma cell lysates treated with temozolomide (193). Apart from the short half-life (1 hr) of the reporter protein luc2p, which may provide a false readout of p62 degradation, the need for ratio metric measurement of luciferase activity along with luc2p-p62 Δ U possess limitation for *in vivo* application.

Poly-80/poly-19-FL2 is the only luciferase based autophagy sensor that has been applied for monitoring starvation and rapamycin induced autophagic flux *in-vivo* by electroporation of the sensor in the skeletal muscle of normal and Atg16L1 hypomorphic mice. The sensor quantitates autophagic flux by estimating the degradation of aggregated (poly-80) to non-aggregated poly glutamine repeats (poly-19) (194). However, the ratio metric nature of the assay system is difficult to be adapted in *in vivo* system. Along with the demerits of FL2 having a short half-life, poly-glutamine aggregates are not selective autophagy substrates and can be degraded by ubiquitin-proteasome system which adds up compounding factor in quantifying the autophagic flux (195). Thus it is of utmost importance to develop an autophagy assay system capable of monitoring real-time autophagy flux *in-vivo*.

1.2.4 Cancer stem cell in chemoresistance

Tumor heterogeneity is one of the factors that contribute to the failure of treatment. Recent evidence suggests presence of a small subpopulation of cancer cells capable of self-renewal and differentiation that evade the cytotoxic effects of common chemotherapeutics to promote disease relapse and resistance (196, 197). Majority of the chemotherapeutic drugs

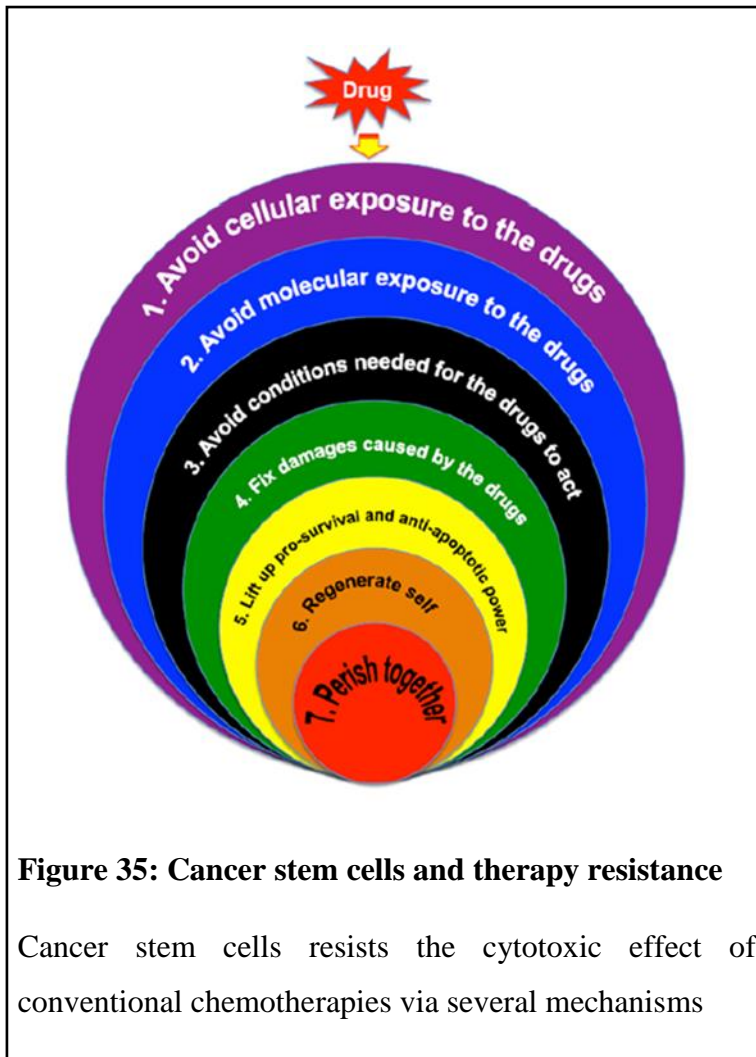
target the actively dividing tumor cell population, while cancer stem cells (CSC) remain largely unaffected due to their quiescent nature and cause disease relapse after the end of chemotherapeutic regimen. Multiple reports including our own which indicate the tumor initiation capability of cancer stem cells (Figure 14) (149, 198-200). In 1997, Bonnet and Dick first confirmed the existence of CSCs in leukemic cells based on the presence of CD34⁺ and CD38⁻ cell population, which were capable of tumor initiation in immunocompromised mice that led to the vast knowledge on the role of cancer stem cells or stem like cells in cancer biology (201).



CSCs are the driver of therapy resistance against cisplatin, paclitaxel, temozolomide, etoposide and doxorubicin in gliomas, glioblastoma breast, lung, colorectal, pancreatic, prostate and ovarian cancer(202). Chemotherapeutic treatments which fail to target CSCs, may also cause increase in CSC population in tumor as reported by the expansion of preleukemic DNMT3A mutant stem cells in the bone marrow post chemotherapy (203). Increase in percentage of glioma stem cells (GSCs) were reported in patient derived cell lines post treatment with temozolomide and these GSCs were functionally and phenotypically interconvertible between cancer cells and cancer stem cells. (204).

Similar increase in CSC population was observed in glioblastoma multiforme post treatment with bevacizumab (205). It was elegantly reported that in bladder cancer cell lines, the pool of quiescent label retaining cells divide unexpectedly and exponentially in between the chemotherapeutic cycles to repopulate tumor (206).

There are several mechanisms by which CSCs evade cytotoxic effect of conventional chemotherapeutics (Figure 15). The increased tolerance of CSCs against chemotherapeutics is contributed to the increased expression of drug transporters like MDR1, ABCG2 and ABCB1 and this property of enhanced drug efflux is also utilized to identify stem cells in tumor population using side population assay (207, 208). CSCs also reduce the damaging effect of various chemotherapeutics by reducing the level of ROS generation due to the increased expression of aldehyde dehydrogenase as observed in leukemia, breast cancer, lung cancer, bladder cancer and head and neck squamous cell carcinoma (209). Increased expression of ALDH can also detoxify chemotherapeutic drugs such as cyclophosphamide, temozolamide, paclitaxel and epirubicin (210-212). Altered epigenetic profile of CSCs also lead to inactivation of chemotherapeutics. Increased expression of DNA methyl transferases in CSCs inhibit the expression of thymidine phosphorylase which is essential for conversion of capecitabine to 5-FU leading to therapy resistance (213). Chemotherapeutic drugs



generally induce DNA damage which ultimately trigger cell death, however CSCs show increased expression of DNA repair genes to mitigate DNA damaging effect of CSCs. Interestingly, a small population of CD29^{High} CD24^{High} Lin⁻ breast cancer cells capable of tumor initiation *in-vivo* also showed increased expression of DNA damage response and repair genes like Nek1, Brca1,

Chk1, Hus1, Ung, Xrcc5, Sfpq, Uhrf1 etc (214). Inhibition of Chk1 or ATM was reported to sensitize CD24⁺/CD44⁺/ESA⁺ breast and pancreatic cancer cells to gemcitabine and radiation respectively (215, 216). Knockdown of O6-methylguanine-DNA methyltransferase (MGMT) was reported to sensitize glioma cells to temozolomide (217).

Current theory suggests that therapeutic regimen targeting both tumor cells and CSC will be more beneficial than conventional chemotherapeutic regimen. However, targeting CSCs have been challenging till now and is in its early development. Various signaling pathways like Wnt/b-catenin, Notch, PI3K/AKT and Hedgehog (HH) found to be crucial for maintenance of stemness properties have been targeted in in-vitro and pre-clinical settings (218). The HH pathway inhibitor Vismodegib, was approved by both FDA and European

Medicines Agency for therapy against metastatic and locally advanced basal cell carcinoma (219). Due to the presence of multi drug transporters and drug detoxification systems, cancer stem cells also demonstrate a multi drug resistant phenotype. Thus it is crucial to identify drugs or drug combination that can target these CSCs along with main tumor population in order to prevent disease relapse and therapy resistance.

1.3 Multi drug resistance:

Development of resistance to one class of chemotherapeutics sometimes may promote the development of resistance to other class of drugs having a different mode of cytotoxicity. Classically this phenotype is termed as multi-drug resistance (MDR) and is contributed to the increased expression of ATP binding cassette family of drug transporters like P-glycoprotein and multidrug resistance related proteins (MRP) which efflux the drug out of the cytoplasm (220). MDR phenotype can also be contributed by the severe down regulation of apoptosis, drug detoxification, epithelial-mesenchymal transition, increased DNA repair and presence of CSC (104, 221).

Several in-vitro and clinical studies report the development of resistance to one drug can severally alter the effectivity of another unrelated drug, thus indicating the importance of designing an optimal therapeutic regimen especially against tumour cells resistant to first line of therapy (222-224). Breast cancer patients who display resistance to doxorubicin rarely respond to second line paclitaxel treatment indicating development of multi drug resistance (225). Further studies reported that selection of cells in presence of doxorubicin with significantly increased expression of P-glycoprotein and breast cancer resistance protein (BCRP) levels while reducing procaspase-9 expression lead to the development of cross resistance to paclitaxel (226). However, selection of cells in presence of paclitaxel did

not confer cross resistance to doxorubicin in the similar extent when the sequence of drug administration was reversed. In another report, Borris et al (2020) using pharmacological screening reported that cells that are resistant to paclitaxel show cross resistance to EGFR directed tyrosine kinase inhibitors (227).

Interestingly, activation of the two key signaling hubs, the PI3K/AKT and MAPK/ERK have been reported to promote development of MDR phenotype in multiple cancers (228, 229). Activation of AKT was reported to upregulate expression of MDR genes via activation of NF κ B in HL-60 acute myeloid leukemia cell line (230). Inhibitory phosphorylation of GSK3 β by AKT accelerates transcription of c-Myc, c-Jun, and cyclin D1 via accumulation of β -catenin, which in turn upregulates expression of MDR1 and survivin to promote a MDR phenotype in breast cancer cells (231). Increased AKT activation in five acute lymphoblastic leukemia VCR-resistant cell lines was reported to impart cross resistance to prednisolone, dexamethasone, daunorubicin and doxorubicin. Upregulation in ERK1/2 activation also increases expression of drug transporters imparting a single or multi drug resistant phenotype (232). ERK1/2 mediated phosphorylation of HIF-1 α induces Pgp expression in chemoresistant lymphocytic leukemia, colon, breast, pancreatic and non-small lung cancer cells. ERK1/2 activation was also reported to positively regulate expression of other drug transporters like BCRP and MRP1 (233). Ectopic expression of Raf in breast cancer cell lines was reported to increase expression of MDR-1 and Bcl-2 via activation of ERK1/2 (234). Adriamycin resistant hepatocellular carcinoma cells (HepG2) show increased ERK1/2 activation to promote MDR phenotype, inhibition of which reduces the expression of P-gp and MRP-1 expression and sensitizes cells to therapy (235). Similar sensitization of gemcitabine resistant pancreatic cancer cells by gefitinib reduced expression of MDR via downregulation of ERK1/2 (236).

The efficacy of any given chemotherapeutics is the measure of its ability to induce cell death by overcoming the apoptotic threshold of cancer cells with minimum toxicity. The development of multidrug resistant clones under the selection pressure of commonly prescribed chemotherapeutics often show alteration in several molecular resistance pathways. Unlike resistance developed against targeted therapies which has acquired a defined mechanism of resistance, resistance to chemotherapeutics is less well defined. Further the response to a given therapeutics or therapeutics combination also depends individual receiving it i.e. the common drug for a given tumor may not perform optimally in all patients (237). Thus prior prediction of efficacy of clinically approved therapies by ex-vivo chemo-sensitivity assay systems before the onset of therapy can be highly beneficial for selection of optimal drug or drug combination, especially in the context of cancers like ovarian cancer, wherein majority of patients show resistance to primary therapy of platinum-taxol.

1.4 Ovarian cancer

Ovarian cancer is one of the most lethal gynaecological malignancies accounting to the seventh highest mortality rate in women in the world and third in India (238, 239). The risk factors for ovarian cancer includes age, genetic history, obesity and parity. Majority of the ovarian cancer cases are of epithelial origin with dismal 5-year survival rate of 35-40% (240, 241). The poor success of ovarian cancer treatment is contributed to late diagnosis of the disease at an advanced stage and acquirement of therapy resistance which is a major impediment in ovarian cancer management

1.4.1 Subtypes of ovarian cancer

Based on the site of origin of primary tumour, ovarian cancer can be mostly classified into three main categories, epithelial ovarian carcinoma (EOC), germ cell and sex cord or

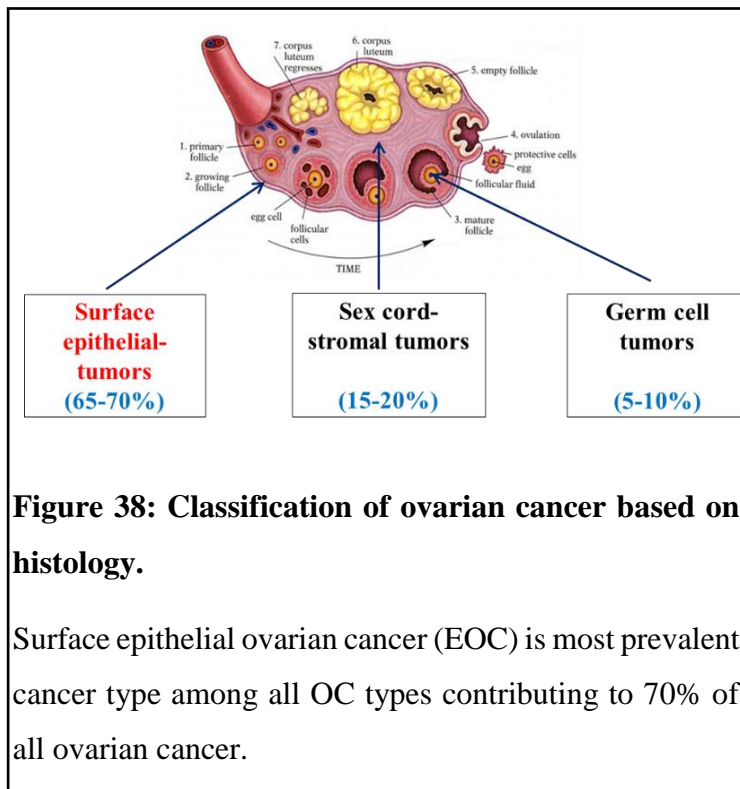


Figure 38: Classification of ovarian cancer based on histology.

Surface epithelial ovarian cancer (EOC) is most prevalent cancer type among all OC types contributing to 70% of all ovarian cancer.

stromal cell tumours (Figure 16) (242). Majority of the ovarian cancer (>90%) originate from the ovarian surface epithelium though some reports suggest the fallopian origin of surface epithelial tumours (243). Histopathological classification of EOC further subdivides this group into four subgroups

consisting of serous (70%), the major type of EOC followed by endometrioid (15%), mucinous, clear cell, having similar frequency of approximately 5% and mixed or carcinosarcomatous müllerian tumours, which is a rare type of EOC having less than 5% frequency. These subtypes are also characterized by distinct genetic signatures, therapy response and disease prognosis (242). Based on pathology and gene signatures, the serous ovarian cancer was classified into type I and type II tumours. Low grade serous, endometrioid, clear cell and mucinous tumours were included in type I tumours with predominant activating BRAF, KRAS and β -catenin mutation along with high microsatellite instability while high grade serous and mixed ovarian tumours with predominant p53 mutation (>90%) and PI3KCA amplification were characterized as Type II. Type II tumours

are more prevalent and aggressive than Type I tumours. Thus in our study we have majorly focused on high grade serous ovarian carcinoma (HGSOC) (244).

1.4.2 Disease management and treatment

Optimal tumour resection and platinum-taxol based chemotherapy are mainstays of ovarian cancer management. Based on these treatment modalities, currently there are five accepted treatment regimens for stage II to stage IV epithelial ovarian cancer (245):

1. Cytoreductive surgery followed by six cycles of platinum-taxol-based chemotherapy injected intravenously or intra peritoneally.
2. Cytoreductive surgery trailed by intra venous administration of platinum-taxol-based chemotherapy along with bevacizumab, which is continued as a maintenance therapy
3. Neo adjuvant chemotherapy of platinum-taxol for 3-6 cycles followed by cytoreductive surgery and few more rounds of chemotherapy which can be administered intravenously or in some context intra-peritoneal chemotherapy with hyperthermia (heated intraperitoneal chemotherapy [HIPEC])
4. Chemotherapy along with PARP inhibitor for patients with BRCA mutation
5. Only chemotherapy for patient associated with high risk of surgical mortality/morbidity

The choice of methodology depends upon the extent of disease progression, mutation status, health performance of patient and the risk associated with surgery. Debulking surgery is performed for complete macroscopic resection of tumor to best possible extent and subsequent cycles of chemotherapy is administered for targeting the residual microscopic disease. The success of optimal debulking surgery is directly correlated to disease prognosis (246, 247).

Platinum based compounds such as cisplatin and carboplatin along with intermittent paclitaxel remain the first choice of chemotherapy for high grade serous ovarian cancer. These drugs are generally administered by intravenous route or intraperitoneally.

Majority of the HGSOC cases respond well to the initial challenge of platinum-taxol, however in 70% of the cases they show disease recurrence within a short period of time. Based on the time of relapse from end of first chemotherapy cycle, which is termed as platinum free interval (PFI), the cases are categorized into three groups: i) platinum refractory which accounts to 20% the total cases which do not respond to platinum from the very beginning of therapy ii) 30% of the total cases show disease relapse within 6 months of therapy and do not respond to platinum again and are termed as platinum resistant ii) cases which show disease relapse after 6 months of therapy is classified as platinum sensitive, this cases are likely to respond to platinum again (4, 248). However, after several rounds of relapse and therapy, majority of the cases eventually acquire resistance to platinum thus necessitating the usage of non-platinum agents. The currently practiced second or subsequent line therapeutic agents are doxorubicin, gemcitabine, irino/topotecan and etoposide. All these chemotherapeutic agents display a similar response rates of 15-20% having a progression free survival of three to four months and an overall survival of 12 months thus confounding the choice of therapeutics for a given case (Figure 17) (4, 249). Further, there is a severe lack of targeted therapies for ovarian cancer. Currently PARP inhibitors are approved for BRCA mutant cases while Bevacizumab, monoclonal antibodies targeting angiogenesis, have been approved for maintenance therapy in platinum-sensitive cases (249-251). Therefore management of therapy resistant disease remains the major hurdle for EOC and contributes to low five year overall survival of 40%. Thus it is critical to identify molecular processes or targets that would allow

- 1) The platinum-resistant tumor cells be sensitized to targeted therapy or
- 2) Delay in acquirement of platinum-resistance or
- 3) Predict response of non-platinum drugs to identify the right choice and avoid excessive side-effects.

All these three or any one of them will impart improved treatment response and may involve critical signaling pathways.

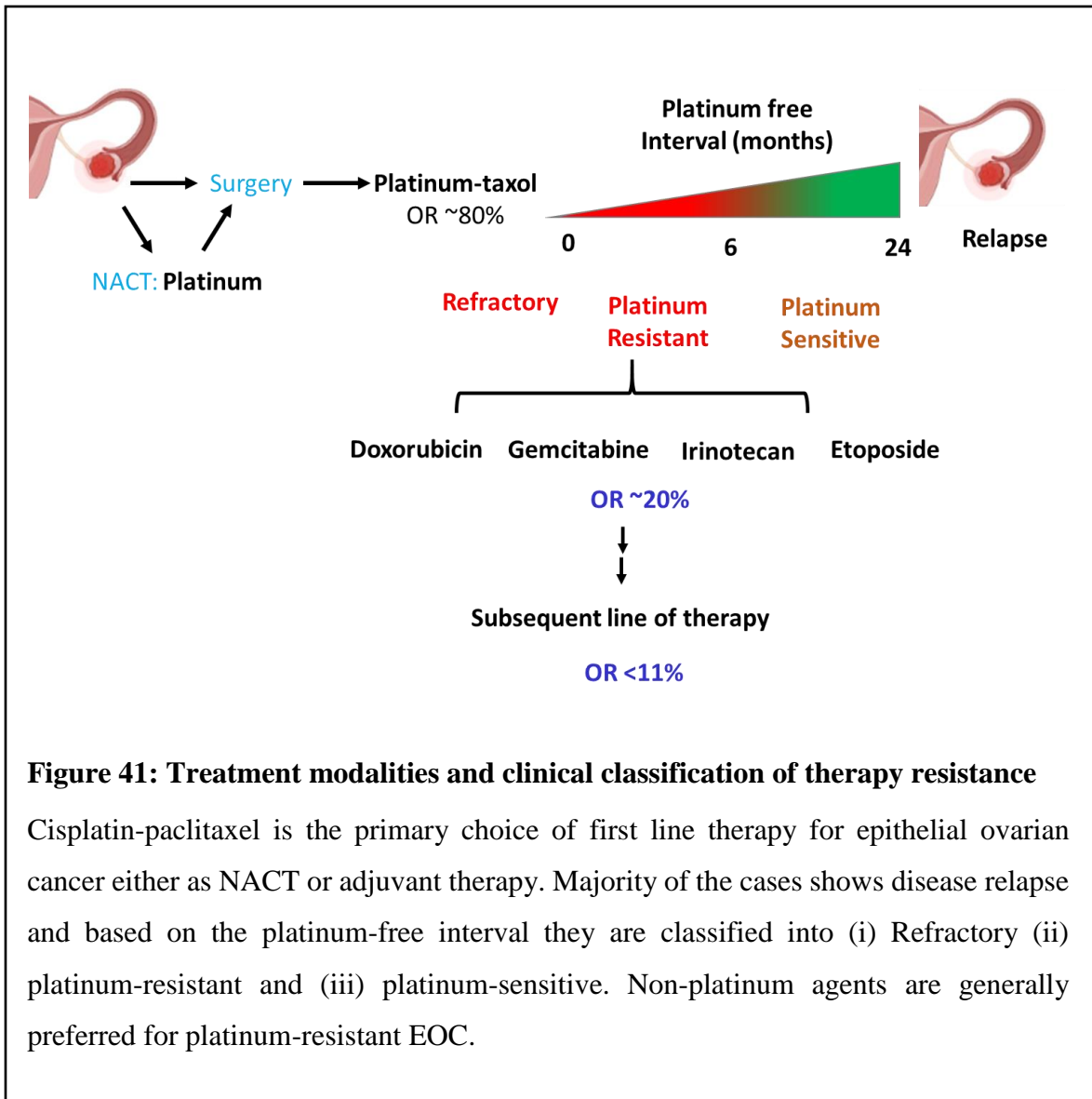


Figure 41: Treatment modalities and clinical classification of therapy resistance

Cisplatin-paclitaxel is the primary choice of first line therapy for epithelial ovarian cancer either as NACT or adjuvant therapy. Majority of the cases shows disease relapse and based on the platinum-free interval they are classified into (i) Refractory (ii) platinum-resistant and (iii) platinum-sensitive. Non-platinum agents are generally preferred for platinum-resistant EOC.

1.4.3 Acquirement of therapy resistance to platinum-taxol in EOC

Since majority of the EOC cases initially respond well to platinum and then show relapse of disease, understanding the molecular mechanisms governing the acquirement of therapy resistance remains to be the major challenge in comparison to intrinsic mode of resistance. Acquired resistance is a multistep process involving alteration in several molecular

pathways that bestows a cell the ability to tolerate cytotoxic effect of platinum and taxol. Several reports suggest upregulation of multi drug transporters in ovarian cancer cells which contributes towards developing resistance to cisplatin, paclitaxel and doxorubicin. These upregulation in MDR genes are regulated through several signaling pathways like Hedgehog, hyaluronic acid receptor and AKT (252-254). Also a reduction in platinum drug uptake via downregulation of hCTR1 and hCTR2 was reported in EOC cell line post platinum challenge (255). Upregulation of anti-apoptotic genes like Bcl-2, Mcl-1, Bcl-xL and XIAP with downregulation of pro-apoptotic proteins Fas, Bim, Bak and Bax was reported in platinum resistant and refractory cases (256-258). Increased DNA repair also contributes to platinum resistance along with a concomitant increase in the expression of ERCC1 and ERCC4 were also reported post platinum therapy in EOC patients (259). Data from our own lab suggests upregulation of PI3K/AKT signaling confers platinum resistance via enrichment of CSC population and activation of NF κ B (260).

Recent evidences however call for a paradigm shift in understanding therapy resistance by investigating the gradual process of acquiring resistance rather than comparing sensitive and its resistant counterpart. Our lab has previously established two dynamic model of cisplatin-paclitaxel dual resistance in A2780 and OAW42 EOC cell lines, developed using pulse method of chemotherapy, to study gradual modulation of signaling pathway during acquirement of chemoresistance. The gradual evolution of a cancer cell to highly resistant disease can be categorized into various stages based on the resistance index thereby investigating molecular alterations. Previously we observed intriguing oscillatory pattern of IGF-1R expression which peaked at the early stage of therapy resistance and then gradually diminished as the cells acquired a highly resistant phenotype governed by an active PI3K/AKT signaling. Targeting IGF-1R using picropodophyllin specifically sensitized cells

at the early stage of resistance to platinum while the hyperactive AKT signaling maintained a highly chemoresistant phenotype by enriching cancer stem cell population (5, 149).

IGF1R signalling mainly relays extra cellular signal to the nucleus through PI3K/AKT and MAPK/ERK pathways. Several reports demonstrate the involvement of these pathways in chemoresistance in ovarian cancer cells (6-9). It has been reported that cisplatin treatment activates PI3K/AKT signalling and blocking this signalling pathway sensitizes resistant ovarian cancer cells to chemotherapeutic drugs (6, 261). It has been also demonstrated that AKT signalling abrogates cisplatin induced apoptotic response in the ovarian cancer cells (7). On the other hand a gene microarray study of 28 patients with highgrade serous ovarian cancer demonstrated that samples relatively resistant to platinum chemotherapy showed enrichment of genes involving IGF1/NFkB/ERK signaling when compared to those tumors remaining sensitive (8). Also it was demonstrated that treatment of ovarian cancer cell line with chemotherapeutic drugs induces apoptosis through activation of JNK/p38 in sensitive cells while resistant cells show prolonged activation of ERK1/2 (262). Though there are several studies which show activation of these signalling pathways in chemoresistant ovarian cancer cells there are no such reports on whether these signalling pathways are modulated as an ovarian cancer cell gradually become more and more resistant to platinum-taxol treatment. The implication of such modulation in governing acquirement of therapy resistance is still not understood. Further the role of these pathways in development of collateral resistance to non-platinum drugs in cisplatin-paclitaxel resistant ovarian cancer cells has not yet been addressed. ***Thus, we aim to understand the biological relevance of these pathways in our dynamic model of chemoresistance to identify and target these key molecular components in order to 1) prevent promotion of resistance or 2) delay the development of a highly chemoresistant disease or 3) predict therapeutic response of alternate non-platinum agents to identify the optimal choice.***

Aim:

Understanding the role of MAPK/ERK and PI3K/AKT signalling during gradual acquirement of chemoresistance to design stage specific intervention to tackle development of platinum-taxol dual resistance in high grade serous ovarian cancer

Key questions:

1. Whether MAPK/ERK and PI3K/AKT signalling are modulated during the gradual acquirement of chemo resistance in ovarian cancer cells?
2. Is it possible to target and pause promotion of resistance at the onset of cisplatin-paclitaxel dual resistance in ovarian cancer cells?
3. Is it possible to impede development of a highly chemoresistant phenotype?
4. Is it possible to utilize the dynamic modulation in MAPK/ERK and PI3K/AKT signaling to predict therapeutic efficacy of second line non-platinum agents in platinum-taxol resistant cells?

Objectives:

1. Understanding the biological relevance of MAPK/ERK and PI3K/AKT signaling in dual chemo resistant ovarian cancer model
2. Development of BRET based sensors to monitor PI3K/AKT signaling and MAPK/ERK signaling during the acquirement of chemoresistance

Chapter 2: Hyper activated ERK1/2 kinase drives autophagy to promote survival of ovarian cancer cells at the onset of chemoresistance

2.1 Introduction

The PI3K/AKT and MAP/ERK are the two keystone signalling hub that can regulate several cellular phenotypes like survival, proliferation, differentiation and therapy resistance in cancer cells. Activating PI3K mutation and PTEN deletion, a negative regulator of AKT activation, are not frequent in high grade serous ovarian cancer, however genomic amplification of PI3K and AKT are observed in 20 and 10-15% of cases. Increase expression of AKT or its downstream target mTOR was reported to be associated with poor overall and disease free survival in TCGA cohort (263). In a cohort of 230 EOC cases, increased phospho AKT (p-AKT) level was associated with poor overall and progression free survival in comparison to cases having reduced p-AKT (264). Increased AKT phosphorylation at serine 473 residue has been correlated with histological grade and chemoresistance in 118 FFP tumor samples (265). Similarly, increase activation of AKT signalling pathway, evaluated in terms of the level of p-AKT, p-mTOR and p70S6K was observed by immunohistochemistry in tissue section of 18 chemoresistant (88.89%, 94.44% and 100% respectively) cases in comparison to 25 chemosensitive (64 %, 68 % and 72% respectively) cases (266). Several reports including data from our lab suggested a hyperactive AKT signalling governs a highly chemoresistant phenotype of EOC cell lines and inhibition of which was reported to sensitize these cells to therapy. Mechanistically, increased AKT activation was reported to promote platinum resistant phenotype via multiple mechanisms like regulation of G2-M transition by upregulation of Chk-1 activity and stabilization, inhibition of p53 dependent apoptosis, modulation of pro and anti-apoptotic genes, by upregulation of DNA damage repair, promotion of epithelial-mesenchymal transition and stemness properties (6, 141, 149, 228, 254, 267).

Activating mutation in upstream regulators of MAPK/ERK1/2, i.e., KRAS and BRAF are rare in HGSOC in comparison to low grade serous ovarian carcinoma, however several members of the pathway show local genetic gains and mRNA overexpression indicating an active signalling

cascade in HGSOC (263, 268). Increased activation of ERK1/2 was reported in HGSOC tissue sections and tumor lysates in comparison to normal fallopian tube (268). High level of phospho MEK, the upstream regulator of ERK1/2, was correlated with poor prognosis in 408 HGSOC cases from TCGA cohort (269). Increased activation of ERK1/2 along with its upstream and downstream kinases was reported in 14 ascites derived xenograft model (270). Interestingly, platinum-taxol, the primary line of therapy in HGSOC, are reported to increase ERK1/2 phosphorylation in cisplatin or paclitaxel resistant ovarian cancer. Activated of ERK1/2 promotes activation of several downstream targets like p90^{RSK1/2}, MNK to promote cisplatin and paclitaxel resistance in EOC cell line (271). However, it is interesting to note, the activation of MAPK/ERK in HGSOC occurs in absence of any activating mutation in KRAS, BRAF and MEK suggesting that activation of ERK1/2 occurs via activation of far upstream pathway drivers like rector tyrosine kinases. Intriguingly, Liu L et al (2018) reported that in a co-culture system of tumor associated macrophages derived from mouse bone marrow monocytes show an increased level of IGF-1 to promote proliferation and migration of ID8 mouse EOC cells via activation of ERK1/2 and AKT signalling (272). Previously, utilizing a dynamic model of cisplatin-paclitaxel dual resistance our lab has demonstrated that increase in IGF1R expression supports the onset of resistance and targeting IGF1R using natural compound picropodophyllin significantly sensitizes these cells to cisplatin-paclitaxel specifically at the early stage of therapy resistance. Interestingly, as the cells acquire a highly chemoresistance phenotype, the IGF1R expression declines with increased activation of AKT which maintain this highly chemoresistant phenotype by promoting stem cell like properties (5). Acquired chemoresistance is a multi-step process developed through series of molecular and biochemical changes involving modulation in several key kinases. Though association of the MAPK/ERK and PI3K/AKT pathway with EOC chemoresistance is apparent, the dynamic modulation of this pathways and its implications during evolution of a cancer cell to a highly resistant disease

has yet not been understood. Thus utilizing our indigenously developed cisplatin-paclitaxel dual resistant model we aim to ask following questions

1. Whether MAPK/ERK and PI3K/AKT signalling are modulated during the gradual acquirement of chemo resistance in ovarian cancer cells?

2. Is it possible to target and pause promotion of resistance at the onset of cisplatin-paclitaxel dual resistance in ovarian cancer cells?

Upregulation in drug transporters, down regulation of drug detoxification system and apoptotic machineries, faster DNA repair, upregulation of survival pathways are shown to be associated with resistance development. In recent time, autophagy, a catabolic cellular process has been implicated in tumour initiation as well as maintenance of chemoresistance in various cancers including EOC (163). In a cohort of 45 EOC patients suffering from recurrent disease, elevated autophagic flux in tumor cells derived from the ascites was reported to promote enhanced survival against cisplatin (273). Several studies showed that genetic or pharmacological inhibition of autophagy lead to sensitization of chemo-resistant cells to therapy (274). Mechanistically several altered molecular pathways are held responsible for increased autophagic flux in chemoresistant ovarian cancer cells. Increased ERK1/2 activation and expression YAP, a transcriptional regulator is reported to regulate induction of autophagy in cisplatin treated ovarian cancer cells (9, 275). Unbiased proteomic screen in paclitaxel treated ovarian cancer cells identified increased expression of an autophagy regulator, TXNDC17 (276, 277). Expression of autophagy adaptor protein, p62 is also reported to be higher in cisplatin resistant SKOV3 cells and knockdown of p62 sensitized these cells to cisplatin. (278, 279). Two clinical trials designed at targeting autophagy in ovarian cancer are currently being held. NCT03081702, a phase I/II study, is aimed at determining the dose and clinical benefits of

hydroxyl-chloroquine that can be administered with itraconazole in platinum-resistant epithelial ovarian cancer patients. In another phase I clinical trial (NCT01634893), combination of oral HCQ with sorafenib is being tested in stage III or IV refractory or relapsed epithelial ovarian cancer, extra ovarian peritoneal carcinoma, or fallopian tube carcinoma patients.

Alteration in several key kinase pathways during acquirement of chemoresistance can fine tune the autophagic flux in cancer cells which in turn can protect cells against chemotherapeutic stress in several cancers including EOC. Macroautophagy, henceforth denoted as autophagy, is a conserved catabolic process induced by various types of nutritional, pH, hypoxic and chemotherapeutic stress (157). AMPK, a central kinase modulated by metabolic stress promotes chemoresistance in osteosarcoma, gastric cancer and lung adenocarcinoma via upregulation of autophagic flux by inhibition of mTORC1 and activation of ULK1 (10, 13, 14). Activation of PI3K/AKT which in turn activates mTOR promotes a chemoresistant phenotype in EOC, head & neck, breast, endometrial and several other cancers and is well established autophagy suppressor (12, 15, 280, 281). Interestingly, the role of MAPK/ERK1/2 signalling in regulation of autophagic flux is context dependent, activation of MAPK/ERK is shown to positively regulate autophagic flux in chemoresistant gastric, breast and ovarian cancer cells while MAPK/ERK pathway mediated repression of autophagic flux was reported in basal or BRAF inhibitor resistant lung, breast and PDAC cells (11, 176, 282). *Though there are multiple studies which implicates the role of autophagy in promotion of chemoresistance, all these studies described a onetime relation between autophagic flux and chemoresistance and did not evaluate whether an increased autophagic flux is required for both initiation as well as maintenance of chemoresistance or sufficient for one of the either steps.* Thus understanding the role of chemotherapy induced autophagic flux during the process of acquirement of chemoresistance and its modulation by MAPK/ERK and PI3K/AKT pathway would enable us

a better understanding of the molecular process governing the gradual evolution of therapy resistance in ovarian cancer cells in order to design targeting strategies.

Pre-clinical evaluation of any novel drug or novel therapeutic strategy provides the basis for future clinical trials. The development of novel autophagy activators/inhibitors or evaluation the efficacy of known autophagy modulators are somewhat hindered due to lack of assay system to monitor autophagic flux *in-vivo* settings. Autophagy is a dynamic, multi-step process involving the formation of phagophore or isolation membrane which gradually expands and sequesters bulk cargo and ultimately closes to become autophagosome, which then fuses with lysosomes/endosomes to form autophagolysosome leading to the degradation of cargo proteins and organelles. LC3-I to LC3-II conversion by ubiquitin-like protein conjugation system is an indispensable process for autophagosomes formation and is initiated through cleavage of LC3 by cysteine protease Atg4 and the cleaved product is then conjugated with phosphatidylethanolamine by E2-like enzymes Atg 7 and Atg 3 to form LC3-II which then associates with nascent autophagosome membranes (283). The conversion of LC3-I to LC3-II serves as a marker of induction of autophagic flux while the fusion of autophagosome with lysosome and subsequent degradation of the sequestered cargo marks the end point of autophagic process and is characteristically detected by degradation of autophagy adaptors like Sequestosome-1 or p62 (284, 285). This dynamicity in autophagic flux involving autophagosome formation and autophagosome lysosome fusion is classically monitored in real time utilizing various fluorescent based LC3 sensors (GFP-LC3, mCherry-GFP-LC3 and GFP-LC3-RFP-LC3 Δ G) by live cell imaging (186, 191, 286). However, application of these fluorescent based autophagy sensors in non-invasive *in vivo* imaging of mouse models are severely limited due to auto-fluorescence, tissue penetration and signal attenuation of fluorescent reporter. Utilization of Luciferase based probes can circumnavigate these limitations and proficiently be applied for non-invasive real-time monitoring of autophagic flux in pre-clinical

animal models (287, 288). Currently, only poly80/poly19-FL2 luciferase based autophagy sensor has been utilized for ratometric estimation of real-time autophagic flux *in vivo*, adaptation of this sensor for assessing the autophagy kinetics in a high-throughput manner is however difficult. Autophagy independent degradation of the poly80 repeats and FL2 further complicates the estimation of autophagy flux (192-194). Thus there is a persistent need to develop an *in vivo* autophagy sensor which can dynamically monitor the progression or stalling of autophagic flux in response to various autophagy modulators and/or chemotherapeutic drug non-invasively in pre-clinical mouse models.

Utilizing the dynamic model of cisplatin-paclitaxel dual resistance we aimed to understand the modulation in ERK1/2 and AKT signaling arms during gradual acquirement of chemoresistance. We further evaluate the role of ERK1/2 in regulation of therapy induced autophagic flux to promote onset of therapy resistance. Utilizing a novel autophagy sensor, we assessed the efficacy of ERK1/2 targeted therapies in modulation of autophagic flux and development of platinum-taxol resistance.

2.2 Methodology

2.2.1 Development of chemoresistant model

Cisplatin-paclitaxel dual resistant A2780 and OAW42 cellular models were established by treatment of cells with incremental doses of platinum-taxol for a period of 6 months (5). At each stage of resistance development cells were treated with platinum-taxol for 2 hours, following which cells were allowed to recover to 80-90 % confluency in absence of drug. The drug concentration was kept fixed for 3 cycles following which an increased concentration was applied for three successive cycles. The process was continued till acquirement of a highly resistant (~90% viable at IC₅₀ of sensitive sells) phenotype (Figure 18). Based upon resistance

index, cells were categorized into early resistant (Dual^{ER}), i.e cells at the onset of chemoresistance (5 times higher than IC₅₀ of sensitive cells) and late resistant (Dual^{LR}), i.e cells that achieved a highly resistant phenotype (10 times higher than IC₅₀ of sensitive cells) (287).

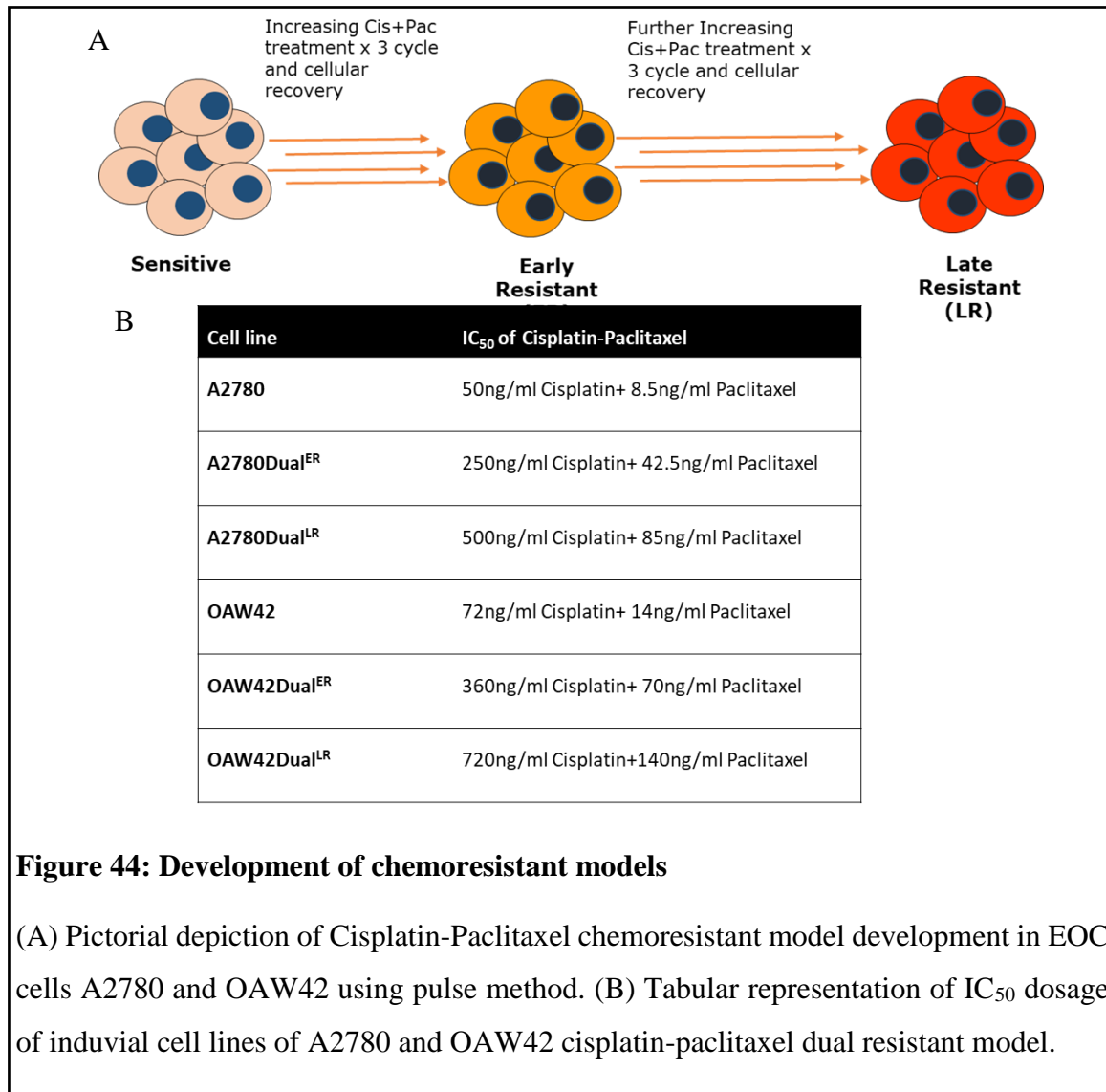


Figure 44: Development of chemoresistant models

(A) Pictorial depiction of Cisplatin-Paclitaxel chemoresistant model development in EOC cells A2780 and OAW42 using pulse method. (B) Tabular representation of IC₅₀ dosage of individual cell lines of A2780 and OAW42 cisplatin-paclitaxel dual resistant model.

2.2.2 Immunoblotting

Immunoblotting for Phospho/total ERK, phospho/total AKT, phospho/total p90^{RSK1/2}, Fra-1, LC3B, p62, cleaved PARP, UVRAG, Rubicon, Rab7 was performed from whole cell lysate as

elaborated in section 5. Images were captured in chemidoc (Biorad) and quantified using Image J software (NIH) as described in section 6.5.

2.2.3 Transmission electron microscopy

TEM images were captured for A2780 and OAW42 chemoresistant model post treatment with either cisplatin-paclitaxel alone or in combination with U0126, a MEK1/2 inhibitor for quantitation of autophagic flux. Cell pellets were processed electron microscopy and images were capture on JEOL 1400 plus transmission electron microscope operated at 120 kV as described in section 6.6.

2.2.4 Confocal and immunofluorescence microscopy

Chemotherapy induced autophagic flux was measured monitored in cells expressing puro-mCherry-EGFP-LC3 plasmid post treatment with cisplatin-paclitaxel either alone or in combination with U0126 by confocal microscopy as described in section 6.7.1. The data was analysed to determine the extent of mCherry-EGFP colocalization in terms of Mander's colocalization coefficient and mCherry/EGFP ratio as described in detail in section. LC3 and LAMP1 dual immunostaining was performed to estimate number, size and volume of autophagosome (LC3^{+ve} puncta) and autophagolysosome (LC3^{+ve}LAMP1^{+ve} puncta) as described in section 6.7.2.

2.2.5 Generation of firefly luciferase/mutant thermostable firefly luciferase-p62 fusion construct (Fl-p62/ mtFL-p62)

GFP-p62 plasmid, purchased from Addgene, deposited by Dr.Noboru Mizushima. The p62 CDS was first cloned at EcoR1 site of pcDNA3.1+. The mtFL or FL gene was inserted upstream of p62 using Nhe1 and Hind III restriction enzymes to generate pCMV-mtFL-p62 or pCMV-FL2-p62 fusion construct.

2.2.6 ERK1 silencing by lentiviral mediated sh-RNA constructs

Lentiviral knockdown of ERK1 was performed as described in section 5 using a target sequence against ERK1 (5'-GACCGGATGTTAACCTTTA-3') [71, 72]. Constructs were verified by restriction digestion and sequencing. Lentivirus particles were produced in HEK293FT and transduced in A2780Dual^{ER} cells. Stable cells expressing ShERK1 construct were FACS sorted using eGFP as a marker using protocol described in section 6.12.

2.2.7 Apoptosis detection with Annexin/PI

Classical Annexin V and PI dual staining was performed in order to detect necrotic, early apoptotic and late apoptotic population in A2780Dual^{ER} and OAW42Dual^{ER} cells post treatment with Cisplatin-Paclitaxel, Trametinib and Cisplatin-Paclitaxel+Trametinib for 12 and 24 hours as per detailed protocol in section 6.8.1. Flow cytometric assessment of each group was performed in Attune NxT Flow cytometer and data analysis was performed using FlowJo version 10 software.

2.2.8 Real-time cell death assessment using CellToxTM

CellToxTM assay is based on the principle of passive uptake of dye by dead cells, which upon entering dead cells interacts with their DNA to generate fluorescence signal. The cytotoxic effect of Cisplatin-Paclitaxel, Trametinib and Cisplatin-Paclitaxel+Trametinib was quantified in terms of fluorescent signal emitted by dead cell population in A2780Dual^{ER}. The detailed staining procedure is described in section 6.4.2. The fluorescence signal was measured for 56 hours at an interval of every 6 hours in Biotek cytation5 imaging system using 485-500 nm excitation filter and 520-530 nm emission filter.

2.2.9 Cell viability assay

Cell viability assay was performed by standard thiazolyl blue tetrazolium bromide method as described in section 6.4.1.

2.2.10 Generation of stable clones expressing

A2780Dual^{ER} cells stably expressing mCherry-EGFP-LC3 or mtFL-p62 was generated against puromycin or G418 selection respectively as described in detail in section 6.3.7.

2.2.11 Luciferase assay

Luciferase assay was performed in chemoresistant cells of A2780 and OAW42 model transiently or stably transfected with mtFL-p62, FL-p62 along with pCMV-Renilla luciferase for normalization as described in section 6.9. All transfection experiments were performed in triplicates and repeated thrice.

2.2.12 Live-cell imaging

Live cell imaging was in chemoresistant cells stably expressing mtFL-p62 performed as described in section 6.10 and using IVIS spectrum imaging system (Perkin-Elmer). Bioluminescence signals were quantified using the Live Image (4.4) software.

2.2.13 *In-vivo* imaging

Tumor xenograft model of A2780Dual^{ER} cells stable clones expressing mtFL-p62 construct were generated by subcutaneous injection in female CD1-NUDE mice as described in section 6.16. These animals were divided into six groups having 8 mice in each group and followed for 15 days to monitor dynamic modulation in autophagic flux. The animals were monitored for further 10 days to assess the effect of each line of therapy in tumors growth. **Group-I: Untreated**, **Group-II: CisPac**, treated with 2mg/kg of Cisplatin and 1mg/kg-Paclitaxel thrice on day 1, day 7 and day 13 **Group-III: Trametinib**, a therapeutically relevant and FDA approved MERK1/2 inhibitor was administered daily at dosage of 1mg/kg for 15 days and **Group-IV: Chloroquine**, a well-established lysosomal inhibitor administered daily at dosage of 40mg/kg for 15 days **Group-V: Trametinib+Cisplatin-paclitaxel**, combinatorial treatment

of Trametinib (1mg/kg, daily for 15 days) along with cisplatin-paclitaxel on 1st, 7th and 12th day and **Group-VI:** CisPac+Chloroquine, combinatorial treatment of chloroquine (40mg/kg, daily for 15 days) along with platinum-taxol on 1st, 7th and 12th day. Each drug or drug combinations were intraperitoneally injected. Bioluminescence imaging of autophagic flux was performed on alternate days following intraperitoneal D-luciferin (30mg/kg) injection in Xenogen-IVIS imaging systems. Images were processed and analysed using Living Image software 4.4.

2.2.14 Statistical analysis

All experiments have been performed at least and represented as mean \pm SEM. For determination of statistical significance unpaired student's t-Test was performed with exception of *in vivo* experiments, which were analyzed using two way ANOVA. A p-value cut-off of less than 0.05 was considered to be significant and represented by *. P value of less than 0.005 was represented by ** and *** represents a P value of less than 0.0005. The term “ns” represents statistically non-significant change.

2.3 Results:

2.3.1 ERK1/2 activation predominates in the onset of therapy resistance

To investigate whether ERK1/2 and AKT activation are differentially modulated during gradual acquirement of cisplatin-paclitaxel dual resistant model, we estimated the basal as well as cisplatin-paclitaxel (CisPac) induced level of phospho ERK1/2 and AKT in our indigenously established cellular models of platinum-taxol resistance developed by treating A2780 and OAW42 EOC cells with incremental doses of both drugs for a period of six months. These chemoresistant cells were classified into sensitive, early (onset of resistance; A2780Dual^{ER} or OAW42Dual^{ER}) and late (stabilized resistance: A2780Dual^{LR} or OAW42Dual^{LR}) resistant cells

based on their resistant indices. The Dual^{ER} cells showed 5 times higher resistance index while the Dual^{LR} cells had 10 times higher resistance index than their sensitive parental counterpart. The basal level of phosphorylated ERK1/2 was highest in A2780Dual^{ER} cells compared to the A2780 and A2780Dual^{LR} cells which did not enhance further after drug treatment, while, the A2780 and A2780Dual^{LR} showed increased ERK1/2 phosphorylation post drug treatment indicating. A similar pattern of basal and drug induced ERK1/2 activation was also observed in the OAW42 chemoresistant model. Interestingly, the Dual^{ER} cells also showed increased basal level of two downstream targets of ERK1/2, the phospho p90^{RSK1/2} and the Fra-1 (Figure 19A-B and 20 A-B). Increased nuclear localization of pERK was specifically evident in the A2780Dual^{ER} cells in comparison to the sensitive and late resistant cells, altogether indicating a hyperactive ERK1/2 signalling specifically in the early stage of resistance (Figure 19C-D). Knocking down of IGF1R expression in the early stage of resistance specifically reduced the level of p-ERK1/2 in comparison to parental counterpart, indicating an increased IGF1R expression activates ERK1/2 in these cells (Figure 19E and 20 E-F). To test the dependency of Dual^{ER} cells on the activated ERK1/2 signalling, we inhibited ERK1/2 activation using U0126 (10 μ M), a MEK1/2 inhibitor and its cytotoxic effects alone or in combination with platinum-taxol were measured. An additive cytotoxic effect was observed specifically in A2780Dual^{ER} cells (26.15%) and OAW42Dual^{ER} cells (23.28%) on combinatorial treatment compared to CisPac or U0126 alone (Figure 19F-G). In comparison to the increased ERK1/2 activation in the Dual^{ER} cells, basal activation of AKT was highest in the Dual^{LR} cells in comparison to the Dual^{ER} and sensitive cells of both A2780 and OAW42 model. When cells of various stages of resistance were challenged with drugs, slight increase in AKT activation was observed only in ER but not in the LR cells that possess maximum level of phospho-AKT (Figure 19A-B and 20C-D).

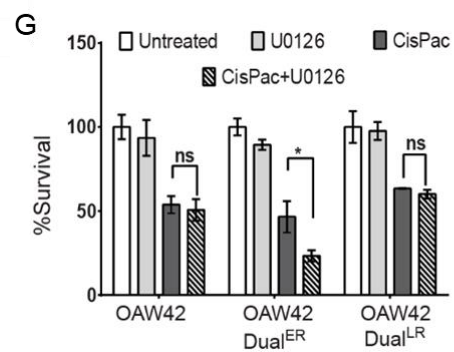
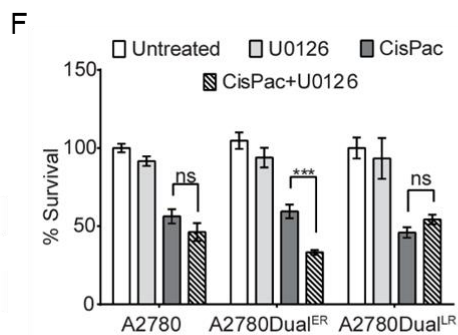
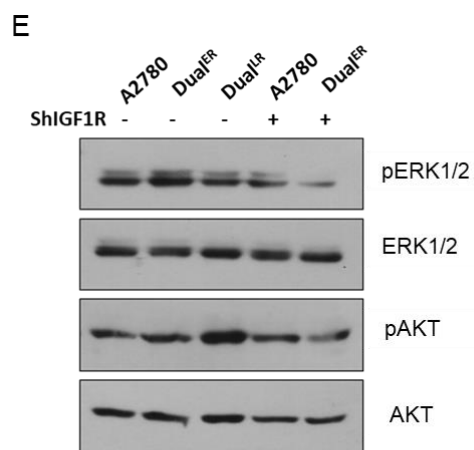
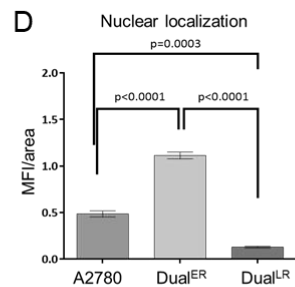
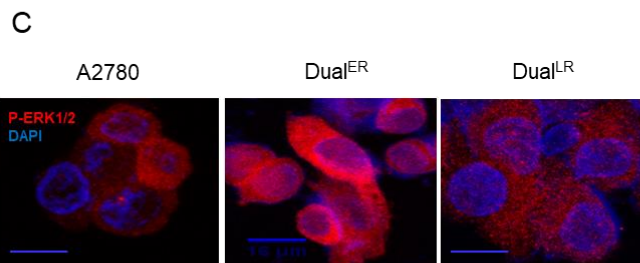
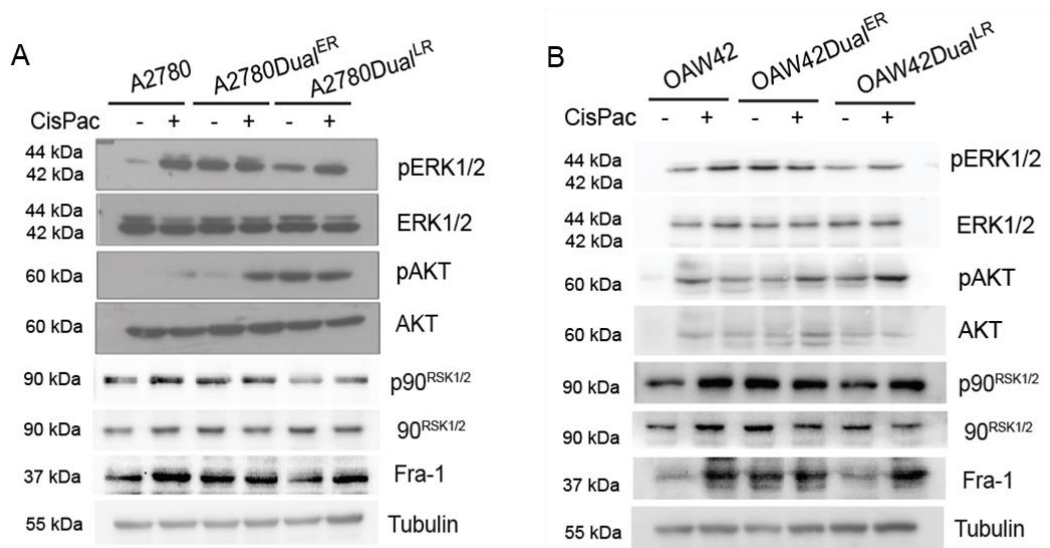


Figure 19: Basal ERK1/2 activation peaks during the onset of platinum-taxol dual resistance

(A-B) Immunoblot depicting increased basal level of phospho ERK1/2, p90^{RSK1/2} and FRA-1 in A2780Dual^{ER} and OAW42Dual^{ER} cells compared to sensitive and Dual^{LR} cells of both model, on the other hand Dual^{LR} cells of both model showed maximal basal level of AKT phosphorylation in comparison to sensitive and Dual^{ER} cells (C) Representative immunofluorescence microscopy image depicting increased nuclear localization of pERK1/2 in the Dual^{ER} cells (scale 16µm) (D) Quantification of nuclear localization of pERK1/2, highest mean fluorescence intensity (MFI) was observed in Dual^{ER} cells. (E) Immunoblotting analysis revealed a significantly reduced pERK1/2 level in Dual^{ER} while pAKT level did not alter significantly post IGF1R knockdown (F-G) Graph representing an additive cytotoxic effect of combinatorial treatment of Cisplatin-Paclitaxel and U0126 (CisPac+U0126) over only Cisplatin-Paclitaxel (CisPac) administered at IC50 dosage and only U0126 in A2780Dual^{ER} and OAW42Dual^{ER} cells

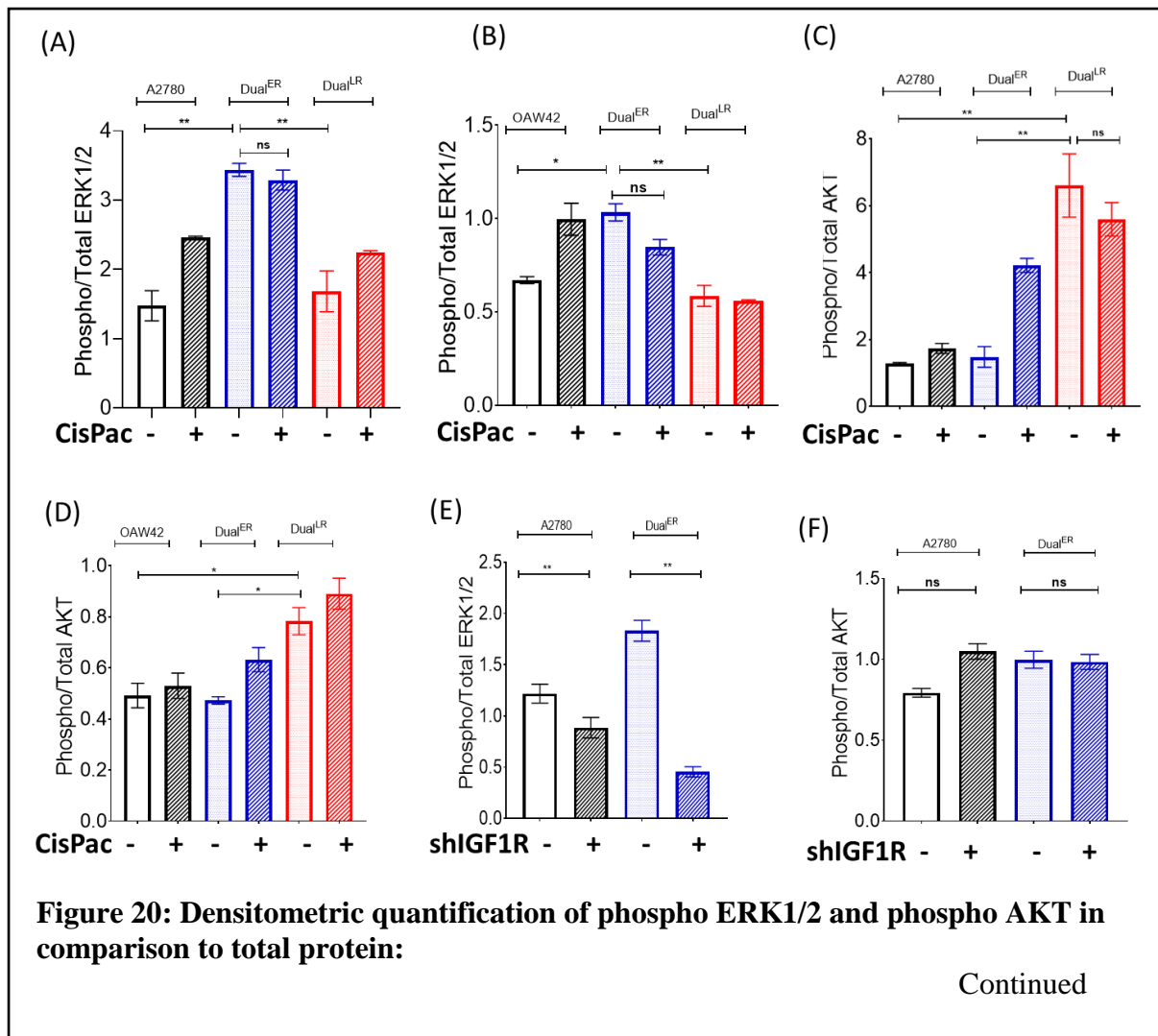


Figure 20: Densitometric quantification of phospho ERK1/2 and phospho AKT in comparison to total protein:

Continued

(A-B) Graph representing increased ratio of phospho ERK1/2 to total ERK1/2 was observed in Dual^{ER} cells in comparison to sensitive and Dual^{LR} cells of both A2780 and OAW42 model. (C-D) Graph representing increased ratio of phospho AKT to total AKT was observed in Dual^{LR} cells in comparison to sensitive and Dual^{ER} cells of both A2780 and OAW42 model. (E-F) IGF1R knockdown specifically reduced ratio of phospho to total ERK1/2 ratio in Dual^{ER} while no significant alteration in phospho to total AKT ratio was observed.

2.3.2 Autophagic flux remains upregulated at the early stage of platinum-taxol dual resistance

In order to investigate the role of autophagy during initiation or in maintenance of chemoresistance we treated sensitive, Dual^{ER} and Dual^{LR} cells with a very high dosage (10 times the respective IC₅₀) of platinum-taxol for 12 and 24 hour. CisPac treatment showed increased LC3 I-II conversion in sensitive (A2780 and OAW42) and Dual^{ER} (A2780Dual^{ER} and OAW42Dual^{ER}) cells at 12 and 24 hours by immunoblotting while similar treatment led to minimal LC3 I-II conversion in Dual^{LR} cells of both models (Figure 21A-B). Enhanced LC3II/LC3I ratio [1.39±0.04 (0hr) to 1.96±0.15 (12hr) to 2.42±0.08 (24hr)] and [1.03±0.12 (0hr) to 1.6±0.05 (12hr) to 1.9±0.19 (24hr)] were observed (average of three immunoblots) in CisPac treated A2780 and A2780Dual^{ER} cells respectively. There was no significant change in LC3II/LC3I ratio in A2780Dual^{LR} cells. A similar trend in LC3II/LC3I ratio was observed in OAW42 chemoresistant model (Figure 21C, E). p62 degradation, which marks the completion of autophagy, was most evident specifically in A2780Dual^{ER} and OAW42Dual^{ER} cells post 24 hours of CisPac treatment and was quantified by the reduction in p62/tubulin ratio [1.39±0.09 (0hr) to 0.63±0.06 (24hr) in A2780Dual^{ER}] and [1±0.08 (0hr) to 0.23±0.05 (24hr) in OAW42Dual^{ER}]. However, changes in p62 level in sensitive and Dual^{LR} cells were found to be non-significant (Figure 21A-B, D, F). Chloroquine (10µM) along with CisPac treatment led to highest change in LC3 conversion and p62 stabilization in A2780Dual^{ER} cells compared to A2780 and A2780Dual^{LR} cells, indicating maximal autophagic flux in these cells (Figure 21G-D).

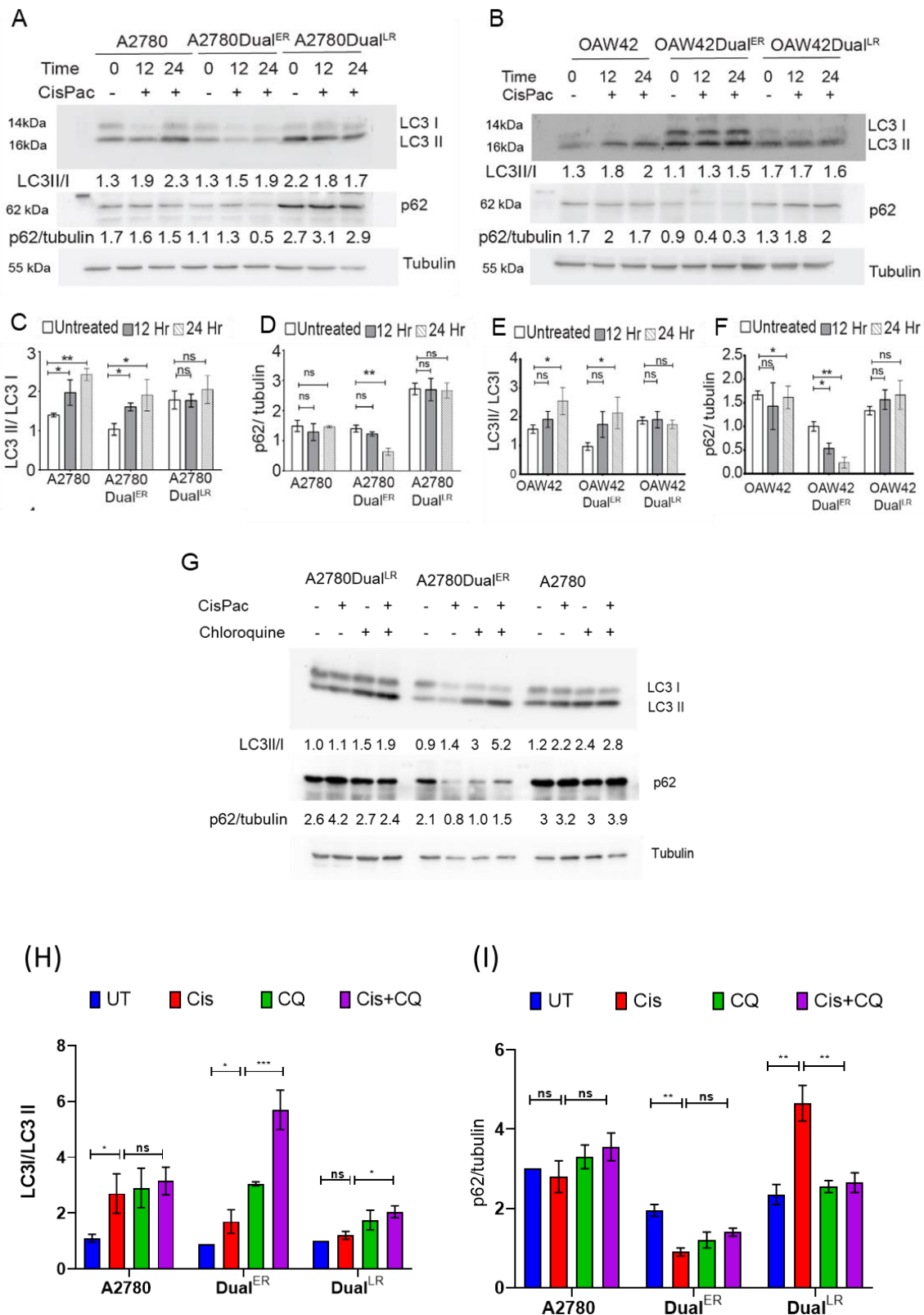


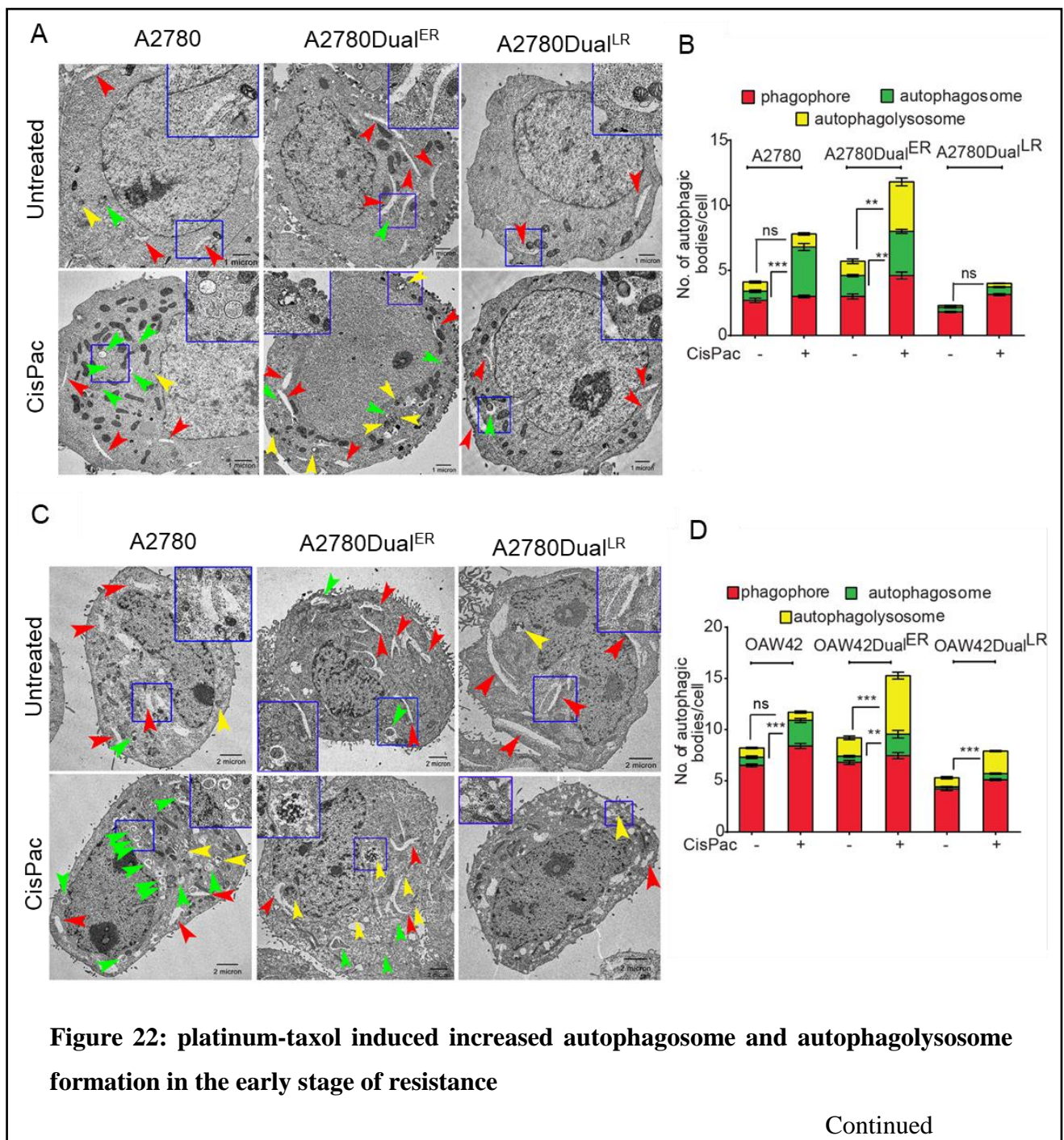
Figure 21: platinum-taxol induced autophagic flux remains high at the early stage of resistance

continued to next page

(A-B) Immunoblot depicting cisplatin-paclitaxel induced increased LC3 I-II conversion and p62 degradation specifically in A2780Dual^{ER} and OAW42Dual^{ER} cells while sensitive cells showed increased LC3I-II conversion without significant p62 degradation compared to respective untreated cells. Dual^{LR} cells of both models showed significantly reduced LC3 I-II conversion and p62 degradation in comparison to its untreated counterpart. (C-F) Graph representing significantly increased LC3 II/LC I ratio and reduced p62/tubulin ratio in the Dual^{ER} cells of both models as quantified from 3 independent immunoblotting experiments (G) Immunoblot depicting highest differences in LC3I-II conversion and p62 accumulation in A2780Dual^{ER} cells treated with CisPac in presence and absence of chloroquine (CQ) compared to sensitive and A2780Dual^{LR} cells (H-I) Graph representing significantly increased LC3 II/LC I ratio and reduced p62/tubulin ratio in the A2780Dual^{ER} cells compared to A2780 and A2780Dual^{LR} cells

Transmission electron microscopy (TEM) is a classical method to monitor autophagic flux through identification of distinct autophagic bodies (phagophore, autophagosome and autophagolysosome) present at the initiation, maturation and degradation steps of autophagic process. TEM analysis revealed differential number of autophagic structures in sensitive, early and late resistant A2780 and OAW42 cells upon chemotherapeutic insult. The total number of autophagic bodies were found to be significantly higher in A2780Dual^{ER} ($12 \pm 1.39/\text{cell}$) compared to A2780 ($8 \pm 1.10/\text{cell}$) and A2780Dual^{LR} ($3 \pm 0.59/\text{cell}$) cells after CisPac treatment (Figure 22A, B). Similarly, the numbers of autophagic bodies in the OAW42Dual^{ER} cells ($15 \pm 1.11/\text{cell}$) were higher than the OAW42 ($12 \pm 1.02/\text{cell}$) and OAW42Dual^{LR} ($8 \pm 0.58/\text{cell}$) after chemotherapeutic challenge (Figure 22C, D). When each of the autophagic bodies were analysed and compared amongst sensitive, Dual^{ER} and Dual^{LR} cells post drug treatment, a sharp increase in both autophagosomes (2.1 and 3.4 fold respectively) as well as autophagolysosomes (3.4 and 3.2 fold respectively) number were found in A2780Dual^{ER} and OAW42Dual^{ER} cells indicating a continued autophagic flux while increase in only autophagosomes in A2780 (5.3

fold) and OAW42 (3.1 fold) cells without any change in autophagolysosome number indicated a blockade in completion of autophagic flux (Figure 22B, D). A minimal increase in the number of phagophore, autophagosomes and autophagolysosomes in both A2780Dual^{LR} and OAW42Dual^{LR} cells suggested a low level of autophagy (Figure 22B, D). Overall, these data conclusively suggest that the chemotherapy induced autophagic flux remains high specifically at early stage of resistance and then decrease as cells acquire maximal resistant stage.



(A, C) Representative electron microscopy images of sensitive, Dual^{ER} and Dual^{LR} cells of A2780 and OAW42 chemoresistant model pre and post 24 hours of cisplatin-paclitaxel treatment. Red arrow represents phagophore, green arrow represents autophagosome and autophagolysosomes are indicated by yellow arrow (scale 1 μ m for A2780 model and 2 μ m for OAW42 model) (B, D) Graph representing the number of individual and total autophagic structure pre and post platinum-taxol treatment. A significant increase in number of both autophagosome and autophagolysosome was observed in Dual^{ER} cells while sensitive cells

2.3.3 Activated ERK1/2 promotes autophagic flux at onset of platinum-taxol resistance

The basal level of phosphorylated ERK1/2 was highest in A2780Dual^{ER} and OAW42Dual^{ER} cells compared to sensitive and Dual^{LR} cells, which did not enhance further after drug treatment. Contrarily, the sensitive and Dual^{LR} cells of both models showed increased ERK1/2 phosphorylation but not enhanced autophagic flux post drug treatment indicating that the basal level of activated ERK might be a molecular regulator of autophagy. We reasoned that the high basal level of ERK1/2 may play a role in maintaining active autophagic flux and thus effect of both pharmacological and genetic inhibition of ERK were assessed. While CisPac treatment alone led to LC3 I-II conversion and p62 degradation, addition of U0126 resulted in higher LC3 I-II conversion and p62 accumulation at 12 and 24 hours in both the A2780Dual^{ER} and OAW42Dual^{ER} cells (Figure 23A-B and 24A-D). To investigate the role of ERK1/2 in regulation of autophagic flux, we administered combinatorial treatment of chloroquine (CQ, a lysosomal inhibitor) along with CisPac and U0126 which, however, did not further supplement the increased LC3 and p62 accumulation observed upon CisPac+U0126, treatment, while addition of chloroquine along with CisPac significantly upregulated LC3 conversion and p62 level in comparison to cells treated with only CisPac, indicating that inhibition of ERK1/2 activation blocks the late stage of autophagy (Figure 23C and 24E-F). To further confirm the

above observation was not U0126 specific, we replaced U0126 with Trametinib (10 nM), another ERK1/2 inhibitor, which showed similar changes in LC3 and p62 accumulation in presence of CisPac alone or in combination with CQ (Figure 23D and 24E-F).

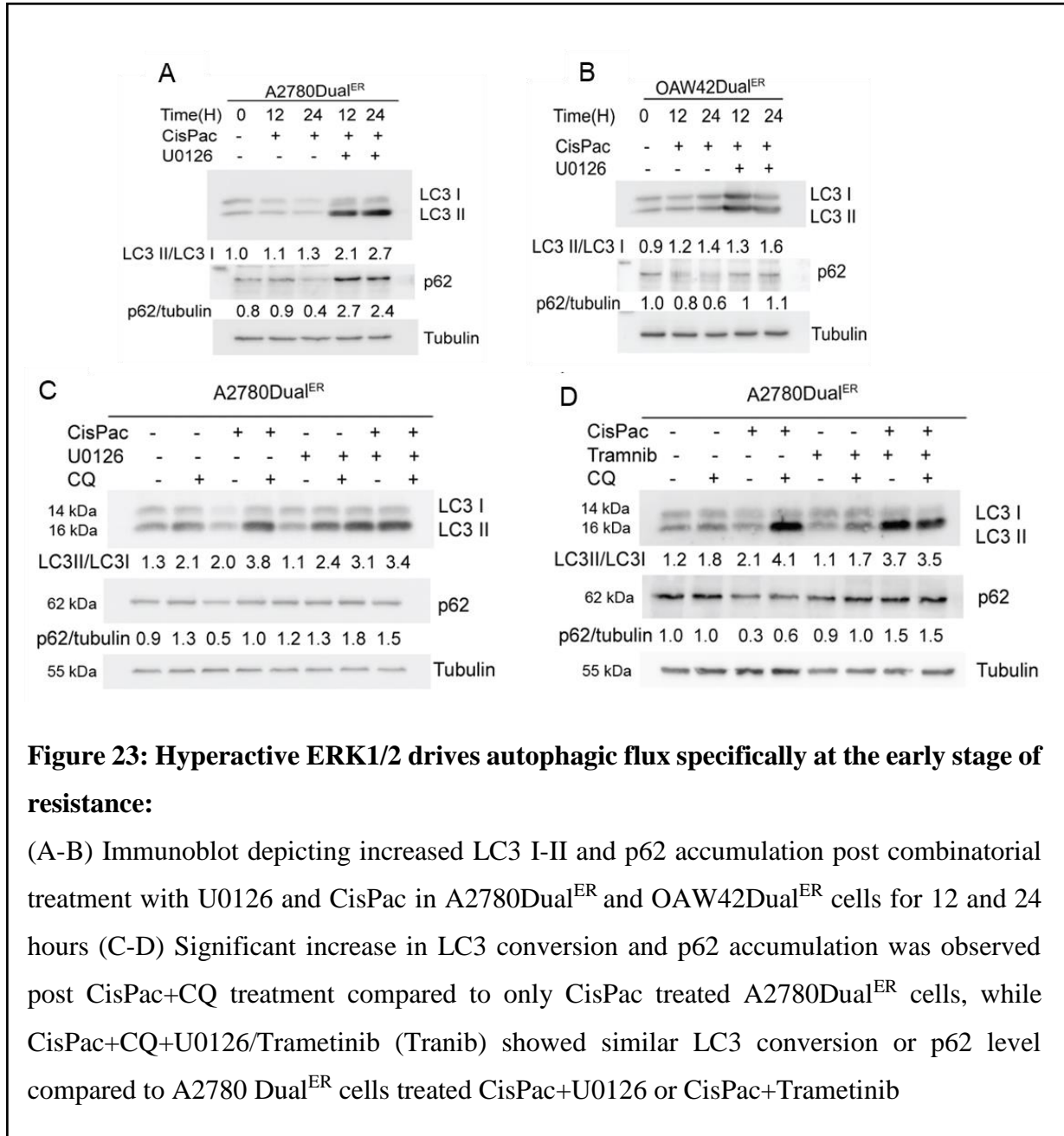


Figure 23: Hyperactive ERK1/2 drives autophagic flux specifically at the early stage of resistance:

(A-B) Immunoblot depicting increased LC3 I-II and p62 accumulation post combinatorial treatment with U0126 and CisPac in A2780Dual^{ER} and OAW42Dual^{ER} cells for 12 and 24 hours (C-D) Significant increase in LC3 conversion and p62 accumulation was observed post CisPac+CQ treatment compared to only CisPac treated A2780Dual^{ER} cells, while CisPac+CQ+U0126/Trametinib (Tranib) showed similar LC3 conversion or p62 level compared to A2780 Dual^{ER} cells treated CisPac+U0126 or CisPac+Trametinib

To assess the precise effect of ERK1/2, lentiviral mediated knock down of ERK was carried out in the A2780Dual^{ER} cells. The efficiency of ERK knockdown was estimated based on the

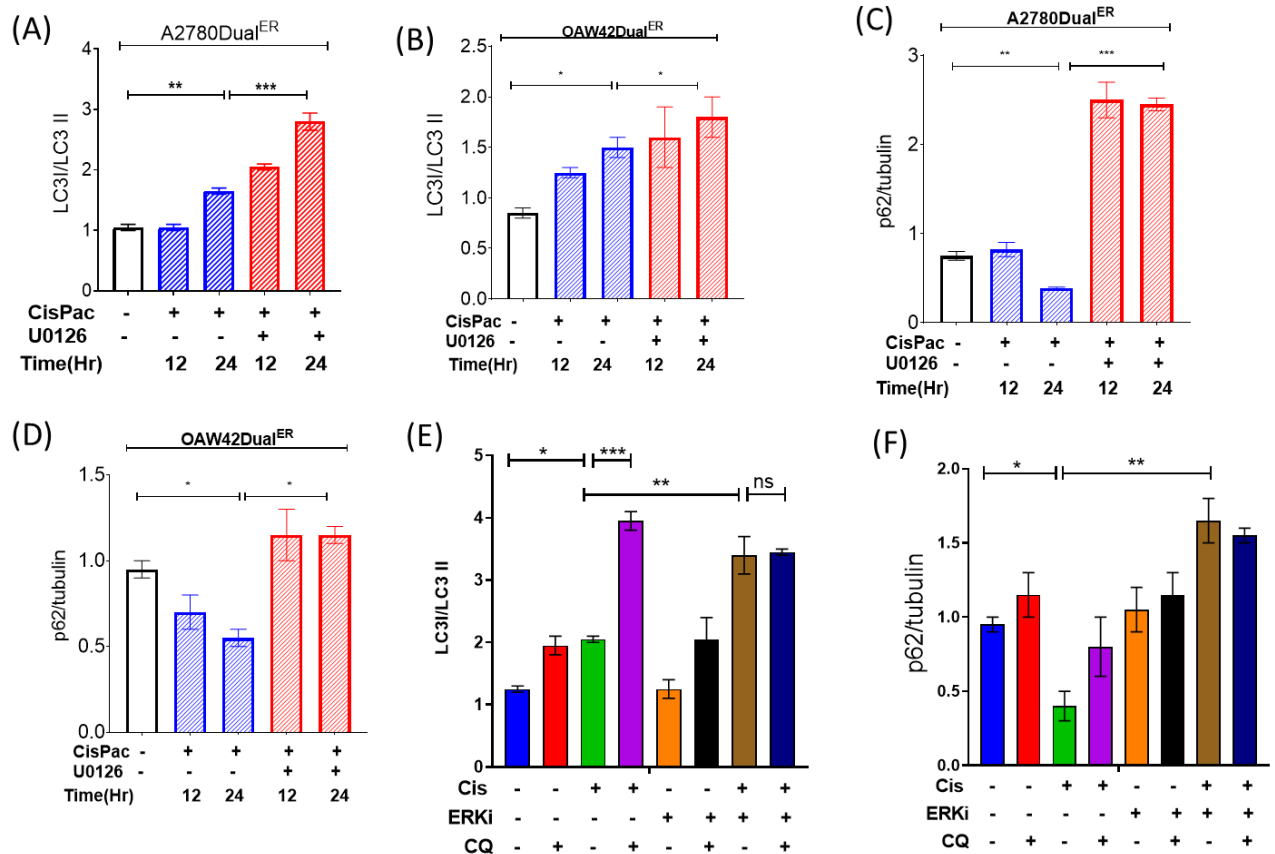
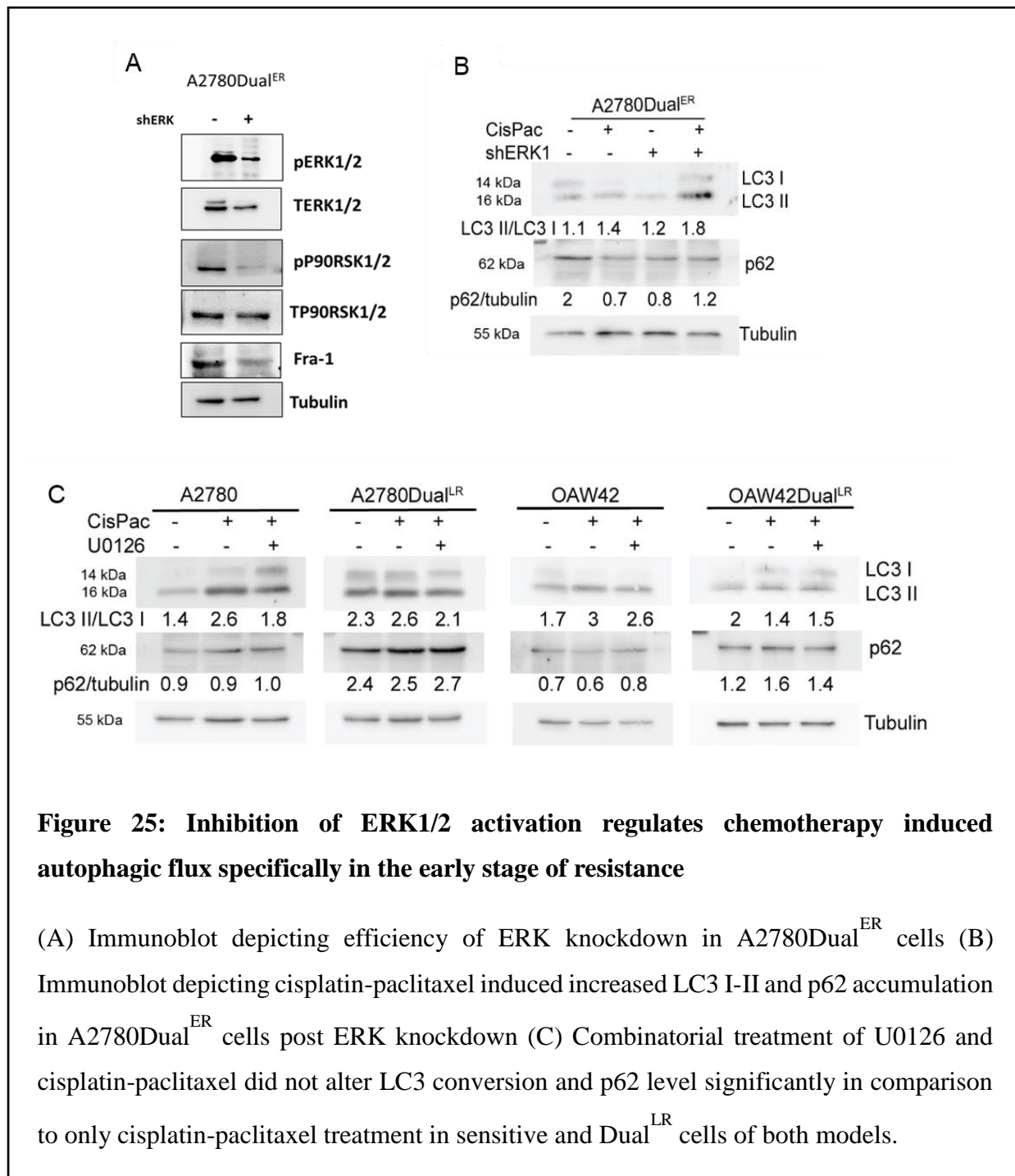


Figure 24: Densitometric quantification of LC3II conversion and p62 degradation

(A-B) Graph representing increased LC3II/LC3I ratio post combinatorial treatment with U0126 and CisPac in A2780Dual^{ER} and OAW42Dual^{ER} cells for 12 and 24 hours (C-D) Graph representing reduced p62/tubulin ratio post CisPac treatment which increases significantly post combinatorial treatment with U0126 and CisPac in A2780Dual^{ER} and OAW42Dual^{ER} cells for 12 and 24 hours (E-F) Graph representing a significant increase in LC3 conversion and p62 accumulation was observed post CisPac+CQ treatment compared to only CisPac treated A2780Dual^{ER} cells, while CisPac+CQ+U0126/Trametinib showed similar LC3 conversion or p62 level compared to A2780 Dual^{ER} cells treated CisPac+U0126 or CisPac+Trametinib

reduction in level of phospho ERK1/2 and its downstream targets p90^{RSK1/2} and FRA-1 (Figure 25A). CisPac treatment in A2780Dual^{ER/ERK1-} cells increased accumulation of both LC3I-II and p62 compared to A2780Dual^{ER/ERK+} cells (Figure 25B and 26A-B). Chemical inhibition of ERK1/2 activation along with CisPac in A2780 and A2780Dual^{LR} cells did not show any significant changes in LC3I-II conversion or p62 level than their drug treated counterparts. A similar trend was observed in OAW42 and OAW42Dual^{LR} cells suggesting

that the basal level rather than therapy induced activated ERK1/2 regulates completion of autophagy particularly at the onset of resistance development (Figure 25C and 26C-D).



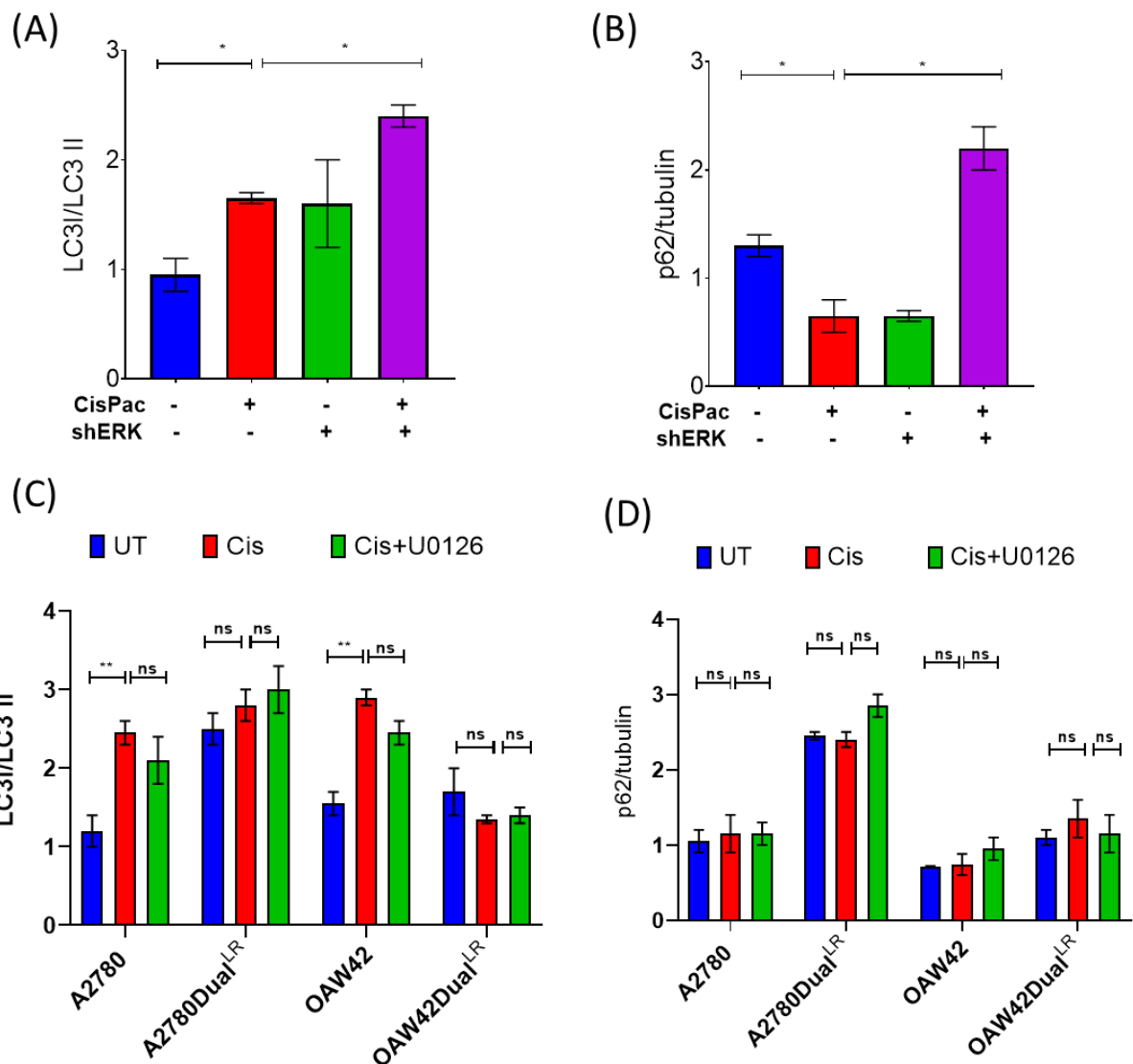
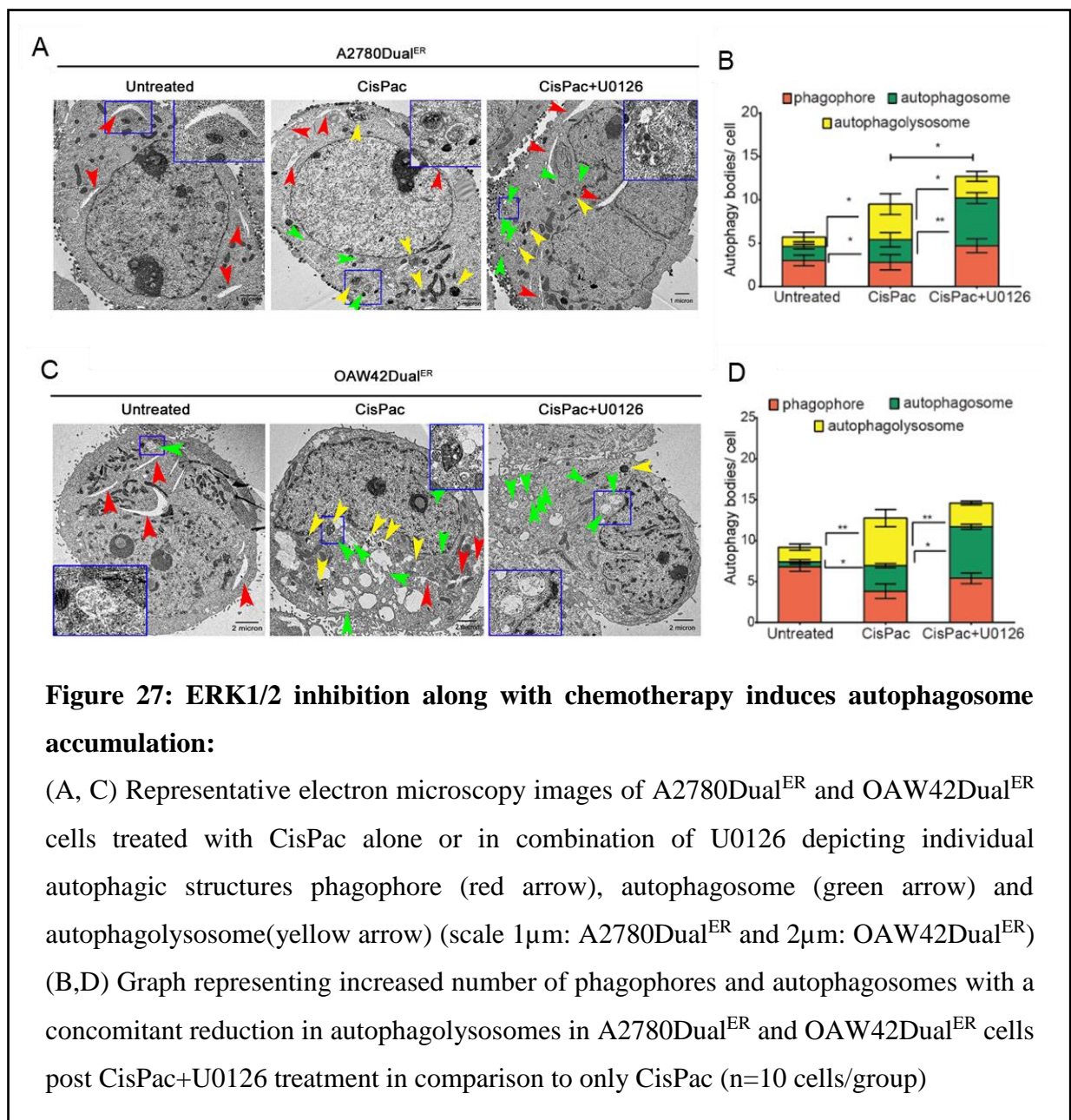


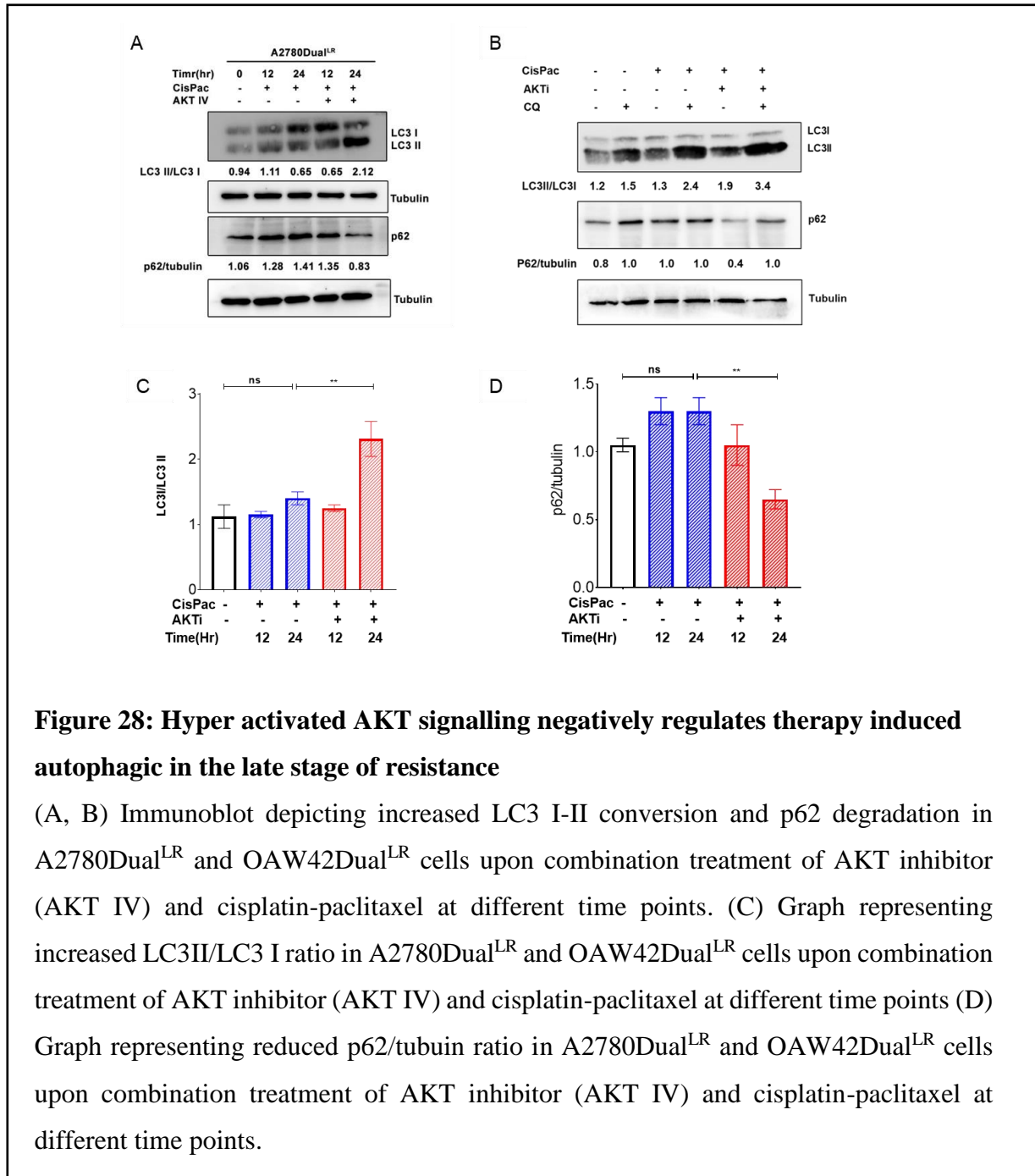
Figure 26: Densitometric quantification of LC3II conversion and p62 degradation

(A) Graph representing a significant increase in CisPac induced LC3II/LC3I ratio post ERK Knockdown (B) Graph representing cisplatin-paclitaxel induced increased p62/tubulin ratio post ERK knockdown in comparison to wild type Dual^{ER} cells (C-D) Combinatorial treatment of U0126 and cisplatin-paclitaxel did not significantly alter LC3II/LC3I and p62/tubulin ratio in comparison to only cisplatin-paclitaxel treatment in sensitive and Dual^{LR} cells of both models.

We reasoned if basal level of ERK1/2 activation is crucial for the autophagosome-lysosome fusion, then the ER cells would show maximum level of defective autophagy upon ERK1/2 inhibition. Indeed, evaluation of autophagic bodies by TEM revealed a 1.67 fold increase in phagophores, and a 2.1 fold increase in autophagosomes with a concomitant reduction (0.6 fold) in autophagolysosomes in A2780Dual^{ER} cells subjected to combinatorial treatment of U0126 and CisPac in comparison to only platinum-taxol (Figure 27A-B). In OAW42Dual^{ER} cells, 0.5 fold reduction in autophagolysosomes with 1.44 fold increase in phagophores and 2.1 fold increase in autophagosomes were observed post combinatorial treatments (Figure 27C-D).



Absence of a positive correlation between drug induced autophagic flux with augmenting resistance in our models was intriguing. AKT, a negative regulator of autophagy is found to be gradually activated with increasing resistance in these models (5, 289). Combinatorial treatment of an AKT inhibitor with the drugs induced higher LC3I-II conversion and p62 degradation in these A2780Dual^{LR} cells (Figure 28A-D).

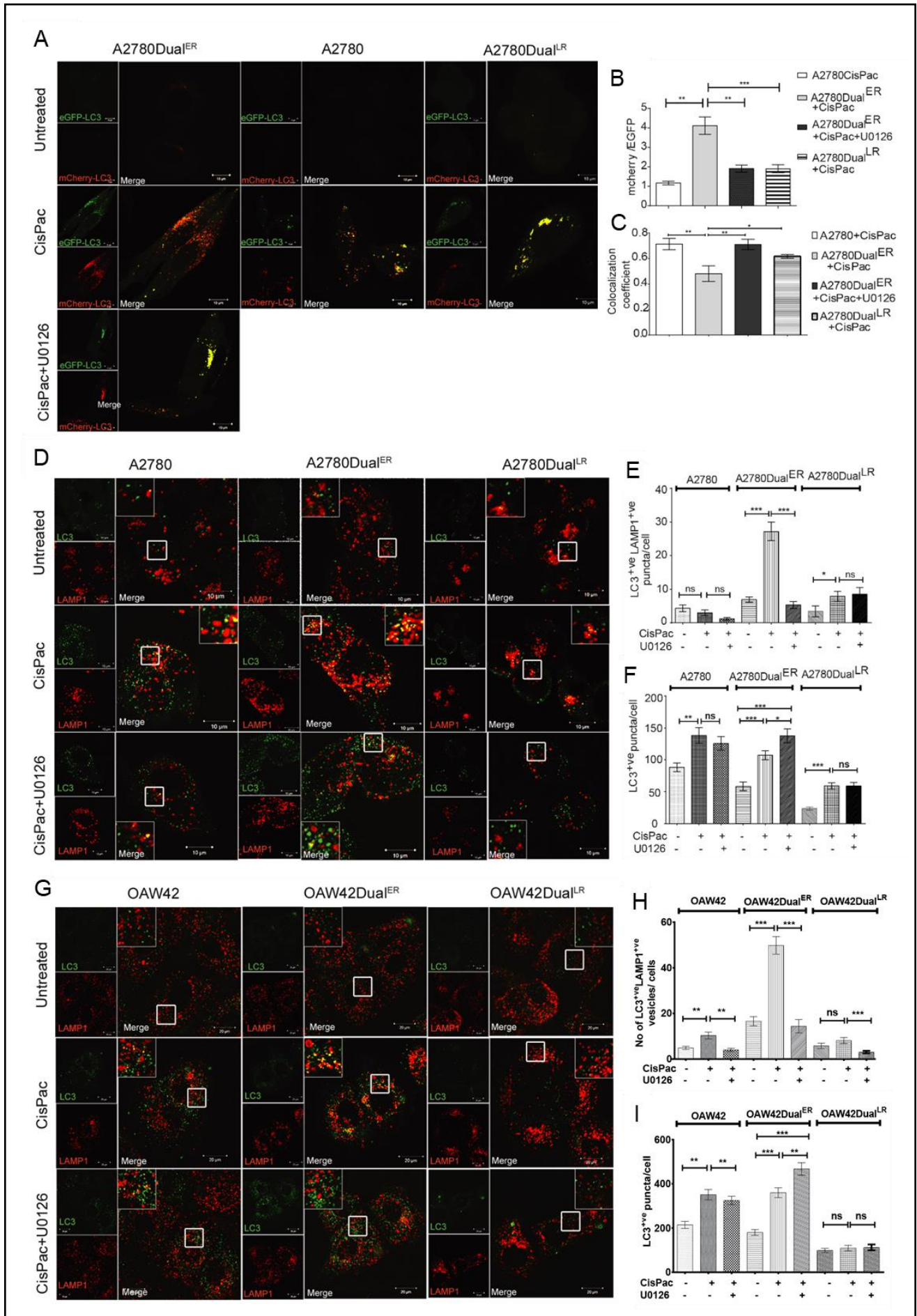


2.3.4 Activated ERK 1/2 kinase regulates autophagosome–lysosome fusion

Proper completion of autophagy pathway requires the fusion of autophagosome with lysosomes leading to degradation of the damaged and internalized biomolecules along with the cargo proteins which when blocked by chemical or genetic manipulation adversely affect cellular homeostasis (290). In order to understand whether ERK1/2 plays any role in autophagosome maturation and its subsequent fusion to lysosome, we utilized the classical

Figure 29: ERK1/2 inhibition abrogates autophagolysosome formation in the early stage of resistance development

(A) Representative images of sensitive, early and late resistant cells of A2780 model expressing mCherry-EGFP-LC3 treated with CisPac alone or CisPac+U0126. Co-localized mcherry and EGFP puncta depicting autophagosome are highlighted as yellow, while autophagolysosomes are indicated by isolated red puncta. CisPac treatment increased the number of red puncta in A2780Dual^{ER} cells, which reduced significantly post CisPac+U0126 treatment. Increased number of yellow puncta were observed in A2780 and A2780Dual^{LR} cells (scale 10 μ m). (B-C) Graphical representation of mCherry/EGFP ratio and Mander's co-localization coefficient of mCherry and EGFP puncta. CisPac treatment induced increase in mcherry/EGFP ratio with concomitant reduction in yellow puncta post CisPac treatment while reduced mcherry/EGFP ratio and increased yellow puncta was observed in A2780Dual^{ER} cells post CisPac+U0126 treatment. CisPac treatment reduced mcherry/EGFP ratio and increased yellow puncta in A2780 and A2780Dual^{LR} cells (n>35 cells/group). (D, G) Representative images of LC3 (Green, autophagosome) and LAMP1 (Red, lysosome) dual immunostained sensitive, early and late resistant cells of both A2780 and OAW42 chemoresistant models treated with CisPac alone or in combination with U0126. Autophagosome-lysosome fusions were depicted as yellow puncta. The white square insets represent the magnified images (scale 10 μ m for A2780 model and 20 μ m for OAW42 model). (E, H) Graphical representation of the number of LC3^{+ve}LAMP1^{+ve} puncta in sensitive, early and late resistant A2780 and OAW42 cells treated with CisPac alone or in combination U0126. A2780Dual^{ER} and OAW42Dual^{LR} cells treated with CisPac show increased LC3^{+ve}LAMP1^{+ve} puncta compared to other groups, which reduced post CisPac+U0126 treatment (F, I) Number of LC3^{+ve} puncta in sensitive, early and late resistant A2780 and OAW42 cells treated with CisPac alone or in combination U0126 (n>35 cells).



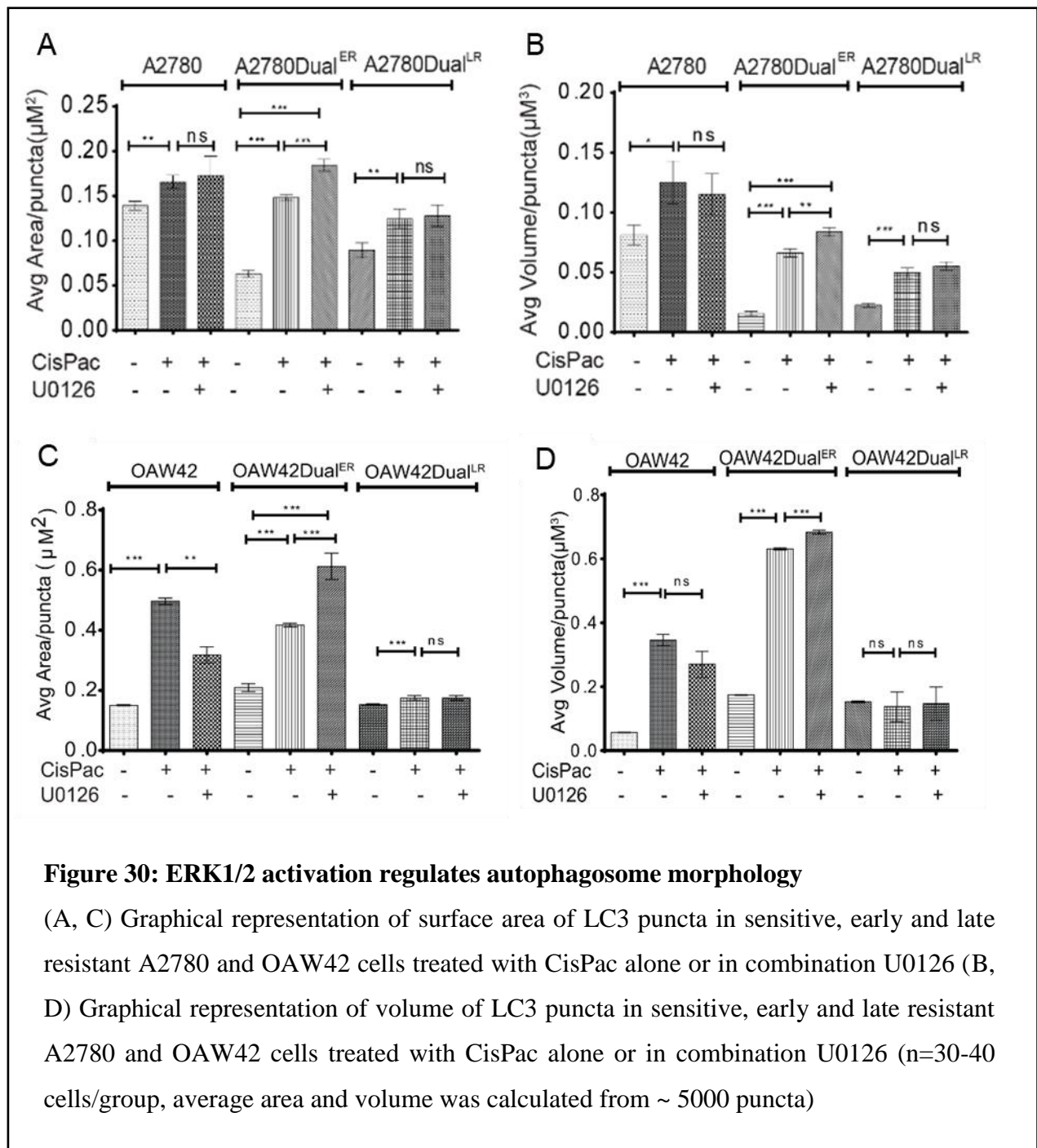
mCherry-EGFP-LC3 reporter that produces yellow puncta, as a result of mcherry and EGFP colocalization, upon formation of autophagosomes and red puncta post autophagosome-lysosome fusion, as result of quenching of EGFP in the acidic environment of lysosome. Thus the extent of mCherry EGFP colocalization is inversely proportional to the number of autophagolysosome formation. This increase in autophagolysosome formation is characterized by increase mCherry/EGFP ratio as a result of reduction in number of EGFP puncta and increase in number of mCherry puncta (186). Combinatorial treatment of CisPac along with U0126 in A2780Dual^{ER} cells stably expressing mCherry-EGFP-LC3 reporter resulted in reduced mcherry/EGFP ratio (1.91) along with accumulation of yellow puncta due to increased co-localization (co-localization coefficient: 0.70 ± 0.04) of LC3 EGFP and mCherry puncta in the perinuclear region, compared to only CisPac treated cells, which displayed increased red puncta (mcherry/GFP ratio 4.11) with reduced co-localization (co-localization coefficient: 0.48 ± 0.06) at 24 hours. In comparison to A2780Dual^{ER} cells, CisPac treatment showed significantly reduced red puncta (mcherry/GFP ratio 1.90) and increased yellow puncta (co-localization coefficient: 0.61 ± 0.01) in A780Dual^{LR} cells, while sensitive cells showed the least number of red puncta (mcherry/GFP ratio 1.17) and increased number yellow puncta (co-localization coefficient: 0.71 ± 0.04) indicating severe defect in autophagolysosome formation (Figure 29A-C). To determine whether ERK1/2 regulates the process of autophagosome-lysosome fusion we performed dual immuno-staining with LC3 (autophagosome marker) and LAMP1 (lysosomal marker) in our A2780 and OAW42 chemoresistant model post CisPac treatment either alone or in combination with U0126. CisPac treatment enhanced LC3^{+ve}LAMP^{+ve} puncta in A2780Dual^{ER} cells in comparison to untreated cells (27.16 ± 2.71 vs. 6.89 ± 0.78 puncta/cell) which were reduced by 5-fold (5.3 ± 0.59 puncta/cell) after combinatorial treatment of U0126 and CisPac. CisPac treatment in A2780 cells did not lead to any noticeable increase in LC3^{+ve}LAMP^{+ve} puncta than control (2.96 ± 0.83

vs. 4.31 ± 0.99 puncta/cell) but showed no significant change (1 ± 1.93 puncta/cell) after combinatorial treatment. In A2780Dual^{LR} cells, drug treatment resulted in ~2.2 fold increase in LC3^{+ve}LAMP^{+ve} puncta than the untreated cells (7.8 ± 1.5 vs. 3.4 ± 1.6 puncta/cell), with no significant change upon combinatorial treatment (8.5 ± 1.91 puncta/cell) (Figure 29D-E). A similar trend of drug induced enhancement of LC3^{+ve}LAMP1^{+ve} puncta in OAW42Dual^{ER} cells were observed compared to the untreated cells (49.8 ± 3.77 vs. 16.5 ± 1.98 puncta/cell) which was reversed upon application of U0126 and CisPac (14.4 ± 2.85 puncta/cell). The OAW42 and OAW42Dual^{LR} cells showed similar trend as A2780 and A2780Dual^{LR} cells for all treatments (Figure 29G-H).

The LC3^{+ve} puncta primarily detects the autophagosome formation which increases upon induction or blockade in autophagic flux. CisPac treatment in A2780Dual^{ER} cells enhanced LC3^{+ve} puncta than untreated cells (107 ± 6.95 vs. 58 ± 6.71 puncta/cell), which increased further post combinatorial treatment (107 ± 6.95 vs. 137.6 ± 10.62 puncta/cell). CisPac also increased LC3^{+ve} puncta (138.14 ± 11.98 vs. 88.5 ± 2.31 puncta/cell) in A2780 cells which did not alter significantly post combinatorial treatment (125 ± 10.56 puncta/cell). Treatment with either CisPac alone or in combination to U0126 induced least number of LC3^{+ve} puncta in A2780Dual^{LR} cells (58 ± 4.76 , 58 ± 5.42 puncta/cell in both cases), indicating a low induction of autophagic flux (Figure 29D-F). A similar trend was observed in OAW42 model as well (Figure 29G-I).

Next we estimated the surface area and volume of these LC3^{+ve} puncta pre and post treatment across the resistant stages. Assuming these autophagic bodies to be spherical, an increase in surface area and volume of these puncta were observed after CisPac treatment in A2780Dual^{ER} ($0.14 \pm 0.003 \mu\text{m}^2$ and $0.06 \pm 0.003 \mu\text{m}^3$ respectively) compared to untreated cells ($0.06 \pm 0.004 \mu\text{m}^2$ and $0.015 \pm 0.002 \mu\text{m}^3$ respectively) which increased further upon CisPac+U0126 treatment ($0.184 \pm 0.007 \mu\text{m}^2$ and $0.083 \pm 0.004 \mu\text{m}^3$ respectively). In contrast, the surface area

and volume of LC3⁺ puncta changed marginally in A2780 and A2780Dual^{LR} cells post drug treatment which remained unchanged after combinatorial treatment (Figure 30A-B). CisPac treatment increased surface area and volume of LC3⁺ puncta was observed in OAW42 cells, although the volume of autophagosome in OAW42 cells were smaller compared to OAW42Dual^{ER} cells while the OAW42Dual^{LR} cells reduced volume and area of LC3⁺ puncta (Figure 30C-D).



Autophagosome maturation and autophagosome-lysosome fusion involve a large number of molecular players of which UV radiation resistance-associated (UVRAG) and Rubicon (RUBCN) are reported to regulate endocytic transport, autophagosome maturation and/or autophagosome-lysosome fusion via Rab7 (24, 25, 291). UVRAG promotes autophagosome-lysosome fusion by interacting with VPS16 while Rubicon inhibits the fusion (24, 292). Interestingly, CisPac treatment increased both UVRAG and Rab7 level at 24 hrs which decreased following the combinatorial treatment in both A2780Dual^{ER} and OAW42Dual^{ER} cells indicating a blockage at the autophagosome-lysosome fusion step (Figure 31A, C-D and 32A-B). Similar treatments did not alter Rubicon level significantly (Figure 31B). Cisplatin-paclitaxel treatment reduced UVRAG and Rab7 level in A2780Dual^{ER/Erk-} cells as well, thus clearly indicates a new role of basal ERK1/2 in facilitation of proper autophagosome-lysosome fusion (Figure 31E and 32C).

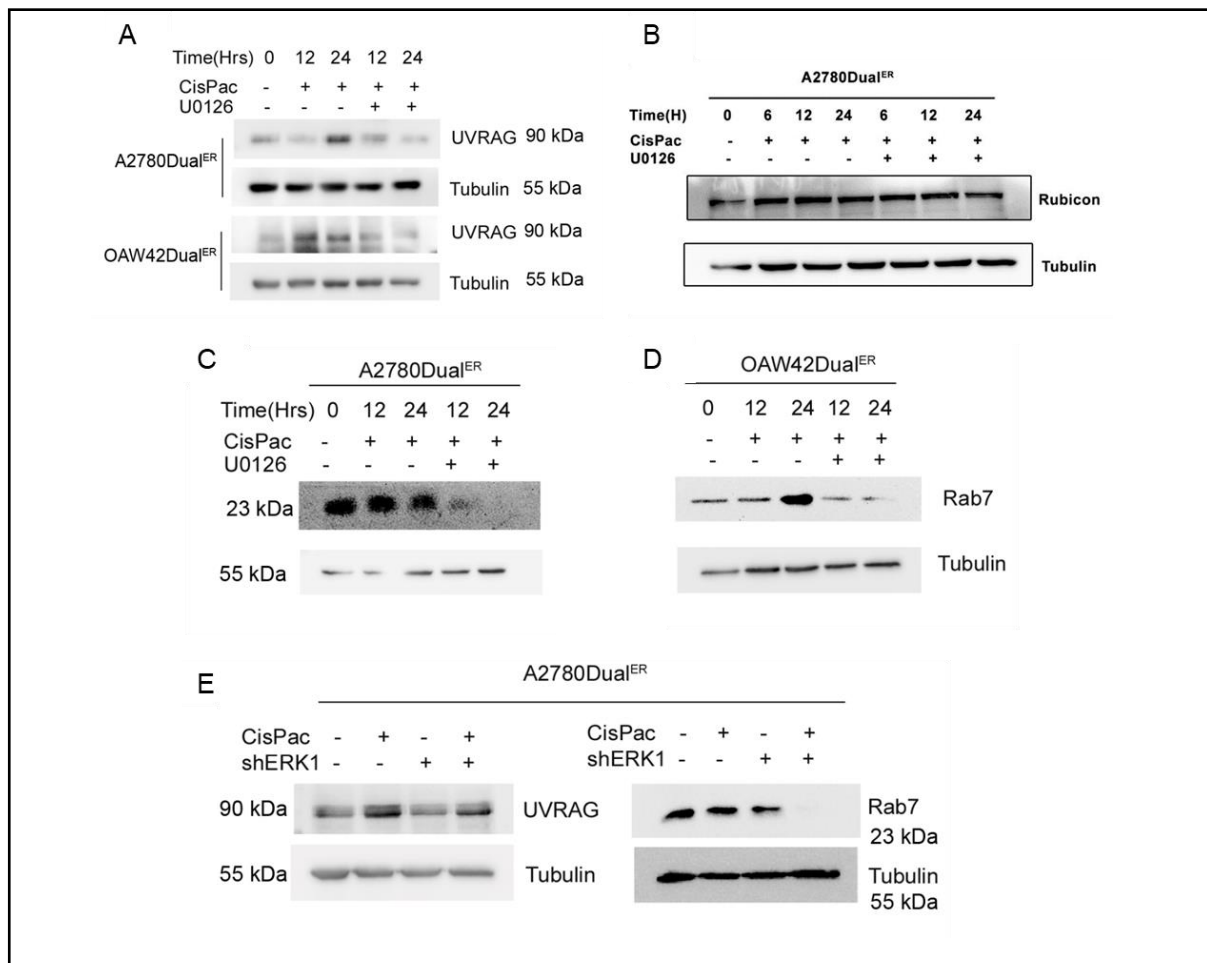


Figure 31: ERK1/2 regulates multiple components of autophagosome-lysosome fusion

(A) Immunoblot depicting CisPac induced increase in UVRAG level of A2780Dual^{ER} and OAW42Dual^{ER} cells, which reduces significantly post combinatorial treatment of CisPac+U0126 (B) Immunoblot depicting no alternation in Rubicon level in A2780Dual^{ER} cells treated with cisplatin-paclitaxel alone or in combination of U0126. (C, D) Immunoblot depicting significant reduction in Rab7 level post combinatorial treatment with U0126 and platinum-taxol in A2780Dual^{ER} and OAW42Dual^{ER} cells (E) A significantly reduced UVRAG and Rab7 level was observed in A2780Dual^{ER/ERK1-} (shERK1) post CisPac treatment in comparison to parental counterpart.

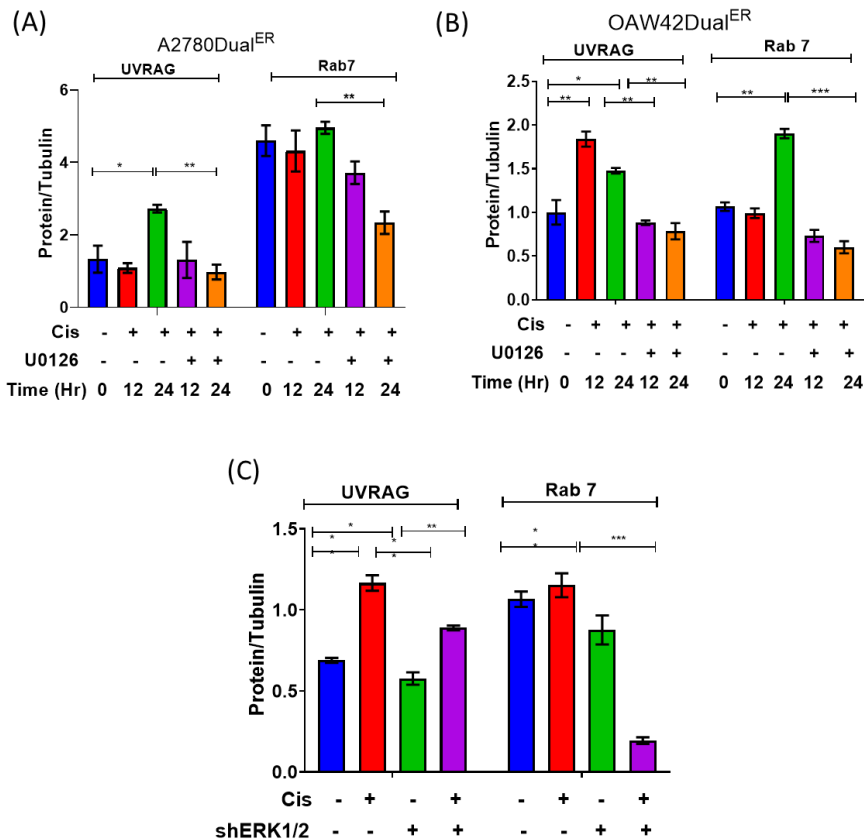


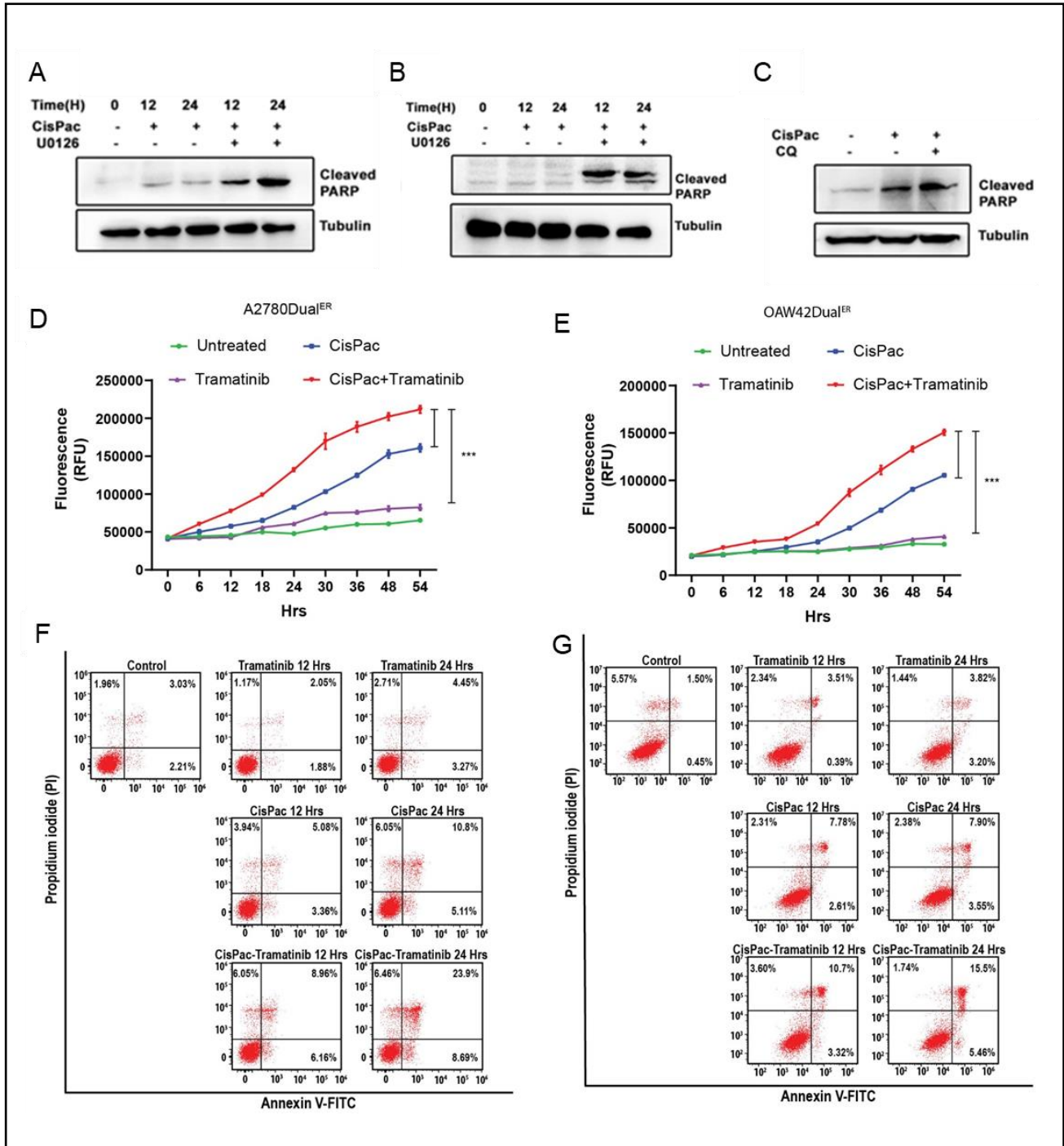
Figure 32: Densitometric quantification of UVRAG and Rab7 in Dual^{ER} cells (A-B) Graph representing CisPac induced increased UVRAG/tubulin and Rab7/tubulin ratio in A2780Dual^{ER} and OAW42Dual^{ER} cells, which reduces significantly post combinatorial treatment of CisPac+U0126

(C, D) Graph representing significantly reduced UVRAG/tubulin and Rab7/tubulin ratio in A2780Dual^{ER/ERK1-} (shERK1) post CisPac treatment in comparison to parental counterpart.

2.3.5 ERK1/2 inhibition promotes platinum-taxol induced apoptosis in early stage of resistance

To understand whether inhibition of autophagy via ERK1/2 inhibition switches the balance towards apoptosis we measured the level of cleaved PARP, which increased significantly post combinatorial treatment of CisPac along with U0126 or CQ in Dual^{ER} cells of both A2780 and OAW42 model (Figure 33A-C). Combinatorial treatment of CisPac along with Trametinib induced a significantly rapid cell death kinetics indicated by 2 fold increased cell death at 24 hour in comparison to cells treated with either CisPac which showed similar effect at 36 hours or Trametinib which did not induced noticeable cell death (Figure 33D). CisPac+Trametinib also showed significantly higher cell death (~3.3-fold) in comparison to only CisPac (~2.5 fold). A significantly higher and faster cell death kinetics was also observed in OAW42Dual^{ER} cells treated with CisPac+Trametinib (Figure 33E). A significantly higher percentage of early (Annexin^{+ve}) and late apoptotic (Annexin^{+ve}/PI^{+ve}) population was observed post combinatorial treatment CisPac+Trametinib at 12 (8.96% and 15.12% respectively) and 24 (23.9% and 32.59% respectively) hours in comparison to 12 (5.08% and 8.44% respectively) and 24 (10.8% and 15.91% respectively) hours of only CisPac treatment. Treatment of cells with only Trametinib showed marginal increase in early and late apoptotic population at both time points (Figure 33F, H). Similar treatment of CisPac+Trametinib in OAW42Dual^{ER} cells significantly increased percentage of early and late apoptotic cells in comparison to only CisPac, indicating

increased promotion of CisPac induced apoptosis in absence of ERK1/2 activation (Figure 33G, H).



H

A2780Dual ^{ER}			
Cell line and Time	Early Apoptosis (EA)	Late Apoptosis (LA)	Total Apoptosis (EA+LA)
Untreated	2.21	3.03	5.24
CisPac 12 Hr	3.36	5.08	8.44
CisPac 24 Hr	5.11	10.8	15.91
Trametinib 12 Hr	1.88	2.05	3.93
Trametinib 24 Hr	3.27	4.45	7.72
CisPac+Trametinib 12 Hr	6.16	8.96	15.12
CisPac+Trametinib 24 Hr	8.69	23.9	32.59
OAW42Dual ^{ER}			
Untreated	0.45	1.5	1.95
CisPac 12 Hr	2.61	7.78	10.39
CisPac 24 Hr	3.65	7.9	11.55
Trametinib 12 Hr	0.39	3.51	3.9
Trametinib 24 Hr	3.2	3.82	7.02
CisPac+Trametinib 12 Hr	3.32	10.7	14.02
CisPac+Trametinib 24 Hr	5.46	15.5	20.96

Figure 33: ERK1/2 inhibition sensitize Dual^{ER} cells to platinum-taxol induced apoptosis (A-C) Enhanced PARP cleavage in A2780Dual^{ER} and OAW42Dual^{ER} cells treated with platinum-taxol and U0126/chloroquine (CQ) for 12 and/or 24 hours. (D-E) Real-time cell death kinetics indicating significantly increased cell death post combinatorial treatment of CisPac+Trametinib in comparison to only platinum-taxol (CisPac), only Trametinib and untreated in A2780Dual^{ER} and OAW42Dual^{ER} cells. (F-G) Scatter plot showing time dependent increase in Annexin^{+ve} (early apoptotic) and Annexin^{+ve}/PI^{+ve} (late apoptotic) cells post combinatorial treatment of CisPac+Trametinib in comparison to only CisPac, only Trametinib and untreated cells in A2780Dual^{ER} and OAW42Dual^{ER} cells. (H) Table representing percentage of Annexin^{+ve} (early apoptotic) and Annexin^{+ve}/PI^{+ve} (late apoptotic) cells post combinatorial and single treatment.

2.3.6 mtFL-p62 sensor captures inducer/inhibitor induced differential autophagic flux

The above results suggest a promising role of ERK inhibitor to combat chemoresistance at very early stage through inhibition of drug induced autophagic flux. However, to evaluate the therapeutic efficacy of autophagy modulator/s in living subjects, an appropriate non-invasive

sensor is required. Completion or perturbation of autophagy is well correlated with p62 degradation, thus monitoring p62 kinetics through a reporter (e.g., luciferase) protein would allow us to reliably estimate the autophagy kinetics (293)[54]. Increased accumulation of p62 due to blocked autophagy would increase luciferase activity while an enhanced clearance of p62 due to ongoing autophagic flux would reduce luciferase activity (Figure 34A). We utilized a mutant thermostable Firefly Luciferase (mtFL) to prevent reporter protein mediated p62 degradation, mtFL displayed significantly longer half-life compared to its wild type counterpart (wtFL) (9 vs 3 hours) (Figure 34B) and developed a new autophagy sensor (mtFL-p62). Serum starvation (2 hours), a well-known autophagy inducer, decreased mtFL-p62 luciferase activity by 0.60 fold while addition of CQ (2 hours) led to 2.2 fold higher luciferase activity compared to the control. Similar treatments induced no reduction or minimal enhancement in luciferase activity in cells expressing only mtFL or wtFL-p62 indicating the ability of mtFL's to accurately monitor autophagic flux through p62 kinetics (Figure 34C). Further, treatment of cells with known autophagy inducers like rapamycin and etoposide reduced (0.53 and 0.45 fold respectively) luciferase activity while Wortmannin and Bafilomycin increased luciferase activity (1.7 and 2.3 fold respectively) after 24 hours of treatment in A2780 cells transfected with mtFL-p62, confirming the potential of the sensor (Figure 34D). Next, we utilized the mtFL-p62 to monitor chemotherapy (CisPac) induced autophagic flux in A2780 and OAW42 EOC cells for different time points. Moderately enhanced luciferase activities (1.4 & 1.6 fold at 12 and 24 hours) were found in drug treated A2780 cells transiently expressing the mtFL-p62 compared to the untreated counterparts. Combinatorial treatment of CisPac and chloroquine led to 2.2 and 2.1 fold increase in luciferase activity respectively in similar conditions. Contrarily, luciferase activity remained unaltered post 24 hours of CisPac and CisPac with Chloroquine treatment in A2780 cells expressing wtFL-p62, indicating the inability of this reporter to portray changes in p62 level (Figure 34E).

Similar increase in mtFL-p62 activity was also observed in OAW42 cells post 12 and 24 hours of CisPac alone (1.9 and 2.1 fold) or CisPac with chloroquine (2.5 and 3.5 fold) treatments, indicating a stalled autophagic flux in A2780 and OAW42 cells upon chemotherapeutic stress (Figure 34F).

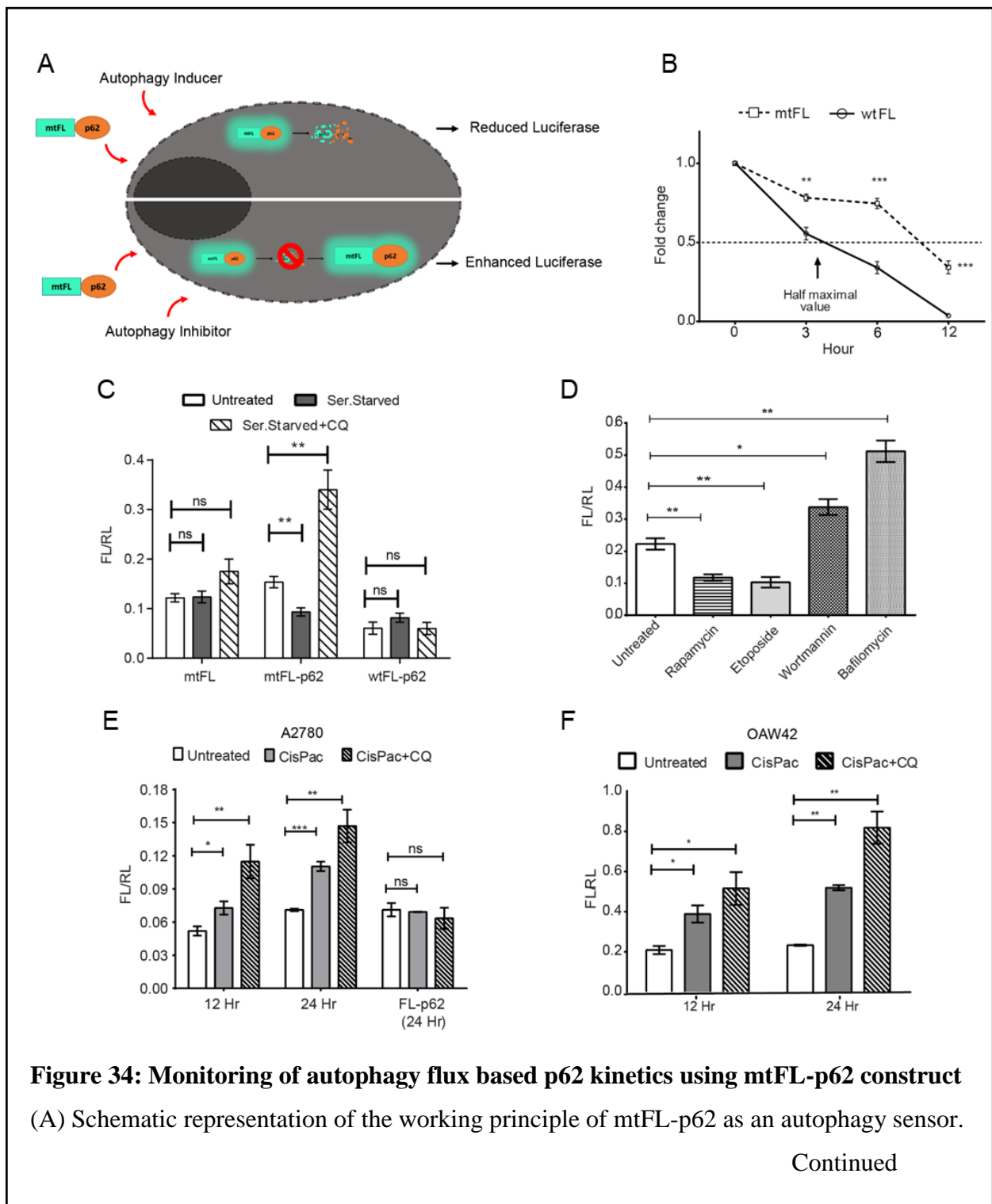


Figure 34: Monitoring of autophagy flux based p62 kinetics using mtFL-p62 construct

(A) Schematic representation of the working principle of mtFL-p62 as an autophagy sensor.

Continued

(B) Graph representing fold change in luciferase activity with respect to pre-treatment condition (0 hour) over time period. A 50% reduction in wtFL luciferase activity was observed post 3 hours of cyclohexamide treatment while mtFL showed similar reduction post 9 hours. (C) Graph representing reduction in luciferase activity post 2 hours of serum starvation (Ser. Starved) and increase in luciferase activity post 2 hours of Ser. Starved+chloroquine (CQ) specifically in cells transfected with mtFL-p62 but not in cells transfected with either wtFL-p62 or only mtFL. (D) Reduced luciferase activity was observed upon Rapamycin and Etoposide treatment (24 hours) respectively while increased luciferase activity was observed upon Wortmannin and Bafilomycin treatment (24 hours) in A2780 cells transfected mtFL-p62. (E, F) p62 degradation kinetics monitored by luciferase activity in sensitive A2780 and OAW42 cells. Both the cells show a significantly increased luciferase activity post 24 hours of CisPac and CisPac+CQ treatment. Similar treatment did not alter luciferase activity significantly in A2780 cells transfected with wtFL-p62.

2.3.7 mTFL-p62 reveals differential autophagic flux at different stages of chemoresistance

Acquired chemoresistance is a dynamic process and ongoing autophagy is known to aid in tumour cell survival, however, the association of active autophagy with different stages of chemoresistance has never been investigated. CisPac treatment alone for 12 and 24 hours in A2780Dual^{ER} cells expressing the mtFL-p62 sensor reduced luciferase activity by 0.7 and 0.5 fold respectively while a significant increase in luciferase signal was observed when U0126 (2.25 and 3.28 fold) was added with platinum-taxol, at 12 and 24 hour respectively (Figure 35A). An increased luciferase activity was observed in A2780Dual^{LR} cells (1.3 & 2 fold respectively), indicating existence of an enhanced ERK1/2 driven autophagic flux at early stages but a stalled one at late resistant stages (Figure 35B). Combinatorial treatment of chloroquine with CisPac for 12 and 24 hours led to a time dependent increase in luciferase activity in both A2780Dual^{ER} (2.95 and 3.71 fold) and A2780Dual^{LR} (3.29 and 5.11 fold) cells

(Figure 35A, B). Similarly, 0.6 and 0.3 fold reduction in mtFL-p62 activity was observed in OAW42Dual^{ER} cells post 12 and 24 hours of drug treatment, which increased by 2.23 and 2.53 fold post combinatorial treatment of U0126 and CisPac (Figure 35C). An increased luciferase activity was observed in OAW42Dual^{LR} (1.9 and 1.8 fold) cells post drug treatment (Figure 35D). Combinatorial treatment of CisPac and chloroquine for 12 and 24 hours increased luciferase activity in both OAW42Dual^{ER} (3.8 and 3.75 fold) and OAW42Dual^{LR} (4 and 4.5 fold) cells (Figure 35C-D). Moreover, proteasome inhibitor (Bortezomib) failed to increase the CisPac induced reduction in mtFL-p62 luciferase activity in A2780Dual^{ER} cells indicating autophagy specific degradation of mtFL-p62 (Figure 35E).

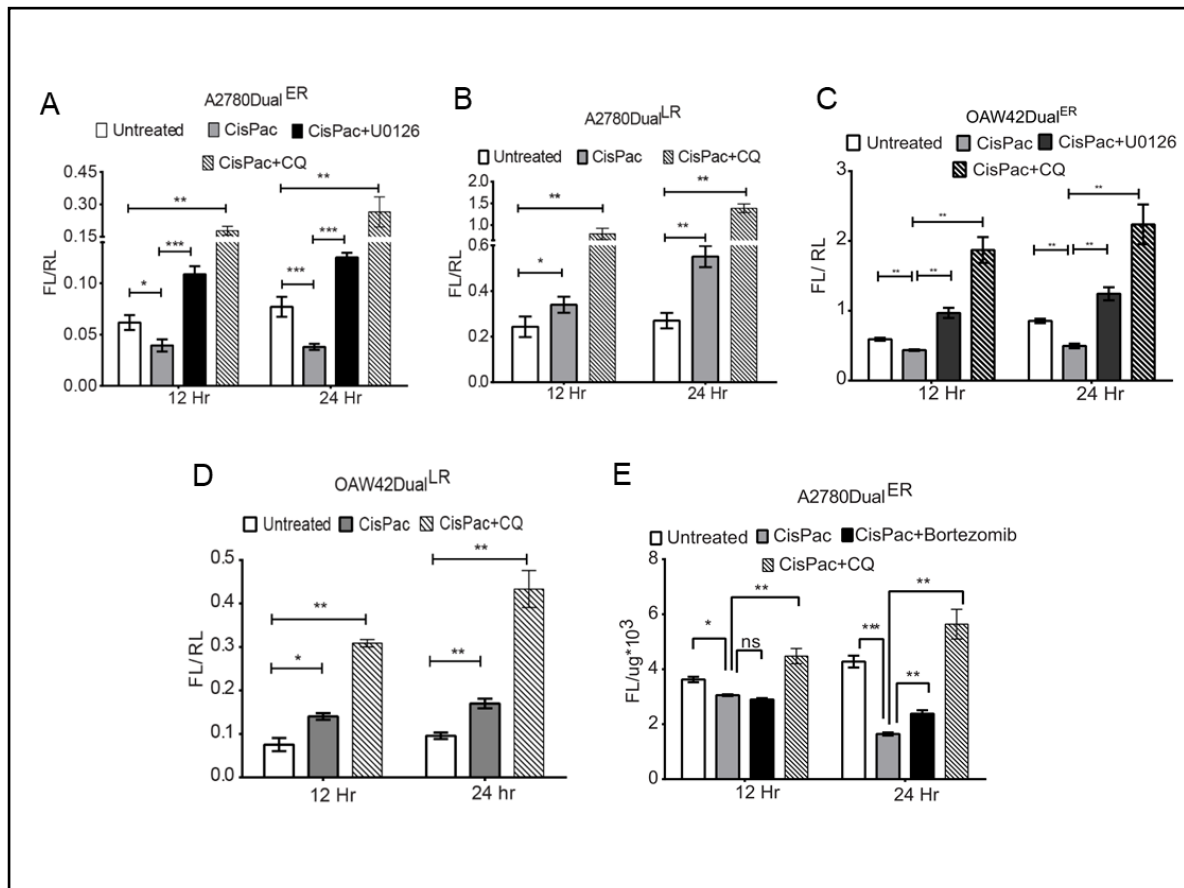


Figure 35: mtFL-p62 portrays differential autophagic flux depending on the stage of platinum-taxol resistance

(A, C) Luciferase activity from A2780Dual^{ER} and OAW42Dual^{ER} cell lysate depict increased luciferase activity post combinatorial treatment of U0126/Chloroquine along CisPac compared to cells treated with only CisPac at 12 and 24 hour

Continued

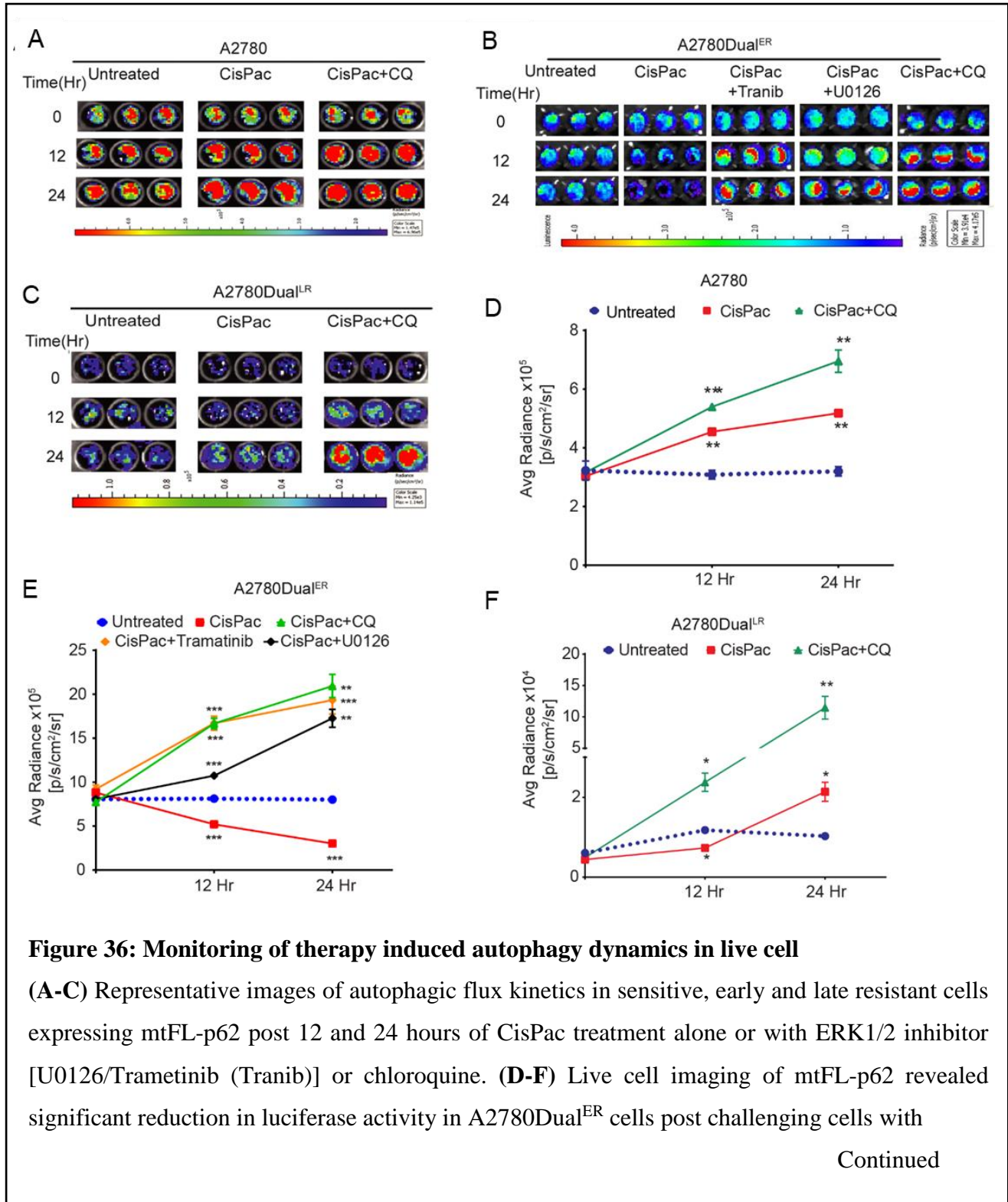
(B, D) CisPac treatment significantly increased luciferase activity in A2780Dual^{LR} and OAW42Dual^{LR} cells, which increased further upon combinatorial treatment of CisPac+CQ at both 12 and 24 hour (E) Application of chloroquine along with CisPac but not proteasome inhibition with Bortezomib, rescued only CisPac mediated reduction in luciferase activity at both 12 and 24 hours.

2.3.8 mtFL-p62 sensor tracks real time autophagy kinetics in live cells and mouse model

Encouraged by the ability of mtFL-p62 to capture autophagy dynamics in-vitro we aim to test its potential as a real-time autophagy sensor. To monitor the therapy induced modulation of autophagy kinetics in live cells in real-time, A2780, Dual^{ER} and Dual^{LR} cells were transfected with mtFL-p62 and luciferase signal was captured from live cells following respective treatments. Interestingly, chemotherapeutic treatment increased luminescence signal in A2780 cells (1.5 and 1.72 fold at 12 and 24 hours respectively) and A2780Dual^{LR} cells (1.5 and 4.8 fold at 12 and 24 hours respectively) compared to respective pre-treatment condition (0 hour) (Figure 36A, C, D, F). A reduction in luminescence signal was observed in A2780Dual^{ER} cells (0.62 and 0.39 fold) post 12 and 24 hours of cisplatin-paclitaxel treatment respectively. An enhanced luciferase signal was observed after combinatorial treatments of CisPac along with Trametinib (1.8 and 2.2-fold respectively) or U0126 (1.4 and 2-fold respectively) (Figure 36B, E). Administration of chloroquine along with platinum-taxol enhanced luminescence signal in all three cells post 12 and 24 hours of treatment (Figure 36A-F).

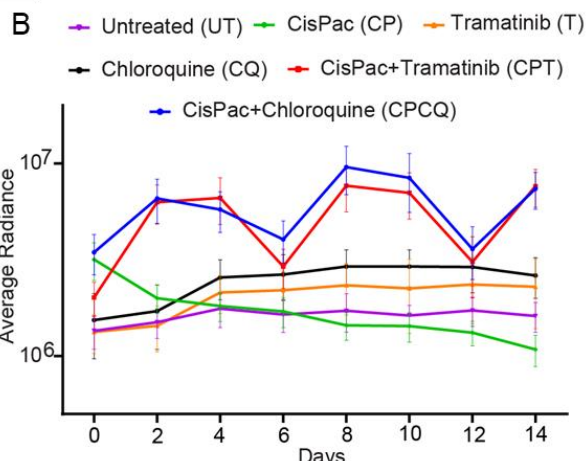
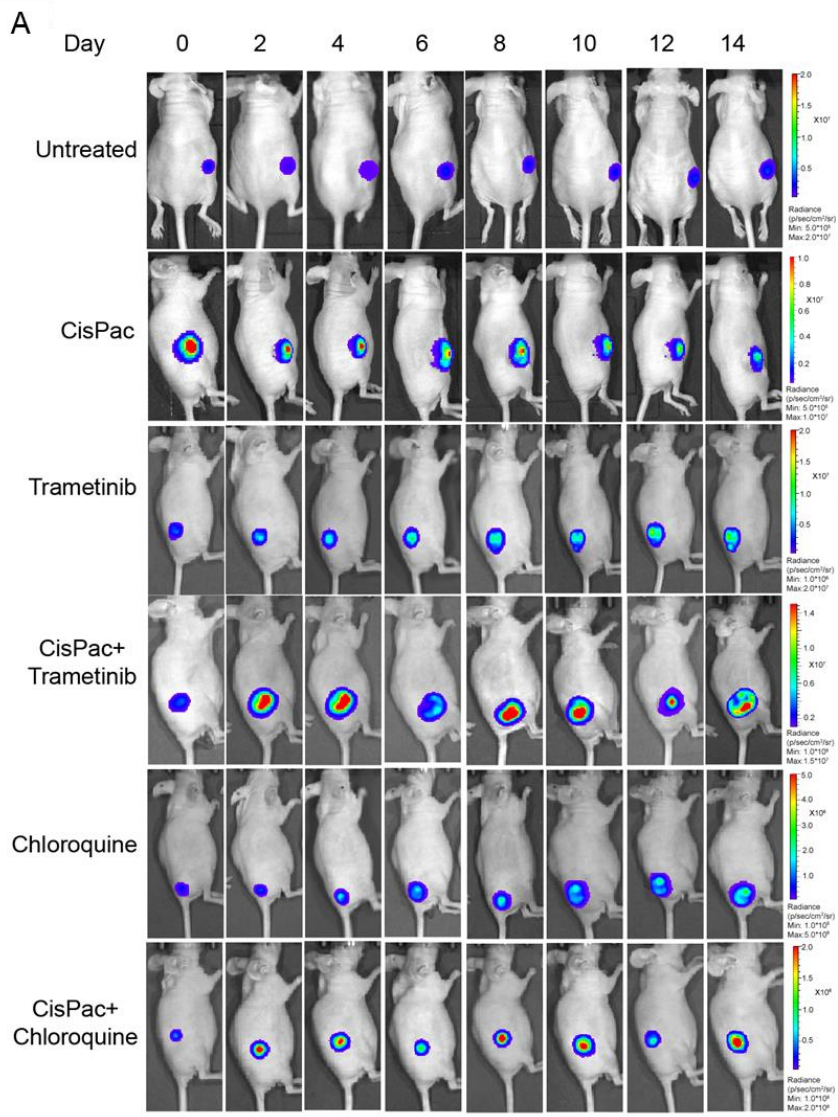
Next therapy induced autophagic flux was monitored for 14 days in A2780Dual^{ER} tumour xenografts stably expressing mtFL-p62 reporter (Figure 37A). Trametinib treatment alone enhanced bioluminescence on day-4 (1.60-fold) over day 0 which then remained stationary till 14 days. Treatment of chloroquine alone showed a similar kinetics with a 1.66-fold increased

luminescence on day-4, which then remained stationary till 14th day. In contrast, CisPac treatment resulted in reduction in luminescence signal on day 2 by 0.62-fold, which again reduced further following second and third dose by 0.45- (day 8) and 0.32-fold (day 14), indicating a continued degradation of p62 and an active autophagic flux. Intriguingly,



CisPac at both 12 and 24 hours while combinatorial treatment of CisPac long with Trametinib/U0126/Chloroquine increased luciferase activity in comparison to respective pre-treatment condition (0 Hour). Platinum-taxol treatment increased luciferase activity in A2780 and A2780Dual^{LR} cells at both 12 and 24 hours. Combinatorial treatment of CisPac and Chloroquine increased luciferase activity in both A2780 and A2780Dual^{ER} cells.

combinatorial treatment of CisPac along with Trametinib showed a 3.12 fold increase in luminescence signal on day-2 which remained steady till day 4 and then reduced on day 6. Administration of second and third doses on day 7 and day 12 respectively, again induced an increase in luminescence signal on day 8 (3.80-fold) and day 14 (3.78 fold), indicating the role of Trametinib in inhibition of CisPac induced autophagic flux. Application of chloroquine along with CisPac also induced an increased bioluminescence on day-2 (1.9-fold) which then gradually decreased till the administration of second and third combinatorial dose on day 7 and day 12, following which a 2.76 and 2.13-fold increased bioluminescence signal was observed on day 8 and day 14 respectively. (Figure 37A-B). Though demonstrating an incremental trend, the change of luciferase signals post treatment with single agents (CQ and Trametinib) over 14 days were not found to be statistically significant compared to control and CisPac treated groups by two way ANOVA analysis. This indicates that Trametinib and CQ may not be enough to block autophagy to a significant extent within 14 days. However, when the modulation in luminescence signals of the combinatorial groups (CisPac with Trametinib or Chloroquine) were compared among days and with other groups by two way ANOVA analysis, highly significant differences ($p=0.0015$ and 0.02 respectively) were observed indicating such combinatorial treatments are sufficient to arrest autophagy in short duration. Trametinib treatment also reduced ERK1/2 activation as observed from tumour lysates by immunoblotting (Figure 37B).



Two-way ANOVA UT, CP, CPT, CPCQ

Source of Variation	% of total variation	P value	P value summary
Row Factor	5.981	0.0015	**
Column Factor	25.49	0.0254	*

Two-way ANOVA UT, CP, T, CQ

Source of Variation	% of total variation	P value	P value summary
Row Factor	0.9365	0.3276	ns
Column Factor	4.893	0.5937	ns

Figure 37: Non-invasive bioluminescence imaging of therapy induced autophagy flux in live animals

Continued

(A) Representative bioluminescence images of real time mtFL-p62 kinetics in A2780Dual^{ER} tumour xenograft post treatment with vehicle (untreated), CisPac, chloroquine, Trametinib, CisPac+Trametinib and CisPac+Chloroquine and observed over 14 days. (B) Graphical representation of kinetics of quantified bioluminescence signal from mice revealed Trametinib treatment alone enhanced bioluminescence on day-4, which remained stationary till day-14. A similar kinetics was observed with chloroquine treatment alone. In contrary, CisPac treatment resulted in slow but continued reduction in bioluminescence over the course of 14 days. Application of Trametinib along with CisPac tripled luminescence signal by day-2 then remained steady at day 4 followed by a reduced luciferase activity on day 6, which again peaked on day 8 and day 14 post second (day 7) and third (day 13) dose . Application of chloroquine along with CisPac also increased bioluminescence till day-2 which then gradually reduced till the administration of second combinatorial dose on day-7, following which an increased bioluminescence signal was observed on day-8. The luminescence signal again peaked on day 14

After administration of individual therapeutic regimen for 15 days, tumour growth was monitored till day 25. Single treatment of Trametinib showed 0.36-fold reduction in tumour volume while only CisPac showed 0.56 fold reduction in tumour volume in comparison to untreated cells. Interestingly, combinatorial treatment of CisPac along with Trametinib significantly reduced (0.08-, 0.14- and 0.22-fold at day 25) tumour volume in comparison to untreated, CisPac and only Trametinib treated group respectively. Similar reduction in tumour volume was observed in CisPac+chloroquine group in comparison to untreated (0.19-fold), CisPac (0.34-fold) and only chloroquine (0.26-fold) group, indicating the effectivity of combinatorial treatment over single agent (Figure 38A, C). Enhanced p62 staining was observed in tumours treated with Trametinib or chloroquine along with platinum-taxol, while a reduction in p62 staining was observed in CisPac treated group (Figure 38C-D).

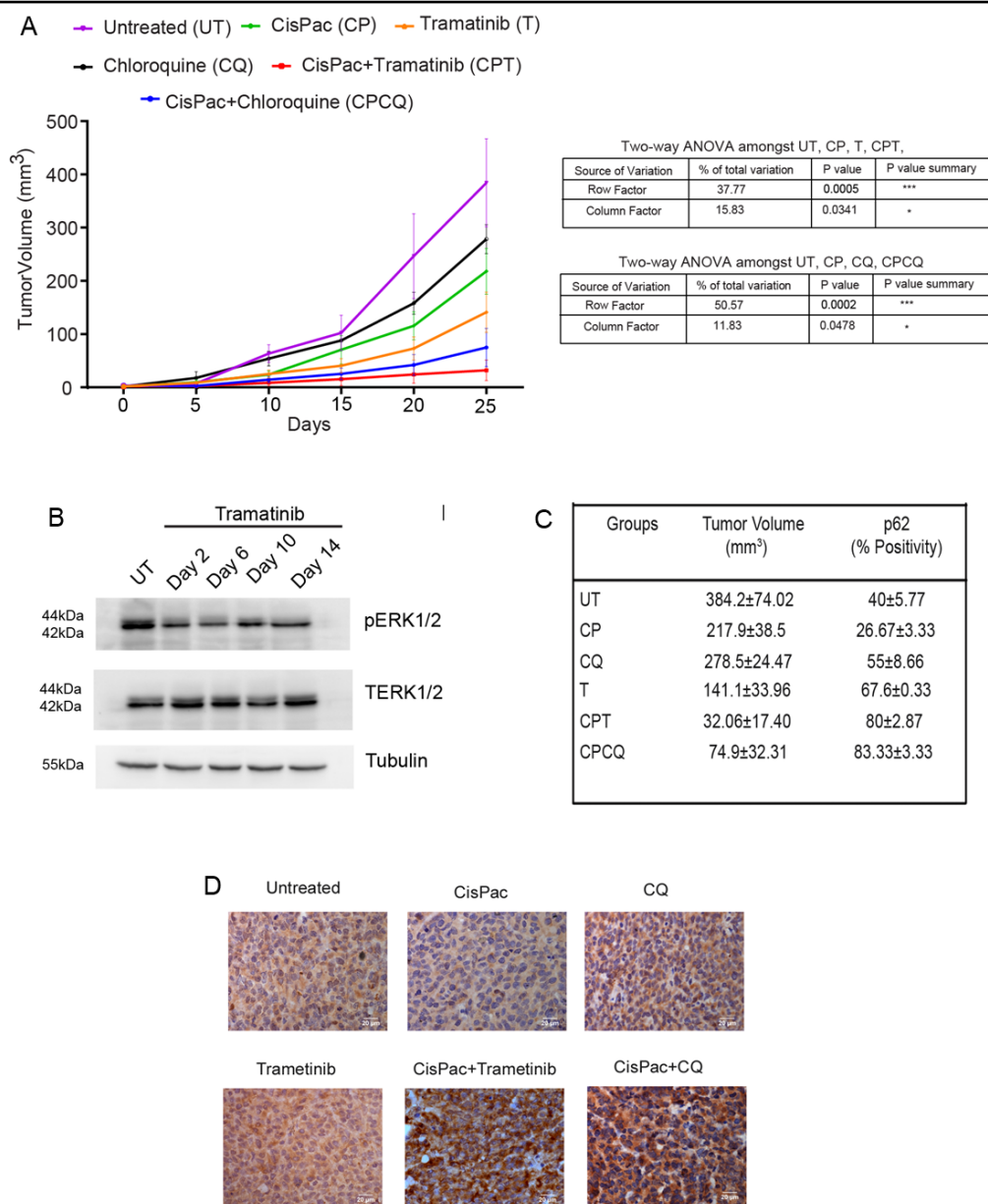


Figure 38: Inhibition of ERK1/2 or autophagy sensitizes Dual^{ER} tumour xenografts to therapy

(A) Graphical representation of alteration in tumour volume at day 25, revealed the efficacy of combinatorial treatment of Trametinib/ chloroquine along with CisPac in reducing tumour growth compared to untreated, only CisPac, only Trametinib and only CQ group. Table depicting the two way Annona statistics on the right (n=8) (B) Immunoblot depicting reduction in phospho ERK level following administration of Trametinib in mouse on day 2, 6, 10 and 14.

Continued

(C) Tabular representation of p62 percent positive cells in tumour sections and tumor volume.

(D) Immunohistochemical staining of p62 in mice tumour tissue revealed increased p62 staining in tissue section harvested from tumours treated with CisPac+Trametinib/chloroquine in comparison to tissue obtained from untreated, only cispac, only Trametinib or only chloroquine group. Lowest p62 staining was observed in tumour sections obtained from only CisPac group.

2.4 Discussion

Understanding the key signalling event governing the gradual acquirement of therapy resistance has become a dire necessity in this era of personalized medicine. The five year survival rate for stage III/IV advanced ovarian carcinoma is 35% and this poor survival rate can be accounted to the acquirement of resistance to first line platinum therapy (294). Currently, there are only limited number of targeted therapy against HGSOc due to absence of a targetable driver mutation/over activated signalling (295). ERK1/2 and AKT are the key effector kinase that activates several molecular pathways to prevent therapy induced cell death. Several reports suggests that increased activation of these pathways in chemoresistant ovarian cancer cells imparts survival advantage against conventional therapy. Though a small subset of tumour cells remain refractory to commencement of standard therapy, majority of the cancer cells progressively develop resistance through successive alteration in several molecular and biochemical pathways (5, 112). Though many studies highlight the benefit of targeting ERK1/2 and AKT in chemoresistant cells, these studies fails to understand how these signalling pathways are gradually modulated during evolution of chemoresistance and the implication of such modulation to promote development of a highly chemoresistant phenotype is yet to known. Understanding these molecular events in a stepwise manner may help in identifying an optimal therapeutic window to target these pathways in order to prevent development of a highly chemoresistant phenotype.

Employing the indigenously developed cisplatin-paclitaxel dual resistant cellular model of ovarian cancer (5), we showed that that an increased basal activation of ERK1/2 kinase stimulates cisplatin-paclitaxel induced autophagic flux at the early stage of resistance development, inhibition of ERK1/2 activation impedes autophagic flux by obstructing autophagosome-lysosome fusion and promotes CisPac induced apoptosis. Intriguingly, therapy induced autophagic flux became dispensable as the cells acquire a highly resistant phenotype, these reduced autophagic flux was attributed to the hyper activated AKT signalling at late stage of resistance. Both pharmacological and genetic inhibition of ERK1/2 kinase in combination with chemotherapy led to increase in number and size of autophagosomes with concomitant reduction in autophagolysosome number. ERK1/2 inhibition along with platinum-taxol significantly reduced the level of UVRAG and Rab7, the two key regulators of autophagosome-lysosome fusion in Dual^{ER} cells. In order to assess the therapeutic efficacy of ERK inhibitor, we developed a novel autophagy sensor mtFL-p62, which enabled us to monitor the autophagy kinetics through degradation/stabilization of p62 in live cells and in tumour bearing mice through real time bioluminescence imaging. Chemotherapy treatment reduced bioluminescence signal specifically in Dual^{ER} cells but not in the chemosensitive or Dual^{LR} cells, which in conjunction with chloroquine showed enhanced bioluminescence signal across all the stages due to p62 stabilization. Interestingly, administration of Trametinib, a FDA approved MEK1/2 inhibitor, along with chemotherapy simulated a comparable effect like chloroquine, a classical lysosomal inhibitor, in Dual^{ER} cells. Combinatorial treatment of Trametinib or chloroquine along with CisPac led to significant increase in p62 accumulation for period of 72 hours as revealed by real time bioluminescence imaging of Dual^{ER} tumour xenograft. Further the combinatorial regimen of CisPac+Trametinib/CQ for 15 days significantly reduced tumour growth in comparison to treatment with individual drugs. In summary our data suggests that an active ERK1/2 kinase specifically drives the onset of

chemoresistance by sustaining an increased autophagic flux in chemotherapy treated ovarian cancer cells, inhibition of which primes the cells towards apoptosis, thus identifying a therapeutic window for targeting ERK1/2 driven autophagic flux for maximizing the effect of a therapy.

Chemotherapy induced autophagy was reported to play both pro-survival and pro-death role in a context dependent manner (174, 175, 296, 297). In majority of cancers including epithelial ovarian cancer the induction of autophagy in response to chemotherapy ultimately leads to development of resistance (10, 11, 14, 176, 281). Enhanced autophagic flux mediated by YAP oncoprotein in cisplatin-resistant OV2008 cells, by up regulated TXNDC17 in paclitaxel resistant cells or by activated ERK1/2 in response to cisplatin treatment in ovarian cancer cells describe the intimate association of autophagy, drug treatment and chemoresistance (9, 11, 275, 276). However, all these cell line based studies reported a onetime relation between chemoresistance and autophagic flux and did not investigate the dynamic association of autophagy across different stages of resistance. We previously reported dynamic models of chemoresistance in ovarian cancer cells which can be distinctly divided into early (onset) and late (maximal) resistant cells based on their resistance index and are characterised with $IGF1R^{high}/pAKT^{low}$ (in early stage) and $IGF1R^{low}/pAKT^{high}$ (at late stage) pathways (5). Utilizing these models (developed in A2780 and OAW42 cells) we report an increased LC3I-II conversion rate in sensitive and ER cells indicating an increased initiation of autophagy, however only Dual^{ER} cells showed completion of autophagy indicated by increased p62 degradation. The Dual^{LR} cells were characterized with low level of initiation and completion of autophagy likely due to presence of hyper activated AKT. Inhibition of AKT indeed promoted active autophagy in these cells as demonstrated by other studies (289, 298, 299). At par with molecular data, TEM images revealed lowest number of autophagic bodies (phagophore, autophagosome and autophagolysosome) in the Dual^{LR} cells while the sensitive

cells displayed increased number of phagophore and autophagosomes with reduced number of autophagolysosomes. CisPac treatment increased the number both of autophagosomes and autophagolysosomes to a similar extent in the Dual^{ER} cells. Increased autophagic flux is classically characterized by increased number of autophagosomes and autophagolysosome (285, 300). Higher autophagosomes as well as autophagolysosomes were observed in UC13 bladder cancer cells after knockdown of ZKSCAN3, a negative transcriptional regulator of autophagy (301). Cisplatin treatment in T24 bladder cancer cells was reported to induce autophagosome and autophagolysosome numbers, while pre-treatment of these cells with chloroquine prevented the formation of autophagolysosome but not autophagosome (302). Defect in autophagy upon genetic knockdown of CD38 in coronary arterial myocytes was reported to increased formation of autophagosome without any change in autophagolysosome number (303). In line with these published literature, we observed enhanced number of both autophagosomes and autophagolysosomes in the ER cells following drug treatment. Our data indicates that an upregulated autophagic flux allows cells to survive chemotherapy stress at the onset of resistance and foster development of a highly chemoresistant phenotype where autophagy becomes dispensable.

Cellular kinases are the key modulators of autophagic flux (10, 13, 289, 298, 299). Therapy induced ERK1/2 activation was reported to positively regulate autophagic flux in oesophageal, breast, bladder, hepatocellular carcinoma cells as well as in a panel of cisplatin resistant ovarian cancer cells (176, 304-306). Cisplatin-paclitaxel treatment induced ERK1/2 activation in sensitive and Dual^{LR} cells but not in the Dual^{ER} cells, having highest basal level of activated ERK. Pharmacological inhibition of ERK1/2 using U0126 and Trametinib or stable ERK knockdown led to significant accumulation of LC3 and p62, when combined with platinum-taxol specifically in the Dual^{ER} cells, indicating a blockade in autophagic flux. Combinatorial treatment of U0126 along with platinum-taxol also increased autophagosome accumulation

and reduced number of autophagolysosome. Similar treatment did not significantly alter LC3 conversion or p62 degradation in sensitive and Dual^{LR} cells in comparison to only platinum-taxol treated cells. Thus indicating that the basal but not the induced level of phospho-ERK seemed to be critical for maintenance of autophagy and cell survival under therapeutic stress. Prolonged activation of ERK1/2 kinase by Lindane in sertoli cells prevented maturation of autophagosome to autophagolysosomes (307). Increased autophagic flux in PDAC cells with mutated *Ras* or *Raf* and brain tumour cells resistant to BRAFi, was reported upon inhibition of Ras-Raf-MEK-ERK signalling. These differential role of ERK in regulation of autophagy can be attributed to the difference of cellular model systems, here in we measured the effect of ERK1/2 in regulation of cisplatin-paclitaxel induced autophagy in cisplatin-paclitaxel resistant cells in comparison to cancer cells having constitutive and hyperactivated MAPK signalling or in untransformed cells exposed to carcinogen. Platinum induced ERK1/2 activation was reported to increase autophagic flux in cisplatin-resistant A2780/CP70 cells (11). Although the extent of platinum resistance between A2780/CP70 and our dual resistant cells is difficult to compare, both the reports suggests the role of activated ERK1/2 in promotion of autophagic flux, suggesting that an optimal level of ERK activation (basal or drug induced) is critical for proper completion of autophagy.

A complete autophagy cycle comprises of several steps which include phagophore formation, autophagosome formation and maturation and finally degradation of autophagosome through autophagosome-lysosome fusion (284). Increase in the LC3^{+ve}LAMP1^{+ve} puncta and reduction in colocalization of GFPPLC3 and mCherryLC3 puncta are bonafide signatures of increased autophagolysosome formation (285, 300). Blockade of autophagolysosome formation by mevastatin or withaferin in MDA-MB-231 and MCF7 cells was reported to increase colocalization of GFP and RFP puncta (308, 309). Treatment of A375 melanoma cells with N6-isopentenyladenosine was reported to prevent autophagosome-lysosome fusion leading

into reduced the number of LC3⁺LAMP1⁺ puncta (310). Interestingly, enhanced autophagolysosome formation indicated by increased number LC3⁺LAMP1⁺ and mCherry LC3 puncta was also observed in cisplatin resistant ovarian cancer cells on O-GlcNAc transferase knockdown (311). Inhibition of ERK1/2 activation by ROS during severe ER stress was reported to block autophagolysosome fusion in HeLa cells (312). Enhanced co-localization of EGFP mCherry puncta (0.70 ± 0.04) was also observed in ER cells treated with combination of U0126 and CisPac, as well in sensitive and LR cells (having low basal ERK1/2 activation) post drug treatment. A drastic increase LC3⁺LAMP1⁺ puncta was observed in ER cells post platinum-taxol treatment, which again returned to basal level upon ERK1/2 inhibition, highlighting the role of ERK1/2 in autophagosome lysosome fusion. Induction of autophagy by amino acid starvation and its blockade by vinblastine at the autophagosome lysosome fusion step was reported to increase autophagosome size in CHO cell line (313). Intriguingly, we also observed increased size (both by area and volume) of the LC3 puncta in ERK inhibited and drug treated ER cells which were not evident in sensitive and LR cells. Regulation of such phenotype by ERK1/2 is still not reported.

Autophagosome maturation and autophagosome-lysosome fusion are regulated by several proteins in sequential and interconnected steps. HCV and *M. Tuberculosis* infected macrophages show impaired autophagolysosome formation and increased autophagosome accumulation due to reduced UVRAG expression. Tissue specific UVRAG knockdown in murine cardiac muscles also led to similar defect in autophagolysosome formation (314). Recently, phosphorylation of UVRAG via mTOR was reported to inhibit UVRAG function leading into reduced autophagolysosome formation (315). Interestingly, ER cells showed enhanced UVRAG level post drug treatment, while inhibition (both genetic and pharmacological) of ERK clearly reduced UVRAG level. Rab7 is a critical regulator of autophagolysosome fusion and knocking down of Rab7 was reported to reduce

LC3^{+ve}LAMP1^{+ve} structure in Hela cells post serum starvation. Overexpression of Rab7 T22N dominant negative mutant also led reduction LC3^{+ve}LAMP1^{+ve} puncta but did not prevent initial maturation of autophagosome (316). Similar observation was reported in CHO cells upon amino acid starvation where accumulation of large autophagosomes and impairment in autophagolysosome formation were observed upon overexpression of dominant negative Rab7 (317). We observed increased size of autophagosomes upon combinatorial treatment of U0126 and platinum-taxol. Further genetic or pharmacological inhibition of ERK1/2 reduced Rab7 level, indicating a mechanistic link between autophagosome-lysosome fusion and ERK1/2 activation in Dual^{ER} cells. Altogether, our data suggests the role activated ERK1/2 in regulation autophagolysosome formation via UVRAG and Rab7. Till date, a direct connection between activated ERK1/2 with autophagosome-lysosome fusion regulators has not been established. Although regulation of genes involved in autophagosome-lysosome fusion by EGR1 or miR-138, two downstream ERK1/2 targets may potentially influence the process and such studies are currently ongoing in our laboratory. Interestingly, inhibition of ERK1/2 activation along with platinum-taxol led to significant increase in the level of cleaved PARP, percent cell death and apoptosis, indicating that inhibition of ERK1/2 sensitizes Dual^{ER} cells to platinum-taxol induced apoptosis.

ERK1/2 regulated therapy induced autophagic flux specifically at early stage of resistance development indicates a therapeutic window to target therapy resistance at the onset. In order to estimate the *in-vivo* therapeutic potential of targeting ERK regulated autophagy axis, we developed a novel luciferase based autophagy reporter, mtFL-p62. Currently available fluorescent based mCherry-GFP-LC3 and GFP-LC3-RFP-LC3ΔG reporter are only amenable monitor autophagic flux in live cells or *ex-vivo* microscopic analysis of tissue section harvested from transgenic animals, thus these approaches fails to monitor autophagic flux in real-time (182). Even with the known benefits of luciferase based reporter system in optical imaging,

currently there are only 3 luciferase based autophagy reporter, out which only polyQ80/polyQ19 sensor has been tested *in-vivo*. Both the LC3-Rluc^{C124A} Luc2p-p62 reporters has been utilized for ratio metric estimation autophagic flux in cell line model. Only the polyQ80/polyQ19 sensor has been utilized to monitor autophagic flux in the skeletal muscles of ATG16L hypomorphic and normal mice by ratio metrically quantifying the degradation of aggregated poly glutamine repeats (polyQ80-luciferase) in comparison to its non-aggregated form (polyQ19). However, ratio metric analysis are difficult to adapt system in pre-clinical models for drug screening and validation (194). Moreover, the autophagy independent degradation of FL2 and poly-glutamine repeats may add confounding factors for estimation of autophagic flux. The mtFL-p62 fusion construct is standalone reporter system, which does not necessitate the use normalization reporters due to the enhanced stability of mtFL (half-life: 9 hours) in comparison to wtFL (half-life 3 hours) which reduces the autophagy independent degradation of the reporter protein thus minimizing the probability of inaccurate measurement of autophagic flux. Utilizing various known autophagy inducers and inhibitors we have validated the accuracy of mtFL-p62 in monitoring autophagic flux. Cisplatin-paclitaxel induced reduction in luciferase activity specifically in Dual^{ER} cells and increased luciferase activity in sensitive and Dual^{LR} cells along with concomitant increase in luciferase activity post combinatorial treatment with U0126/chloroquine highlights the potential of the sensor in real-time monitoring of autophagic flux.

The actual strength of this mtFL-p62 sensor lies in real-time monitoring of autophagic flux from live cells and pre-clinical mouse models, which has never been demonstrated by any of the existing autophagy sensors. In mice model, drug treatment gradually diminished the luciferase signal over 14 days signifying ongoing autophagic flux in the tumours, which was further reflected by immunohistochemical staining of p62 in tumour tissues. Compared to Trametinib or chloroquine treatment alone, which showed a non-significant increase in

luciferase signal, combinatorial treatment of Trametinib or chloroquine with platinum-taxol resulted in more pronounced blockade in autophagic flux by 48-96 hours. Intriguingly, Trametinib was found to block autophagic flux for a period of 24-96 hours in a similar extent as chloroquine, a well-established autophagy inhibitor, indicating the potential of Trametinib

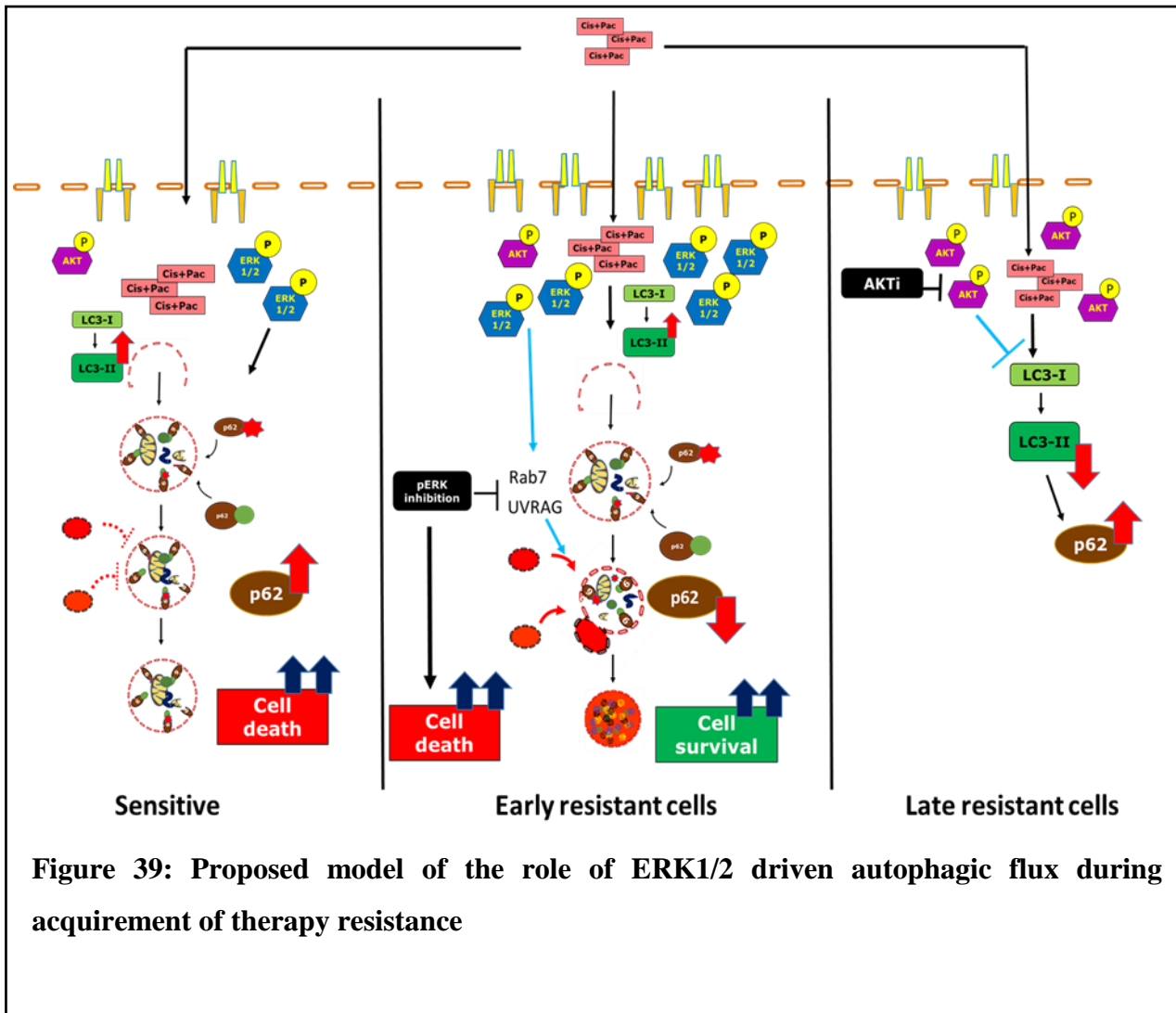


Figure 39: Proposed model of the role of ERK1/2 driven autophagic flux during acquisition of therapy resistance

in regulation of autophagic flux in clinical settings. Administration of CisPac along with Trametinib significantly reduced tumour volume and increased p62 staining intensity compared to untreated and single agent treated group indicating the therapeutic potential of combinatorial regimen of platinum-taxol and Trametinib in management of platinum resistant ovarian cancer. Identification of molecular drivers of cisplatin-paclitaxel dual resistance can significantly improve the therapeutic management of ovarian cancer. Herein, we report that

HGSOC cells responds to chemotherapeutic stress by sustaining a continued autophagic flux driven by hyper activated ERK1/2 at the early stage of resistance development. Addition of these cells to the hyper activated ERK1/2 driven autophagy signalling was observed in both cell line and pre-clinical animal model (Figure 39). Till date, Trametinib and Cobimetinib, are the two FDA approved MEK inhibitors for treatment of BRAF mutant unresectable or metastatic malignant melanoma and non-small cell lung cancer (318, 319). Recently, Ulixertinib (BVD-523), a potent ERK1/2 inhibitor, has shown favourable pharmacokinetics and clinical benefits in *NRAS*- and *BRAF* V600- and non-V600-mutant solid-tumour malignancies with acceptable side effects (NCT01781429). These and other future ERK inhibitors might be able to exert therapeutic benefit to EOC patients by regulating the autophagic flux in the tumour cells particularly after few cycles of platinum-taxol therapy which is known to initiate resistance development. Our unique autophagy sensor would be a valuable resource for such clinical studies.

Although an increased autophagic flux drives the onset of cisplatin-paclitaxel dual resistance, chemotherapy induced autophagic flux remains subdued as the cells acquire a highly chemoresistant phenotype. Thus targeting of ERK1/2 driven autophagic flux may not be successful in the late stage of resistance. Additionally, it is difficult to accurately identify various stages of chemoresistance in clinical settings. Thus, we aimed to investigate alternate strategies to tackle development of highly chemoresistant cells.

**Chapter 3: Repurposing metabolic drug to impede development of
platinum-taxol resistance in ovarian cancer**

3.1 Introduction

Platinum-taxol resistance is the major contributor of poor therapeutic outcome in management of high grade serous ovarian cancer (HGSOC). We have shown in previous chapter that targeting ovarian cancer cells specifically at the onset of development of chemoresistance by inhibiting the ERK1/2 driven autophagy axis provides a possible strategy to manage cisplatin-paclitaxel dual resistance. However, this strategy may not be successful against highly resistant (platinum-taxol) cells, which are characterized by reduced autophagic flux. Attainment of a highly chemoresistant phenotype severely rewires signalling networks making it difficult to design targeted therapy. Majority of the published research are focused on reversing/sensitizing chemoresistant phenotype by targeting key signalling axes rather than identifying preventative measures to delay its acquirement. Thus development of alternate strategies to delay the acquirement of the highly chemoresistant phenotype may be explored. Discontinuous dosing of small molecule inhibitor, vemurafenib, was reported to delay acquirement of therapy resistance in two independently derived primary human melanoma xenografts harbouring BRAFV600E mutation. This strategy was reported to exploit fitness advantage of sensitive cells to proliferate at a higher rate than resistant cells, thus reducing the level of resistance of the overall tumour (320). Treatment of ovarian cancer cell line with combination of ethacrynic acid or selenite along with melphalan was reported to prevent development of melphalan resistance by reducing the activity of glutathione S-transferase (321, 322). Though the success of MDR inhibitors were fairly limited in clinical setting, continuous exposure of paclitaxel in presence of MDR inhibitors NSC23925 was reported to prevent development of paclitaxel resistance in ovarian cancer cells (323). Altogether, these studies indicate the therapeutic potential of developing a strategy to impede the development of therapy resistance is possible. However, no such studies are reported to delay acquirement of platinum resistance in any

cancer cells. Thus utilizing our dynamic cellular model of cisplatin-paclitaxel dual resistance we aimed to ask

5. Is it possible to impede development of a highly chemoresistant phenotype?

Amongst several molecular mechanisms that maintain a highly chemoresistant phenotype, the presence of a small sub-population of cancer cells having self-renewal and tumour initiation properties, termed as Cancer Stem Cells (CSC) significantly contribute to this phenotype (324, 325). Since majority of the chemotherapeutic drugs targets a population of actively proliferating cancer cell, CSCs due to their quiescent nature and increased expression of drug transporters evade the cytotoxic effect of chemotherapeutics (200). Previous reports from our lab suggest enrichment of CSC population in late resistant cells contributes to the highly chemoresistant phenotype in Dual^{LR} cells for both A2780 and OAW42 models (149, 260). Herein, we explore a strategy to achieve delay in development of chemoresistance by lowering the CSC population through targeting their metabolic pathways.

Rewiring of cellular metabolism from TCA cycle to aerobic glycolysis is a critical mechanism which regulates maintenance and differentiation of CSCs (326, 327). Alteration in the level of cellular metabolites like Carnitine and acetylcarnitine can regulate mitochondrial metabolism which in turn regulates differentiation of adipose-derived mesenchymal stem cell (328). Cellular metabolites like methionine also affects the epigenetic make up for maintenance of stemness via histone methylation (329). Taurine, a semi-essential amino acid synthesised in the body as by product of cysteine and methionine metabolism, has been reported to promote differentiation of neuronal and mesenchymal stem cells (26, 27)(26, 27)(26, 27)(26, 27)(26, 27)(319, 320)(319, 320)(319, 320)(16, 17). However, the role of these metabolites in regulation of CSCs are yet to be investigated.

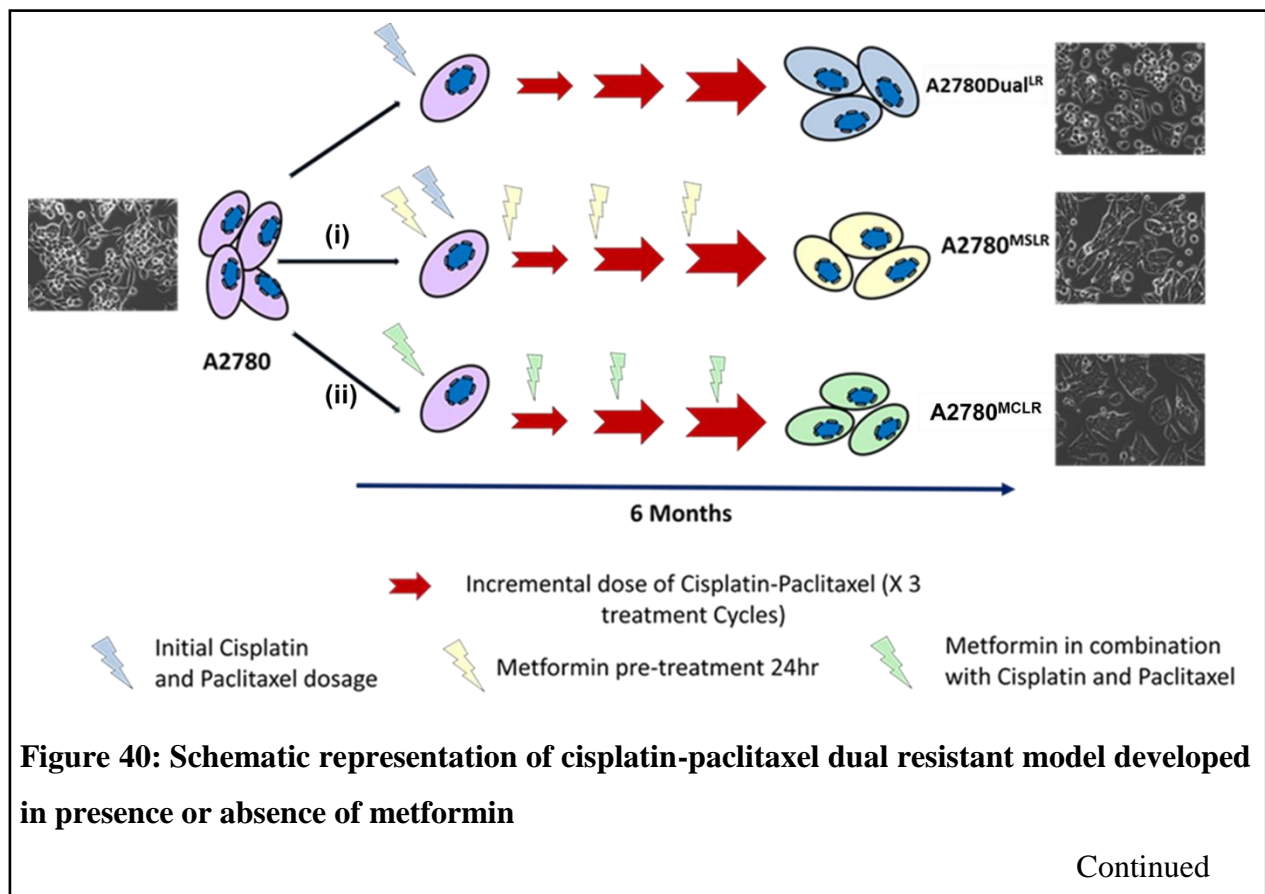
Metabolic drug such as metformin, commonly prescribed for type II diabetes, has been repurposed as anti-tumour agent in several cancers including EOC (330-332). Several reports also suggest the role of metformin in regulation of CSC (330, 333-335). The landmark study by Evans et al reported a reduced incidence of ovarian cancer in diabetic patients receiving metformin (336). In a cohort of 73 EOC patients, administration of metformin was associated with increased survival suggesting the anti-tumour efficacy of metformin (17). Efficacy of metformin as anti-tumour agent has also been demonstrated in pre-clinical SKOV3ip1 xenograft and LSL-Kras^{G12D/+}Pten^{loxP/loxP} mice model of EOC (20). Apart from alteration in glucose metabolism, administration of metformin also regulates lipid metabolism and TCA cycle (337, 338). The anti-proliferative effect of high dose of metformin has been reported in TYKNU, OV90, and OVCAR 433 cell lines. Metformin treatment significantly altered the level of mitochondrial shuttle metabolites and mitochondrial respiration (339). Although, multiple reports described multifunctional effects of metformin on proliferation, sensitization, cellular metabolism and tumour growth, the consequence of administration of low dose of metformin as an adjuvant to platinum-taxol during gradual acquirement of chemoresistance is yet to be investigated.

Herein, we assessed the efficacy of continuous administration of low dose metformin along with platinum and taxol as a therapeutic strategy to impede the development of highly chemoresistant phenotype. We further demonstrated the role of metformin induced alteration in cellular metabolism in maintenance/differentiation of CSC population and therapy resistance.

3.2 Materials and Methods:

3.2.1 Development of cisplatin-paclitaxel dual resistant model in presence of metformin:

Cisplatin-paclitaxel dual resistant A2780 and OAW42 cellular models were developed as described above in Section 2.2.1. Since there no earlier report on the use of metformin as an adjuvant to platinum-taxol, two strategies of metformin administration were implemented : i) MSLR cells of both A2780 and OAW42 were developed by sequential treatment with metformin (24 hours) followed by platinum-taxol for 2 hours and ii) MCLR cells of both models were developed by combinatorial treatment of metformin and cisplatin-paclitaxel (2 hours). The pulse method of cisplatin-paclitaxel treatment were adopted for all the cellular models i.e cisplatin-paclitaxel dosage was escalated after every 3 cycles of chemotherapy for period of six months. In order to avoid metformin induced cytotoxicity, metformin was administered at a low dosage (IC_{20} i.e., 2mM) (Figure 40).



A2780Dual^{LR} was developed by administration of incrementing doses of cisplatin and paclitaxel (doses were escalated after every 3 cycles). Two strategies of metformin administration was followed (i) Pre-treatment with metformin for 24 hours, followed by 2 hours of cisplatin and paclitaxel for development of A2780^{MSLR} cells. (ii) Combinatorial treatment with metformin along with cisplatin-paclitaxel for 2 hours was followed for development of A2780^{MCLR} cells. Phase contrast microscopy images of each cell type is represented alongside.

3.2.2 MTT assay

MTT assay was performed as above and described in section 6.4.1

3.2.3 Trypan blue exclusion assay for cell proliferation

Proliferation rate was estimated using trypan blue exclusion assay by manual cell counting using a haemocytometer as described in detail in section 6.3.5. Using the number of viable cells over a period of 120 hours we calculated doubling time (Td) using an online calculator.

3.2.4 Clonogenic assay

To determine the ability of Dual^{LR}, MSLR and MCLR to tolerate the cytotoxic effect of cisplatin-paclitaxel, long term survival of each cells were measured in terms of colony forming ability in presence of two increasing dosage of platinum taxol. The detailed method for quantitation of clonogenic potential of each cells is described in section 6.4.3.

3.2.5 Immunoblotting

Immunoblotting was performed to estimate the level of phospho and total ERK1/2 and AKT as described in section 6.5.

3.2.6 Quantitative real-time PCR

Real time PCR was performed to quantitate the expression of Sox-2, Oct-4 and Nanog with respect to internal control GAPDH as described in section 6.11. Sequence of each gene is described in section 6.11.5

3.2.7 Side population assay

Side population assay was performed to estimate the percentage of CSCs in the sensitive, Dual^{LR}, MSLR and MCLR cells. Side population assay distinguishes CSCs from non-CSCs based on their increased ability to efflux drug in presence and absence a drug transporter inhibitor Verapamil. The detailed method has been described in section 6.13.

3.2.8 Surface biomarker based CSC quantification

CD133 is a well-established marker of CSC population in ovarian cancer. Percentage of CD133^{+ve} cells was estimated by staining cells with anti-CD133 antibody followed by flow cytometric analysis as described in section 6.8.2.

3.2.9 Cell Metabolome Quenching and Metabolites Extraction for NMR Analysis

Cell metabolites were quenched using liquid nitrogen and extracted using phase separation as described in section 6.14.1.

3.2.10 NMR experimentation and metabolite identification

¹H-Nuclear Magnetic Resonance spectra was acquired on an 800MHz Bruker Avance AV III spectrometer using water signal suppression programme at 298K. Metabolites were identified using literature survey and 2D-NMR spectra followed by TOSCY and COSY analysis as described in section 6.14.2..

3.2.11 Statistical analysis

To determine whether observations are statistically significant student T-test, Mann–Whitney U test, and one-way analysis of variance (Kruskal Wallis test) were performed as mentioned in result section and described in detail in section. A p value of less than 0.05 was considered statistically significant.

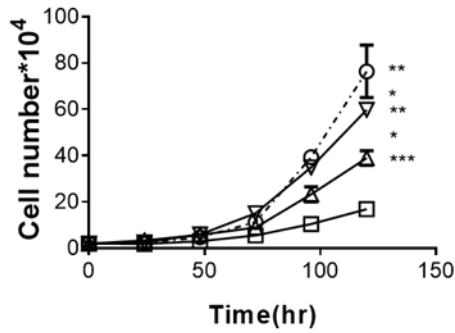
3.3 Results:

3.3.1 Metformin intervention during acquirement of platinum-taxol resistance promotes proliferation

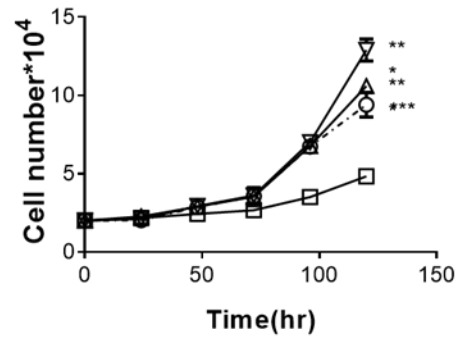
Since metformin is reported to alter proliferation of ovarian cancer cells, we estimated the proliferation rate of cisplatin-paclitaxel dual resistant cells developed in presence or absence

of metformin in both our indigenously developed cellular (A2780 and OAW42 models) of EOC. The proliferative capacity was highest in parental of A2780 and OAW42 cells. Intriguingly both A2780^{MCLR} and A2780^{MSLR} cells displayed an increased proliferation rate than A2780Dual^{LR} cells from 96 hours onwards (Figure 41A). Similarly, OAW42^{MSLR} and OAW42^{MCLR} cells displayed increased proliferation potential in comparison to OAW42Dual^{LR} cells from 72 hours onwards (Figure 41B). The proliferation data was used to quantitate the doubling time of A2780^{MSLR} and A2780^{MCLR} cells which were 28.05 ± 0.60 hours and 24.18 ± 0.14 hours respectively in comparison to A2780Dual^{LR} cells having longest doubling time of 39 ± 0.93 hours, while parental A2780 cells doubled in 23.02 ± 0.74 hours. Also a significantly reduced doubling time was observed in OAW42^{MSLR} (43.59 ± 1.02 hours) and OAW42^{MCLR} (36.66 ± 0.11 hours) cells with respect to doubling time of 84.25 ± 11.42 hours in OAW42Dual^{LR} cells. The doubling time of parental OAW42 cells was 43.73 ± 3.11 hours (Figure 41C), thus indicating the Dual^{LR} cells have reduced proliferative capacity in comparison to MCLR and MSLR cells in both Models. Since ERK1/2 activation promotes a proliferative phenotype in comparison to AKT activation which sustains an increased survival potential we compared the level of basal ERK1/2 and AKT activation in our chemoresistant model, which revealed an increased ERK1/2 phosphorylation in dual resistant cells developed in presence of metformin (MSLR and MCLR) in both A2780 and OAW42 model. A2780Dual^{LR} and OAW42Dual^{LR} cells showed increased phosphorylation of AKT in comparison to respective MSLR and MCLR cells. The parental sensitive A2780 and OAW42 cells showed reduced phosphorylation of both ERK1/2 and AKT, indicating long term presence of metformin promotes activation of ERK1/2 while AKT activation remains low in comparison to Dual^{LR} cells (Figure 41D-H).

A \circ A2780 \square A2780^{LR}
 \triangle A2780^{MSLR} ∇ A2780^{MCLR}



B \circ OAW42 \square OAW42^{LR}
 \triangle OAW42^{MSLR} ∇ OAW42^{MCLR}



C \square A2780 \square A2780^{LR}
 \blacksquare A2780^{MSLR} \square A2780^{MCLR}
 \square OAW42 \square OAW42^{LR}
 \blacksquare OAW42^{MSLR} \square OAW42^{MCLR}

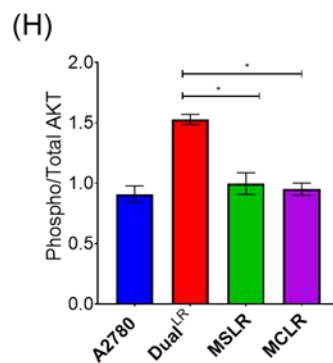
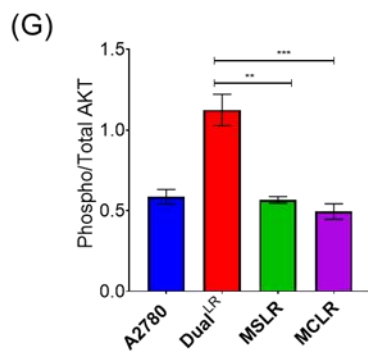
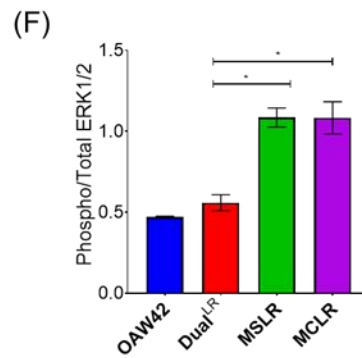
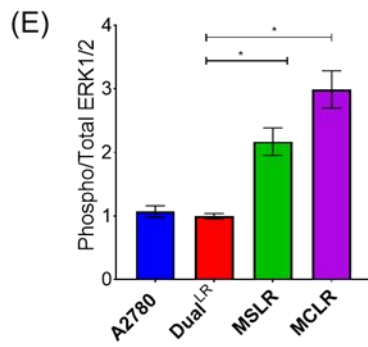
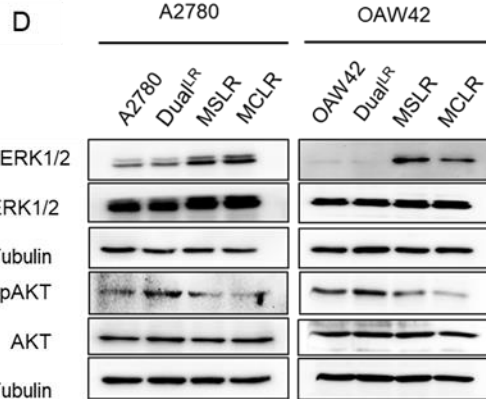
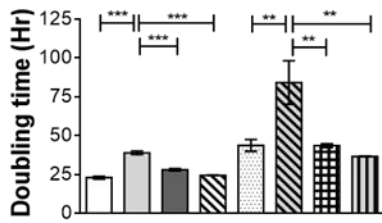


Figure 41: Presence of metformin during acquirement of resistance promotes a proliferative phenotype

(A-B) Graph depicting proliferation rate of A2780 and OAW42 resistant cells over a span of 120 hours. MSLR and MCLR cells had a higher proliferation rate than Dual^{LR} cells in both models. (C) Quantification of doubling time revealed a significantly reduced doubling time in MCLR and MSLR cells compared to Dual^{LR} cells of both model (D) Immunoblot depicting enhanced ERK phosphorylation in MSLR and MCLR cells, and enhanced AKT phosphorylation in LR cells in both the A2780 and OAW42 resistant models.

3.3.2 Long term metformin treatment impedes development of chemoresistance and reduce CSCs

To comprehend the effect of continuous and sequential administration of metformin in cisplatin-paclitaxel dual resistance, we quantified the cell viability in presence of chemotherapeutics. Interestingly, combinatorial treatment of A2780Dual^{LR} cells with cisplatin (50 ng/ml) and paclitaxel (8.5 ng/ml) for 72 hours induced a mere 4.5±2 % cell death while similar treatment significantly increased cell death in A2780^{MSLR} (33±2.73%) and A2780^{MCLR} (39±0.46 %) cells. Similarly, an 18.51±2.4 % and 32.26±2.9% death was observed in OAW42^{MSLR} and OAW42^{MCLR} cells respectively in comparison to 6.2±4.2% cell death in OAW42Dual^{LR} post 72 hours of platinum taxol treatment. Similar dosage induced ~50% cell death in parental A2780 and OAW42 cells (Figure 42A). The long term survival potential of these cells in presence of two increasing dosage of platinum-taxol were estimated using clonogenic assay which revealed a significantly greater fraction of colonies in the A2780Dual^{LR} cells in both dosage (~90% surviving fraction in 100ng/ml cisplatin+13ng/ml paclitaxel and 65% surviving fraction against 200ng/ml cisplatin+26ng/ml paclitaxel). While the similar treatment reduced surviving fraction in A2780^{MSLR} (~66% and 18% respectively),

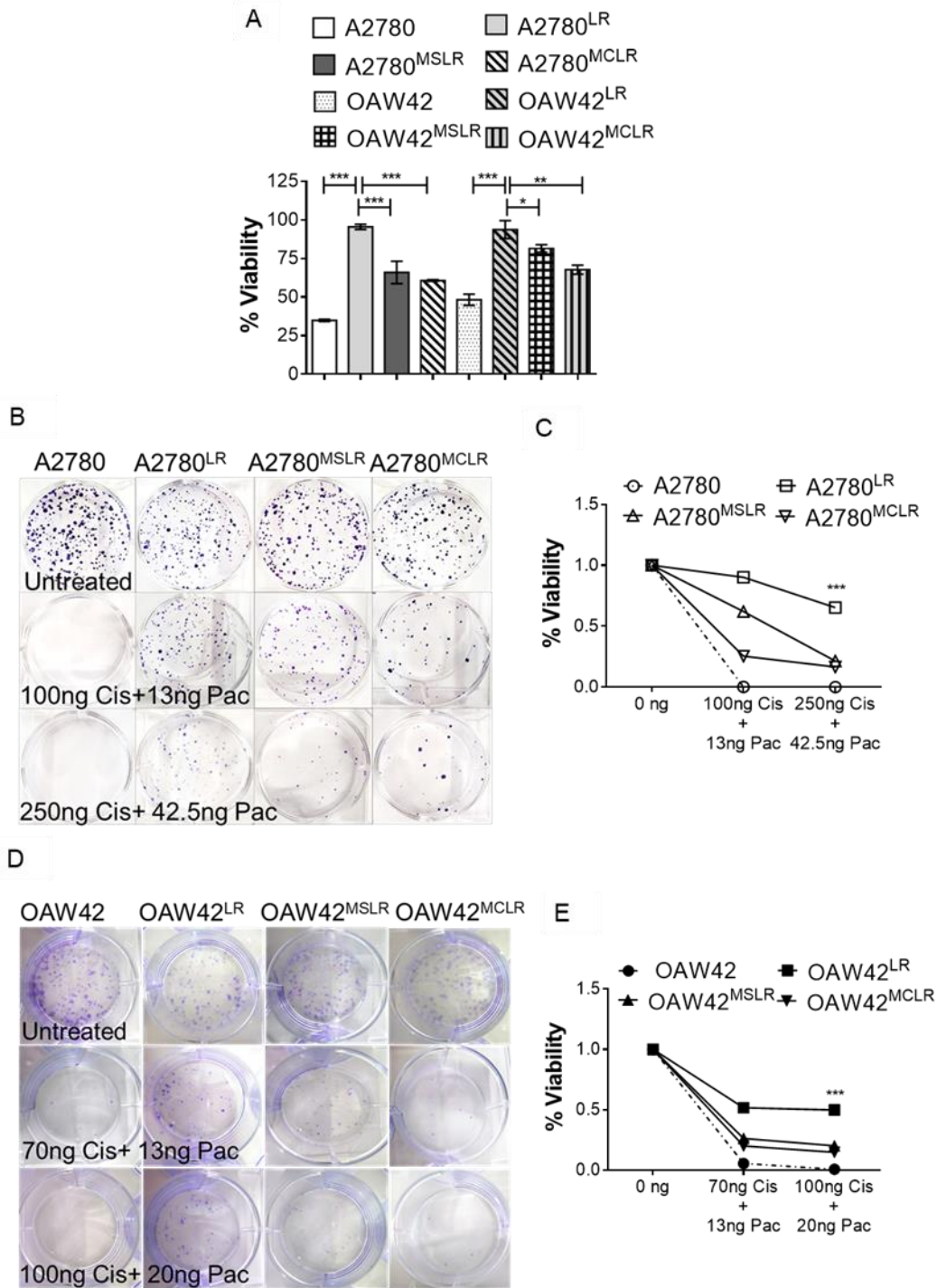


Figure 42: Presence of metformin reduces tolerance of resistance cells to therapy

(A) MTT assay showing significantly reduced viability of MCLR, MSLR as compared to Dual^{LR} cells, in response to 50ng cisplatin+8.5ng paclitaxel/ml in both A2780 and OAW42 models. (B-E) Long term survival assay of A2780 and OAW42 cell models in response to increasing concentration of cisplatin-paclitaxel treatment displayed significantly higher colony forming ability in LR cells compared to MCLR and MSLR cells in both the cellular models.

and A2780^{MCLR} (~19% and 17% respectively) in both the dosage (Figure 42B-C). Similarly, 50% of OAW42Dual^{LR} colonies survived platinum-taxol treatment while only 21% and 16% survival fraction was observed in OAW42^{MSLR} and OAW42^{MCLR} cells post treatment with 250ng Cisplatin+20ng Paclitaxel/ml (Figure 42D-E). Since, previous reports from our lab suggests the increased CSC fraction in the Dual^{LR} significantly reduces the effectivity of cisplatin-paclitaxel, we quantified the percentage of CSC population using a functional assay based on the increased drug efflux potential of CSCs (149). Highest percentage of CSCs were observed in A2780Dual^{LR} cells (28.6 %) population while a presence of metformin significantly reduced CSCs population in A2780^{MSLR} (15.1%) and A2780^{MCLR} (9.70%) cells. Only 2.16% of parental A2780 cells were CSC (Figure 43A). A significantly higher fraction of CSCs was also observed in OAW42Dual^{LR} cells (22.1%) in comparison to OAW42^{MSLR} (4.13%) and OAW42^{MCLR} (6.79%) cells (Figure 43B). To further validate the alteration CSC population in MSLR and MCLR cells in comparison to Dual^{LR} cells, we quantified the CSC population based on surface expression of CD133, a well-established CSC biomarker of ovarian cancer. A significantly reduced CD133^{+ve} population of 28.5% and 35.5% was observed in A2780^{MSLR} and A2780^{MCLR} cells respectively in comparison to 74.4% CD133^{+ve} population in A2780Dual^{LR} cells (Figure 43C). A similar increased percentage of CD133^{+ve} population was detected in OAW42Dual^{LR} (9.63%) cells in comparison to 4.29% and 0.64% CD133^{+ve} population in OAW42^{MSLR} and OAW42^{MCLR} cells (Figure 43D). The parental A2780 and OAW42 also showed reduced percentage of CSCs based on CD133 expression. Moreover the A2780Dual^{LR} and OAW42Dual^{LR} cells showed increased expression Oct 4, Sox 2 and Nanaog, pluripotent genes with respect to MSLR and MCLR cells of both models, thus indicating the presence of metformin during acquirement of therapy resistance significantly reduces stemness and sensitizes the cells to platinum-taxol (Figure 43E-F).

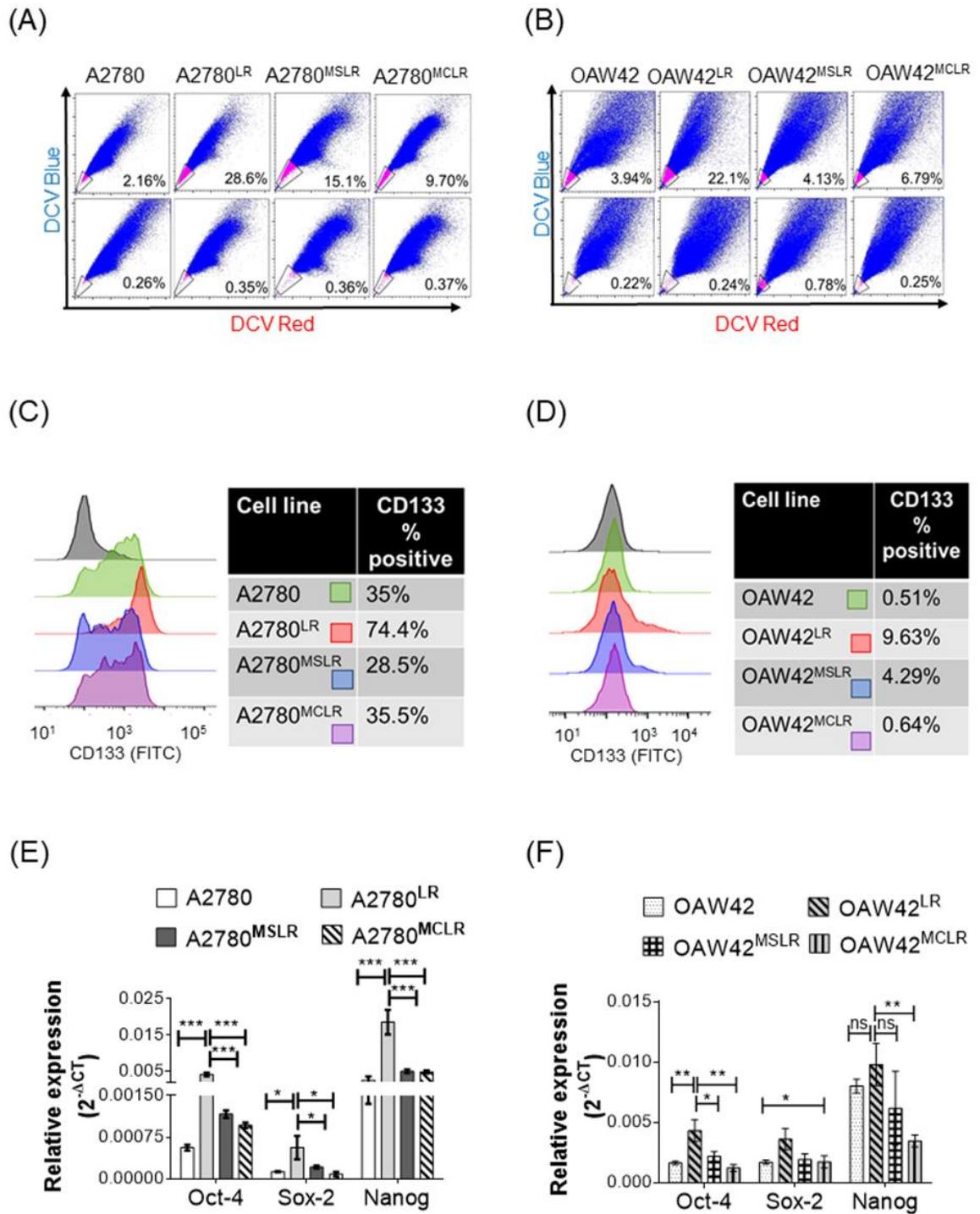


Figure 43: Presence of metformin reduces stemness properties.

Continued

(A-B) FACS dot plot showing side population distribution (tail end of scatter) with and without verapamil in A2780 and OAW42 cellular resistant models. Both the MSLR and MCLR cells of A2780 and OAW42 cellular model had a reduced SP population compared to LR cells. (C-D) Histogram showing an increased expression of CSC biomarker CD133 in LR cells of both the A2780 and OAW42 resistant model in comparison to MSLR and MCLR cells. (E-F) Quantitative PCR showing the relative expression of pluripotent genes (oct-4, sox-2, nanog), in A2780 and OAW42 cellular models. GAPDH was used as an internal control. MSLR and MCLR cells show significantly reduced expression of pluripotent genes compared to LR cells.

3.3.3 Metformin treatment alters the level of semi-essential amino acids

Metformin, a metabolic drug primarily targets complex I of the electron transport chain of mitochondria leading to alteration in cellular metabolism. We aimed to characterize the global metabolome of dual resistant cells developed in presence or absence of metformin by 1D ¹H-NMR spectroscopy. The metabolic profile of A2780^{MSLR} and A2780^{MCLR} cells were distinguishable from A2780Dual^{LR} cells as observed by orthogonal partial least squares discriminant analysis OPLS-DA, a higher supervised clustering method for comparison between two groups (Figure 44A-B). Further this model was utilized to extract/identify the significantly altered metabolites amongst the groups. One dimensional (1D) ¹H-NMR spectral peaks corresponding to specific metabolites were identified using through literature review followed by confirmation using dimensional (2D) NMR experiments [Total Correlation Spectroscopy (TOCSY) and Correlation Spectroscopy (COSY)]. We identified 41 metabolites from the 1D-NMR spectra. Interestingly, a significant increase in the level of taurine and histidine were observed in A2780^{MCLR} and A2780^{MSLR} cells in comparison to A2780Dual^{LR} cells by both the multi and uni-variate analysis (Figure 44C-D). A 2-fold and 1.9-fold increase in taurine level was observed in A2780^{MSLR} and A2780^{MCLR} respectively in comparison to

A2780 cells while taurine level remained similar in A2780Dual^{LR} (~1.2 fold) (Figure 44E). A significant increase in histidine level was observed in A2780^{MCLR} (~3 fold) and A2780^{MSLR} (~2.33 fold) cells compared to A2780 cells. A 1.3-fold increased histidine level was observed in A2780Dual^{LR} (Figure 44F). Analysis of the metabolic profile revealed significant alteration in only two metabolites, which is indeed expected as the resistant cells were developed in a synchronous manner thus alteration in multiple metabolites were not expected. Identification of only 2 significantly upregulated metabolites specifically in metformin treated ones increased our confidence.

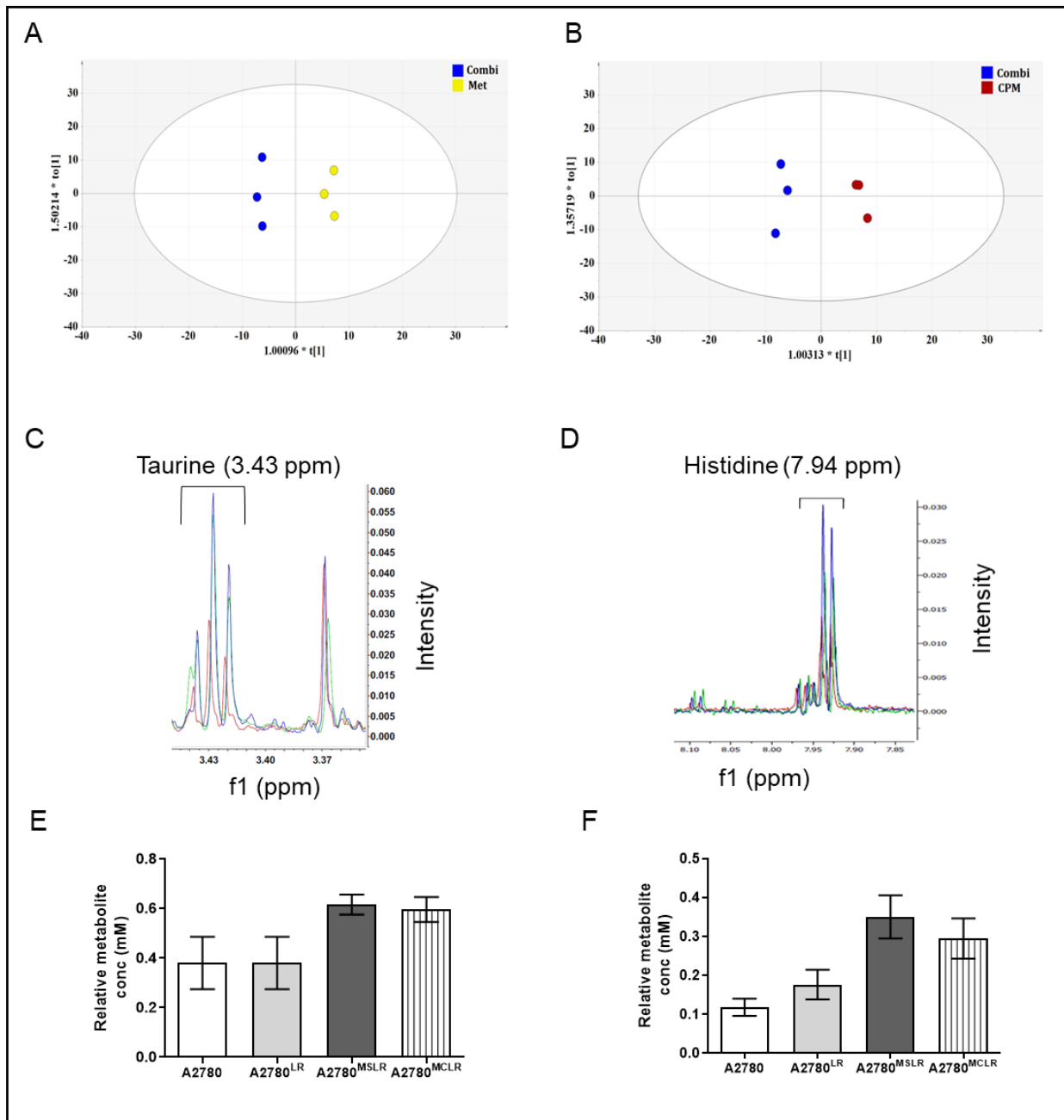


Figure 44: Continuous presence of metformin during development of resistance alters amino acid metabolism

(A-B) Orthogonal partial least squares discriminant analysis (OPLS-DA) showing optimized discrimination between (A) A2780Dual^{LR} (COMBI) vs. A2780^{MCLR} (MET) (R2X=0.578, R2Y=0.404 and Q2=0.404), A2780Dual^{LR}(COMBI) vs. A2780^{MSLR} (CPM) (R2X=0.897, R2Y=0.989 and Q2=0.738). (C-D) Inset representing regions from the superimposition of the mean NMR spectra of A2780Dual^{LR} (Red), A2780^{MSLR} (Blue), A2780^{MCLR} (Green), indicating differential level of taurine and histidine (E-F) Concentration of Taurine (E) and Histidine (F) relative to loading control TSP across A2780, A2780Dual^{LR}, A2780^{MSLR} and A2780^{MCLR}

3.3.4 Taurine regulates CSC differentiation and sensitizes cells to therapy

Increased taurine level or its external supplementation promotes differentiation of stem cells. Interestingly, the MCLR and MSLR cells of both models had reduced CSCs population, which prompted us to investigate the consequence of taurine supplementation on CSCs. In order to avoid cytotoxicity, taurine treatment was administered at a low dosage (Figure 45C). A 5.7% and 10.6% reduction in s population was observed post 10mM (IC₂₀) and 25mM (IC₃₀) of taurine treatment respectively compared to the untreated A2780 cells (Figure 45A). Similar treatment of taurine in SKOV3, an intrinsically platinum EOC cell line led to 3.81% and 5.33% reduction in SP population in comparison to its untreated counterpart (Figure 45B), indicating external supplementation of taurine reduces CSCs population in therapy resistant EOC cell line. Intriguingly, combinatorial treatment of platinum-taxol (50ng Cisplatin + 8.5 ng paclitaxel/ml) along with taurine (10mM and 25mM) in A2780Dual^{LR} cells significantly induced 27.22±2.62% and 49±2.35% cell death respectively in comparison to cells treated with only platinum-taxol (7.61±2.28%) (Fig 45C).

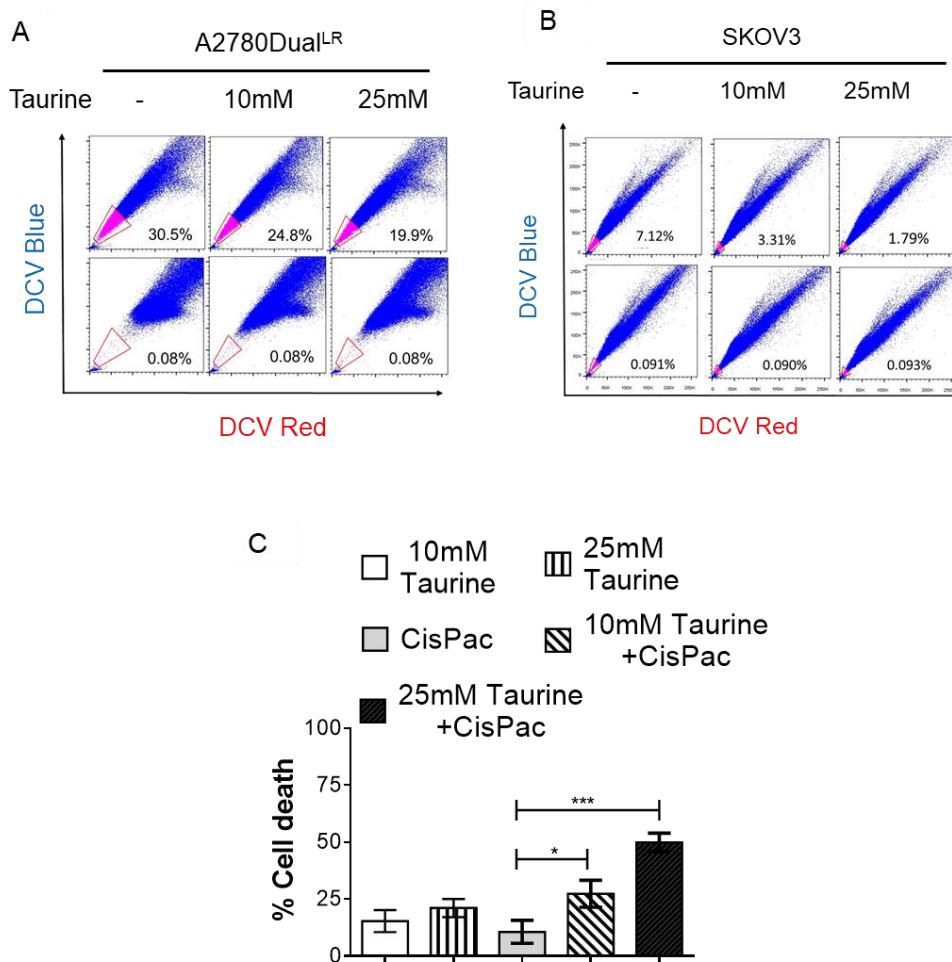


Figure 45: Taurine promotes CSC differentiation and sensitizes cells to therapy:

(A-B) FACS dot plot depicting the side population distribution in A2780^{LR} and SKOV3 cells treated with taurine. Treatment of taurine for 24 hours reduced stem cell like population as compared to untreated in both the cell lines. (C) D) MTT assay showing percentage of cell death in response to taurine and cisplatin-paclitaxel. Combination of taurine+cisplatin-paclitaxel significantly sensitized A2780^{LR} cells towards platinum-taxol.

3.4 Discussion:

Relapse of chemoresistant disease within a short period from the end of initial cisplatin-paclitaxel therapy is a significant challenge for ovarian cancer management. Development of highly chemoresistant phenotype renders platinum-taxol in-effective for successive rounds of therapy (4). Enrichment of small sub-population of sparing CSCs after the initial therapy can

likely contribute to the disease relapse and chemoresistant phenotype (325). Therapy induced increase in cell population expressing ALDH1A1, CD44 and CD133 had been reported in EOC (340, 341). Thus targeting CSC population can offer therapeutic benefit in ovarian cancer management and identification and validation of novel therapeutic strategies against CSCs are crucial. CSCs show an altered metabolic profile which regulates its quiescent nature (342, 343). Herein, we aimed to repurpose a commonly prescribed metabolic drug “metformin” to target cellular metabolism and CSCs in order to prevent development of a highly chemoresistant phenotype. To evaluate the role of low dose of metformin as an adjuvant to platinum-taxol, we developed platinum-taxol dual resistant cellular models of EOC by treatment of sensitive A2780 and OAW42 cells with incremental dosage of cisplatin-paclitaxel either alone or in presence of metformin. Administration of metformin during gradual acquirement of chemoresistance significantly altered the proliferative capacity, level of ERK1/2 and AKT activation and also sensitized the cells to therapy by targeting the CSC population in both model of acquired resistance. The effect of metformin in reduction of CSC population was evident by the reduction in side population, percentage of CD133 expressing cells and reduced expression of pluripotent genes like Sox 2, Oct 4 and Nanog. Presence of metformin during acquirement of resistance significantly increased the level of two amino acids, histidine and taurine, in comparison to sensitive and cisplatin-paclitaxel dual resistant cells. Interestingly, treatment of highly resistant cisplatin-paclitaxel dual resistant A2780Dual^{LR} and intrinsically platinum resistant SKOV3 cells with low dose of taurine significantly reduced the reduced the CSC like population and promoted platinum-taxol induced cell death (Chemo-sensitization). Altogether, we propose a therapeutic strategy to impede the development of a highly chemoresistant phenotype by repurposing metformin, administration of which at a low dose significantly promotes CSC differentiation by upregulating the taurine level. Our study also highlights, the

potential of a common health supplement, taurine in CSC differentiation and chemosensitization.

Repurposing of therapeutics approved for treatment of one particular disease to manage another different pathological condition is a cost and time effective strategy for implementation of novel therapeutic strategies. The repurposed molecule can be directly tested of its efficacy in clinical trials since the initial research on its pharmacokinetics, side-effects and other pharmacological characteristics remains largely understood. Thus can be readily approved and integrated in the management of the disease of interest. A large body of clinical and pre-clinical research supports the notion of repurposing metformin for management of EOC. In a cohort of 239 EOC cases, 61 patients who received metformin showed a significantly ($p=0.007$) higher 5 year disease free survival (67%) in comparison to patients without metformin treatment (47%). Metformin was reported to be independent predictor of survival with a hazard ratio of 3.7 (17). Xu et al, 2018 reported that combinatorial treatment of metformin along with cisplatin impairs NF κ B activation, thus reducing the level IL-6 in the tumour stroma of EOC patients which turns delays tumour growth (344). Metformin treatment at a very high dosage was reported to impart anti-proliferative effect in EOC cell lines (8 mM for 48 hours) and tumour xenografts (200mg/kg) (19, 21). Developing a cellular model closely mimicking the clinical scenario of patients suffering from platinum-taxol dual resistant EOC, we investigated the molecular and cellular alterations as a consequence of continuous metformin treatment during acquirement of therapy resistance. Surprisingly, the MSLR and MCLR cells developed by sequential and combinatorial treatment of metformin along with cisplatin-paclitaxel respectively displayed an increased proliferation rate of 2.5-fold and 3.5-fold respectively in comparison to Dual^{LR} cells of both models after 72-96 hours. This discordance with previous reports might be the result of the high dosage used in other reports in comparison to a low dosage used in our study and the one-time nature of treatment versus

the continuous administration of metformin. Thus our data indicates that continuous administration of sub-lethal (IC₂₀) dosage of metformin promotes cellular proliferation when administered in combination with chemotherapeutics. Application of metformin had been reported to significantly increase the sensitivity of breast, lung and prostate cancer cells to chemotherapy (345, 346). Metformin treatment was also reported to sensitize both cisplatin resistant and paclitaxel resistant EOC cells to therapy (347). In agreement with previous studies, we also report that presence of metformin during evolution of therapy resistance in MSLR and MCLR cells, significantly reduces the tolerance of these cells to cisplatin-paclitaxel in comparison to the Dual^{LR} cells, which were developed in absence of metformin. As the majority of the cytotoxic drugs predominantly targets the proliferative cells, the reduced tolerance of MSLR and MCLR cells towards platinum-taxol may be ascribed to the increased proliferation rate of these cells as compared to slow proliferation rate of Dual^{LR} cells. ERK1/2 activation fosters a proliferative phenotype via upregulation of cell cycle entry genes along with downregulation of genes that impairs the process, in contrast AKT activation reduces cell cycle entry and supports a quiescent cell-survival phenotype (260, 348, 349). Metformin regulates ERK1/2 activation in a context dependent manner, metformin positively regulates ERK1/2 activation in promyelocytic leukemia and acute myeloid cells while metformin treatment in pancreatic cancer cells inhibits ERK activation (132, 350). Herein we observed an increased basal level of activated ERK1/2 in MCLR and MSLR cells for both the cellular models, while the basal level of AKT activation was significantly lower in these cells in comparison to Dual^{LR} cells. Thus an increased ERK1/2 signalling in the MSLR and the MCLR cells may promote their high proliferative nature, while the hyperactive AKT signalling in the Dual^{LR} cells may support a quiescence state with enriched CSCs population.

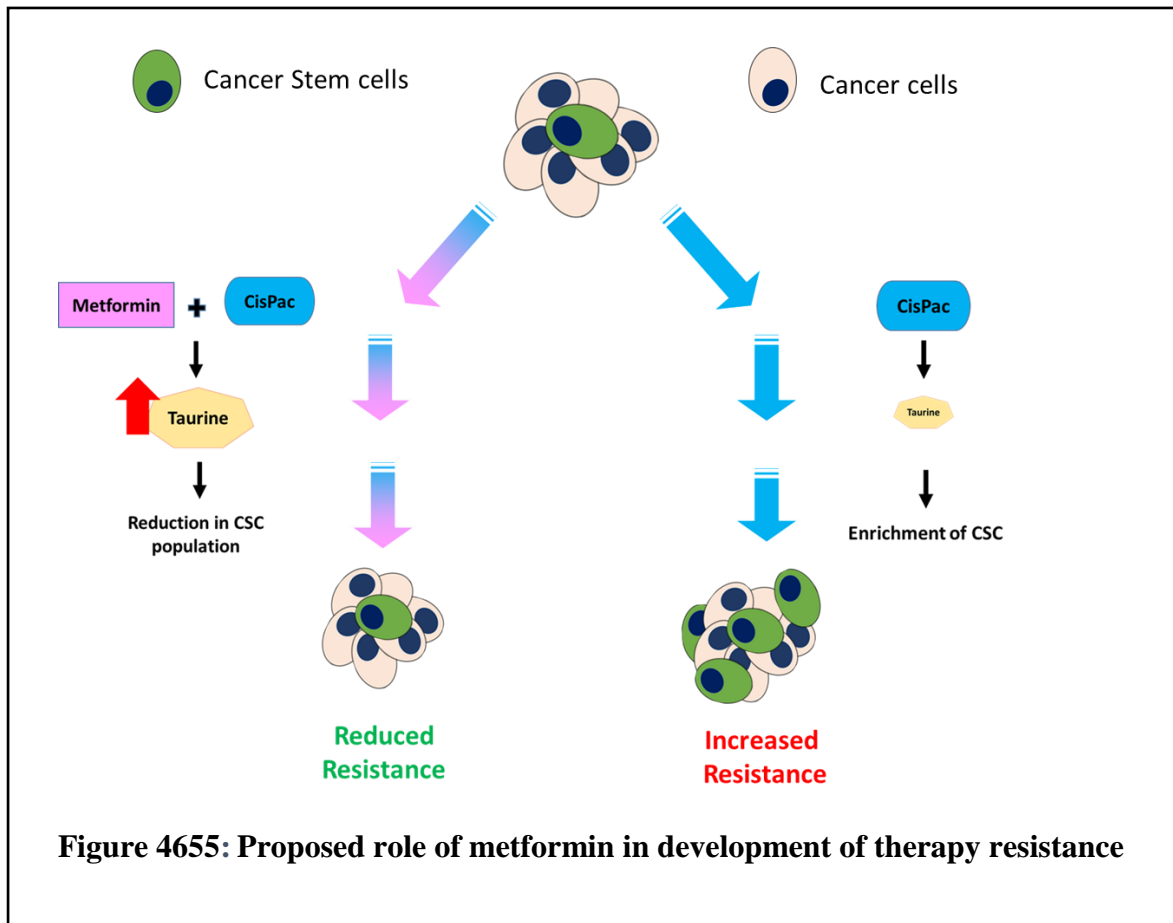
Increased stemness phenotype can significantly promote therapy resistance in several cancers including EOC (202, 207). Previously our lab reported an increase in percentage of CSC

population with acquirement of cisplatin-paclitaxel dual resistance (149). Metformin treatment had been associated with reduced spheroid formation and decrease in percentage of ALDH⁺ cells in SKOV3 and A2780 cells (351). Reduced formation of mamosphere was reported in metformin treated breast cancer cells (330). Interestingly, we observed a reduction in CSC population in cisplatin-paclitaxel resistant cells developed in presence of metformin indicating the role of metformin in promoting CSC differentiation in comparison to their Dual^{LR} counterpart which were developed in absence of metformin in both A2780 and OAW42 resistant models. The percentage of CD133⁺ ovarian cancer cells also reduced in MSLR and MCLR cells of both cellular models. The reduced expression of Nanog, Sox-2 and Oct 4 in MSLR and MCLR cells in comparison to Dual^{LR} cells point to the increased differentiation of CSCs to non-CSC population in presence of metformin in both the cellular models. These results substantially advocates the role of metformin in promoting differentiation of stem like population in EOC cells, which in turn could result in to reduced tolerance of these cells to platinum-taxol.

Stemness phenotype of cancer cells are also regulated by cellular metabolism and bioenergetics, alteration in which can promote differentiation of CSCs in to non-CSCs (335, 352). Metformin, is a metabolic drug that primarily targets the complex I of the mitochondria (353). Deletion of TCA cycle intermediates was reported in metformin treated breast and non-small cell lung cancer cell lines (354, 355). Metformin treatment prior to upfront surgery was reported to alter mitochondrial metabolism, nucleotide metabolism, TCA cycle and redox pathways in EOC patients (356). Intriguingly, we detected an alteration in both purine metabolism (Histidine level) and semi-essential amino acid metabolism (Methionine/Cysteine-Taurine level) as a result of administration of low dose of metformin for a prolonged period during development of cisplatin-paclitaxel dual resistant cellular models. Since we synchronously developed our cellular models of chemoresistance we did not expect a global

changes in tumour metabolome, indeed we observed alteration in two specific metabolites as a result of combination treatment of metformin and platinum-taxol. The metabolic profile of MSLR (sequential treatment) and MCLR (combinatorial treatment) cells were similar as was the other cellular properties like proliferation, stemness and chemoresistance, indicating an equivalent therapeutic outcome irrespective of the treatment strategies. Taurine is a semi-essential amino acid synthesized in presence of vitamin B₆ from cysteine or methionine, it plays a crucial role in retinal function and calcium homeostasis in neurons (357). Major physiological function of taurine include antioxidant activities, anti-inflammatory effects, osmoregulatory actions (358). Apart from its physiological functions, supplementation of taurine at a high dosage was reported to promote apoptosis in colon and lung cancer cells (359, 360). Taurine treatment also promotes differentiation of mesenchymal stem cell via increased ERK1/2 activation in neuronal and retinal stem cells (27). However, the role of taurine on CSC homeostasis has yet not been explored. Taurine supplementation to standard culture condition at a low dosage of 10 and 25mM for 24 hours significantly decreased the percentage of SP population to 24.6% and 19.9% respectively in comparison to untreated A2780Dual^{LR} (30.5%) cells, indicating the role of taurine in inducing differentiation of CSCs into non-CSC population. Similar treatment of taurine also reduced SP population in a dose dependent manner in SKOV3, an inherently platinum resistant EOC cell line. Also, increased taurine level was negatively correlated with reduced CSC like population in the MSLR and MCLR cells. Further we observed that the combinatorial treatment of taurine (10mM and 25mM) along with platinum-taxol induced a 2.65- and 4.68-fold increased cell death in Dual^{LR} cells in comparison to only chemotherapy, indicating the chemo-sensitization effect of taurine, which may be contributed to the increased differentiation of CSC population. Thus we identified a novel role of a common health supplement taurine on CSC homeostasis and chemoresistance, which may serve as novel approach to combat chemoresistance. Altogether our data signifies that the

continuous presence of metformin impedes the development of a highly chemoresistant phenotype by regulating taurine level which in turn promotes CSC differentiation (Figure 46).



**Chapter 4: Development of BRET based bio-molecular interaction
platform to predict response of non-platinum drugs**

4.1 Introduction:

The evolution of a highly chemoresistant phenotype can be prevented at the onset of resistance development by targeting ERK1/2-autophagy axis or can be delayed by metformin intervention (361, 362). However, attainment of a highly chemoresistant phenotype may render these strategies unsuccessful. In such scenarios, alternate drugs that act by attacking other critical pathways are the only choice to achieve some response. Clinically, platinum resistance is defined by time course (progression free interval, PFI) within which disease relapses after completion of first line therapy. The term “platinum-resistant relapse” defines a condition wherein the disease relapses within 6 months of completion of front-line platinum-taxol therapy and these patients never respond to platinum-again. While cases with PFI of greater than 6 months are termed “platinum-sensitive relapse” and these cases respond to platinum again with or without an alternate drug. However, these cases also develop platinum resistance over the course of multiple relapse and therapy. Platinum-resistant relapse cases have a dismal progression free (3-4 months) and overall survival (approximately a year) (363). Currently, there is no effective targeted therapy against platinum-resistant ovarian cancer. The only targeted therapy that has progressed from phase-2 to phase-3 was bevacizumab, which showed a response rate of 16-21% when used as a single agent and showed a higher response rate in combination with paclitaxel (364). However, the phase 3 “AURELIA” study recently reported that bevacizumab alone in combination with chemotherapeutics does not significantly improve the overall survival and show 3 months benefit in progression free survival (365). Thus, the platinum-resistant cases resort to the available second line chemotherapeutics, which comprises liposomal doxorubicin, topo/irinotecan, gemcitabine and etoposide (4).

The majority of the second line chemotherapeutics show a similar response rate of 15-30%. Gemcitabine, a cytidine analogue which incorporates in DNA to block DNA synthesis and liposomal doxorubicin, a topoisomerase II inhibitor are generally preferred for managing the

platinum-resistant disease, shows a response rate of 25% and 22.4% respectively. Irinotecan, a topoisomerase I inhibitor and oral etoposide, another topoisomerase II inhibitor also shows a similar response rate of 19.9% and 18% respectively (249, 366). A recent clinical trial, aimed at determining the optimal second line chemotherapy for platinum-resistant disease, reported no significant benefit of liposomal doxorubicin over topotecan (367). Thus the choice of second line therapy for individual patients relies upon treatment history, cost, availability, associated toxicities and convenience of treatment but rarely on molecular pathways. Since the response rate of majority of the available therapies is similar, a prior subject specific assessment of the efficacy of these drugs can guide the choice of second or third line chemotherapeutics to improve response rate.

MAPK/ERK1/2 and PI3K/AKT are the two key signalling axes that governs the development of platinum-taxol dual resistance in our indigenously developed chemoresistant cellular models. These effector kinases are the focal point of several signal transduction pathways and are master regulators of therapy resistance. However, the modulations in these key signalling arms in response to second line non-platinum agents in chemoresistant ovarian cells is yet to be investigated. Thus, utilizing the dynamic model of chemoresistance and cells derived from patient ascites we aim to ask:

1. Is it possible to utilize the dynamic modulation in MAPK/ERK and PI3K/AKT signalling to predict therapeutic efficacy of second line non-platinum agents in platinum-taxol resistant cells?

Predicating efficacy of chemotherapeutic drugs on cancer cell lines or cells derived from patient tumours prior to initiation of chemotherapeutic regimen holds a high prognostic significance. Classically, the efficacy of chemotherapeutic drugs was estimated as a function of reduction in mitochondrial respiration or ATP production (368). Significant correlation of clinical response with Area Under Curve (AUC) and IC_{50} was reported in primary cells

harvested from 70 chemo naïve and 30 refractory ovarian tumours by ATP luminescence assay (369). A similar correlation of overall and progression free survival with in-vitro cytotoxicity was also reported for 83 patients (370). Although these assays serve as a gross indicator of sensitivity, they fail to evaluate therapy induced molecular responses, which are crucial determinants in predicting therapy resistance. Chemotherapeutic insults result in a myriad of molecular responses regulated through alterations in molecular interactions (protein-protein interaction [PPI or protein-lipid [PLI]) which in turn leads to activation of key signalling pathways. Thus, evaluation of these key molecular interactions to estimate activation of key survival promoting pathways in response to chemotherapeutic stress may help to determine the most effective choice of non-platinum agents against platinum resistant ovarian cancer cell lines or primary cells isolated from ascites.

In recent years, Bioluminescence Resonance Energy Transfer (BRET) based proximity assay, has emerged as a powerful system for studying PPI (35, 371, 372). Application of BRET in the assessment protein-lipid interaction by directly labelling the interacting partners has yet not been explored. However, utilizing membrane localized acceptor (fluorescent) protein, interaction between membrane lipids such as phosphatidyl inositol-3-phosphate (PIP3) with PH domain of proteins has been evaluated through BRET based platforms. These assays work on the virtue of the close proximity between membrane localized acceptor protein and donor tagged PH-domain upon interaction with membrane lipids. This lipid assisted PPI framework was utilized to monitor AKT activation in MCF7 cells and human serum samples by Rluc-PH/AKT-YFP-mem BRET sensor. A Renilla Luciferase (Rluc) based BRET sensor, Rluc-EKAR-Venus, was reported to precisely predict the activation of ERK1/2 in neurons isolated from hippocampus of mice embryos (88, 89). Though both the sensors were useful in estimating the activation of PIP3/AKT and ERK1/2 pathway, the low quantum yield of Rluc and low spectral resolution of these BRET pairs significantly limit the application of the

sensors. Several reports suggest the advantage of NanoBRET system over classical BRET, especially due to the high quantum yield and sustained luciferase signal of nanoluciferase (Nluc) (92). Thus, development of highly sensitive and cost-effective Bioluminescence Resonance Energy Transfer (BRET) based platforms that can monitor chemotherapy induced ERK1/2 and AKT activation may help to monitor the molecular modulation in survival signals and predict the efficacy of commonly used second line chemotherapeutics against platinum-taxol resistant ovarian cancer cells.

4.2 Methodology

4.2.1 Development of chemoresistant model

Cisplatin-paclitaxel resistant A2780 and OAW42 cells were developed following pulse method strategy, with incremental doses of platinum-taxol over a period of 6 months as described in section 2.2.1.

4.2.2 Enrichment of tumour cells from ascitic fluid

Patient studies were performed as per Institutional Ethics Guidelines. The ascitic fluid was subjected to centrifugation to obtain cell pellet which was treated with RBC lysis buffer to remove contamination of red blood cells. To enrich the tumour cells, depletion of CD90 positive fibroblasts was carried out by Magnetic Assisted cell sorting. CD90 negative fraction was further sorted by FACS for EpCAM positive cells. CD90-/EpCAM+ cells thus obtained were cultured in MCDB:M199 media and experiments were performed within one week of obtaining the cells.

4.2.3 Development of PIP3/AKT BRET construct (NAT)

The NAT BRET sensor comprises of PH-AKT-Nluc fusion construct (Pleckstrin Homology (PH) domain of AKT fused to nanoluciferase) and the membrane localized Turbo635 protein. The PH-AKT domain was PCR amplified with Nhe-1 and Bgl-II restriction site from PH-AKT-EGFP construct and column purified. The PCR amplified product was then substituted in place of Turbo in the Turbo-Nluc plasmid using the Nhe-I and Bgl-II site to generate PH-AKT-Nluc. Synthetically synthesized oligonucleotides coding for membrane localization signal was annealed and column purified. The membrane localization sequence was derived from N-terminal of neuronal protein GAP3 (20 amino acid). The annealed oligonucleotide was substituted in place of Stat3 in Stat3-Turbo construct using Nhe1 and Sal1 to generate GAP-Turbo. The BRET pair together was termed NAT.

4.2.4 Development of BRET sensor for monitoring ERK1/2 activation (NEO)

The Cerulean-EKARcytoplasmic-Venus and Cerulean-EKARnuclear-Venus was purchased from Addgene. The full length cytoplasmic and nuclear EKAR was PCR amplified with Bgl-II and Xho-I site and column purified. The PCR amplified product was then introduced in the Nlu-mOrange vector using the Bgl-II and Xho-I site to generate nanoluc- EKARcyto/nucl-mOrange (NAT). For construction of Nluc-CEKAR as BRET donor construct for normalization, the CEKAR was PCR amplified and cloned downstream of Nluc by replacing mOrange in the Nluc-mOrange vector using XhoI and BamHI restriction enzyme.

4.2.5 Side directed mutagenesis

The PH-AKT domain mutant were made in the background of PH-AKT-EGFP and PH-AKT-Nluc by replacing the 14th codon expressing lysine with alanine (K14A_PH-AKT-EGFP/Nluc)

by standard site directed mutagenesis (SDM) protocols and using SDM primers as described in section 6.2.8. All constructs were verified by restriction digestion and sequencing.

4.2.6 Immunoblotting:

Immunoblotting was performed for estimating the level of phosphorylated and total ERK1/2, AKT, p90^{RSK1/2}, BAD and mTOR as described in section 6.5.

4.2.7 Confocal microscopy

A2780 cells were transiently transfected with PHAKT-EGFP or its mutant K14A_PHAKT – EGFP construct and treated with IGF-1 for 15 min. Following treatment each sample was processed for confocal microscopy and imaged in LSM780 for membrane localization as described in section 6.7.1.

4.2.8 Cell viability assay

In order to determine IC₅₀, cells were incubated with each of the non-platinum drugs at different concentration. After 48 hours, MTT assay was performed to determine cell viability as described in section 6.4.1. The data was fitted into a dose-inhibition curve and plotted.

4.2.9 BRET imaging and analysis

Bioluminescence resonance energy transfer measurements in cell populations were performed as described in section 6.15. For NAT, emission spectra was acquired at 500 and 640 nm while NEO spectra was collected at 500 and 550 nm followed by ROI calculation and analysis in Living image software version 4.5. BRET ratio was represented as milliBRET unit (mBU) calculated using the formula:

$$\text{milliBRET unit (mBU)} = \frac{\text{Avg.Rad(acceptor filter)} - Cf * \text{Avg.Rad (Donor filter)}}{\text{Avg.Rad (Donor filter)}} * 1000$$

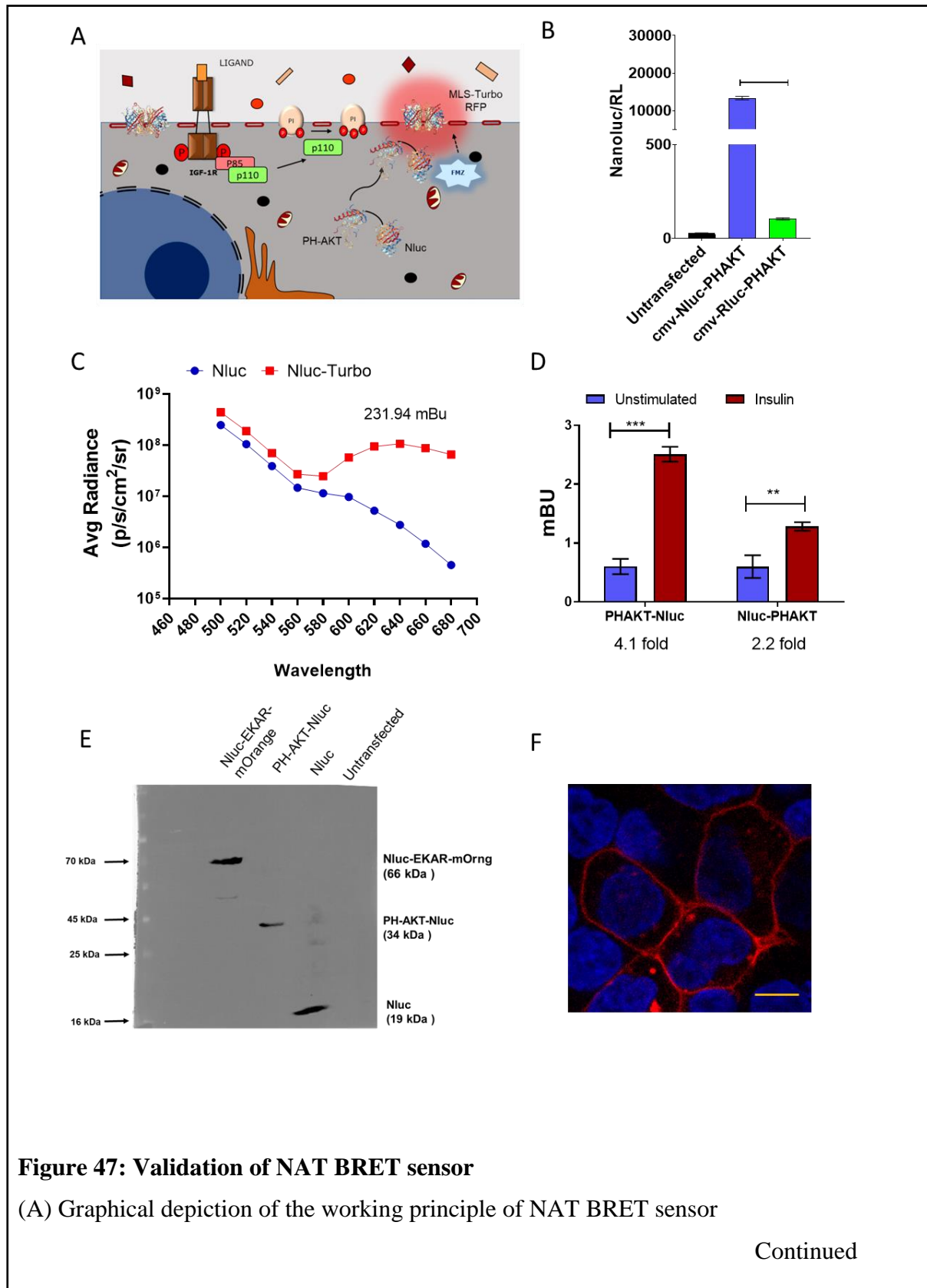
$$Cf = \frac{\text{Avg.Rad(acceptor filter)donor only}}{\text{Avg.Rad(donor filter)donor only}}$$

4.3 Results:

4.3.1 PIP3 BRET biosensor NAT accurately predicts PIP3/AKT activation:

Activation of AKT is initiated at the membrane upon conversion of PIP2 to PIP3 by phosphatidylinositol-3-kinase, which induces membrane translocation of AKT via its PH domain (373). We aimed to monitor the protein-lipid interaction between PH-domain of AKT and PIP3, as a surrogate for AKT activation utilizing an improved BRET biosensor. We developed a nanoBRET platform consisting of fusion construct expressing PH-domain of AKT and Nluc, as BRET donor and membrane targeted TurboFP fluorescent protein as BRET acceptor. Thus, increase in BRET ratio indicates an increased interaction of PH-AKT-Nluc with PIP3 (Figure 47A). The PH-AKT-Nluc displayed a 127-fold increase in luciferase activity in comparison to PH-AKT-Rluc indicating an increased quantum yield of the PH-AKT-Nluc construct (Figure 47B). Efficient energy transfer of Nluc and TurboFP635 BRET pair was observed at the characteristic emission maxima (Nluc: 500 nm and TurboFP: 640 nm) with a BRET ratio of 231.94 mBu in A2780 cells expressing TurboFP635-Nluc fusion protein (Figure 47C). Since, the orientation of donor and acceptor protein influence BRET efficiency, we developed both PH-AKT-Nluc and Nluc-PH-AKT fusion construct. Nluc fused to the C-terminus of PH-AKT (PH-AKT-Nluc) displayed significantly higher BRET ratio in comparison to N-terminal orientation post insulin treatment, indicating the efficiency of C-terminal orientation for optimal energy transfer (Figure 47D). Stability of the PH-AKT-Nluc construct was confirmed by immunoblotting which displayed prominent band at 33kDa (Figure

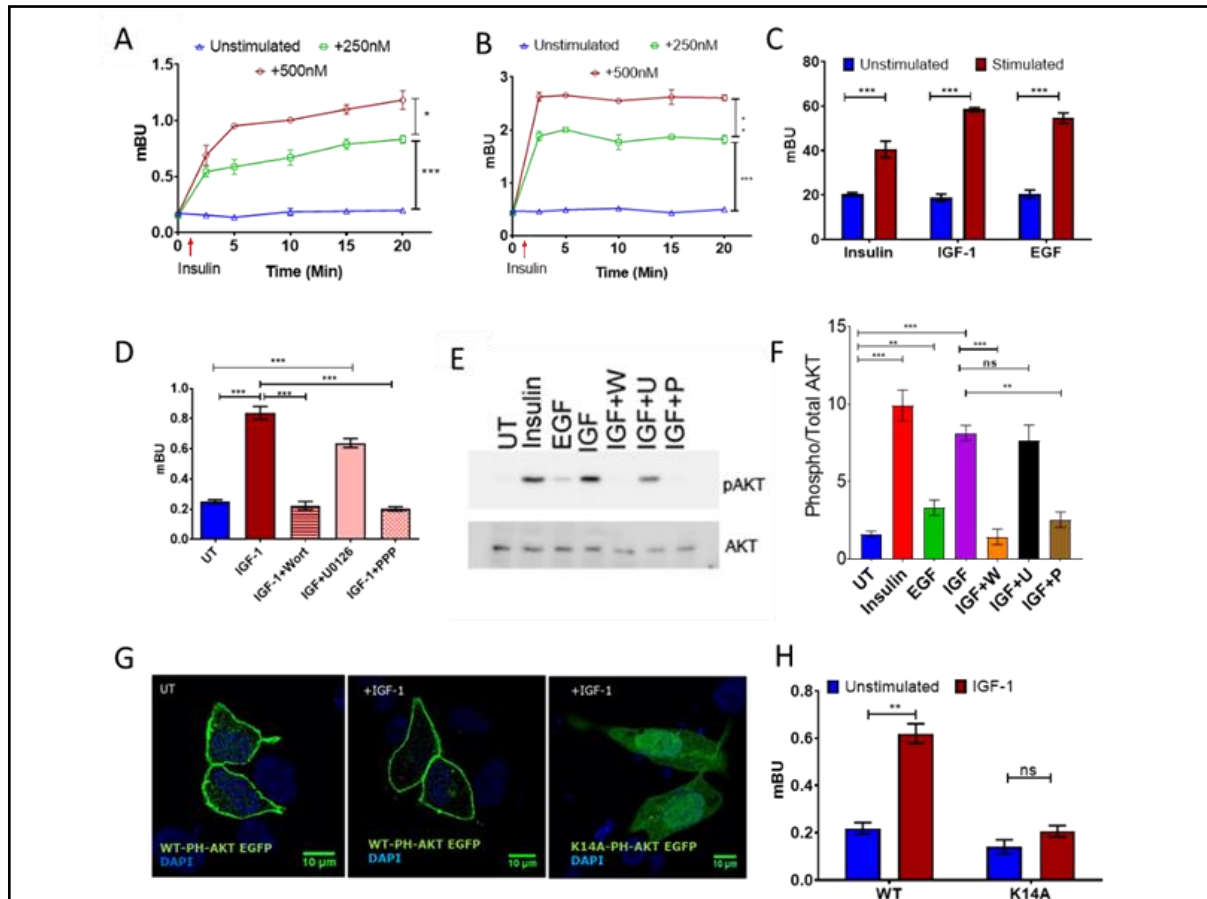
47E). Fusion of GAP domain with TurboFP led to its membrane localization in A2780 cells (Figure 47F).



(B) graph representing increase in luciferase activity in A2780 cells expressing PHAKT-nanoluciferase (PHAKT-Nluc) in comparison to cells expressing AKT-Rluc Turbo at 640 nm in A2780 cells.(C) Spectral scan of nanoluciferase (Nluc) and nanoluciferase-TurboFP (Nluc-Turbo) fusion protein indicating resonance energy transfer (231.9 milliBRET unit, mBu) between Nluc and (D) Fusion of Nluc in the C-terminal of AKT show increased efficiency of resonance energy transfer in comparison to Nluc fused in the N-terminal of AKT when paired with membrane localized TurboFP635 in A2780 cells (E) Immunoblot depicting increased molecular weight of nanoluciferase-AKT fusion protein (33 kDa) and nanoluciferase-EKAR-mOrange (66 KDa) fusion protein in comparison to nanoluciferase (Nluc, 19 kDa) (F) Representative image of A2780 cells expressing GAP-TurboFP, depicting membrane localization of the fusion protein (scale 10 μ m).

Real-time imaging of live A2780 cells post insulin treatment revealed a dose dependent increase in BRET ratio (100 nM:0.58 \pm 0.05, 200 nM:0.95 \pm 0.01), which peaked at 5 min compared to untreated (0.13 \pm 0.02) cells and then remained fairly constant till 15 min, indicating the kinetics of AKT activation post IGF-1 treatment (Figure 48A). A similar dose dependent increase in NAT BRET ratio was observed in MCF7 cells post insulin treatment which peaked at 2.5 min (Figure 48B). An equivalent increase in NAT BRET ratio was observed post 15 min of IGF-1 (200nM, 0.98 \pm 0.03) treatment in comparison to insulin (200nM, 1 \pm 0.02), while a comparatively lower BRET ratio was observed post EGF (200nM, 0.51 \pm 0.03) treatment (Figure 48C). Pre-treatment of cells with wortmannin (PI3KCA inhibitor) and picropodophyllin (IGF1R inhibitor) prevented IGF-1 induced AKT activation (0.22 \pm 0.03 and 0.20 \pm 0.01 mBU respectively) compared to cells treated with only IGF-1 (0.83 \pm 0.04). Pre-treatment of cells with U0126 (MEK1/2 inhibitor, 0.63 \pm 0.03) was able to only partially inhibit IGF-1 induced AKT activation compared to untreated cells (Figure 48D). In parallel to our BRET data, a similar trend in AKT phosphorylation was observed in A2780 cells post treatment with different growth factors and inhibitors by immunoblotting (Figure 48E-F).

Interestingly, introduction of a point mutation (K14A) in the PH-AKT domain completely abolished PIP3 PH-AKT interaction and membrane localization of PH-AKT (Figure 48G). A significantly reduced BRET ratio was observed in cells expressing mutated PHK14A-AKT-Nluc (0.20 ± 0.02) in comparison to cells expressing wild type PH-AKT-Nluc (0.61 ± 0.07) post IGF-1 treatment (Figure 48H).



4.3.2 BRET based ERK activity reporter (NEO) accurately predicts

ERK1/2 activation:

We then constructed a Nluc based BRET sensor for monitoring cdc25c phosphorylation as a surrogate for ERK1/2 activation. The NEO BRET sensor was developed by substituting the fluorophores of FRET based Extracellular signal-regulated Kinase Activity Reporter (EKAR_{cyto} and EKAR_{nucleus}) with NanoLuc and mOrange (Nluc-EKAR-mOrange, NEO). The NEO BRET sensor constituted of a phospho ERK binding domain (FQFP), a consensus ERK target phosphorylation sequence of cdc25 (PRTP), a flexible linker of 72 glycine residue and a proline directed phospho binding domain. Changes in conformation as a result of phosphorylation by ERK1/2 brings the donor and acceptor proteins in close proximity, thus inducing resonance energy transfer (Figure 49A). The NEO BRET sensor comprises of Nluc-EKAR_{cyto}-mOrange and Nluc-EKAR_{nuclear}-mOrange for detection of ERK1/2 activation from both cytoplasm and the nucleus. Efficient energy transfer between the donor Nluc and acceptor mOrange indicated by a BRET ratio of 257.94mBu was observed in A2780 cells expressing mOrange-NanoLuc fusion protein (Figure 49B). An increased efficiency of resonance energy transfer was observed when Nluc was cloned in the N-terminal of EKAR indicated by increased BRET ratio (50.55 ± 2.2 mBu) in comparison to cells expressing mOrange-EKAR-Nluc (36.67 ± 0.42 mBu) (Figure 49C). The nuclear and cytoplasmic localization of Nluc-EKAR_{nuclear}-mOrange and Nluc-EKAR_{cytoplasmic}-mOrange construct was validated by confocal microscopy (Figure 49D).

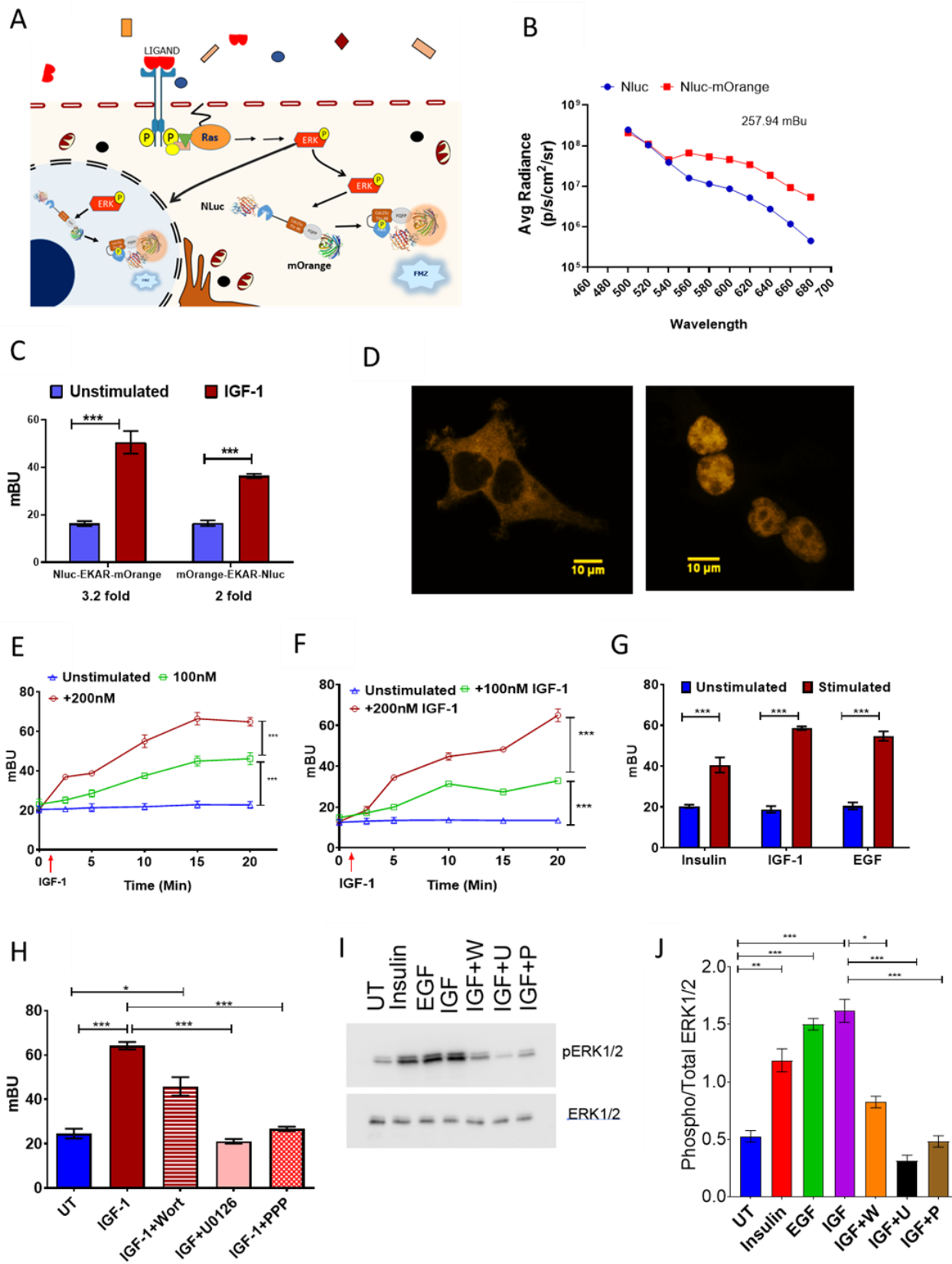


Figure 49: Validation of NEO BRET sensor

(A) Schematic representation of the working principle of NEO biosensor

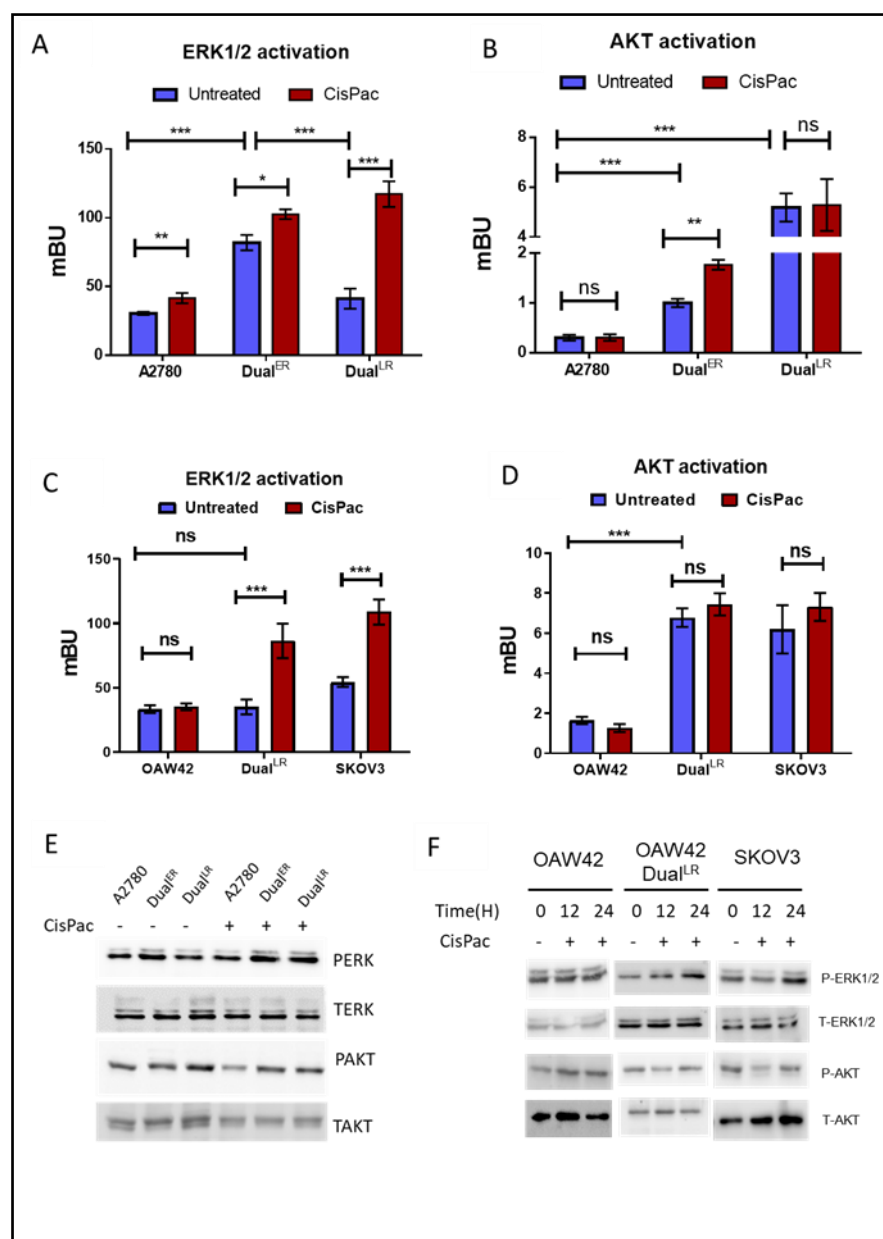
Continued

(B) Spectral scan of nanoluciferase (Nluc) and nanoluciferase-mOrange (Nluc-mOrange) fusion protein indicating resonance energy transfer (257.9 milliBRET unit, mBu) between Nluc and mOrange at 560 nm in A2780 cells (C) Fusion of Nluc in the N-terminal of EKAR show increased efficiency of resonance energy transfer in comparison to Nluc fused in the C-terminal of EKAR in A2780 cells (D) Representative microscopic images showing cytoplasmic localization of Nluc-cytoplasmicEKAR-mOrange and nuclear localization of Nluc-nuclearEKAR-mOrange in A2780 cells (E-F) Graph representing dose and time dependent increase in BRET ratio (mBU) post IGF-1 treatment in A2780 and MCF7 cells (G) IGF-1 and EGF induced highest ERK1/2 activation post 15 min in A2780 cells as indicated by increased BRET ratio in comparison to insulin (H-I) U0126 (10 μ M) and picropodophyllin (PPP, 2 μ M) but not wortmannin (Wort, 200 nM) specifically inhibits IGF-1 induced ERK1/2 activation in A2780 cells as represented by BRET and immunoblotting assay.

Live cell imaging of ERK activation revealed a dose and time dependent increase in BRET ratio (27.44 ± 0.19 and 48.21 ± 0.51 mBu at 15 min respectively) post 100nM and 200 nM IGF-1 treatment in comparison to unstimulated A2780 cells (13.34 ± 0.41 mBu) (Figure 49E). A similar increase in BRET ratio indicating gradual ERK activation was observed in IGF-1 stimulated MCF7 cells (Figure 49F). Treatment of A2780 cells expressing NEO BRET sensor with EGF treatment simulated a comparable effect as IGF-1 (58.55 ± 0.68 and 54.64 ± 1.89 mBu respectively) while insulin induced lowest ERK1/2 activation (40.55 ± 3.03 mBu) (Figure 49G). MEK1/2 inhibitor, U0126 (21.07 ± 0.99 mBu) and IGF1R inhibitor, picropodophyllin (26.72 ± 0.97 mBu) significantly reduced IGF-1 (64.21 ± 1.66 mBU) induced increased NEO BRET ratio while PI3KCA inhibitor, wortmannin (45.85 ± 4.14 mBu) partially prevented ERK1/2 activation (Figure 49H). A comparable level of ERK phosphorylation was observed post treatment with above mentioned inducers or activators by immunoblotting (Figure 49I-J).

4.3.3 Dynamic modulation of ERK and AKT activation in sensitive and chemoresistant ovarian cancer ascites and cell lines

Previously, we have demonstrated the role of ERK1/2 and AKT signalling at onset and late stage of platinum-taxol dual resistance in two indigenously developed ovarian cancer models. Now, we aim to evaluate the level of therapy induced ERK1/2 and AKT activation in dual resistant A2780 model. Interestingly, platinum-taxol treatment at respective IC₅₀ dosage, induced highest fold increase in NEO BRET ratio in A2780Dual^{LR} cells in comparison to



A2780Dual^{ER} and sensitive A2780 cells, indicating the therapy induced ERK1/2 activation remains significantly higher in late stage of resistance and possibly contributes to their survival (Figure 50A). Similarly, an increased BRET ratio was observed in OAW42Dual^{LR} and SKOV3, an inherently platinum resistant ovarian cancer cell

Figure 50: Platinum-taxol induces increased ERK1/2 activation specifically in late stage of resistance

(A, C) Graph representing increased NEO BRET ratio indicating ERK1/2 activation of ERK1/2 in A2780Dual^{LR}, OAW42Dual^{LR} and SKOV3 cells. (B, D) Cisplatin-paclitaxel treatment did not alter NAT BRET ratio in sensitive and Dual^{LR} cells of both A2780 and OAW42 model. (E-F) Immunoblot depicting increased level of p-ERK1/2 specifically in A2780Dual^{LR}, OAW42Dual^{LR} and SKOV3 cells post cisplatin-paclitaxel treatment

line (Figure 50 C). On the other hand, platinum-taxol treatment led to non-significant alteration NAT BRET ratio in both sensitive and Dual^{LR} cells. Although, the basal NAT BRET ratio was highest in these cells, indicating a significantly higher basal level of AKT activation in A2780Dual^{LR} comparison to A2780 and A2780Dual^{ER} cells (Figure 50B). Similarly, platinum-taxol treatment did not enhance NAT BRET ratio in OAW42 chemoresistant model and in SKOV3 cells (Figure 50 D). We also observed a similar modulation in phospho-ERK and phospho-AKT level by immunoblotting (Figure 50 E-F). Next, we aimed to test the specificity and sensitivity of NEO and NAT sensor in live HGSOc cells isolated from patient's ascites by CD90^{-ve}EPCAM^{+ve} sorting. Based on the platinum free interval, the cases were categorized into platinum-resistant, platinum sensitive and chemo naïve. Interestingly, platinum-taxol induced increase in both NEO (4.72-fold) and NAT BRET (10.11-fold) ratio specifically in cells derived from platinum-resistant subjects while no significant alteration in platinum induced NEO or NAT BRET ratio was observed in chemo-naive and platinum-sensitive patients, indicating the ability of resistant cells to activate pro survival signalling pathways in response to chemotherapeutic stress (Figure 51A-B). A similar increase in the level of phospho-ERK and phospho-AKT was also observed in primary cells established from a platinum-resistant patient post cisplatin treatment (Figure 51C). In-vitro cytotoxicity of platinum determined by MTT assays correlated well with clinical definition of therapy resistance as indicated by increased tolerance of cells derived from platinum resistant subjects

to platinum (20 and 16 $\mu\text{g}/\text{ml}$) in comparison to cells derived from chemo-naïve (8 $\mu\text{g}/\text{ml}$) and platinum-sensitive (4 and 5 $\mu\text{g}/\text{ml}$) subject (Figure 51D).

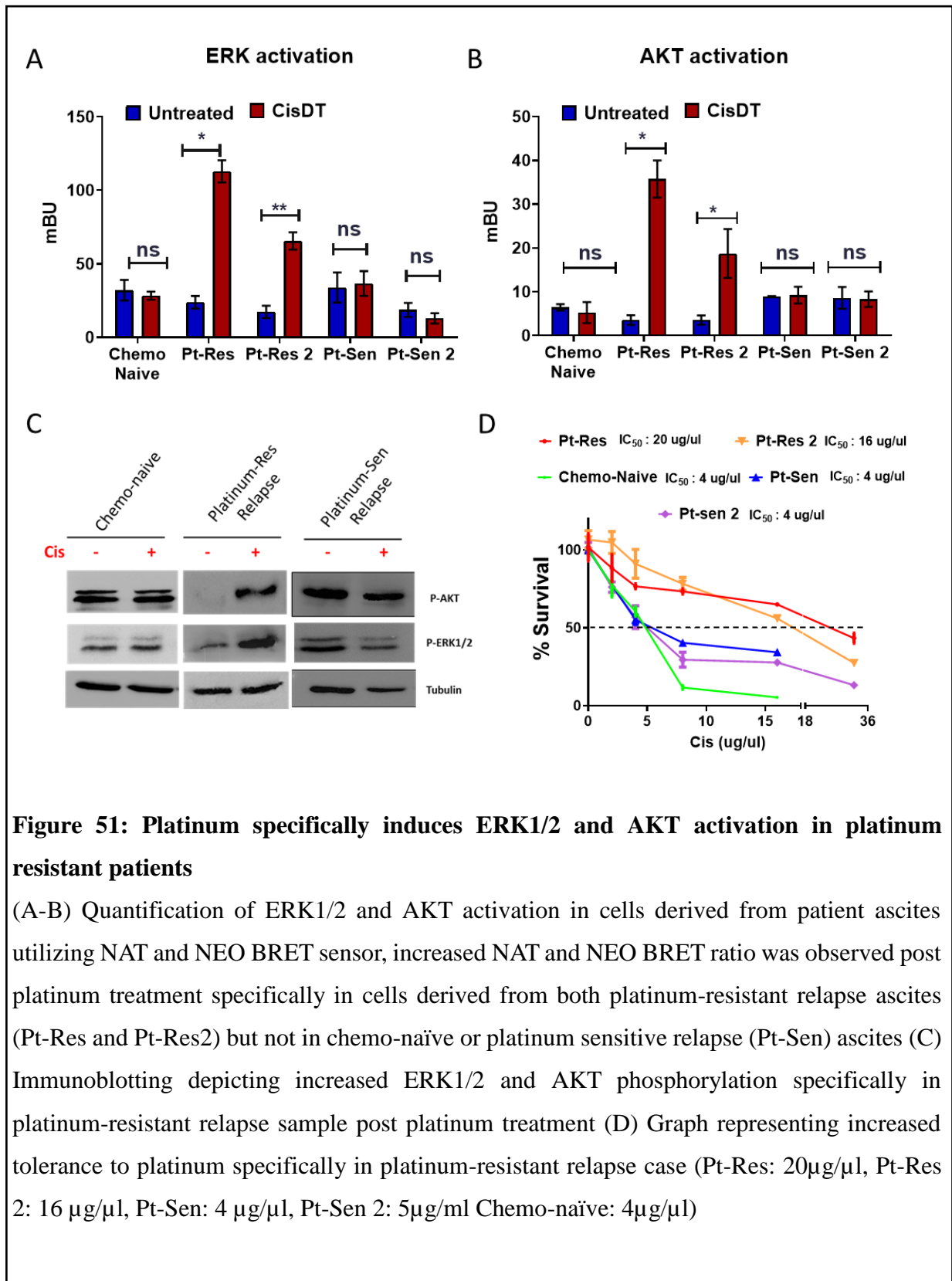


Figure 51: Platinum specifically induces ERK1/2 and AKT activation in platinum resistant patients

(A-B) Quantification of ERK1/2 and AKT activation in cells derived from patient ascites utilizing NAT and NEO BRET sensor, increased NAT and NEO BRET ratio was observed post platinum treatment specifically in cells derived from both platinum-resistant relapse ascites (Pt-Res and Pt-Res2) but not in chemo-naïve or platinum sensitive relapse (Pt-Sen) ascites (C) Immunoblotting depicting increased ERK1/2 and AKT phosphorylation specifically in platinum-resistant relapse sample post platinum treatment (D) Graph representing increased tolerance to platinum specifically in platinum-resistant relapse case (Pt-Res: 20 $\mu\text{g}/\mu\text{l}$, Pt-Res 2: 16 $\mu\text{g}/\mu\text{l}$, Pt-Sen: 4 $\mu\text{g}/\mu\text{l}$, Pt-Sen 2: 5 $\mu\text{g}/\mu\text{l}$ Chemo-naïve: 4 $\mu\text{g}/\mu\text{l}$)

4.3.4 ERK1/2 activation predicts cross-resistance to second line of ovarian cancer therapy

Acquirement of a highly resistant platinum phenotype imposes the use of non-platinum agents. The most commonly used non-platinum agents against platinum resistant ovarian cancer are doxorubicin, gemcitabine, irinotecan and etoposide. Utilizing our highly platinum-taxol resistant Dual^{LR} cells and intrinsically platinum resistant SKOV3 cells we aimed to evaluate influence of second line non-platinum agents on ERK1/2 and AKT activation dynamics through BRET technology. Doxorubicin treatment increased NEO BRET signal by 2.3fold in A2780Dual^{LR} cells, by 3.5fold in OAW42Dual^{LR} cell and by 2.6 fold in SKOV3 cells post 24 hours of treatment, while no significant change in BRET signal was observed in A2780 and OAW42 cells. Increased NEO BRET signal was also observed post 24 hours of gemcitabine treatment in specifically A2780Dual^{LR} (1.96 fold), OAW42Dual^{LR} (3.35 fold) and SKOV3 (2.7 fold) cells but not in sensitive A2780 and OAW42 cells. Etoposide treatment also increased NEO BRET signal specifically in platinum-taxol resistant Dual^{LR} cells of both models and SKOV3 cells. Intriguingly, Irinotecan treatment did not result any significant change in NEO BRET ratio in chemoresistant or chemosensitive cells (Figure 52A). In comparison to the NEO BRET, NAT BRET ratio did not significantly alter post treatment with any of the second line therapeutic agents in both chemoresistant and sensitive cells (Figure 52C). A similar increase in ERK1/2 phosphorylation level was observed post doxorubicin, gemcitabine and etoposide treatment specifically in the platinum resistant cells, while irinotecan treatment did not alter phospho-ERK1/2 level significantly (Figure 52B and 53A-E). On the other hand, the level of AKT phosphorylation remained unaltered post chemotherapeutic treatments in both resistant and sensitive cells (Figure 52D). Intriguingly, platinum-taxol resistant A2780Dual^{LR}, OAW42Dual^{LR} and SKOV3 cells also showed increased resistant against doxorubicin indicated by resistance index of 8.9, 7.70 and 7.45 respectively in comparison to A2780 and

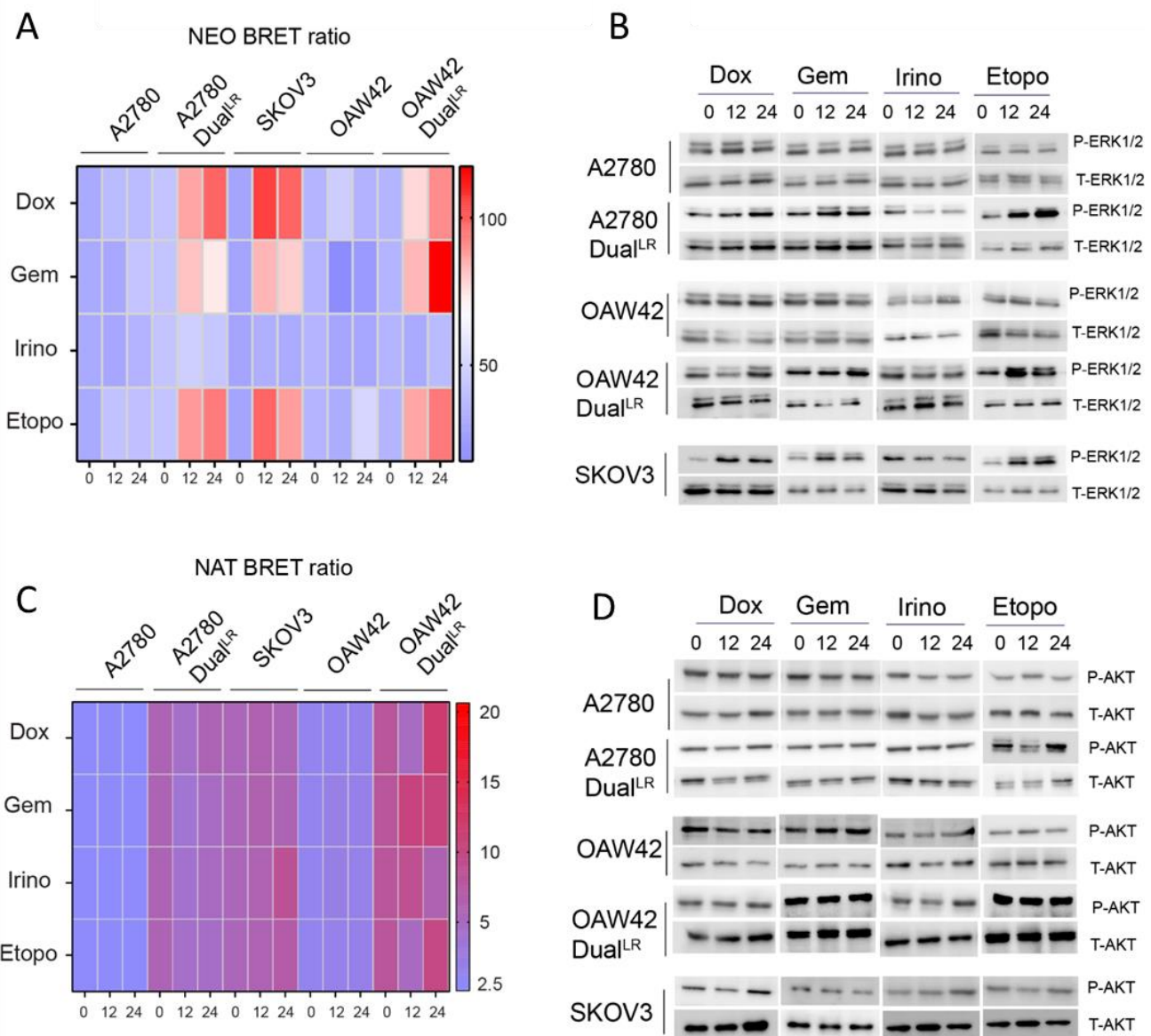


Figure 52: Non-platinum therapy induced modulation in ERK1/2 and AKT activation in sensitive and platinum-taxol resistant ovarian cancer cells

(A, C) Heat map representing alteration in NEO and NAT BRET signal respectively in sensitive (A2780 and OAW42) and platinum-taxol resistant (Dual^{LR} and SKOV3) cells post treatment with IC₅₀ dosage doxorubicin (Dox), Gemcitabine (Gem), Irinotecan (Irino) and etoposide (Etopo). All the non-platinum agents except irinotecan increased NEO BRET ratio in SKOV3 and Dual^{LR} cells of both A2780 and OAW42 model (B, D) Immunoblot depicting increase in ERK1/2 but not AKT activation post treatment with all the tested non-platinum agents except irinotecan

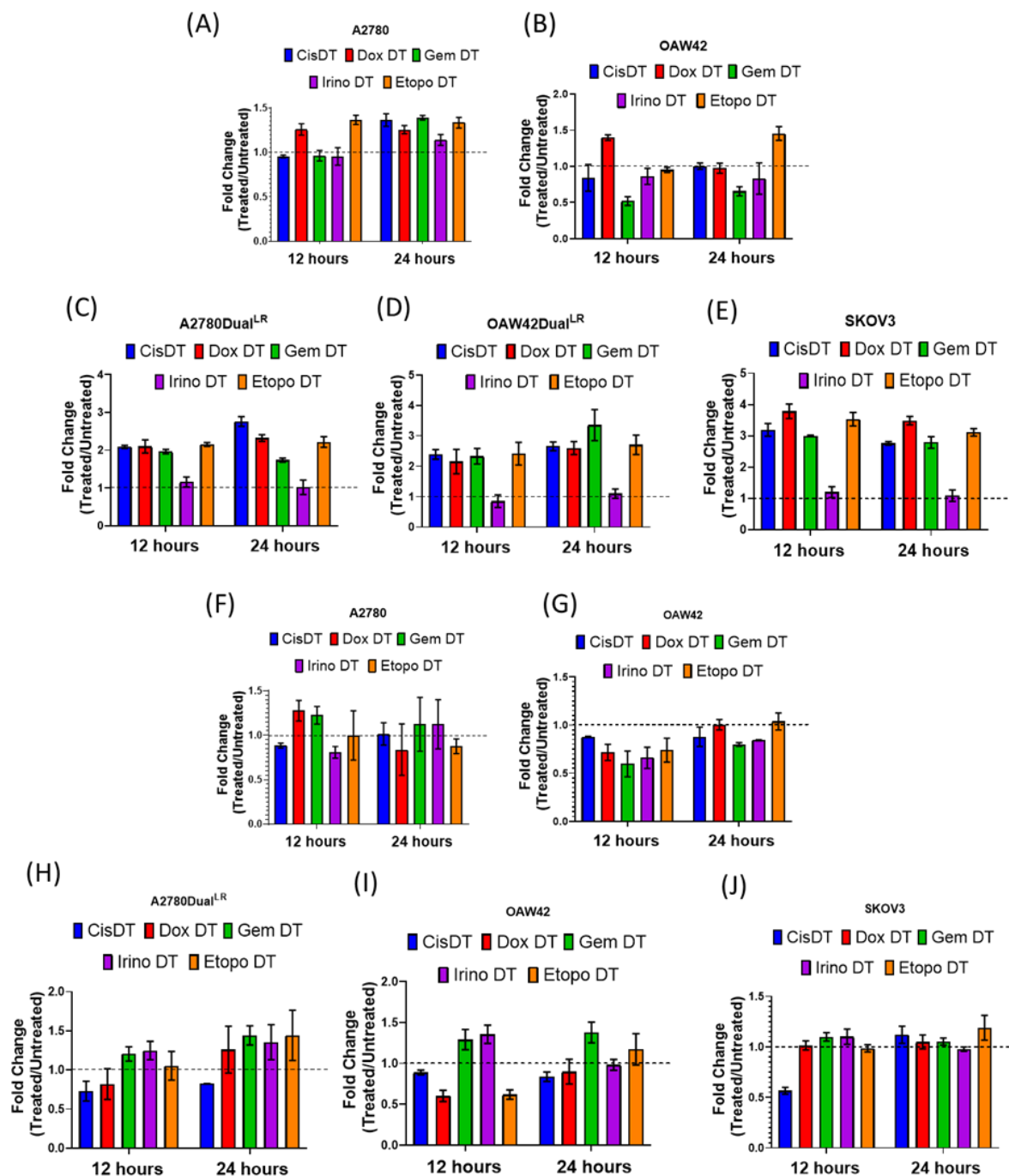


Figure 53: Densitometric quantification of phospho/total ERK1/2 and phospho/total AKT post chemotherapeutic challenge: (A-E) Fold increase in phospho to total ERK1/2 ratio in sensitive and resistant cells post treatment with cisplatin-paclitaxel, doxorubicin, gemcitabine, irinotecan and etoposide in comparison to the untreated cells. Significant higher fold increase in phospho/total ERK1/2 was observed specifically in resistant cells treated with all drugs except irinotecan (F-J) Fold change in phospho to total AKT ratio in sensitive and resistant cells post treatment with cisplatin-paclitaxel, doxorubicin, gemcitabine, irinotecan and etoposide in comparison to the untreated cells. No significant change was observed in either sensitive or resistant cells.

OAW42 cells. Similarly, A2780Dual^{LR} (RI: 9.41 and 10.94), OAW42Dual^{LR} (RI: 10.34 and 8.86) and SKOV3 (RI: 5.01 and 4.86) cells also showed increased tolerance to gemcitabine and etoposide respectively. Interestingly, only irinotecan sensitized the resistant cells to therapy (Fig 54A-D). Altogether our data suggests that chemotherapy induced ERK1/2 activation may support a resistant phenotype and may lead to poorer therapeutic outcome.

4.3.5 ERK1/2 promotes survival and anti-apoptotic signature in platinum-taxol resistant cells

Assessment of the consequence of ERK1/2 activation post doxorubicin treatment as opposed to irinotecan, revealed an increased phospho p90^{RSK1/2} level specifically in chemoresistant cells post doxorubicin treatment but not after irinotecan treatment. Doxorubicin challenge also upregulated inhibitory phosphorylation of pro-apoptotic protein BAD (serine 112) specifically in platinum-taxol resistant A2780 and SKOV3 cells. Irinotecan challenge did not alter phospho-BAD level in both sensitive and resistant cells. No significant alteration in mTORC1 level, a bonafide AKT target, was observed post doxorubicin or Irinotecan treatment in sensitive or chemoresistant cells (Figure 54E). These results indicated that doxorubicin induced increased ERK1/2 activation promote a growth promoting, anti-apoptotic phenotype via p90^{RSK1/2}-BAD signalling axis.

Figure 54: Activation of ERK1/2 signalling negatively correlates with sensitivity of platinum-taxol resistant cells to non-platinum agents

(A-D) Graph representing % survival versus log transformed concentration of second-line non-platinum agents in sensitive (A2780 and OAW42) and therapy resistant (DualLR and SKOV3) cells post 72 hours of treatment. Interestingly, only irinotecan sensitized platinum resistant cells to therapy (E) Immunoblot depicting increased phospho p90RSK1/2 and phospho BAD level specifically in DualLR and SKOV3 cells post doxorubicin treatment in comparison to irinotecan.

Figure in the next page

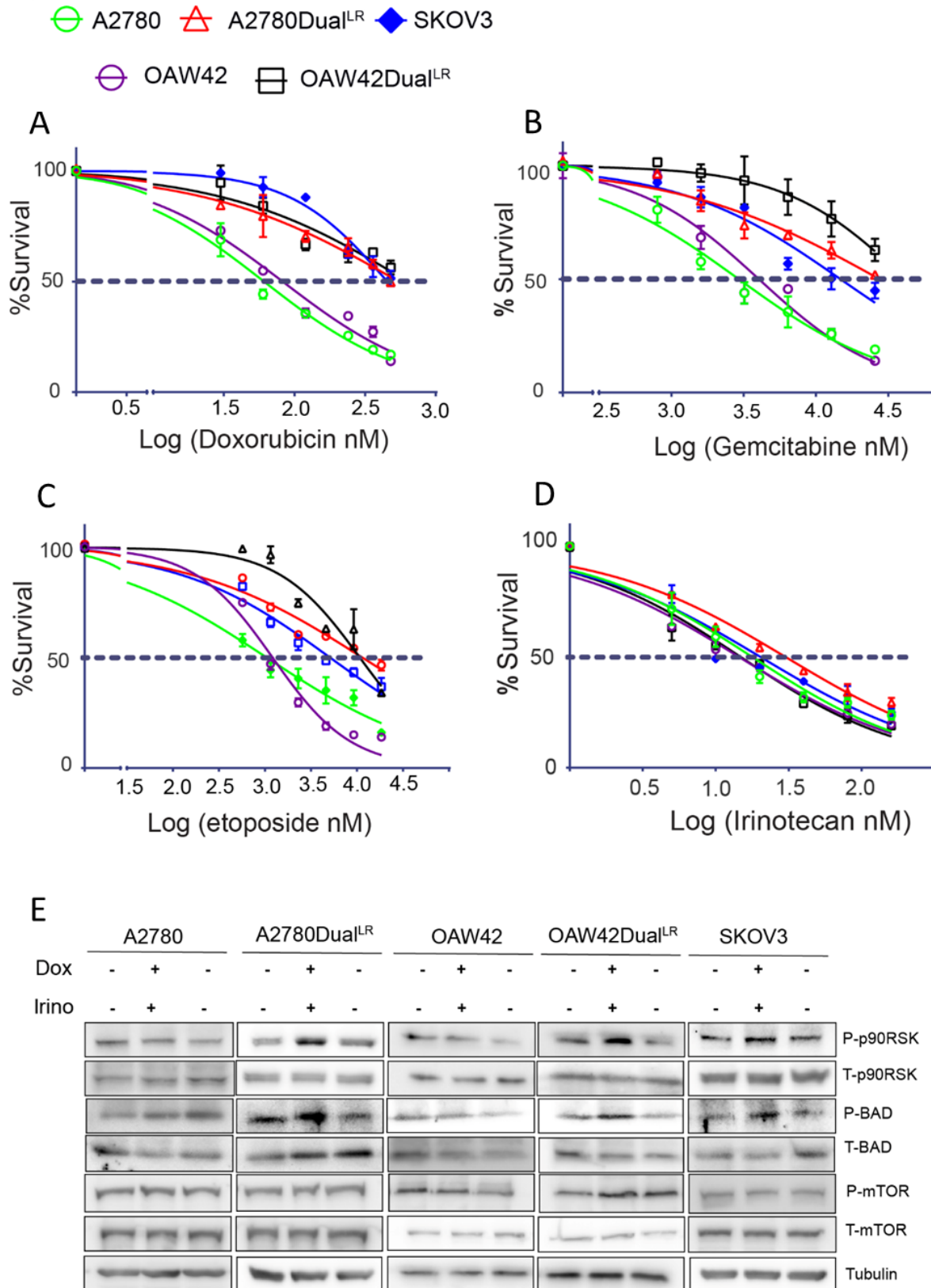


Figure 54: Activation of ERK1/2 signalling negatively correlates with sensitivity of platinum-taxol resistant cells to non-platinum agents

4.4 Discussion:

Acquirement of platinum resistance is a major obstacle in management of HGSOc and several efforts are already underway to target key molecular alterations and pathways. However, it's also important to evaluate and optimize the currently available therapeutic options for management of platinum-resistant disease. Thus, development of a platform for personalised in-vitro or ex-vivo evaluation of the efficacy of the available second line drugs before initiation of therapy could guide the choice of second- or subsequent-line therapy for optimal response. Herein, we have developed two improved BRET based PPI and lipid assisted PPI sensors, for real-time monitoring of ERK1/2 and PIP3/AKT activation in live cells. The NAT and NEO sensors revealed platinum-taxol induced activation of ERK1/2 but not AKT in platinum-taxol resistant Dual^{LR} and platinum resistant SKOV3 cells in comparison to the sensitive counterpart. A similar ERK1/2 activation along with AKT activation were observed in cells derived from platinum-resistant patients but not in cells isolated from chemo-naïve and platinum-sensitive relapse ascites. To the best of our knowledge, this is the first report of BRET based imaging of growth promoting effector kinases, ERK1/2 and AKT in cells derived from ascites of EOC patients. Further, we demonstrated that second line non-platinum agents that failed to act on platinum-taxol resistant cells also led to increased NEO BRET ratio and phospho-ERK1/2 level, indicative of increased ERK1/2 activation. Intriguingly, Irinotecan treatment did not induce ERK1/2 or AKT activation and subsequently sensitized these resistant cells to therapy. This enhanced tolerance of cisplatin-paclitaxel resistant cells to doxorubicin could be attributed to an anti-apoptotic, pro-survival cellular phenotype driven by ERK1/2-RSK-BAD signalling. The diversity of cellular response to external stimuli are governed by multitude of spatially and temporally resolved differential protein-protein or protein-lipid interaction. Alteration in PPI/PLI network can lead to various diseases and also contribute to the aberrant activation of cell survival pathways leading to cancer progression and therapy resistance. Among the several

methods to study PPI/PLI, resonance energy transfer is an attractive assay system due to its physical distance constraint of 10 nm which increase the specificity of the assay system. Forster resonance energy transfer (FRET) was classically used to monitor PPI/PLI in live cells, however, limitations arising from autofluorescence, use of external light source which may lead to photobleaching or phototoxicity prompted the development of BRET based proximity assay, where donor fluorophore is replaced by luciferase (374). In recent years, BRET, has emerged as a powerful tool for studying PPI, post-translational modification and protein conformation. Along with PPI measurements BRET also offers opportunities to measure PLI, utilizing lipid assisted PPI between proteins fused with luciferase and cell membrane targeted acceptor protein. BRET assay system has been employed to monitor several molecular interactions including AKT and ERK. The earlier sensors utilize a BRET1 or BRET3 platform consisting of Rluc or its mutant Rluc8 as BRET donor and YFP or Venus BRET acceptor. Herein, we substituted the Rluc/Rluc8 with brighter and stable nanoluciferase for both NAT and NEO BRET sensor resulting in increased luciferase activity. Further, we paired donor Nluc with Turo635 for NAT, having a spectral resolution of 140 nm and mOrange for NEO, having a spectral resolution of 80 nm in comparison to previously developed Rluc/YFP or Rluc8/Venus having spectral resolution of ~55nm. The increased spectral resolution of Nluc TurboFP/mOrange system significantly reduces background signal resulting from overflow of donor signal in the acceptor channel thus significantly improving the dynamic range and sensitivity of the BRET platform. This enabled us to precisely portrayed real-time modulation in AKT and ERK activation dynamics post treatment with various growth factors and inhibitors in A2780 and MCF7 cells.

PIP3/AKT and ERK1/2 signalling, are key signalling hubs, reported to play a crucial role in development of therapy resistance in multiple carcinoma including ovarian cancer (141, 144, 150, 233, 257). Previous reports from own lab also demonstrated the role of these pathways

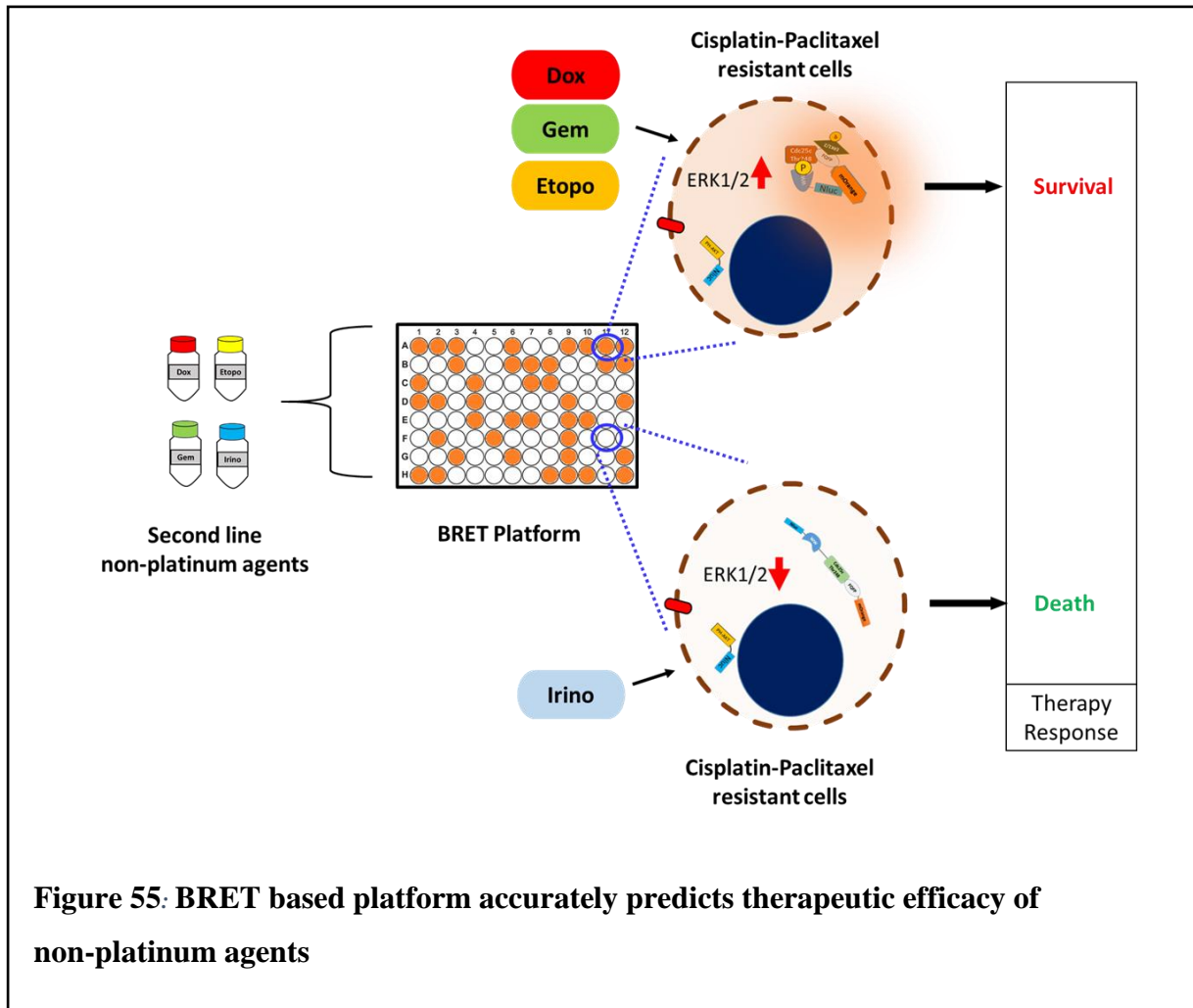
during initiation and maintenance of chemoresistance in two indigenously developed acquired chemoresistant cellular models of ovarian carcinoma (5, 149, 375). Re-challenging platinum-taxol resistant Dual^{LR} cells and intrinsically platinum-resistant SKOV3 cells with cisplatin-paclitaxel specifically increased NEO BRET ratio and ERK1/2 phosphorylation without any significant alteration in the NAT-BRET ratio or AKT phosphorylation, implying the role of ERK1/2 in platinum-taxol induced therapeutic stress. In agreement with our observation, multiple reports suggest platinum induced ERK1/2 activation plays a key role in imparting therapy resistance in hepatocellular as well as ovarian carcinoma.

Classically, tumour cell lysate or paraffin fixed tumour samples are used to evaluate activation of protein kinases by RPPA or IHC based methods. However, both the methods have their shortcomings in measuring the dynamics of activation in live cell. Herein, we dynamically monitored therapy induced modulation in ERK1/2 and AKT activation directly in live cells derived from HGSOC ascites through BRET. We observed an increased BRET ratio for both NEO and NAT constructs in malignant ascites derived cancer cells of Platinum-resistant relapse patients but not in cells derived from treatment-naïve or platinum sensitive relapse patients. This data confirms that platinum induced ERK activation is a molecular signature for platinum-resistance and probably bestows survival advantage for these cells. However, discrepancy in NAT BRET ratio enhancement in primary cancer cells might arise due to heterogeneity and thus the role of activated AKT in imparting platinum resistance cannot be completely ruled out. A detailed study is required to thoroughly understand the contribution of AKT and ERK activation in acquirement of platinum resistance.

Currently available therapeutics for platinum-resistant HGSOC include Doxorubicin, Gemcitabine, Irinotecan (preferred over topotecan due to reduced toxicity) and etoposide. These drugs show a similar response rates (10-15%), PFS (3-4 months), and OS (~12 months) against platinum-resistant HGSOC.(4, 249). The efficacy of these non-platinum agents reduce

further upon attainment of multidrug resistance phenotype (103). Development of resistance to doxorubicin and partially to topotecan had been reported in paclitaxel resistant ovarian cancer cells (376). Thus, prior assessment of the efficacy of a chosen second line drug for a particular patient can be of great benefit. Classically, MTT or other cytotoxicity based assays are utilized to monitor efficacy of chemotherapeutics drugs against cancer cells which however fail to monitor the underlying molecular response. We observed increased NEO BRET ratio indicative of ERK1/2 activation specifically in chemoresistant cells post treatment of doxorubicin, gemcitabine and etoposide but not of irinotecan. This change in NEO BRET was also reflected in western blot analysis where all drugs except irinotecan induced phosphorylation of ERK in therapy resistant cells. However, AKT level remained fairly unaltered in both sensitive and resistant ovarian cancer cells post treatment with non-platinum agents and did not show any change in NAT BRET ratio and phospho-AKT level. Interestingly, we observed that cisplatin-paclitaxel dual resistant A2780/OAW42Dual^{LR} and SKOV3 cells were insensitive to doxorubicin, gemcitabine and etoposide but not toward irinotecan. Further, an increased doxorubicin induced ERK1/2 activation promoted an anti-apoptotic, pro-survival cellular phenotype via p90^{RSK1/2}-BAD signalling while irinotecan treatment did not alter the level of p90^{RSK1/2} and BAD phosphorylation. Activation of ERK1/2 was reported to promote multi-drug resistant phenotype in other cancers as well (377-379). Combinatorial treatment of U0126 and adriamycin was reported to sensitized multidrug resistant HEPG2 cells (235). Increased ERK1/2 activation post gemcitabine treatment in gemcitabine resistant pancreatic cancer cells, Bxpc-3, was reported to promote MDR phenotype, which reversed upon combinatorial treatment of gefitinib and gemcitabine (379). Altogether, our data suggests ERK1/2 activation can act as a crucial indicator of therapeutic efficacy of the second line chemotherapeutics against platinum resistant HGSOc. Thus, real-time monitoring of therapy induced ERK1/2 and AKT activation by utilizing our improved NAT and NEO BRET platform

can indicate the efficacy of non-platinum drugs prospectively in a personalized manner, which may guide the choice of most appropriate therapeutic option (Figure 50). The PPI /lipid assisted PPI based BRET platforms described here would be valuable resource for such clinical studies.



Chapter 5: Summary

An integrated network of signalling pathways maintains cellular growth and homeostasis. Reinforced by genetic reprogramming, cancer cells hijack this regulatory network to support limitless replicative potential and evade death. Depending on the type of cancer, therapeutic targeting of these modified signalling pathways have been attempted and such strategies have relatively improved the therapeutic outcome. However, in absence of a targetable genetic alteration, conventional therapies involving chemo/radio therapy and surgery are applied as forefront strategies for the management of cancers, such as EOC. Platinum-taxol based chemotherapeutic regimen remains the primary choice against EOC, as the majority of the cases initially responds well to therapy. However, nearly 30% of the cases relapse within 6 months of initial therapy complete and do not respond to platinum again, thus termed as platinum-resistant relapse while cases that relapse after 6 months are classified as platinum-sensitive relapse. A few cases classified as platinum-refractory show upfront resistance to platinum. Eventually, platinum sensitive patients also develop platinum resistance after multiple rounds of relapse and therapy. Acquisition of platinum resistance remains the major hurdle for EOC and contributes to a low five year overall survival of ~40%. Acquired chemoresistance is a multi-step process involving therapy induced rewiring of signalling networks. Thus it is critical to identify the alterations in key signalling pathways and evaluate the implication of such alteration during gradual acquisition of chemoresistance.

The process of gradual evolution of chemoresistance can be categorized into multiple stages depending on the degree of resistance which can be manipulated for therapeutic purpose. Utilizing two dynamic models of platinum-taxol resistance in A2780 and OAW42 cells, we aim to identify and target key signalling pathways to **1) target cells at the onset of resistance or 2) impede the development of a highly chemoresistant phenotype or 3) predict the response of highly chemoresistant cells to non-platinum agents for identifying the optimal choice of therapy.**

Increased activation of RTK signalling axis contributes to the development of therapy resistance in various cancers including EOC. Previous reports from our lab suggest that an increased IGF1R expression protect cancer cells from therapeutic stress at the onset of resistance (DualER) while hyperactivated AKT signalling maintains a highly chemoresistant phenotype (DualLR). Monitoring of MAPK/ERK and PI3K/AKT, the two major signalling axis downstream of IGF1R, revealed an oscillatory pattern of ERK1/2 activation which peaked at the early stage of resistance while increased AKT activation was associated with the late resistant stage. This increased ERK1/2 activation was found to promote cytoprotective autophagic flux specifically at the early stage of resistance. Therapy induced autophagic flux was found to be blocked in the sensitive cells while late resistant cells showed reduced autophagic flux, probably due to the presence of hyperactive AKT. Pharmacological or genetic inhibition of ERK1/2 significantly reduced chemotherapy induced autophagic flux indicated by reduced p62 degradation, number of LC3+veLAMP1+ve puncta and autophagolysosome formation. Inhibition of ERK1/2 activation also reduced the level of UVRAG and Rab7, two key proteins involved in autophagosome-lysosome fusion, indicating the role of ERK1/2 in the sustenance of chemotherapy induced autophagic flux. Interestingly, early resistant cells showed oncogenic addiction towards ERK1/2, as combinatorial treatment of platinum-taxol along with Trametinib, an FDA approved MEK inhibitor, significantly promoted cell death and apoptosis. Utilizing a novel autophagy sensor comprised of a mutant thermostable firefly luciferase fused with p62, we longitudinally monitored autophagic flux from live cell and tumour bearing mice. Combinatorial treatment of platinum-taxol along with Trametinib or chloroquine led to increased luminescence signal indicative of p62 accumulation and stalled autophagy while only platinum-taxol treatment induced autophagic flux leading to reduced luminescence signal. Interestingly, Trametinib was found to be equally efficient as chloroquine, in blocking autophagic flux in live cells and tumour xenograft. To the best of our knowledge, this is the

first report of real time monitoring of chemotherapy induced autophagy flux kinetics in live animals. Further, a significant reduction in tumour growth was observed upon combinatorial treatment of platinum-taxol with Trametinib/chloroquine indicating the role of ERK1/2 driven autophagic flux in ameliorating chemotherapeutic stress at the onset of resistance. Altogether our data suggest that therapeutic targeting of ERK1/2 blocks cytoprotective autophagic flux and sensitizes cells at the early stage of resistance to prevent the development of a highly chemoresistant phenotype.

Targeting the ERK1/2 driven autophagic axis though sensitizes cells at the early stage of resistance, the development of a highly resistant phenotype may render this strategy ineffective. Additionally, precise identification of an early resistance stage in clinical settings is difficult, thus an alternate strategy is to impede the development of a highly chemoresistant phenotype. Among several processes, enrichment of CSCs population has been identified as a major regulator of disease relapse and resistance. Therefore, the efficacy of any therapeutic regimen depends on its ability to target this small sub-population of quiescent CSC. Utilizing cisplatin and paclitaxel dual resistant models developed either in the presence or absence of metformin, we demonstrated that continuous administration of a low dose of metformin during acquirement of chemoresistance led to a significant increase in proliferation rate and ERK activation while AKT activation reduced compared to dual resistant cells developed in absence of metformin. Interestingly, the presence of metformin significantly reduced CSC population indicated by the reduction in side population (SP), CD133+ve cell population and expression of pluripotent genes. Reduction in CSC population was concomitant with increased sensitivity of these cells towards platinum-taxol. Further metabolic profiling of the metformin treated platinum-taxol resistant cells identified a significant increase in the level of taurine and histidine in comparison to sensitive cells and platinum-taxol resistant cells. Intriguingly, a low dosage of taurine was found to reduce the percentage of SP (CSC-like population) in

A2780DualLR cells and SKOV3, an inherent cisplatin resistant cell line. Combinatorial treatment of platinum-taxol along with taurine significantly sensitized DualLR cells to therapy. Collectively, our data for the first time demonstrates that metformin impedes the development of platinum-taxol resistance by inducing CSC differentiation through taurine metabolism, and maintains a highly proliferative cellular state, susceptible to chemotherapeutic intervention. We also demonstrate the role of a common health supplement, taurine, in inducing CSC differentiation in ovarian cancer cell lines.

The gradual evolution of a highly platinum-taxol resistant phenotype can be targeted at its onset or can be delayed through metformin administration. However, attainment of a highly chemoresistant phenotype necessitates the use of non-platinum drugs like doxorubicin, gemcitabine, irinotecan and etoposide. The majority of the second line chemotherapeutics show a similar response rate of 15-30% against platinum-resistant disease. Thus a prior subject specific assessment of the efficacy of these drugs can guide the choice of optimally effective non-platinum agents. Biomolecular interactions are the fingerprints of a variety of biological phenomena that measure specific responses of drugs in cancer cells and are superior to currently available cytotoxicity assays for predicting therapy efficacy. Utilizing, a brighter, stable and highly sensitive nanoluciferase, we developed two BRET sensors to monitor specific molecular events through PIP3 mediated AKT activation at the plasma membrane (NAT sensor) and ERK1/2 activation through its substrate phosphorylation in cytoplasm and nucleus (NEO sensor). BRET assessment revealed inducer/inhibitor mediated temporal modulation in AKT and ERK activation in A2780 and MCF-7 cells with high sensitivity and specificity. Intriguingly, platinum-taxol induced only ERK1/2 phosphorylation and not AKT, as observed by live-cell BRET assessment in cisplatin-paclitaxel resistant Dual^{LR} and in SKOV3 cells. This indicates that ERK mediated signalling is crucial for the survival of these drug resistant cells. Platinum challenge significantly increased NAT and NEO BRET signal specifically in cells

derived from platinum-resistant relapse patients but not in treatment-naive or platinum sensitive relapse patients, indicating the ability of platinum-resistant cells to upregulate growth promoting signalling pathways in response to therapy. To the best of our understanding, this is the first report on real-time monitoring of therapy induced ERK1/2 and AKT activation in patient ascites through BRET technology. Further, treatment of A2780/OAW42 Dual^{LR} and SKOV3 cells with doxorubicin, gemcitabine, etoposide and irinotecan showed increased ERK1/2 activation for all except irinotecan as observed by live-cell BRET assessment. Interestingly, only irinotecan among all these drugs was able to sensitize these resistant cells to therapy. Further, doxorubicin treatment led to activation of p90RSK1/2 and inhibition of BAD specifically in resistant cells. Such effects were not observed with irinotecan treatment, implying that activation of ERK1/2 in response to therapy is crucial for the survival of these resistant cells. Altogether, our data suggest that the application of BRET can foresee the efficacy of cancer drugs through activation of two crucial pathways in real-time which may be expanded into a valuable assay for management of therapy-resistant ovarian and other cancers.

Collectively, our data suggest that targeting ERK1/2 driven autophagic flux sensitizes ovarian cancer cell in the early stage of resistance to prevent the development of a highly chemoresistant phenotype. Repurposing of metformin as an adjuvant to platinum-taxol could impede the development of a highly chemoresistant phenotype. However, attainment of highly resistant phenotype necessitates the administration of non-platinum drugs, the choice of which can be guided by our BRET platform.

Chapter 6: Materials and methods

6.1 Bacterial culture

6.1.1 Reagents

Sr. No.	Reagent name	Source
1	Luria-Bertani (LB) broth	HiMedia, India
2	Luria-Bertani (LB) agar	HiMedia, India
3	Yeast extract	HiMedia, India
4	Bactotryptone	HiMedia, India
5	Ampicillin	Sigma, USA
6	Kanamycin	Sigma, USA
7	Zeocin	Invitrogen, USA
8	Dimethyl sulfoxide (DMSO)	HiMedia, India
9	Sodium chloride	HiMedia, India
10	Potassium chloride	HiMedia, India
11	Magnesium sulphate	Sigma, USA
12	Magnesium chloride	Sigma, USA
13	4-(2-hydroxyethyl)-1-piperazineethanesulfonic acid (HEPES)	Sigma, USA
14	Calcium chloride	Sigma, USA
15	Manganese chloride	HiMedia, India
16	Potassium hydroxide	HiMedia, India
17	Sucrose	Sigma, USA

6.1.2 Bacterial strains

Sr. No.	Bacterial strain	Source
1	<i>Escherichia coli</i> DH5 α	ATCC

6.1.3 Bacterial culturing media preparations

Luria Broth: 20 grams (g) of Luria Broth powder was dissolved in 1 litre of milliQ water and sterilized by autoclaving.

Luria Agar: 34gms of Luria agar powder was dissolved in 1 liter of milliQ water and sterilized by autoclaving.

Super Optimal Broth: 2g-bactotryptone, 0.5g-yeast extract, 50mg-Nal, 18.6mg-KCl. 1M-MgCl₂ (10 ml): 2.033g and 1M- MgSO₄ (10 ml): 2.465g was dissolved in 100ml of media.

Antibiotics were added as necessary for propagation of plasmids

6.1.4 Plasmids used in the study and their selection markers

Sr. No	Construct name	Selection marker
1.	pCMV-Nluc-mOrange	Zeocin
2.	pCMV-Turbo-Nluc	Zeocin
3.	pCMV-PH-AKT-EGFP	Kanamycin
4.	pCMV-PH-AKT-Nluc	Ampicillin
5.	pCMV-PH-AKT-Rluc8.6	Zeocin
6.	pCMV-GAP-Turbo	Ampicillin
7.	pCMV-Cerulean-EKARcytoplasmic-Venus	Ampicillin
8.	pCMV-Cerulean-EKARnuclear-Venus	Ampicillin
9.	pCMV-Nluc-EKARcytoplasmic-mOrange	Zeocin
10.	pCMV-Nluc-EKARnuclear-mOrange	Zeocin
11.	pCMV-FL2	Ampicillin
12.	pCMV-mtFL	Ampicillin
13.	pCMV-RL	Ampicillin
14.	pCMV-mtFL-p62	Ampicillin
15.	pCMV-FL-p62	Ampicillin

6.1.5 Bacterial culturing technique

All bacterial cultures were grown aseptically in LB media or LB agar in presence or absence of antibiotics and incubated at 37°C for growth. For bacterial culture grown in media, tubes were kept under mild stirring at 180 RPM

6.1.6 Preparation of Competent cells

1. Single *E.Coli* colonies were obtained by streaking DH5 α strain on LB agar and grown at 37°C for 16 hours
2. Starter culture were prepared by suspending well isolated colony in 1 ml of LB medium and grown for 6 hours in 1.5 mL Eppendorf tube at 37°C, 180 RPM
3. 200 μ l of the starter culture was added to 100 mL SOB in 1 litre conical flask and incubated at 20°C at 150 RPM. Culture were grown till the absorbance of the medium reached 0.5 at 600 nm
4. Next, culture was chilled on ice for a minimum of 10 minutes and kept on ice for all the following steps
5. The bacterial suspension was then aliquoted in pre-chilled 50 ml sterile centrifuge tubes and centrifuged at 4°C for 10 minutes at 3000 RPM
6. The supernatant consisting of clear media was discarded and bacterial pellet was processed for making competent cells
7. Bacterial pellet was gently re-suspended in 50 ml of freshly prepared ice-cold TB buffer by gentle tapping and incubated for 10 minutes on ice
8. After 10 minutes bacterial suspension was centrifuged at 4°C for 10 minutes at 3000 RPM and supernatant was discarded

9. Bacterial pellet was gently re-suspended in 2 ml of ice-cold TB buffer containing 7% DMSO by tapping and incubated on ice for 10 minutes
10. After incubation, 100 µl of bacterial suspension were aliquoted in pre-chilled 1.5 mL micro centrifuge tubes on ice
11. The aliquots were flash-frozen in liquid nitrogen and stored at -80°C till use

6.1.7 Bacterial transformation

1. 10ng of plasmid DNA was added to 100 µl of competent cells were thawed on ice and mixed with 10ng of plasmid DNA and incubated on ice for 30 minutes
2. After incubation, competent cell were incubated at 42°C for 60 sec for heat-shock and followed by incubation on ice for 5 minutes
3. 900µl of LB medium was added to the cells and incubated at 37°C for 60 minutes at 180 RPM
4. Desired volume of bacterial culture were then plated on an LB agar plate with the appropriate antibiotic

6.1.8 Plasmid isolation

NucleoSpin® Plasmid kit manufactured by MACHEREY-NAGEL (MN), Germany was used for all plasmid isolation.

1. 10 ml of bacterial culture containing desired plasmid were grown overnight at 37°C at 180 RPM
2. Bacterial culture were pelleted by centrifugation at 3000RPM for 10 minutes at 4°C and resuspended in 250 µl Buffer A1 containing RNase A
3. For cell lysis, 250 µl of Buffer A2 was added and mixed gently

4. 300 µl of neutralization buffer A3 was added and centrifuged at 12,000 RPM for 5 minutes for pelleting cell debris
5. Clear supernatant containing plasmid of interest was loaded on to NucleoSpin column and centrifuged at 12,000 RPM for 1 minute
6. Columns were washed with buffer A4 to remove salts and dried by additional step of centrifugation at 12,000 RPM for 1 minute and heating at 70°C
7. Plasmids were eluted using milliQ water pre-warmed to 70°C
8. Plasmid yield was quantified using Nanodrop spectrophotometer, Thermo Scientific, USA

6.2 Molecular Cloning

6.2.1 Reagents

Sr. No.	Reagent name	Source
1	Glacial acetic acid	Fisher Scientific, USA
2	EDTA	Invitrogen, USA
3	Tris base	Sigma, USA
4	Agarose	Sigma, USA
5	Ethidium bromide (EtBr)	Sigma, USA
6	6X DNA loading dye	NEB, USA
7	DNA molecular weight standards	NEB, USA
8	NucleoSpin® Gel and PCR Clean-up kit	Macherey-Nagel, Germany
9	Restriction enzymes and buffers	NEB, USA
10	T4 DNA Ligase kit	NEB, USA
11	PrimeSTAR GXL DNA Polymerase Kit	Clontech-Takara-Bio, USA

6.2.2 Electrophoresis Buffers:

Tris acetate EDTA buffer (TAE): 40mM Tris base, 20mM glacial acetic (20mM) and 1mM Sodium EDTA

6.2.3 DNA gel electrophoresis

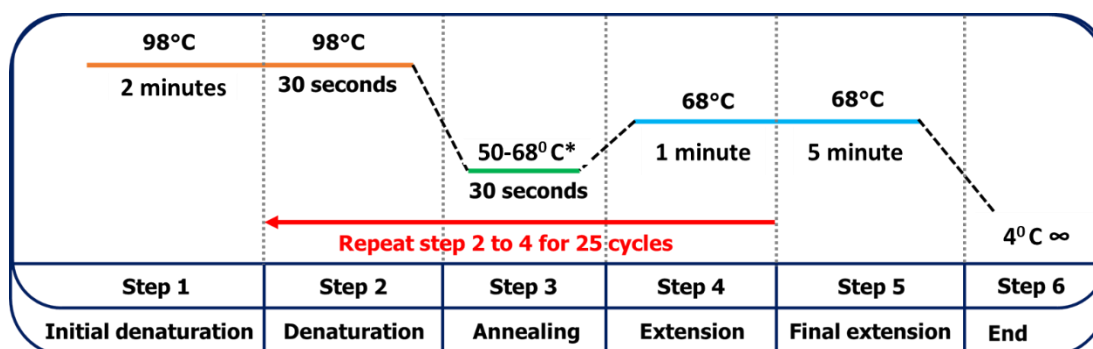
1. Desired percentage of agarose gel depending on the size of the DNA was made and EtBr was added for visualization of nucleic acids at concentration of 0.2g/ml
2. Samples were prepared by mixing appropriate volume of 6X loading dye and loaded on to agarose gel along with molecular weight standard
3. Gel was run at 60-80V in TAE buffer for desired time for optimal resolution of the band of interest and visualized in gel doc under UV light

6.2.4 Polymerase chain reaction (PCR)

1. All PCR reaction mixture of 25µl reaction volume were made to as given in the following table

Components and stock concentration	Volume
5X PCR buffer	5 µl
2.5mM dNTPs	4 µl
Forward Primer 10µM	0.25 µl
Reverse Primer 10µM	0.25 µl
PrimeSTAR GXL DNA Polymerase	0.5 µl
Template DNA 20 ng/µl	2
milliQ water	13 µl
Total volume	25 µl

2. PCR reaction conditions



*Annealing temperature was calculated using online tool using the formula:

$$T_m (\text{°C}) = [(\text{the number of A and T}) \times 2] + [(\text{the number of G and C}) \times 4] - 5$$

** For colony PCR all reaction conditions were kept similar apart from initial denaturation which was 4 minutes instead of 2 minutes

6.2.5 Restriction digestion

1. Appropriate restriction enzymes with incompatible ends were selected
2. All restriction digestion were made using following table

Component	Volume/concentration
Plasmid DNA / PCR amplified DNA	1µg
10X-NEB restriction buffer (according to restriction enzymes of choice)	5µl (1X)
Restriction enzyme 1	10 units / 1µg of DNA
Restriction enzyme 2	10 units / 1µg of DNA
Nuclease free water	Volume make up to 50µl

3. Reaction mixture were incubated at 37°C water bath for 16-20 hours
4. Efficiency of restriction digestion was assessed by DNA gel electrophoresis

6.2.6 DNA purification from gel, PCR product and restriction digestion reactions

1. Desired DNA fragment was cut from agarose gel under UV-illuminator
2. Agarose pieces containing DNA fragment were collected in micro centrifuge tube and weighed
3. DNA was purified from gel using NucleoSpin® Gel and PCR Clean-up kit
4. Gel piece was melted at 55°C in NT1 buffer (volume of NT1 buffer= 2*weight of gel in mg)

* Same kit was used for purifying DNA from PCR product and restriction digestion reaction with modification in volume of NT1 buffer (volume of NT1 buffer= 2*volume of reaction)

5. Solution contacting the DNA fragment of interest was loaded in the nucleospin column and centrifuged at 12,000 RPM for 1 minute

6. Columns were washed with buffer NT3 to remove salts and dried by additional step of centrifugation at 12,000 RPM for 1 minute and heating at 70°C

8. DNA fragment were eluted using milliQ water pre-warmed to 70°C

8. Yield was determined using Nanodrop spectrophotometer, Thermo Scientific, USA

6.2.7 Ligation

1. Purified cut vector and insert (vector to insert ratio: 1:3) were ligated at 16⁰ C for 16-20 hours using T4 DNA ligase using the following protocol

Component	Volume/concentration
Vector Plasmid DNA (1X)	50-100 ng
Insert plasmid DNA (3X)	150-300 ng
10X-NEB T4 DNA ligase buffer	2µl (1X)
T4 DNA Ligase enzyme	1µl
milliQ water	Volume make up to 20µl

2. Ligated products were transformed in *E. Coli* DH5α and screened by colony PCR or restriction digestion followed by plasmid purification

6.2.8 Side Directed Mutagenesis (SDM)

1. Mutagenesis primers containing desired mutation of interest were designed.

SDM Primer for introduction of K14A mutation in PH domain of AKT

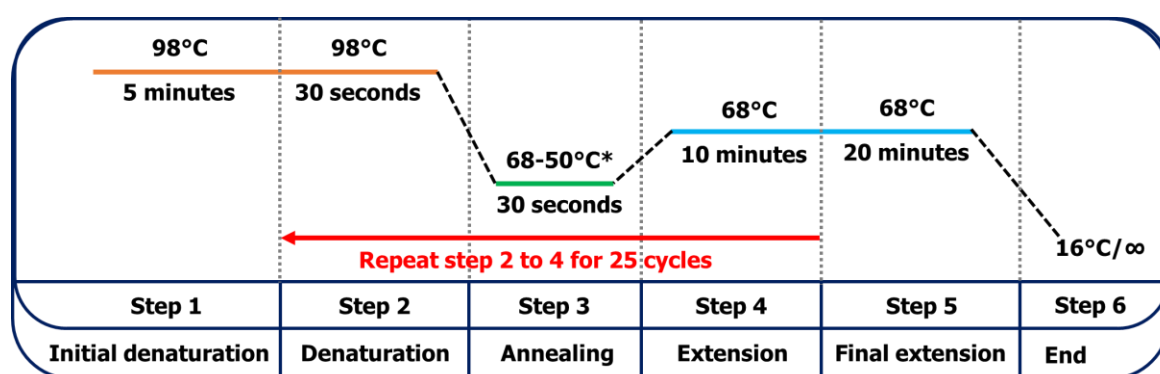
Forward SDM primer: ggctgcacGCCcgaggggaatatattaaaacc

Reverse SDM primer: cctcggGCgtgcagccagcctcct

2. PCR reaction mixture using the plasmid DNA (PH-AKT-Nluc/PH-AKT-EGFP) of interest was constituted following the below table

Component	Volume/Concentration
Plasmid DNA	125 ng
Forward SDM primer	125 ng
Reverse SDM primer	125 ng
2.5 mM dNTPs mix	4µl
5X-Primestar GXL buffer	10µl
Primestar GXL enzyme (high fidelity)	1µl
Nuclease free water	Volume make up to 50µl

3. PCR reaction conditions:



*Annealing temperature was calculated using online tool using the formula:

$$T_m (\text{°C}) = [(\text{the number of A and T}) \times 2] + [(\text{the number of G and C}) \times 4] - 5$$

- The PCR products were analysed based on their predicted size by gel electrophoresis
- The PCR product and the original template DNA were digested with DpnI restriction enzyme following restriction digestion protocol mentioned above
- Following digestion, PCR products were purified and transformed in *DH5α* in presence of antibiotic
- 5-10 isolated colonies were grown overnight in LB broth containing antibiotic for amplification of mutated plasmid DNA

8. Plasmid DNA was purified and screened using Sanger sequencing to identify construct/s harbouring desired mutation

6.3 Cell culture

6.3.1 Reagents and chemicals

Sr. No.	Reagent name	Source
1	Media – DMEM, MEM and RPMI	Gibco, USA
2	Foetal bovine serum (FBS)	HiMedia, India
3	100X-Penicillin – Streptomycin (Pen-Strep)	HiMedia, India
4	Trypsin-0.25% – (EDTA)-0.02%	Sigma, USA
5	Dimethyl sulfoxide (DMSO)	Sigma, USA
6	G418	Sigma, USA
7	Puromycin	Sigma, USA
8	Superfect transfection reagent	Qiagen, USA
9	Lipofectamine 2000	Invitrogen, USA
10	Trypan blue solution (0.4%)	Sigma, USA
11	Vybrant DyeCycle Violet (DCV) stain	Thermo Fisher Scientific, USA
12	Verapamil hydrochloride	Sigma, USA
13	Polybrene	Sigma, USA
14	Charcoal stripped serum	HiMedia, India

6.3.2 Buffers

Phosphate Buffer Saline: 137mM NaCl, 2.7mM KCl, 10mM Na₂HPO₄ and 2mM KH₂PO₄, pH 7.4.

6.3.3 Cell lines

List of cell lines used in this study with culture media.

Sr. No.	Cell line name	Origin	Source	Culture media
1	A2780	Ovarian cancer	ATCC	DMEM

2	OAW42	Ovarian cancer	ATCC	MEM
3	SKOV3	Ovarian cancer	ATCC	RPMI
4	MCF7	Breast cancer	ATCC	RPMI
5	HEK293FT	Human embryonic kidney	ATCC	DMEM

6.3.4 Cell culture Methods

Standard aseptic practice was followed for performing cell culture, All the cell lines were maintained in their respective media supplemented with the 10% FBS and 1% Pen-Strep and incubated under 5% CO₂ at 37°C in a humidified incubator. Cells with 70-80% confluence were used for experiments.

*for BRET assay to measure growth factor induced ERK and AKT activation, culture media was supplemented with 10% charcoal stripped serum instead of normal FBS

6.3.4.1 Sub culturing of Cells

1. Old culture media was aspirated from culture plate using sterile glass pipette and cells were washed with 1X PBS buffer
2. Required volume of Trypsin-EDTA solution was added to the plate to cover the entire surface and the cells were then incubated in 37°C incubator for 3-4 minutes
4. Activity of trypsin was neutralized by complete medium in ratio of 1:3
- 5 Single cell suspension was made by gently pipetting and cells were centrifuged at 800 RPM for 4 minutes. Supernatant was discarded and the cells were resuspended in complete medium
6. Viable cell count was determined using trypan blue dye exclusion method followed by manual cell counting in a haemocytometer. Number of cells/ml were calculated using the following formula: No of cells/ml= average number of cells per WBC chamber*dilution factor*10⁴
7. A portion of cell suspension was reseeded according to the requirement in new culture plate/s with fresh complete medium

6.3.4.2 Cryopreservation

1. Adherent cells were trypsinized and collected in 15ml tube
2. Cells were washed twice with 1XPBS and collected by centrifugation at 800 RPM for 4 minutes at 4°C
3. 1 million cells were resuspended well in freezing medium containing 30% FBS and 8% DMSO (950µl FBS and 50µl DMSO)
4. Vials were kept in freezing container filled with isopropanol and transferred to -80°C
5. On the following day, the vials were transferred to liquid Nitrogen for long term storage of the cells

6.3.4.3 Revival of Cryopreserved vials

1. Vial removed from liquid N₂ was immediately transferred to water bath set at 37°C
2. Thawed cells were resuspended in 1ml complete medium and centrifuged at 800RPM for 4 minutes at 4°C
3. Cells were washed once with 1X PBS and centrifuged at 800 RPM for 4minutes at 4°C
4. Cells were resuspended in culture medium and plated in 60mm dish containing complete medium
5. Cells were allowed to recover and revive at 37°C incubator with 5% CO₂ supply overnight

6.3.5 Cell proliferation assay

1. 2×10^4 cells were seeded in each well of a 6 well plate in triplicate
2. Viable cell count was determined using trypan blue dye exclusion method followed by manual cell counting in a haemocytometer at every 24 hours till 120 hours

3. Cell number was plotted against time to determine proliferation rate and doubling time was calculated using online doubling time calculator

6.3.6 Transient transfection of mammalian cell lines

All transfections were performed using Superfect, Qiagen, USA transfection reagent according to manufacturer guidelines at 70 % confluency

For luciferase assay: Transfection of luciferase construct of interest and normalization vector was done in a ratio of 9:1

For BRET assay: Transfection of donor and acceptor plasmid was done in a ratio of 1:1. For normalization, cells were transfected with only donor

6.3.7 Stable transfection (mtFL-p62) of mammalian cell line (A2780Dual^{ER})

1. Cells were trypsinized post 24 hours of transfection with mtFL-p62 and split into 100 mm tissue culture dish at single cell density

2. Cells were cultured in complete media containing 4 µg/ml of Puromycin

3. Fresh sterile media with adequate quantity of Puromycin was added every 72 hours

4. Once well isolated colonies emerged in cell culture dish, they were picked using pipette and transferred to a 96-well plate containing selection media

5. Each colony was screened using luciferase assay to identify cells expressing transgene

6. Colonies were expanded and cryopreserved as per requirement

6.4 Cell viability assay

6.4.1 MTT assay

1. 2×10^3 cells were seeded in each well of a 96 well plate in triplicate and incubated overnight in a humidified incubator at 37°C and 5% CO₂

2. Cells were treated with various drugs at desired concentration

3. All the cytotoxicity test were performed after 48 hours of drug treatment and the cells were incubated for 72 hours
4. At end points, 20µl of MTT (5mg/ml) reagent (Sigma, USA) was added to each well and incubated for 3 hours
5. The spent media from each well were removed completely
6. 100µl DMSO per well was added to solubilise the dye
7. Absorbance from each well was measured at 560nm and 670nm and percent cell viability was calculated using the formula

$$\text{Percent cell viability} = \frac{\text{Test Absorbance 560} - \text{Test Absorbance 670}}{\text{Control Absorbance 560} - \text{Control Absorbance 670}} \times 100$$

6.4.2 CellTox assay

1. 1×10^4 cells were seeded in each well of a black clear bottom 96 well plate in triplicate and incubated overnight in a humidified incubator at 37°C and 5% CO₂
2. Cells were treated with various drug at a concentration mentioned below along with CellTox dye (1:1000 dilution)

Drug	Concentration	Source
Cisplatin-paclitaxel	250ng of cisplatin-42.5ng of paclitaxel	Sigma, USA
Trametinib	10 nM	Cayman Chemicals, USA

3. Real time cell death kinetics was measured at every 6 hour interval at 485-500 nm_{EX}/520-530 nm_{EM} in Biotek cytation5 (VT, USA) imaging system

6.4.3 Clonogenic assay

- a) Cells were trypsinized and viable cell count was determined using haemocytometer
- b) 500 cells were seeded per well in 6-well plates and incubated under at 37°C under 5% CO₂ in a humidified incubator
- c) On the following day, cells were treated with increasing dose of platinum-taxol for 2 hours

A2780 model: 100ng cisplatin+13 ng paclitaxel, 250ng cisplatin+ 42.5 ng/ml of paclitaxel

OAW42 model: 70 ng cisplatin+13 ng paclitaxel, 100 ng cisplatin+ 20 ng/ml of paclitaxel

- d) After treatment spent media was removed and fresh complete media was added
- e) Cells were incubated at 37°C under 5% CO₂ in a humidified incubator for 10-14 days till visible colonies appear
- f) After the end of the incubation period, plates were washed once with PBS and fixed using pre-chilled mixture 90% methanol and 10% glacial acetic acid at -20°C for 5 minutes
- g) Cells were stained with staining solution (0.5% crystal violet in 90% methanol + 10% glacial acetic acid) and incubated for 1 hour at room temperature
- h) Excess staining solution was then discarded and plates were washed once with 1X PBS
- i) Plating efficiency was calculated using following formula

$$\text{Plating efficiency} = \frac{\text{Number of colonies formed}}{\text{Number of cells seeded}} \times 100$$

j) Surviving fraction was determined using the formula,

$$\text{Surviving fraction} = \frac{\text{Plating efficiency of treated sample}}{\text{Plating efficiency of control sample}}$$

6.5. Immunoblotting

6.5.1 Reagents

Sr. No.	Reagent name	Source
1	Bradford reagent	Sigma, USA
2	Tris-base	Hi media, India
3	Sodium dodecyl sulphate (SDS)	Hi media, India
4	β -mercaptoethanol	Sigma, USA
5	100X-Protease inhibitor cocktail	Sigma, USA
6	Sodium orthovanadate	Sigma, USA
7	Sodium fluoride	Sigma, USA
8	Sodium chloride	Sigma, USA
9	Sodium EDTA	Sigma, USA
10	Sodium deoxycholate	Sigma, USA
11	Nonidet P-40 (NP-40)	Sigma, USA
12	Triton-X-100	Sigma, USA
13	Acrylamide	Hi media, India
14	Bis-acrylamide	Sigma, USA
15	Ammonium persulfate	Sigma, USA
16	Tetramethylethylenediamine (TEMED)	Sigma, USA
17	Pre-stained protein ladder	Hi media, India
18	Methanol	SRL Chemicals, India
19	Polyvinylidene difluoride (PVDF) membrane	PALL, USA
20	Bovine serum albumin (BSA)	Hi media, India
21	Skimmed non-fat milk	Hi media, India
22	Tween 20	Sigma, USA
23	Enhanced chemiluminescent substrate	Clonotech Takara, USA

24	Horseradish peroxidase (HRP)-conjugated secondary antibodies	Sigma, USA
----	--	------------

6.5.2 Primary antibodies

Sr. No	Antibody	Dilution	Source
1	Phospho ERK1/2	(1:2000)	CST, USA
2	Total ERK1/2	(1:2000)	CST, USA
3	Phospho AKT	(1:2000)	Sigma, USA
4	Total AKT	(1:2000)	Sigma, USA
5	Phospho p90 ^{RSK1/2}	(1:1000)	R&D systems, USA
6	Total p90 ^{RSK1/2}	(1:1000)	R&D systems, USA
7	Fra-1	(1:1000)	Santacruz biotechnology, USA
8	LC3	(1:1000)	CST, USA
9	P62	(1:2000)	Abcam, UK
10	UVRAG	(1:1000)	Abclonal, USA
11	Rubicon	(1:1000)	Abclonal, USA
12	Rab7	(1:1000)	CST, USA
13	Phospho mTOR	(1:2000)	CST, USA
14	Phospho mTOR	(1:2000)	CST, USA
15	Phospho BAD	(1:1000)	CST, USA
16	Total BAD	(1:1000)	CST, USA
17	Tubulin	(1:4000)	Sigma, USA

6.5.3 Buffers

Sr. No.	Buffer name	Compositions

1	Radio immunoprecipitation assay (RIPA) buffer	50mM Tris-HCl pH 8.0, 150mM NaCl, 1% Nonident P-40 or 1% Triton-X100, 0.5% Sodium deoxycholate and 0.1% SDS.
2	Resolving gel buffer	1.5 M Tris-HCl, pH 8.8
3	Stacking gel buffer	0.5 M Tris-HCl, pH 6.8.
4	5X-Protein loading buffer	0.5 M Tris-HCl pH 6.8, 10% SDS, 50% Glycerol, 0.01% Bromophenol blue and 25% β -mercaptoethanol.
5	Gel running buffer	25mM Tris base, 190mM Glycine and 0.1% SDS.
6	30% Acryl amide mix	29g Acryamide + 1g of Bis-acrylamide in 100ml double distilled water.
7	Transfer buffer	48mM Tris, 39mM glycine, 0.04% SDS and 20% methanol.
8	Tris-buffered saline (TBS)	20mM Tris, 150mM NaCl, pH 7.4.
10	Wash buffer (TBST)	TBS with 0.1% Tween 20.
11	Blocking buffer	5% BSA or 5% Skimmed-non-fat milk in TBST
12	Stripping buffer	62.5mM Tris, 20% SDS and 0.8% β -mercaptoethanol

6.5.4 Immunoblotting

6.5.4.1 Lysate preparation

- 1) Cells were collected by trypsinization and required amount of the RIPA lysis buffer supplemented with 1X-protease inhibitor cocktail, 1mM-Sodium orthovanadate and 5mM-Sodium fluoride was added to cell pellet

- 2) Cells were incubated on ice for 1 hour and sonicated in water cooled sonicator (Biorupter) at high amplitude for 3-5 cycles (30-seconds-on/30-seconds-off)
- 3) Cell lysates were centrifuged at 14000RPM for 30 minutes at 4°C to remove cell debris
- 4) Clear supernatant was collected as cell lysates for further use

6.5.4.2 Bradford assay

- 1) BSA standards were made by serially diluting 1mg/ml stock (Concentration range 0.2mg/ml-1mg/ml)
- 2) 5 µl of each of standard concentration was added to 250 µl of Bradford reagent in triplicate
- 3) Absorbance was measured at 595nm, values were subtracted against the blank and a standard curve was plotted by using the linear regression analysis. The formula derived from the standard curve was used for estimating protein concentration of the cell lysates
- 4) Cell lysates were diluted 10 times with PBS and 5 µl of diluted cell lysate was added to 250 µl of Bradford reagent in triplicate
- 5) Colorimetric absorbance was taken at 595nm using Biotek citation 5
- 6) Absorbance values were subtracted against the blank and protein concentration was calculated using the formula derived from the standard curve

$$\text{Protein } (\mu\text{g}/\mu\text{l}) = \frac{\text{Absorbance} + y \text{ intercept of standrad curve}}{\text{slope of standard curve}} \times \text{Dilution factor}$$

- 7) Protein samples were prepared by mixing 30-60 µg of protein lysates with 5X-loading buffer
- 8) Samples were heated at 95°C for 5 minutes and used for loading on poly-acrylamide gel

6.5.4.3 Poly-acrylamide gel casting

- 1) Gel percentage was determined according to the molecular weight and casted by following the below table
- 2) Resolving gel was poured first and allowed to polymerize for 30 minutes
- 3) Stacking gel was poured over resolving gel and allowed to polymerize for 30 minutes after placing the comb

% Acrylamide	8%	12%	4% (stacking)
Proteins detected	AKT, mTOR, UVRAG, Rubicon, p90 ^{RSK1/2}	ERK1/2, LC3, p62, Rab7, BAD, Fra-1	-
Milli Q water	4.6 ml	3.3 ml	1.25 ml
30% Acrylamide	2.7 ml	4 ml	0.25 ml
1.5 M Tris pH 8.8	2.5 ml	2.5 ml	-
0.5 M Tris pH 6.8			0.5 ml
10% SDS	100 μ l	100 μ l	20 μ l
10% APS	50 μ l	50 μ l	10 μ l
TEMED	5 μ l	5 μ l	2 μ l

6.5.4.4 Procedure for immunoblotting

- 1) The solidified gel was placed in the cassette and fitted with electrodes in the tank.
- 2) The tank was filled with 1X running buffer completely
- 3) The comb was then gently removed and the wells were washed with the buffer to remove un-polymerized gel pieces

- 4) The prepared samples (as mentioned in section point 8 section 6.5.4.2) were then loaded into respective wells
- 5) The gel was then allowed to run at 60V, 400mA. After the sample entered the resolving gel the voltage was gradually increased to 80V. The run was stopped as soon as desired resolution has been achieved
- 6) The PVDF membrane was activated by soaking in methanol for 60 seconds
- 7) The gel, blotting paper and activated PVDF membrane were then soaked in 1X transfer buffer and incubated for 10 minutes
- 8) Onto the base of the Trans blot system the two soaked blotting papers were placed one after another, the transfer buffer was poured on top of the membrane and the air bubbles were removed carefully. Then, the PVDF membrane was placed and the gel was carefully placed over it
- 9) The remaining two blotting papers were placed on the top of the gel and same as before the transfer buffer was poured, ensuring that the bubbles were removed
- 10) Transfer of proteins were performed at 13V, 400mA for 1 hr
- 11) After complete transfer, the membrane was removed carefully and then incubated in 40 ml of 5% blocking buffer for 1 hr on a shaker
- 12) After blocking, the membrane was probed with primary antibody(s) and incubated overnight at 4°C with gentle shaking
- 13) Next day, the membrane was washed thrice with the wash buffer (1X TBST) and then incubated with the secondary antibody for 2 hour at room temperature
- 14) After the secondary Ab incubation the membrane was again washed thrice with the wash buffer.
- 15) Proteins were detected using chemiluminescent substrate and imaged in chemidoc imaging system (Biorad)

16) Blots were stripped by incubating with stripping buffer for 10 minutes under vigorous shaking and reprobed with Tubulin antibody (loading control) and proceed as mentioned before for detection of protein band

6.6 Transmission Electron Microscopy

- 1) 5×10^6 cells were collected by trypsinization and centrifuged in 15 ml tube at 1000 RPM for 4 minutes
- 2) Cell pellets were collected in a 1.5 ml micro-centrifuge tube and fixed using 2.5% glutaraldehyde (Volume: Volume) in 0.1 M cacodylate buffer (pH: 7.4)
- 3) Fixed cells were treated with 1% osmium tetroxide (weight: volume) in 0.1 M cacodylate buffer and incubated at 4⁰ C for 1 hour
- 4) Samples were dehydrated in graded series of ethanol (30%-50%-70%-90%-100%). In each step samples were dipped in ethanol solution for 15 minutes
- 5) Samples blocks were prepared by embedding in araldite resin and incubated at 70°C for 24 hours for polymerization
- 6) Ultrathin sections of approximately 50-70nm were made using Lieca UC7 ultramicrotome
- 7) Sections were mounted on 300 mesh copper grids and stained with 10% Uranyl acetate alcoholic and lead citrate for contrast enhancement
- 8) Samples were imaged on a JEOL 1400plus transmission electron microscope operated at 120 kV using Tengra camera and acquired with iTEM software
- 9) Autophagic bodies were identified and quantified on the basis of their morphology and staining intensity in 10-15 cells across different fields

6.7 Confocal and Immuno-fluorescence microscopy

6.7.1 Confocal microscopy

- 1) 5×10^5 cells were seeded in 35 mm tissue culture dish containing 22 mm coverslips and incubated at 37⁰ C humidified incubator at 5% CO₂
- 2) On the following day, cells were transfected with mCherry-EGFP-LC3/PH-AKT-EGFP/NAT constructs/GAP-TurboFP635 as mentioned previously
- 3) Cells were then treated* as necessary and fixed with 4% paraformaldehyde for 15 minutes at 37⁰ C incubator.
- 4) Coverslips were then mounted on glass slide using Vectasheild (Vector labs, USA) and imaged on LSM780, Ziess confocal microscope
- 5) Images were analysed using image J or Zen software.

* mCherry-EGFP-LC3 assay:

- 1) A2780, Dual^{ER} and Dual^{LR} cells were transfected with mCherry-EGFP-LC3 plasmid and treated for 24 hours with platinum-taxol (at concentration 10 times the respective IC₅₀) alone or in combination with U0126 (10 μM)
- 2) Cells were imaged in LSM780 microscope using 488 and 633 laser with 40X optical zoom and 2X digital zoom
- 3) Images were analysed for colocalization and ratio of mCherry and EGFP puncta. For colocalization analysis Ziess Zen imaging software's "*coloc*" function was used. Pixel intensity spatial correlation analysis was used to determine the extent of co-localization of mCherry and EGFP puncta and data was represented as mean Manders colocalization coefficient derived from total number of cells counted. The values of Mander colocalization coefficient ranges between 0 to 1, where 0 depicts no colocalization and 1 represents perfect colocalization. A value over 0.5 signifies the extent of proper co-localization. For calculation of mCherry/EGFP ratio, a fixed intensity threshold was set before estimating the number of

EGFP or mCherry puncta. Number of puncta was calculated using “*find maxima function*” of Image J software at respective green and red channel. The ratio of red vs green puncta was then calculated for each cell and represented as mean of total number of cells analysed (n< 40 cells)

*** For monitoring membrane localization of PH-AKT**

1) A2780 cells were transfected PH-AKT or K14A-PH-AKT construct and treated with 100nM of insulin for 15 minutes

6.7.2 Immunofluorescence

6.7.2.1 Primary antibodies

Sr. No	Antibodies	Dilution	Source
1	Phospho ERK1/2	(1:200)	CST, USA
2	LC3	(1:100)	CST, USA
3	LAMP1	(1:200)	DSHB

6.7.2.2 Protocol

- 1) Cells were seeded on 22 mm coverslips on the previous day of experiment
- 2) After overnight incubation cells were treated as required
- 3) Cells were then fixed with 4% paraformaldehyde for 15 minutes at 37⁰C room temperature
- 4) After fixation, the coverslips were washed twice with 1X PBS and then permeabilized with 0.2% Triton X-100 in 4% PFA for 15 minutes
- 5) Cells were then washed with 1X PBS thrice and blocked with 3% BSA for 30 minutes at room temperature.
- 6) 40µL of the primary antibody solution was added on a parafilm and then coverslips were inverted onto the solution
- 7) These parafilms with the coverslips were then kept overnight at 4⁰ C in a humidified chamber.

8) On the following day, the cells were washed with 1X PBS for three times and incubated for 2 hours at room temperature with respective secondary antibodies (1:200) diluted in 3% BSA in 1X PBS

9) After incubation, the cells were again washed with 1X PBS thrice and DNA was labelled using DAPI

10) Coverslips were then mounted on glass slides using Vectashield (Vector Laboratories, USA)

6.7.2.3 Analysis

For counting LC3⁺/LAMP1⁺ puncta: colocalized puncta LC3 and LAMP1 puncta were first identified using “*coloc*” function of Zen imaging software and then counted using “*find maxima*” function of image J software.

For morphometric analysis of LC3⁺ puncta: area of LC3 puncta was deduced from the pixel size using image J software in the following manner

1) A scale was set according to the known distance

2) Images were converted to 8 bit binary images and analysed using “*analysed particles*” function of image J software

3) The diameter of each LC3 puncta was calculated using the formula: Area ($A = 4\pi r^2$) with the assumption that each LC3 puncta are perfect sphere. The value of the diameter obtained above was used to calculate the volume using the formula: Volume ($V = 4/3 \pi r^3$)

6.8 Flow cytometry

6.8.1 Annexin-PI assay

1. 3×10^5 A2780/OAW42Dual^{ER} cells were seeded and treated with either platinum-taxol (10 times the IC₅₀ dosage of respective cells), only Trametinib (10 nM) or their combination for 12 and 24 hours

2. Cells were harvested after treatment and washed with ice cold PBS (1X)
2. 1X annexin binding buffer was prepared by adding 1 ml of 5x annexin binding buffer with 4 ml deionized water
3. 100 µg/mL working solution of PI was prepared by diluting 5 ul of 1mg/ml PI stock solution with 45 ul of 1X annexin binding buffer
4. The washed cells from step 2 were pelleted down again, supernatant discarded and resuspended in 100 ul 1X annexin binding buffer
5. To this, 5 µL of Alexa Fluor® 488 annexin V and 1 µL of 100 µg/mL PI working solution was added
6. The cells were incubated at Room temperature for 15 minutes
7. After the incubation, 400 µL 1X annexin-binding buffer was added, mixed gently and analysed the stained cells through Flow Cytometry, measuring the florescence emission at 530 nm band pass filter and 575 nm high pass filter

6.8.2 Staining with CD133 for flow cytometry

1. 3×10^5 Cells were harvested and washed with ice cold PBS
2. Cells were resuspended in blocking buffer containing 3% FBS in 1X PBS for 20 minutes on ice
3. The cells were centrifuged at 1500 RPM for 5 minutes and the supernatant was discarded
4. Anti-CD133 antibody (1:100) was added to the cells and incubated on ice for 30 minutes
5. The cells were then washed with PBS, centrifuged at 1500 RPM for 5 minutes and resuspended in secondary anti-rabbit alexaflour 488 (1:200)
6. The cells were incubated for 30 minutes on ice in the dark
7. The cells were then washed in ice cold PBS three times, resuspended in FACS buffer for analysis in flow cytometer.

6.9 Luciferase assay

6.9.1 Reagents

Sr. No.	Reagent name	Source
1	5X-Passive lysis buffer	Promega, USA
2	Lar-II (Firefly luciferase substrate)	Promega, USA
3	1mg/ml Coelenterazine in 100%-Methanol (Renilla luciferase substrate)	Biosynth, USA

6.9.2 Protocol

1) Cells with desired reporter plasmids (pCMV-mtFL-p62/FL-p62) were transfected along with normalization vector (pCMV-RL) as described previously and transfected cells were seeded in triplicates in a 24-well plate. In context of stables cell lines, cells were directly seeded in triplicates in a 24-well plate

2) Cells were treated with drugs as mentioned below for 24 hours

Cell line	Chemotherapeutic drugs	Inhibitors
A2780/OAW42	Cisplatin (500ng/ml)+paclitaxel (85ng/ml)	Chloroquine (CQ, 10 μ M)
		Wortmanin (500ng/ml)
		Rapamycin (200ng/ml)
		Etoposide (30nM)
Dual ^{ER}		U0126 (10 μ M)

	Cisplatin (2500ng/ml)+paclitaxel (425 ng/ml)	Trametinib (10 nM)
		Bortezomib (100 ng/ml)
		Chloroquine (CQ, 10µM)
Dual ^{LR}	Cisplatin (5000ng/ml)+paclitaxel (850 ng/ml)	Chloroquine (CQ, 10µM)

3) After 24 hours of incubation with each drug cells were washed twice with PBS and lysed with 80µl of 1X-Paasive lysis buffer containing protease inhibitor

4) Cell lysate was incubated at room temperature for 10 minutes with continuous shaking

5) Cell lysates were collected in 1.5 ml micro-centrifuge tube and cell debris were removed by centrifugation at 14000 RPM for 30 minutes at 4°C

6) Clear supernatant was collected for luciferase assay and protein estimation

7) Luciferase assay was performed in a white 96-well plate by adding 10-20µl of lysate with 50µl of Lar-II substrate

8) Bioluminescence reading was immediately measured in open filter for 1 second in Biotek citation 5.

9) To measure Renilla luciferase activity, coelenterazine (1mg/ml, dilution: 1:50) was used in the same way as described for Lar-II substrate

10) Protein concentration was measured using Bradford assay as described in section 6.5.4.2

11) Reporter activity was calculated as mentioned below:

- [Relative reporter activity from transient transfection experiment,](#)

Relative reporter activity

$$= \frac{\text{Relative light units of test reporter gene/Protein}}{\text{Relative light units of constitutively active reporter gene/Protein}}$$

- Relative reporter activity from cells stably expressing reporter gene,

$$\text{Reporter activity (RLU}/\mu\text{g}/\text{sec}) = \frac{\text{Relative light units of test reporter gene}}{\text{Protein concentration of sample}}$$

6.10 Live cell imaging of autophagic flux

- 1) 5×10^4 cells expressing mtFL-p62 were seeded in each well of a clear bottom 96 well black plates and incubated overnight at 37°C in a humidified incubator at 5% CO_2
- 2) On the following day, cells were treated with drugs (as mentioned in point 2 section 5.8) for 12 and 24 hours
- 3) 1mg/ml D-luciferine was added to each wells after end of 12 and 24 hours
- 4) Images were acquired in IVIS spectrum (Perkin-Elmer, USA) using open filter settings to collect the total light output. A subject height of 0.50 cm with medium sized field of view (C setting in IVIS software) was used to acquire bioluminescence signal after every 1 minute to capture the peak luciferase activity
- 5) For quantification of bioluminescence signal average radiance were measured by drawing ROI over each well and quantified using the Live Image (4.4) software.

6.11 Quantitative Real-time PCR

6.11.1 Reagents

Sr. No.	Reagent name	Source
1	RNeasy total RNA isolation minutes i kit	Qiagen, Germany
2	SuperScript™ First-Strand cDNA Synthesis kit	Invitrogen, UK
3	PowerUp SYBR Green	Applied Biosystems, USA
4	Ethanol	Sigma, USA
5	Diethyl pyrocarbonate (DEPEC)	Sigma, USA
6	Sodium acetate	Fisher scientific
7	Sodium-EDTA	Invitrogen, USA
8	Formaldehyde	Sigma, USA
9	Formamide	Sigma, USA
10	Ethidium bromide	Sigma, USA
11	6X-RNA loading dye	
12	Agarose	Sigma, USA

6.11.2 Buffers

MOPS buffer (1X): 4.186g-MOPS (20mM), 0.411g-Sodium acetate (5mM), 0.372g-Sodium EDTA (1mM) in 1 litre of milliQ and pH (7.0) adjustment was done using NaOH to 7.0

Denaturation mix: 13µl of 37% Formaldehyde, 22µl of Foarmamide and, 65µl of 10X-MOPS buffer.

6.11.3 RNA isolation

- 1) Cells were trypsinized and centrifuged at 1000 RPM for 5 minutes at 4°C
- 2) Cell pellet was used to isolate total RNA from cells using RNeasy mini kit as per protocol
- 3) RNA yield was determined using Nanodrop spectrophotometer

4) 1 µg of RNA samples were mixed with 1.8 µl of denaturation mix preparation and heated at 55°C for 15 minutes in a dry bath

5) An appropriate volume of 6X loading dye was added to the denatured RNA samples and loaded on 0.8% formaldehyde-agarose denaturing gel (0.32g of agarose, 4 ml of 10X MOPS buffer and 36 ml of milliQ)

6) Gel was run in 1X MOPS buffer at 60 V for 45 minutes and the bands were visualized in a UV-transilluminator.

6.11.4 CDNA synthesis

1) 2 µg of good quality RNA was reverse transcribed into cDNA using Superscript™ first strand synthesis kit, Invitrogen

2) Two separate reaction mixture was

Reaction-1

S. No.	Component	Amount
1	RNA (2 µg)	X µl
2	10 mM dNTP mix	1 µl
3	Random Hexamers	1 µl
4	DEPC-treated water	To 10 µl

Reaction-2

S. No.	Component	Amount
1	10X RT buffer	2 µl

2	25 mM MgCl ₂	4 µl
3	0.1 M DTT	2 µl
4	RNase OUT (40 U/ µl)	1 µl

- 3) Reaction-1 was incubated at 65⁰ C for 5 minutes
- 4) Reaction -1 and Reaction-2 were mixed and incubated at room temperature for 2 minutes
- 5) 1 µl of Superscript reverse transcriptase enzyme was added to the reaction mixture and incubated at room temperature for 10 minutes
- 6) PCR reaction was set using following conditions: 42⁰ C for 50 minutes and 70⁰ C for 15 minutes
- 7) 1 µl of RNase H was added to each tube and incubated at 37⁰C for 20 minutes.

6.11.5 Real time polymerase chain reaction

6.11.5.1 List of primers used

Sr. No	Primer name	Sequence
1	OCT4 Forward	GTGGAGAGCAACTCCGATG
2	OCT4 Reverse	TGCAGAGCTTTGATGTCCTG
3	SOX2 Forward	AACCCCAAGATGCACAACCTC
4	SOX2 Reverse	GCTTAGCCTCGTCGATGAAC
5	NANOG Forward	AAAGCTTGCCTTGCTTTGAA
6	NANOG Reverse	AAGTGGGTTGTTTGCCTTTG
7	GAPDH Forward	TGCACCACCAACTGCTTAGC
8	GAPDH Reverse	GGCATGGACTGTGGTCATGAG

6.11.5.2 Protocol

1) The qPCR reaction mixture was prepared for each gene as follows

Sr. No	Ingredients	Amount/Volume
1	2X SYBR Green master mix	5 µl
2	Forward primer (10 pmol/µl)	1 µl
3	Reverse Primer (10 pmol/µl)	1 µl
4	cDNA (10ng/µl)	1 µl
5	milliQ water	To 10 1 µl

2) Samples were run in triplicates for all genes using standard qPCR protocol at an annealing temperature of 60⁰ C

3) The relative expression of each target gene was calculated using GAPDH as an internal control as follows: Relative expression = $2^{-\Delta Ct}$ where $\Delta Ct = Ct$ of target gene - Ct of GAPDH.

6.12 Lentiviral mediated genetic knock down

6.12.1 Reagents

Sr. No	Reagents	Source
1	Lipofectamine 2000	Invitrogen, USA
2	Polybrene	Sigma, USA

6.12.2 Preparation of lentiviral particles

1) One day prior to co-transfection 1×10^6 HEK293FT cells were seeded in a 60mm dish

- 2) Plasmids mix was made as mentioned below and co-transfected in HEK293FT cells
 - a. 2 μ g of VSVG plasmid+ 4 μ g of p Δ plasmid+ 6 μ g of pLL3.7 containing ERK1 shRNA in 500 μ l of incomplete media
 - b. ERK1 shRNA sequence: 5'-GACCGGATGTTAACCTTTA-3'.
- 3) 30 μ l of Lipofectamine 2000 reagent was mixed with 470 μ l of incomplete sterile media
- 4) Both tubes were incubated at room temperature for 5 minutes
- 5) Both the tubes were mixed and incubated at 37°C for 20 minutes
- 6) After the end of incubation period, 2ml of complete media was added to the above mixture and mixed gently
- 7) Spent media from the culture plate was removed and the transfection mix was added to cells and incubated under 5% CO₂ at 37°C humidified incubator
- 8) Post 16-20 hours of transfection media containing transfection complex was removed and replenished with fresh complete media
- 9) Cells were incubated under 5% CO₂ at 37°C humidified incubator for 48-60 hours and syncytia formation was checked
- 10) At the end of the 48-60 hours of incubation, spent media was collected into a 15 ml centrifuge tube aseptically and centrifuged at 2000 RPM for 10 minutes to remove cells
- 11) Culture supernatant was then filtered through a 0.45 μ sterile syringe into a fresh tube and ultra-centrifuged at 30,000 RPM for 90 minutes at 4°C. Ultra-centrifuge was set at highest acceleration while no brake was applied for deceleration

- 12) A white viral pellet was collected at the bottom of ultra-centrifuge
- 13) Supernatant was carefully discarded into a hypo-chloride solution to remove any left-over viral particle
- 14) 1ml of fresh complete media was added to the pellet and resuspended by gentle tapping followed by incubation at 4⁰C overnight for proper mixing
- 15) Aliquot of viral particle containing media was stored at -80⁰C for future use.

6.12.3 Viral transduction

- 1) 4×10^5 to 5×10^5 cells were seeded in a 60 mm culture dish at a confluency of 60%–70% and incubated overnight at 37⁰C under 5% CO₂ in a humidified incubator
- 2) Viral particle were diluted in fresh media supplemented with 4 µg/ml of Polybrene were added to culture plate after removal of spent media and incubated at 37⁰C under 5% CO₂ in a humidified incubator for 16 hours
- 3) Stable clones expressing EGFP were enriched by FACS sorting.

6.13 Side population assay

- 1) DyeCycle Violet staining (Invitrogen, USA) was used to detect SP (CSC) population
- 2) Verapamil stock (5mM) was prepared by dissolving 1.23 mg of Verapamil hydrochloride in 500µl of DMSO
- 3) 5×10^6 cells were seeded in 10 cm dish and incubated overnight at 37⁰C under 5%CO₂ in a humidified incubator
- 4) Cells were trypsinized and equally divided in two facs tubes after cell counting
- 5) Cells in each tubes were resuspended in 1 ml of media

- 6) In one of the tubes, labelled as control, 10µl of verapamil stock solution was added and incubated for 15 minutes at 37°C water bath. The other tube was labelled as test
- 7) 1µl DyeCycle Violet stain solution was added to both the tubes and incubated for 90 minutes at 37°C water bath in dark. Tubes were tapped at every 15 minutes intervals to prevent cell clumping
- 8) After the end of the incubation period, the tubes were kept on ice for 10 minutes and then centrifuged at 1000RPM for 5 minutes at 4°C
- 9) Supernatant was discarded and cells were resuspended in sterile PBS for flow cytometry.
- 10) Flow cytometry data was analysed using Flow Jo software.

6.14 Metabolite extraction and NMR

6.14.1 Metabolites extraction

- 1) 4×10^6 cells were seeded in four 10 cm dish and incubated overnight at 37°C under 5% CO₂ in a humidified incubator
- 2) Cells were extensively washed with ice-cold PBS (1X) for four times in order to completely remove any residue of culture medium
- 3) A total of 15×10^6 cells was then collected in 5.4 ml of ice cold PBS by scrapping
- 4) Tubes were snap frozen in liquid nitrogen for quenching cellular metabolism
- 5) Cell suspension was thawed gradually over ice bath
- 6) Cell suspension was sonicated for 6 cycles (30 sec ON and 30 sec OFF at maximum amplitude) to extract inter-cellular metabolites from the quenched cells.

- 7) Dual phase extraction of metabolite was performed using following mixture:
 - i. 6 ml of -20⁰C chloroform + 6 ml of methanol+ 5.4 ml of cell lysate
(Total volume 17.4 ml). Volume ratio (0.9:1:1)
- 8) Lysed cell solutions were incubated for 20 minutes on ice and vortexed frequently to facilitate metabolite extraction
- 9) The cell extracts were centrifuged at 4000 g at 4⁰ C for 20 minutes
- 10) A two-phase extract was formed with upper layer containing water-soluble intracellular metabolites, a middle layer of proteins and lipids and lower layer of apolar metabolites
- 11) The upper layer was carefully collected in multiple 1.5 ml centrifuge tubes and vacuum dried

6.14.2 NMR experimentation

- 1) The vacuum dried metabolites were resuspended in D₂O (600 μl) with 3-(trimethylsilyl) propionic-2, 2, 3, 3, d₄ acid (TSP, 0.1% W/V) and loaded into 5 mm NMR tubes
- 2) ¹H-NMR spectra were acquired at 298K on an 800MHz Bruker Avance AV III spectrometer using ZGPR 1D pulse sequence for efficient water signal suppression
- 3) The spectra were recorded with spectral width of 14,367.8Hz, 256 transients, 1.5 seconds relaxation delay, 32K data points and an acquisition time of 1.14 seconds
- 4) For metabolite identification purposes, 2D NMR spectra were obtained using TOCSY and COSY software. Following manual phase and baseline correction, the 1D spectra were referenced to TSP (δ=0.0 ppm) in MestReNova version 7.1.0 (Mestrelab Research, Santiago de Compostela, Spain)

- 5) For minimizing the chemical shift variations, NMR spectra(s) were bucketed with a binning width of 0.02 ppm. After removal of the water signal regions (δ 4.5–5.10 ppm), the spectral regions of δ 0.5–4.5 and δ 5.10–9.0 were subjected to further multivariate and univariate analysis. Spectra were normalized using constant sum normalization using MetaboAnalyst 4.0 and scaled with unit variance scaling (SIMCA 13.0.2, Umetrics, Sweden)

6.14.3 Data analysis

- 1) Partial Least squares-discriminates ant analysis (PLS-DA) and Orthogonal Partial Least squares-discriminates ant analysis (OPLS-DA) were generated using SIMCA 13.0.2 (Umetrics, Sweden)
- 2) Robustness and validation of the OPLS-DA model was confirmed by R² and Q² score
- 3) S-plot and variable important for projection (VIP) plot with threshold of >0.60 and ≥ 1 respectively were used to identify significant regions discriminating the groups
- 4) The identified significant variables underwent spectral integration (MestReNova version 7.1.0, Mestrelab Research, Santiago de Compostela, Spain). These metabolite integral values were constant sum normalized and subjected to univariate analysis

6.15 BRET

6.15.1 Transfection

- 1) 6×10^5 cells were seeded in 60 mm culture dish and incubated overnight at 37°C under 5% CO₂ in a humidified incubator

2) a. For measuring NAT BRET ratio: PH-AKT-Nluc and GAP-TurboFP635 plasmids were transfected in 1:1 ratio in one plate (donor + acceptor) and only PH-AKT-Nluc was transfected in another plate (donor alone) using Superfect transfection reagent

b. For measuring NEO BRET ratio: Nluc-ERKAR_{cytoplasmic}-mOrange and Nluc-ERKAR_{nuclear}-mOrange plasmids were transfected in 1:1 ratio in one plate (donor + acceptor) and only Nluc was transfected in another plate (donor alone) using Superfect transfection reagent

3) After 5 hours of transfection, 1×10^4 cells were reseeded in each well of 96-black well plate (in triplicates) and incubated overnight at 37⁰C under 5% CO₂ in a humidified incubator

* For measurement of growth factor induced ERK1/2 and AKT activation cells were washed twice with 1X PBS and seeded in charcoal stripped media

** For measurement of platinum induced NAT and NEO ratio in cells derived from patient ascites:

4) 5×10^3 cells were seeded in each well of each well of 96-black well plate (in triplicates) and incubated overnight at 37⁰C under 5% CO₂ in a humidified incubator

5) Cells were transfected with NAT or NEO plasmids as previously performed for cancer cell lines

6.15.2 Treatment

1) For measurement of **growth factor induced NAT and NEO kinetics**: After 36 hours of transfection, cells were treated with various growth factors for 15-20 minutes as mentioned below:

Sr. No	Growth Factor	Concentration/s	Source

1	Insulin	250nM and 500Nm	Sigma, USA
2	IGF-1	100 nM and 200 nM	Sigma, USA
3	EGF	200 nM	Sigma, USA

2) For measurement of **inhibitor dissuade NAT and NEO kinetics**: Transfected cells were pre-treated with various inhibitors for 24 hours as mentioned below and then stimulated with IGF-1 (200 nM)

Sr. No	Inhibitors	Concentration/s	Source
1	Wortmanin	200 nM	Calbiochem, Germany
2	U0126	10 μ M	CST, USA
3	Picropodophyllin	2 μ M	Calbiochem, Germany

3) For measurement of **chemotherapy induced NAT and NEO kinetics**: Transfected cells were treated with various chemotherapeutic drugs for 24 hours as mentioned below

Cell line	Concentration				
	Cisplatin- paclitaxel	Doxorubicin	Gemcitabine	Irinotecan	Etoposide
A2780	50 ng/ml+8.5 ng/ml	60 nM	2.9 nM	17.9 nM	1.4 μ M
OAW42	72 ng/ml+14 ng/ml	82 nM	4 nM	14.6 nM	1.2 μ M

SKOV3	300 ng/ml+30 ng/ml	454 nM	18.9 nM	20.46 nM	9.3 μ M
A280Dual ^{ER}	250 ng/ml+42.5 ng/ml				
A280Dual ^{LR}	500 ng/ml+85 ng/ml	540 nM	27.5 nM	32.5 nM	11.53 μ M
OAW42Dual ^{LR}	720 ng/ml+ 140 ng/ml	548 nM	41.7 nM	14.9 nM	10.7 μ M

4) For measurement of platinum induced NAT and NEO ratio in cells derived from patient ascites: After 24 hours of transfection, cells were treated with respective IC₅₀ dosage of platinum for 24 hours

6.15.3 Imaging and analysis

1) Cells were imaged using furimazine substrate at 1:1000 dilution in IVIS spectrum at appropriate filters (as mentioned below) with integration time of 30-60 sec per filter. Subject height was set at 0.50cm (standard for plate imaging) and FOV (field of view) used was C, to capture the entire plate image. Binning was set as medium for all acquisition

2) For monitoring temporal kinetics of growth factor induced ERK1/2 and AKT activation: Immediately after ligand and substrate addition, acquisition was performed for 15-20 minutes at an interval of every 30 secs using same settings as mentioned above

Constructs	Donor Filter	Acceptor Filter
NAT and its only donor (PH-AKT-Nluc) constructs	500 nm	640 nm
NEO and its only donor (Nluc) constructs	500 nm	560 nm

- 3) All imaging analysis were done on IVIS living imaging software 4.5.
- 4) For calculating BRET ratio, following steps were followed:
- Acquisition file was opened in IVIS software and scan for individual time point was loaded in the software
 - For any particular time-point, an ROI of same size was drawn on all the wells in donor channel and acceptor filter
 - Average radiance (Avg. Rad) from each well was measured for both donor and acceptor filter
 - Background correction was performed by subtracting signal from wells with untransfected cells
 - BRET ratio is determined using avg. radiance values utilizing the formula
- $$\text{milliBRET unit (mBU)} = \frac{\text{Avg.Rad(Acceptor filter)} - Cf * \text{Avg.Rad (Donor filter)}}{\text{Avg.Rad (Donor filter)}} * 1000$$
- $$Cf = \frac{\text{Avg.Rad(Acceptor filter)donor only}}{\text{Avg.Rad(donor filter)donor only}}$$
- Corrected BRET ratio was represented in milliBRET unit.

6.16 In-Vivo imaging

6.16.1 Reagents and chemicals

Sr. No.	Reagent name	Source
1	D-Luciferin	Biosynth, UK
2	Isoflurane	Baxter, USA

6.16.2 Methods

6.16.2.1 Cell preparation

- 1) A2780Dual^{ER} cells stably expressing mutant thermostable firefly luciferase fused with p62 (mtFL-p62) reporter construct were grown completed media at 70-80% confluency
- 2) Cells were trypsinized and counted using haemocytometer to determine viable cell count
- 3) 5×10^6 viable cells were resuspended in 100 μ l ice cold 1X PBS

6.16.2.2 Cell implantation in mice

- 1) Animal handling and euthanasia was performed as per the guidelines of Institutional Animal Ethics Committee of ACTREC, TMC
- 2) Non-obese diabetic-severe combined immunodeficient (NOD-SCID) mice were used for all experiments
- 3) Mice were anesthetized using isoflurane to remove fur using electronic razor with utmost care to avoid injuries
- 4) The site of injection was sterilized with 70% alcohol
- 5) 5×10^6 A2780Dual^{ER} cells were injected subcutaneously using 26 gauge injection

6.16.2.3 Drug treatment in mice

- 1) Treatment regimen was started after 20 days of cell implantation as palpable tumours were observed
- 2) Animals were divided into 6 groups with 8 animals in each group and treated as mentioned below

Drug	Dosage	Days
------	--------	------

		1	2	3	4	5	6	7	8	9	10	11	12	13	14	15
Cisplatin- Paclitaxel	2mg 1mg	✓						✓						✓		
Trametinib	1mg	✓	✓	✓	✓	✓	✓	✓	✓	✓	✓	✓	✓	✓	✓	✓
Chloroquine	40 mg/kg	✓	✓	✓	✓	✓	✓	✓	✓	✓	✓	✓	✓	✓	✓	✓
Cisplatin- Paclitaxel +Trametinib	2mg/kg 1mg/kg 1mg/kg	✓						✓						✓		
Cisplatin- Paclitaxel +Chloroquine	2mg/kg 1mg/kg 40mg/kg	✓						✓						✓		
		✓	✓	✓	✓	✓	✓	✓	✓	✓	✓	✓	✓	✓	✓	✓

* ✓ denotes Cisplatin-Paclitaxel treatment ✓ denotes Trametinib treatment

✓ denotes Chloroquine treatment

6.16.2.4 Bioluminescence imaging of mice

- 1) Bioluminescence and bright field images of mice were captured every alternate day for 15 days in IVIS-Spectrum pre-clinical optical imager
- 2) 100µl of D-luciferin with stock concentration of 30mg/ml was intraperitoneally injected into mice
- 3) Animals were then euthanatized by isoflurane in air-tight chamber with steady flow of oxygen

- 4) Mice were then imaged inside IVIS-Spectrum pre-clinical optical imager under isoflurane euthanasia and bioluminescence images were acquired every 2 minutes till peak luciferase signal was acquired using sequence mode with field of view C and image height of 1.5 cm,
- 5) Bioluminescence images were analysed using LIVING IMAGE 4.4 software

6.16.2.5 Tumour volume measurement

Tumour volume was measured on every 5th day till day 25 using digital Vernier calliper and volume was calculated using the formula:

$$\text{Tumour Volume (mm}^3\text{)} = \frac{1}{2} * \text{length} * \text{breadth}^2$$

6.17 Statistics

1. All statistical analysis was performed using GraphPad prism version 8 or Microsoft excel 13 software.
2. Unpaired Student T-test was used for comparing cell line data.
3. Kurskal-wallis test was performed for metabolomics data.
4. Two way ANOVA was performed for in-vivo animal data.
5. Statistical significance was set to $p < 0.05$ where ns indicates non-significant, * indicates $p < 0.05$, ** $p < 0.005$, *** $p < 0.0005$ as calculated by respective statistical test.

References

1. Colombo PE, Fabbro M, Theillet C, Bibeau F, Rouanet P, Ray-Coquard I. Sensitivity and resistance to treatment in the primary management of epithelial ovarian cancer. *Critical reviews in oncology/hematology*. 2014;89(2):207-16.
2. Markman M, Bookman MA. Second-Line Treatment of Ovarian Cancer. *The Oncologist*. 2000;5(1):26-35.
3. Pujade-Lauraine E, Combe P. Recurrent ovarian cancer. *Annals of oncology : official journal of the European Society for Medical Oncology*. 2016;27 Suppl 1:i63-i5.
4. Pujade-Lauraine E, Banerjee S, Pignata S. Management of Platinum-Resistant, Relapsed Epithelial Ovarian Cancer and New Drug Perspectives. *Journal of clinical oncology : official journal of the American Society of Clinical Oncology*. 2019;37(27):2437-48.
5. Singh RK, Gaikwad SM, Jinager A, Chaudhury S, Maheshwari A, Ray P. IGF-1R inhibition potentiates cytotoxic effects of chemotherapeutic agents in early stages of chemoresistant ovarian cancer cells. *Cancer letters*. 2014;354(2):254-62.
6. Peng DJ, Wang J, Zhou JY, Wu GS. Role of the Akt/mTOR survival pathway in cisplatin resistance in ovarian cancer cells. *Biochemical and biophysical research communications*. 2010;394(3):600-5.
7. Abedini MR, Muller EJ, Bergeron R, Gray DA, Tsang BK. Akt promotes chemoresistance in human ovarian cancer cells by modulating cisplatin-induced, p53-dependent ubiquitination of FLICE-like inhibitory protein. *Oncogene*. 2010;29(1):11-25.
8. Koti M, Gooding RJ, Nuin P, Haslehurst A, Crane C, Weberpals J, et al. Identification of the IGF1/PI3K/NF kappaB/ERK gene signalling networks associated with chemotherapy resistance and treatment response in high-grade serous epithelial ovarian cancer. *BMC Cancer*. 2013;13:549.
9. Wang J, Wu GS. Role of autophagy in cisplatin resistance in ovarian cancer cells. *The Journal of biological chemistry*. 2014;289(24):17163-73.
10. Wu T, Wang MC, Jing L, Liu ZY, Guo H, Liu Y, et al. Autophagy facilitates lung adenocarcinoma resistance to cisplatin treatment by activation of AMPK/mTOR signaling pathway. *Drug design, development and therapy*. 2015;9:6421-31.
11. Zhang XY, Zhang M, Cong Q, Zhang MX, Zhang MY, Lu YY, et al. Hexokinase 2 confers resistance to cisplatin in ovarian cancer cells by enhancing cisplatin-induced autophagy. *The international journal of biochemistry & cell biology*. 2018;95:9-16.
12. Lin Q, Wang Y, Chen D, Sheng X, Liu J, Xiong H. Cisplatin regulates cell autophagy in endometrial cancer cells via the PI3K/AKT/mTOR signalling pathway. *Oncology letters*. 2017;13(5):3567-71.
13. Che L, Yang X, Ge C, El-Amouri SS, Wang QE, Pan D, et al. Loss of BRUCE reduces cellular energy level and induces autophagy by driving activation of the AMPK-ULK1 autophagic initiating axis. *PLoS one*. 2019;14(5):e0216553.
14. Pei G, Luo M, Ni X, Wu J, Wang S, Ma Y, et al. Autophagy Facilitates Metadherin-Induced Chemotherapy Resistance Through the AMPK/ATG5 Pathway in Gastric Cancer. *Cellular physiology and biochemistry : international journal of experimental cellular physiology, biochemistry, and pharmacology*. 2018;46(2):847-59.
15. Peng H, Wang Q, Qi X, Wang X, Zhao X. Orlistat induces apoptosis and protective autophagy in ovarian cancer cells: involvement of Akt-mTOR-mediated signaling pathway. *Archives of gynecology and obstetrics*. 2018;298(3):597-605.
16. Patingre S, Bauvy C, Codogno P. Amino acids interfere with the ERK1/2-dependent control of macroautophagy by controlling the activation of Raf-1 in human colon cancer HT-29 cells. *The Journal of biological chemistry*. 2003;278(19):16667-74.
17. Kumar S, Meuter A, Thapa P, Langstraat C, Giri S, Chien J, et al. Metformin intake is associated with better survival in ovarian cancer: a case-control study. *Cancer*. 2013;119(3):555-62.

18. Xu S, Yang Z, Jin P, Yang X, Li X, Wei X, et al. Metformin Suppresses Tumor Progression by Inactivating Stromal Fibroblasts in Ovarian Cancer. *Molecular Cancer Therapeutics*. 2018;17(6):1291-302.
19. Chan DK, Miskimins WK. Metformin and phenethyl isothiocyanate combined treatment in vitro is cytotoxic to ovarian cancer cultures. *Journal of ovarian research*. 2012;5(1):19.
20. Lengyel E, Litchfield LM, Mitra AK, Nieman KM, Mukherjee A, Zhang Y, et al. Metformin inhibits ovarian cancer growth and increases sensitivity to paclitaxel in mouse models. *American journal of obstetrics and gynecology*. 2015;212(4):479 e1- e10.
21. Rattan R, Graham RP, Maguire JL, Giri S, Shridhar V. Metformin suppresses ovarian cancer growth and metastasis with enhancement of cisplatin cytotoxicity in vivo. *Neoplasia*. 2011;13(5):483-91.
22. Dragulescu-Andrasi A, Chan CT, De A, Massoud TF, Gambhir SS. Bioluminescence resonance energy transfer (BRET) imaging of protein-protein interactions within deep tissues of living subjects. *Proceedings of the National Academy of Sciences of the United States of America*. 2011;108(29):12060-5.
23. Dimri S, Arora R, Jasani A, De A. Dynamic monitoring of STAT3 activation in live cells using a novel STAT3 Phospho-BRET sensor. *American journal of nuclear medicine and molecular imaging*. 2019;9(6):321-34.
24. Matsunaga K, Saitoh T, Tabata K, Omori H, Satoh T, Kurotori N, et al. Two Beclin 1-binding proteins, Atg14L and Rubicon, reciprocally regulate autophagy at different stages. *Nature cell biology*. 2009;11(4):385-96.
25. Sun Q, Westphal W, Wong KN, Tan I, Zhong Q. Rubicon controls endosome maturation as a Rab7 effector. *Proceedings of the National Academy of Sciences of the United States of America*. 2010;107(45):19338-43.
26. Li XW, Gao HY, Liu J. The role of taurine in improving neural stem cells proliferation and differentiation. *Nutritional neuroscience*. 2017;20(7):409-15.
27. Zhou C, Zhang X, Xu L, Wu T, Cui L, Xu D. Taurine promotes human mesenchymal stem cells to differentiate into osteoblast through the ERK pathway. *Amino acids*. 2014;46(7):1673-80.
28. Wu G, Haw R. Functional Interaction Network Construction and Analysis for Disease Discovery. *Methods in molecular biology*. 2017;1558:235-53.
29. Mizuno S, Iijima R, Ogishima S, Kikuchi M, Matsuoka Y, Ghosh S, et al. AlzPathway: a comprehensive map of signaling pathways of Alzheimer's disease. *BMC systems biology*. 2012;6:52.
30. McDermott JE, Arshad OA, Petyuk VA, Fu Y, Gritsenko MA, Clauss TR, et al. Proteogenomic Characterization of Ovarian HGSC Implicates Mitotic Kinases, Replication Stress in Observed Chromosomal Instability. *Cell reports Medicine*. 2020;1(1).
31. Reyna MA, Haan D, Paczkowska M, Verbeke LPC, Vazquez M, Kahraman A, et al. Pathway and network analysis of more than 2500 whole cancer genomes. *Nature communications*. 2020;11(1):729.
32. Mayer BJ. Protein-protein interactions in signaling cascades. *Methods in molecular biology*. 2006;332:79-99.
33. Amala A, Emerson IA. Identification of target genes in cancer diseases using protein-protein interaction networks. *Network Modeling Analysis in Health Informatics and Bioinformatics*. 2019;8(1):2.
34. Li Z, Ivanov AA, Su R, Gonzalez-Pecchi V, Qi Q, Liu S, et al. The OncoPPI network of cancer-focused protein-protein interactions to inform biological insights and therapeutic strategies. *Nature communications*. 2017;8(1):14356.
35. De A, Jasani A, Arora R, Gambhir SS. Evolution of BRET Biosensors from Live Cell to Tissue-Scale In vivo Imaging. *Frontiers in endocrinology*. 2013;4:131.
36. Peng T, Yuan X, Hang HC. Turning the spotlight on protein-lipid interactions in cells. *Current opinion in chemical biology*. 2014;21:144-53.

37. Martinez-Sernandez V, Orbegozo-Medina RA, Romaris F, Paniagua E, Ubeira FM. Usefulness of ELISA Methods for Assessing LPS Interactions with Proteins and Peptides. *PloS one*. 2016;11(6):e0156530.
38. Del Vecchio K, Stahelin RV. Using Surface Plasmon Resonance to Quantitatively Assess Lipid-Protein Interactions. *Methods in molecular biology*. 2016;1376:141-53.
39. Rao VS, Srinivas K, Sujini GN, Kumar GNS. Protein-Protein Interaction Detection: Methods and Analysis. *International Journal of Proteomics*. 2014;2014:147648.
40. Stynen B, Tournu H, Tavernier J, Van Dijck P. Diversity in Genetic *In Vivo* Methods for Protein-Protein Interaction Studies: from the Yeast Two-Hybrid System to the Mammalian Split-Luciferase System. *Microbiology and Molecular Biology Reviews*. 2012;76(2):331-82.
41. Bruckner A, Polge C, Lentze N, Auerbach D, Schlattner U. Yeast two-hybrid, a powerful tool for systems biology. *International journal of molecular sciences*. 2009;10(6):2763-88.
42. Ray P, Pimenta H, Paulmurugan R, Berger F, Phelps ME, Iyer M, et al. Noninvasive quantitative imaging of protein-protein interactions in living subjects. *Proceedings of the National Academy of Sciences of the United States of America*. 2002;99(5):3105-10.
43. Luker GD, Sharma V, Pica CM, Dahlheimer JL, Li W, Ochesky J, et al. Noninvasive imaging of protein-protein interactions in living animals. *Proceedings of the National Academy of Sciences of the United States of America*. 2002;99(10):6961-6.
44. Romei MG, Boxer SG. Split Green Fluorescent Proteins: Scope, Limitations, and Outlook. *Annual review of biophysics*. 2019;48:19-44.
45. Ghosh I, Hamilton AD, Regan L. Antiparallel Leucine Zipper-Directed Protein Reassembly: Application to the Green Fluorescent Protein. *Journal of the American Chemical Society*. 2000;122(23):5658-9.
46. Hu C-D, Chinenov Y, Kerppola TK. Visualization of Interactions among bZIP and Rel Family Proteins in Living Cells Using Bimolecular Fluorescence Complementation. *Molecular Cell*. 2002;9(4):789-98.
47. Hu CD, Kerppola TK. Simultaneous visualization of multiple protein interactions in living cells using multicolor fluorescence complementation analysis. *Nature biotechnology*. 2003;21(5):539-45.
48. Kodama Y, Hu C-D. Bimolecular fluorescence complementation (BiFC): A 5-year update and future perspectives. *BioTechniques*. 2012;53(5):285-98.
49. Paulmurugan R, Umezawa Y, Gambhir SS. Noninvasive imaging of protein-protein interactions in living subjects by using reporter protein complementation and reconstitution strategies. *Proceedings of the National Academy of Sciences of the United States of America*. 2002;99(24):15608-13.
50. Luker KE, Smith MC, Luker GD, Gammon ST, Piwnica-Worms H, Piwnica-Worms D. Kinetics of regulated protein-protein interactions revealed with firefly luciferase complementation imaging in cells and living animals. *Proceedings of the National Academy of Sciences of the United States of America*. 2004;101(33):12288-93.
51. Kaihara A, Kawai Y, Sato M, Ozawa T, Umezawa Y. Locating a protein-protein interaction in living cells via split Renilla luciferase complementation. *Analytical chemistry*. 2003;75(16):4176-81.
52. Massoud TF, Paulmurugan R, De A, Ray P, Gambhir SS. Reporter gene imaging of protein-protein interactions in living subjects. *Current opinion in biotechnology*. 2007;18(1):31-7.
53. Luker KE, Luker GD. Split Gaussia luciferase for imaging ligand-receptor binding. *Methods in molecular biology*. 2014;1098:59-69.
54. Sun Y, Rombola C, Jyothikumar V, Periasamy A. Forster resonance energy transfer microscopy and spectroscopy for localizing protein-protein interactions in living cells. *Cytometry Part A : the journal of the International Society for Analytical Cytology*. 2013;83(9):780-93.
55. Forster T. Energiewanderung und Fluoreszenz. *Naturwissenschaften*. 1946;33(6):166-75.
56. Fluorescence Resonance Energy Transfer. 2020.
57. Ciruela F, Vilardaga JP, Fernandez-Duenas V. Lighting up multiprotein complexes: lessons from GPCR oligomerization. *Trends in biotechnology*. 2010;28(8):407-15.

58. Sekar RB, Periasamy A. Fluorescence resonance energy transfer (FRET) microscopy imaging of live cell protein localizations. *The Journal of cell biology*. 2003;160(5):629-33.
59. Bajar BT, Wang ES, Zhang S, Lin MZ, Chu J. A Guide to Fluorescent Protein FRET Pairs. *Sensors*. 2016;16(9).
60. Margineanu A, Chan JJ, Kelly DJ, Warren SC, Flatters D, Kumar S, et al. Screening for protein-protein interactions using Förster resonance energy transfer (FRET) and fluorescence lifetime imaging microscopy (FLIM). *Scientific reports*. 2016;6(1):28186.
61. Wang Y, Botvinick EL, Zhao Y, Berns MW, Usami S, Tsien RY, et al. Visualizing the mechanical activation of Src. *Nature*. 2005;434(7036):1040-5.
62. Takemoto K, Nagai T, Miyawaki A, Miura M. Spatio-temporal activation of caspase revealed by indicator that is insensitive to environmental effects. *The Journal of cell biology*. 2003;160(2):235-43.
63. Miura H, Matsuda M, Aoki K. Development of a FRET biosensor with high specificity for Akt. *Cell structure and function*. 2014;39(1):9-20.
64. Erard M, Fredj A, Pasquier H, Beltolngar DB, Bousmah Y, Derrien V, et al. Minimum set of mutations needed to optimize cyan fluorescent proteins for live cell imaging. *Molecular bioSystems*. 2013;9(2):258-67.
65. Gavet O, Pines J. Progressive activation of CyclinB1-Cdk1 coordinates entry to mitosis. *Developmental cell*. 2010;18(4):533-43.
66. Harvey CD, Ehrhardt AG, Cellurale C, Zhong H, Yasuda R, Davis RJ, et al. A genetically encoded fluorescent sensor of ERK activity. *Proceedings of the National Academy of Sciences of the United States of America*. 2008;105(49):19264-9.
67. Lam AJ, St-Pierre F, Gong Y, Marshall JD, Cranfill PJ, Baird MA, et al. Improving FRET dynamic range with bright green and red fluorescent proteins. *Nature methods*. 2012;9(10):1005-12.
68. Eichorst JP, Clegg RM, Wang Y. Red-shifted fluorescent proteins monitor enzymatic activity in live HT-1080 cells with fluorescence lifetime imaging microscopy (FLIM). *Journal of microscopy*. 2012;248(1):77-89.
69. Murakoshi H, Shibata ACE, Nakahata Y, Nabekura J. A dark green fluorescent protein as an acceptor for measurement of Förster resonance energy transfer. *Scientific reports*. 2015;5:15334.
70. Hochreiter B, Garcia AP, Schmid JA. Fluorescent proteins as genetically encoded FRET biosensors in life sciences. *Sensors*. 2015;15(10):26281-314.
71. Niba ET, Nagaya H, Kanno T, Tsuchiya A, Gotoh A, Tabata C, et al. Crosstalk between PI3 kinase/PDK1/Akt/Rac1 and Ras/Raf/MEK/ERK pathways downstream PDGF receptor. *Cellular physiology and biochemistry : international journal of experimental cellular physiology, biochemistry, and pharmacology*. 2013;31(6):905-13.
72. He J, Wink S, de Bont H, Le Devedec S, Zhang Y, van de Water B. FRET biosensor-based kinase inhibitor screen for ERK and AKT activity reveals differential kinase dependencies for proliferation in TNBC cells. *Biochemical pharmacology*. 2019;169:113640.
73. Hughes WE, Larijani B, Parker PJ. Detecting protein-phospholipid interactions. Epidermal growth factor-induced activation of phospholipase D1b in situ. *The Journal of biological chemistry*. 2002;277(25):22974-9.
74. Ananthanarayanan B, Ni Q, Zhang J. Signal propagation from membrane messengers to nuclear effectors revealed by reporters of phosphoinositide dynamics and Akt activity. *Proceedings of the National Academy of Sciences of the United States of America*. 2005;102(42):15081-6.
75. Bhuckory S, Kays JC, Dennis AM. In Vivo Biosensing Using Resonance Energy Transfer. *Biosensors*. 2019;9(2).
76. Drinovec L, Kubale V, Nohr Larsen J, Vrecl M. Mathematical models for quantitative assessment of bioluminescence resonance energy transfer: application to seven transmembrane receptors oligomerization. *Frontiers in endocrinology*. 2012;3:104.
77. Dimri S, Basu S, De A. Use of BRET to Study Protein-Protein Interactions In Vitro and In Vivo. *Methods in molecular biology*. 2016;1443:57-78.

78. Boute N, Pernet K, Issad T. Monitoring the activation state of the insulin receptor using bioluminescence resonance energy transfer. *Molecular pharmacology*. 2001;60(4):640-5.
79. Jensen AA, Hansen JL, Sheikh SP, Bräuner-Osborne H. Probing intermolecular protein–protein interactions in the calcium-sensing receptor homodimer using bioluminescence resonance energy transfer (BRET). *European Journal of Biochemistry*. 2002;269(20):5076-87.
80. Shigeto H, Ikeda T, Kuroda A, Funabashi H. A BRET-based homogeneous insulin assay using interacting domains in the primary binding site of the insulin receptor. *Analytical chemistry*. 2015;87(5):2764-70.
81. Dale NC, Johnstone EKM, White CW, Pflieger KDG. NanoBRET: The Bright Future of Proximity-Based Assays. *Front Bioeng Biotechnol*. 2019;7:56.
82. Goyet E, Bouquier N, Ollendorff V, Perroy J. Fast and high resolution single-cell BRET imaging. *Scientific reports*. 2016;6(1):28231.
83. den Hamer A, Dierickx P, Arts R, de Vries JSPM, Brunsveld L, Merckx M. Bright Bioluminescent BRET Sensor Proteins for Measuring Intracellular Caspase Activity. *ACS sensors*. 2017;2(6):729-34.
84. Oishi A, Dam J, Jockers R. β -Arrestin-2 BRET Biosensors Detect Different β -Arrestin-2 Conformations in Interaction with GPCRs. *ACS sensors*. 2020;5(1):57-64.
85. Machleidt T, Woodroffe CC, Schwinn MK, Méndez J, Robers MB, Zimmerman K, et al. NanoBRET—A Novel BRET Platform for the Analysis of Protein–Protein Interactions. *ACS chemical biology*. 2015;10(8):1797-804.
86. Soave M, Stoddart LA, Brown A, Woolard J, Hill SJ. Use of a new proximity assay (NanoBRET) to investigate the ligand-binding characteristics of three fluorescent ligands to the human beta1-adrenoceptor expressed in HEK-293 cells. *Pharmacology research & perspectives*. 2016;4(5):e00250.
87. Blanquart C, Boute N, Lacasa D, Issad T. Monitoring the activation state of the insulin-like growth factor-1 receptor and its interaction with protein tyrosine phosphatase 1B using bioluminescence resonance energy transfer. *Molecular pharmacology*. 2005;68(3):885-94.
88. Kuo MS, Auriou J, Pierre-Eugene C, Issad T. Development of a human breast-cancer derived cell line stably expressing a bioluminescence resonance energy transfer (BRET)-based phosphatidylinositol-3 phosphate (PIP3) biosensor. *PLoS one*. 2014;9(3):e92737.
89. Xu C, Peter M, Bouquier N, Ollendorff V, Villamil I, Liu J, et al. REV, A BRET-Based Sensor of ERK Activity. *Frontiers in endocrinology*. 2013;4:95.
90. Hall MP, Unch J, Binkowski BF, Valley MP, Butler BL, Wood MG, et al. Engineered luciferase reporter from a deep sea shrimp utilizing a novel imidazopyrazinone substrate. *ACS chemical biology*. 2012;7(11):1848-57.
91. Mo XL, Luo Y, Ivanov AA, Su R, Havel JJ, Li Z, et al. Enabling systematic interrogation of protein-protein interactions in live cells with a versatile ultra-high-throughput biosensor platform. *Journal of molecular cell biology*. 2016;8(3):271-81.
92. Dale NC, Johnstone EKM, White CW, Pflieger KDG. NanoBRET: The Bright Future of Proximity-Based Assays. *Frontiers in Bioengineering and Biotechnology*. 2019;7(56).
93. Stoddart LA, Kilpatrick LE, Hill SJ. NanoBRET Approaches to Study Ligand Binding to GPCRs and RTKs. *Trends Pharmacol Sci*. 2018;39(2):136-47.
94. Robers MB, Dart ML, Woodroffe CC, Zimprich CA, Kirkland TA, Machleidt T, et al. Target engagement and drug residence time can be observed in living cells with BRET. *Nature communications*. 2015;6:10091.
95. Wan Q, Okashah N, Inoue A, Nehme R, Carpenter B, Tate CG, et al. Mini G protein probes for active G protein-coupled receptors (GPCRs) in live cells. *The Journal of biological chemistry*. 2018;293(19):7466-73.
96. den Hamer A, Dierickx P, Arts R, de Vries J, Brunsveld L, Merckx M. Bright Bioluminescent BRET Sensor Proteins for Measuring Intracellular Caspase Activity. *ACS sensors*. 2017;2(6):729-34.
97. Hanahan D, Weinberg RA. The hallmarks of cancer. *Cell*. 2000;100(1):57-70.
98. Sever R, Brugge JS. Signal transduction in cancer. *Cold Spring Harbor perspectives in medicine*. 2015;5(4).

99. Samadani AA, Norollahi SE, Rashidy-Pour A, Mansour-Ghanaei F, Nemati S, Joukar F, et al. Cancer signaling pathways with a therapeutic approach: An overview in epigenetic regulations of cancer stem cells. *Biomedicine & Pharmacotherapy*. 2018;108:590-9.
100. Sanchez-Vega F, Mina M, Armenia J, Chatila WK, Luna A, La KC, et al. Oncogenic Signaling Pathways in The Cancer Genome Atlas. *Cell*. 2018;173(2):321-37 e10.
101. Baudino TA. Targeted Cancer Therapy: The Next Generation of Cancer Treatment. *Current drug discovery technologies*. 2015;12(1):3-20.
102. Giamas G, Stebbing J, Vorgias CE, Knippschild U. Protein kinases as targets for cancer treatment. *Pharmacogenomics*. 2007;8(8):1005-16.
103. Bukowski K, Kciuk M, Kontek R. Mechanisms of Multidrug Resistance in Cancer Chemotherapy. *International journal of molecular sciences*. 2020;21(9).
104. Mansoori B, Mohammadi A, Davudian S, Shirjang S, Baradaran B. The Different Mechanisms of Cancer Drug Resistance: A Brief Review. *Advanced pharmaceutical bulletin*. 2017;7(3):339-48.
105. Kampen KR. Membrane proteins: the key players of a cancer cell. *The Journal of membrane biology*. 2011;242(2):69-74.
106. Lin CY, Lee CH, Chuang YH, Lee JY, Chiu YY, Wu Lee YH, et al. Membrane protein-regulated networks across human cancers. *Nature communications*. 2019;10(1):3131.
107. Lazennec G, Richmond A. Chemokines and chemokine receptors: new insights into cancer-related inflammation. *Trends in molecular medicine*. 2010;16(3):133-44.
108. Aoudjit F, Vuori K. Integrin signaling in cancer cell survival and chemoresistance. *Chemotherapy research and practice*. 2012;2012:283181.
109. Du Z, Lovly CM. Mechanisms of receptor tyrosine kinase activation in cancer. *Molecular cancer*. 2018;17(1):58.
110. Gottesman MM. Mechanisms of cancer drug resistance. *Annual review of medicine*. 2002;53:615-27.
111. Luqmani YA. Mechanisms of drug resistance in cancer chemotherapy. *Medical principles and practice : international journal of the Kuwait University, Health Science Centre*. 2005;14 Suppl 1:35-48.
112. Zheng HC. The molecular mechanisms of chemoresistance in cancers. *Oncotarget*. 2017;8(35):59950-64.
113. Tung SL, Huang WC, Hsu FC, Yang ZP, Jang TH, Chang JW, et al. miRNA-34c-5p inhibits amphiregulin-induced ovarian cancer stemness and drug resistance via downregulation of the AREG-EGFR-ERK pathway. *Oncogenesis*. 2017;6(5):e326.
114. Taylor-Harding B, Aspuria PJ, Agadjanian H, Cheon DJ, Mizuno T, Greenberg D, et al. Cyclin E1 and RTK/RAS signaling drive CDK inhibitor resistance via activation of E2F and ETS. *Oncotarget*. 2015;6(2):696-714.
115. Simpkins F, Jang K, Yoon H, Hew KE, Kim M, Azzam DJ, et al. Dual Src and MEK Inhibition Decreases Ovarian Cancer Growth and Targets Tumor Initiating Stem-Like Cells. *Clinical cancer research : an official journal of the American Association for Cancer Research*. 2018;24(19):4874-86.
116. Lee C. Overexpression of Tyro3 receptor tyrosine kinase leads to the acquisition of taxol resistance in ovarian cancer cells. *Molecular medicine reports*. 2015;12(1):1485-92.
117. Dhadve AC, Hari K, Rekhi B, Jolly MK, De A, Ray P. Decoding molecular interplay between RUNX1 and FOXO3a underlying the pulsatile IGF1R expression during acquirement of chemoresistance. *Biochimica et Biophysica Acta (BBA) - Molecular Basis of Disease*. 2020;1866(6):165754.
118. Deo A, Chaudhury S, Kannan S, Rekhi B, Maheshwari A, Gupta S, et al. IGF1R predicts better survival in high-grade serous epithelial ovarian cancer patients and correlates with hCtr1 levels. *Biomarkers in medicine*. 2019;13(7):511-21.
119. Busca R, Pouyssegur J, Lenormand P. ERK1 and ERK2 Map Kinases: Specific Roles or Functional Redundancy? *Frontiers in cell and developmental biology*. 2016;4:53.

120. Dhillon AS, Hagan S, Rath O, Kolch W. MAP kinase signalling pathways in cancer. *Oncogene*. 2007;26(22):3279-90.
121. Pritchard AL, Hayward NK. Molecular Pathways: Mitogen-Activated Protein Kinase Pathway Mutations and Drug Resistance. *Clinical Cancer Research*. 2013;19(9):2301-9.
122. Yoon S, Seger R. The extracellular signal-regulated kinase: multiple substrates regulate diverse cellular functions. *Growth factors*. 2006;24(1):21-44.
123. Yang L, Zheng L, Chng WJ, Ding JL. Comprehensive Analysis of ERK1/2 Substrates for Potential Combination Immunotherapies. *Trends in Pharmacological Sciences*. 2019;40(11):897-910.
124. Fernandez-Medarde A, Santos E. Ras in cancer and developmental diseases. *Genes & cancer*. 2011;2(3):344-58.
125. Hobbs GA, Der CJ, Rossman KL. RAS isoforms and mutations in cancer at a glance. *Journal of cell science*. 2016;129(7):1287-92.
126. Pakneshan S, Salajegheh A, Smith RA, Lam AK. Clinicopathological relevance of BRAF mutations in human cancer. *Pathology*. 2013;45(4):346-56.
127. Jiang X, Jiang X, Yang Z. NRAGE confers poor prognosis and promotes proliferation, invasion, and chemoresistance in gastric cancer. *Gene*. 2018;668:114-20.
128. Li S, Tian J, Zhang H, Zhou S, Wang X, Zhang L, et al. Down-regulating IL-6/GP130 targets improved the anti-tumor effects of 5-fluorouracil in colon cancer. *Apoptosis : an international journal on programmed cell death*. 2018;23(5-6):356-74.
129. Dai G, Deng S, Guo W, Yu L, Yang J, Zhou S, et al. Notch pathway inhibition using DAPT, a gamma-secretase inhibitor (GSI), enhances the antitumor effect of cisplatin in resistant osteosarcoma. *Molecular carcinogenesis*. 2019;58(1):3-18.
130. Meloche S, Pouyssegur J. The ERK1/2 mitogen-activated protein kinase pathway as a master regulator of the G1- to S-phase transition. *Oncogene*. 2007;26(22):3227-39.
131. Xu M, Chen S, Yang W, Cheng X, Ye Y, Mao J, et al. FGFR4 Links Glucose Metabolism and Chemotherapy Resistance in Breast Cancer. *Cellular physiology and biochemistry : international journal of experimental cellular physiology, biochemistry, and pharmacology*. 2018;47(1):151-60.
132. Chai X, Chu H, Yang X, Meng Y, Shi P, Gou S. Metformin Increases Sensitivity of Pancreatic Cancer Cells to Gemcitabine by Reducing CD133+ Cell Populations and Suppressing ERK/P70S6K Signaling. *Sci Rep*. 2015;5:14404.
133. Senthebane DA, Jonker T, Rowe A, Thomford NE, Munro D, Dandara C, et al. The Role of Tumor Microenvironment in Chemoresistance: 3D Extracellular Matrices as Accomplices. *International journal of molecular sciences*. 2018;19(10).
134. Lesniak D, Xu Y, Deschenes J, Lai R, Thoms J, Murray D, et al. Beta1-integrin circumvents the antiproliferative effects of trastuzumab in human epidermal growth factor receptor-2-positive breast cancer. *Cancer research*. 2009;69(22):8620-8.
135. Zhou Y, Zhu Y, Fan X, Zhang C, Wang Y, Zhang L, et al. NID1, a new regulator of EMT required for metastasis and chemoresistance of ovarian cancer cells. *Oncotarget*. 2017;8(20):33110-21.
136. Yang L, Zheng L, Chng WJ, Ding JL. Comprehensive Analysis of ERK1/2 Substrates for Potential Combination Immunotherapies. *Trends Pharmacol Sci*. 2019;40(11):897-910.
137. Moore AR, Rosenberg SC, McCormick F, Malek S. RAS-targeted therapies: is the undruggable drugged? *Nature reviews Drug discovery*. 2020;19(8):533-52.
138. Grimaldi AM, Simeone E, Festino L, Vanella V, Strudel M, Ascierto PA. MEK Inhibitors in the Treatment of Metastatic Melanoma and Solid Tumors. *American journal of clinical dermatology*. 2017;18(6):745-54.
139. Chang F, Lee JT, Navolanic PM, Steelman LS, Shelton JG, Blalock WL, et al. Involvement of PI3K/Akt pathway in cell cycle progression, apoptosis, and neoplastic transformation: a target for cancer chemotherapy. *Leukemia*. 2003;17(3):590-603.
140. Gonzalez E, McGraw TE. The Akt kinases: isoform specificity in metabolism and cancer. *Cell cycle*. 2009;8(16):2502-8.

141. Kim D, Dan HC, Park S, Yang L, Liu Q, Kaneko S, et al. AKT/PKB signaling mechanisms in cancer and chemoresistance. *Frontiers in bioscience : a journal and virtual library*. 2005;10:975-87.
142. Robbins HL, Hague A. The PI3K/Akt Pathway in Tumors of Endocrine Tissues. *Frontiers in endocrinology*. 2015;6:188.
143. Shah KN, Mehta KR, Peterson D, Evangelista M, Livesey JC, Faridi JS. AKT-Induced Tamoxifen Resistance Is Overturned by RRM2 Inhibition. *Molecular Cancer Research*. 2014;12(3):394-407.
144. Ali AY, Kim JY, Pelletier JF, Vanderhyden BC, Bachvarov DR, Tsang BK. Akt confers cisplatin chemoresistance in human gynecological carcinoma cells by modulating PPM1D stability. *Molecular carcinogenesis*. 2015;54(11):1301-14.
145. Heavey S, O'Byrne KJ, Gately K. Strategies for co-targeting the PI3K/AKT/mTOR pathway in NSCLC. *Cancer treatment reviews*. 2014;40(3):445-56.
146. Garcia-Regalado A, Vargas M, Garcia-Carranca A, Arechaga-Ocampo E, Gonzalez-De la Rosa CH. Activation of Akt pathway by transcription-independent mechanisms of retinoic acid promotes survival and invasion in lung cancer cells. *Molecular cancer*. 2013;12:44.
147. Yoon C, Lu J, Yi BC, Chang KK, Simon MC, Ryeom S, et al. PI3K/Akt pathway and Nanog maintain cancer stem cells in sarcomas. *Oncogenesis*. 2021;10(1):12.
148. Bahmad HF, Mouhieddine TH, Chalhoub RM, Assi S, Araji T, Chamaa F, et al. The Akt/mTOR pathway in cancer stem/progenitor cells is a potential therapeutic target for glioblastoma and neuroblastoma. *Oncotarget*. 2018;9(71):33549-61.
149. Singh RK, Dhadve A, Sakpal A, De A, Ray P. An active IGF-1R-AKT signaling imparts functional heterogeneity in ovarian CSC population. *Scientific reports*. 2016;6(1):36612.
150. Gort EH, Groot AJ, Derks van de Ven TLP, van der Groep P, Verlaan I, van Laar T, et al. Hypoxia-inducible factor-1 α expression requires PI 3-kinase activity and correlates with Akt1 phosphorylation in invasive breast carcinomas. *Oncogene*. 2006;25(45):6123-7.
151. Ogawara Y, Kishishita S, Obata T, Isazawa Y, Suzuki T, Tanaka K, et al. Akt Enhances Mdm2-mediated Ubiquitination and Degradation of p53*. *Journal of Biological Chemistry*. 2002;277(24):21843-50.
152. Li Y, Dowbenko D, Lasky LA. AKT/PKB phosphorylation of p21Cip/WAF1 enhances protein stability of p21Cip/WAF1 and promotes cell survival. *The Journal of biological chemistry*. 2002;277(13):11352-61.
153. Yu X, Li R, Shi W, Jiang T, Wang Y, Li C, et al. Silencing of MicroRNA-21 confers the sensitivity to tamoxifen and fulvestrant by enhancing autophagic cell death through inhibition of the PI3K-AKT-mTOR pathway in breast cancer cells. *Biomedicine & pharmacotherapy = Biomedecine & pharmacotherapie*. 2016;77:37-44.
154. Richardson PG, Nagler A, Ben-Yehuda D, Badros A, Hari PN, Hajek R, et al. Randomized, placebo-controlled, phase 3 study of perifosine combined with bortezomib and dexamethasone in patients with relapsed, refractory multiple myeloma previously treated with bortezomib. *eJHaem*. 2020;1(1):94-102.
155. Gdowski A, Panchoo M, Treuren TV, Basu A. Emerging therapeutics for targeting Akt in cancer. *Frontiers in bioscience*. 2016;21:757-68.
156. Andre F, Ciruelos E, Rubovszky G, Campone M, Loibl S, Rugo HS, et al. Alpelisib for PIK3CA-Mutated, Hormone Receptor-Positive Advanced Breast Cancer. *The New England journal of medicine*. 2019;380(20):1929-40.
157. Glick D, Barth S, Macleod KF. Autophagy: cellular and molecular mechanisms. *The Journal of pathology*. 2010;221(1):3-12.
158. Takamura A, Komatsu M, Hara T, Sakamoto A, Kishi C, Waguri S, et al. Autophagy-deficient mice develop multiple liver tumors. *Genes & development*. 2011;25(8):795-800.
159. Salminen A, Kaarniranta K, Kauppinen A. Beclin 1 interactome controls the crosstalk between apoptosis, autophagy and inflammasome activation: impact on the aging process. *Ageing research reviews*. 2013;12(2):520-34.

160. Guo JY, Chen HY, Mathew R, Fan J, Strohecker AM, Karsli-Uzunbas G, et al. Activated Ras requires autophagy to maintain oxidative metabolism and tumorigenesis. *Genes & development*. 2011;25(5):460-70.
161. Huo Y, Cai H, Teplova I, Bowman-Colin C, Chen G, Price S, et al. Autophagy opposes p53-mediated tumor barrier to facilitate tumorigenesis in a model of PALB2-associated hereditary breast cancer. *Cancer discovery*. 2013;3(8):894-907.
162. Singh SS, Vats S, Chia AY, Tan TZ, Deng S, Ong MS, et al. Dual role of autophagy in hallmarks of cancer. *Oncogene*. 2018;37(9):1142-58.
163. Sui X, Chen R, Wang Z, Huang Z, Kong N, Zhang M, et al. Autophagy and chemotherapy resistance: a promising therapeutic target for cancer treatment. *Cell death & disease*. 2013;4:e838.
164. Sun WL, Chen J, Wang YP, Zheng H. Autophagy protects breast cancer cells from epirubicin-induced apoptosis and facilitates epirubicin-resistance development. *Autophagy*. 2011;7(9):1035-44.
165. Li J, Hou N, Faried A, Tsutsumi S, Kuwano H. Inhibition of autophagy augments 5-fluorouracil chemotherapy in human colon cancer in vitro and in vivo model. *European journal of cancer*. 2010;46(10):1900-9.
166. Paillas S, Causse A, Marzi L, de Medina P, Poirot M, Denis V, et al. MAPK14/p38alpha confers irinotecan resistance to TP53-defective cells by inducing survival autophagy. *Autophagy*. 2012;8(7):1098-112.
167. de la Cruz-Morcillo MA, Valero ML, Callejas-Valera JL, Arias-Gonzalez L, Melgar-Rojas P, Galan-Moya EM, et al. P38MAPK is a major determinant of the balance between apoptosis and autophagy triggered by 5-fluorouracil: implication in resistance. *Oncogene*. 2012;31(9):1073-85.
168. Hu YL, DeLay M, Jahangiri A, Molinaro AM, Rose SD, Carbonell WS, et al. Hypoxia-induced autophagy promotes tumor cell survival and adaptation to antiangiogenic treatment in glioblastoma. *Cancer research*. 2012;72(7):1773-83.
169. Shi YH, Ding ZB, Zhou J, Hui B, Shi GM, Ke AW, et al. Targeting autophagy enhances sorafenib lethality for hepatocellular carcinoma via ER stress-related apoptosis. *Autophagy*. 2011;7(10):1159-72.
170. Lagneaux L, Delforge A, Carlier S, Massy M, Bernier M, Bron D. Early induction of apoptosis in B-chronic lymphocytic leukaemia cells by hydroxychloroquine: activation of caspase-3 and no protection by survival factors. *British journal of haematology*. 2001;112(2):344-52.
171. Rosich L, Xargay-Torrent S, Lopez-Guerra M, Campo E, Colomer D, Roue G. Counteracting autophagy overcomes resistance to everolimus in mantle cell lymphoma. *Clinical cancer research : an official journal of the American Association for Cancer Research*. 2012;18(19):5278-89.
172. Moscat J, Diaz-Meco MT. p62 at the crossroads of autophagy, apoptosis, and cancer. *Cell*. 2009;137(6):1001-4.
173. Moscat J, Karin M, Diaz-Meco MT. p62 in Cancer: Signaling Adaptor Beyond Autophagy. *Cell*. 2016;167(3):606-9.
174. Lee YJ, Won AJ, Lee J, Jung JH, Yoon S, Lee BM, et al. Molecular mechanism of SAHA on regulation of autophagic cell death in tamoxifen-resistant MCF-7 breast cancer cells. *International journal of medical sciences*. 2012;9(10):881-93.
175. Hu T, Wang L, Zhang L, Lu L, Shen J, Chan RL, et al. Sensitivity of apoptosis-resistant colon cancer cells to tanshinones is mediated by autophagic cell death and p53-independent cytotoxicity. *Phytomedicine : international journal of phytotherapy and phytopharmacology*. 2015;22(5):536-44.
176. Shen P, Chen M, He M, Chen L, Song Y, Xiao P, et al. Inhibition of ERalpha/ERK/P62 cascades induces "autophagic switch" in the estrogen receptor-positive breast cancer cells exposed to gemcitabine. *Oncotarget*. 2016;7(30):48501-16.
177. Li J-r, Cheng C-L, Yang C-R, Ou Y-C, Wu M-J, Ko J-L. Dual inhibitor of phosphoinositide 3-kinase/mammalian target of rapamycin NVP-BE2235 effectively inhibits cisplatin-resistant urothelial cancer cell growth through autophagic flux. *Toxicology Letters*. 2013;220(3):267-76.
178. Manic G, Obrist F, Kroemer G, Vitale I, Galluzzi L. Chloroquine and hydroxychloroquine for cancer therapy. *Molecular & cellular oncology*. 2014;1(1):e29911.

179. Wolpin BM, Rubinson DA, Wang X, Chan JA, Cleary JM, Enzinger PC, et al. Phase II and pharmacodynamic study of autophagy inhibition using hydroxychloroquine in patients with metastatic pancreatic adenocarcinoma. *The oncologist*. 2014;19(6):637-8.
180. Vogl DT, Stadtmauer EA, Tan KS, Heitjan DF, Davis LE, Pontiggia L, et al. Combined autophagy and proteasome inhibition: a phase 1 trial of hydroxychloroquine and bortezomib in patients with relapsed/refractory myeloma. *Autophagy*. 2014;10(8):1380-90.
181. Rosenfeld MR, Ye X, Supko JG, Desideri S, Grossman SA, Brem S, et al. A phase I/II trial of hydroxychloroquine in conjunction with radiation therapy and concurrent and adjuvant temozolomide in patients with newly diagnosed glioblastoma multiforme. *Autophagy*. 2014;10(8):1359-68.
182. Kuma A, Komatsu M, Mizushima N. Autophagy-monitoring and autophagy-deficient mice. *Autophagy*. 2017;13(10):1619-28.
183. Zhang L, Yu J, Pan H, Hu P, Hao Y, Cai W, et al. Small molecule regulators of autophagy identified by an image-based high-throughput screen. *Proceedings of the National Academy of Sciences of the United States of America*. 2007;104(48):19023-8.
184. Balgi AD, Fonseca BD, Donohue E, Tsang TC, Lajoie P, Proud CG, et al. Screen for chemical modulators of autophagy reveals novel therapeutic inhibitors of mTORC1 signaling. *PloS one*. 2009;4(9):e7124.
185. Mizushima N, Yamamoto A, Matsui M, Yoshimori T, Ohsumi Y. In vivo analysis of autophagy in response to nutrient starvation using transgenic mice expressing a fluorescent autophagosome marker. *Molecular biology of the cell*. 2004;15(3):1101-11.
186. Kimura S, Noda T, Yoshimori T. Dissection of the autophagosome maturation process by a novel reporter protein, tandem fluorescent-tagged LC3. *Autophagy*. 2007;3(5):452-60.
187. Chauhan S, Ahmed Z, Bradfute SB, Arko-Mensah J, Mandell MA, Won Choi S, et al. Pharmaceutical screen identifies novel target processes for activation of autophagy with a broad translational potential. *Nat Commun*. 2015;6:8620.
188. Pampaloni F, Mayer B, Kabat Vel-Job K, Ansari N, Hotte K, Kogel D, et al. A Novel Cellular Spheroid-Based Autophagy Screen Applying Live Fluorescence Microscopy Identifies Nonactin as a Strong Inducer of Autophagosomal Turnover. *SLAS discovery : advancing life sciences R & D*. 2017;22(5):558-70.
189. Li L, Wang ZV, Hill JA, Lin F. New autophagy reporter mice reveal dynamics of proximal tubular autophagy. *Journal of the American Society of Nephrology : JASN*. 2014;25(2):305-15.
190. Hariharan N, Zhai P, Sadoshima J. Oxidative stress stimulates autophagic flux during ischemia/reperfusion. *Antioxidants & redox signaling*. 2011;14(11):2179-90.
191. Kaizuka T, Morishita H, Hama Y, Tsukamoto S, Matsui T, Toyota Y, et al. An Autophagic Flux Probe that Releases an Internal Control. *Molecular cell*. 2016;64(4):835-49.
192. Farkas T, Hoyer-Hansen M, Jaattela M. Identification of novel autophagy regulators by a luciferase-based assay for the kinetics of autophagic flux. *Autophagy*. 2009;5(7):1018-25.
193. Min Z, Ting Y, Mingtao G, Xiaofei T, Dong Y, Chenguang Z, et al. Monitoring autophagic flux using p62/SQSTM1 based luciferase reporters in glioma cells. *Experimental cell research*. 2018;363(1):84-94.
194. Ju JS, Miller SE, Jackson E, Cadwell K, Piwnicka-Worms D, Weihl CC. Quantitation of selective autophagic protein aggregate degradation in vitro and in vivo using luciferase reporters. *Autophagy*. 2009;5(4):511-9.
195. Iwata A, Nagashima Y, Matsumoto L, Suzuki T, Yamanaka T, Date H, et al. Intranuclear degradation of polyglutamine aggregates by the ubiquitin-proteasome system. *The Journal of biological chemistry*. 2009;284(15):9796-803.
196. Al-Hajj M, Wicha MS, Benito-Hernandez A, Morrison SJ, Clarke MF. Prospective identification of tumorigenic breast cancer cells. *Proceedings of the National Academy of Sciences of the United States of America*. 2003;100(7):3983-8.

197. Visvader JE, Lindeman GJ. Cancer stem cells in solid tumours: accumulating evidence and unresolved questions. *Nature reviews Cancer*. 2008;8(10):755-68.
198. Alison MR, Lim SM, Nicholson LJ. Cancer stem cells: problems for therapy? *The Journal of pathology*. 2011;223(2):147-61.
199. Dean M, Fojo T, Bates S. Tumour stem cells and drug resistance. *Nature reviews Cancer*. 2005;5(4):275-84.
200. Islam F, Gopalan V, Wahab R, Smith RA, Lam AK. Cancer stem cells in oesophageal squamous cell carcinoma: Identification, prognostic and treatment perspectives. *Critical reviews in oncology/hematology*. 2015;96(1):9-19.
201. Bonnet D, Dick JE. Human acute myeloid leukemia is organized as a hierarchy that originates from a primitive hematopoietic cell. *Nature medicine*. 1997;3(7):730-7.
202. Zhao J. Cancer stem cells and chemoresistance: The smartest survives the raid. *Pharmacology & therapeutics*. 2016;160:145-58.
203. Shlush LI, Zandi S, Mitchell A, Chen WC, Brandwein JM, Gupta V, et al. Identification of pre-leukaemic haematopoietic stem cells in acute leukaemia. *Nature*. 2014;506(7488):328-33.
204. Auffinger B, Tobias AL, Han Y, Lee G, Guo D, Dey M, et al. Conversion of differentiated cancer cells into cancer stem-like cells in a glioblastoma model after primary chemotherapy. *Cell death and differentiation*. 2014;21(7):1119-31.
205. Hamerlik P, Lathia JD, Rasmussen R, Wu Q, Bartkova J, Lee M, et al. Autocrine VEGF-VEGFR2-Neuropilin-1 signaling promotes glioma stem-like cell viability and tumor growth. *The Journal of experimental medicine*. 2012;209(3):507-20.
206. Kurtova AV, Xiao J, Mo Q, Pazhanisamy S, Krasnow R, Lerner SP, et al. Blocking PGE2-induced tumour repopulation abrogates bladder cancer chemoresistance. *Nature*. 2015;517(7533):209-13.
207. Shervington A, Lu C. Expression of multidrug resistance genes in normal and cancer stem cells. *Cancer investigation*. 2008;26(5):535-42.
208. Golebiewska A, Brons NH, Bjerkvig R, Niclou SP. Critical appraisal of the side population assay in stem cell and cancer stem cell research. *Cell stem cell*. 2011;8(2):136-47.
209. Raha D, Wilson TR, Peng J, Peterson D, Yue P, Evangelista M, et al. The Cancer Stem Cell Marker Aldehyde Dehydrogenase Is Required to Maintain a Drug-Tolerant Tumor Cell Subpopulation. *Cancer research*. 2014;74(13):3579-90.
210. Schafer A, Teufel J, Ringel F, Bettstetter M, Hoepner I, Rasper M, et al. Aldehyde dehydrogenase 1A1--a new mediator of resistance to temozolomide in glioblastoma. *Neuro-oncology*. 2012;14(12):1452-64.
211. Koelling TM, Yeager AM, Hilton J, Haynie DT, Wiley JM. Development and characterization of a cyclophosphamide-resistant subline of acute myeloid leukemia in the Lewis x Brown Norway hybrid rat. *Blood*. 1990;76(6):1209-13.
212. Tanei T, Morimoto K, Shimazu K, Kim SJ, Tanji Y, Taguchi T, et al. Association of breast cancer stem cells identified by aldehyde dehydrogenase 1 expression with resistance to sequential Paclitaxel and epirubicin-based chemotherapy for breast cancers. *Clinical cancer research : an official journal of the American Association for Cancer Research*. 2009;15(12):4234-41.
213. Kosuri KV, Wu X, Wang L, Villalona-Calero MA, Otterson GA. An epigenetic mechanism for capecitabine resistance in mesothelioma. *Biochemical and biophysical research communications*. 2010;391(3):1465-70.
214. Zhang M, Behbod F, Atkinson RL, Landis MD, Kittrell F, Edwards D, et al. Identification of tumor-initiating cells in a p53-null mouse model of breast cancer. *Cancer research*. 2008;68(12):4674-82.
215. Venkatesha VA, Parsels LA, Parsels JD, Zhao L, Zabludoff SD, Simeone DM, et al. Sensitization of pancreatic cancer stem cells to gemcitabine by Chk1 inhibition. *Neoplasia*. 2012;14(6):519-25.
216. Yin H, Glass J. The phenotypic radiation resistance of CD44+/CD24(-or low) breast cancer cells is mediated through the enhanced activation of ATM signaling. *PLoS one*. 2011;6(9):e24080.

217. Sciuscio D, Diserens A-C, van Dommelen K, Martinet D, Jones G, Janzer R-C, et al. Extent and Patterns of MGM Promoter Methylation in Glioblastoma- and Respective Glioblastoma-Derived Spheres. *Clinical Cancer Research*. 2011;17(2):255-66.
218. Pattabiraman DR, Weinberg RA. Tackling the cancer stem cells - what challenges do they pose? *Nature reviews Drug discovery*. 2014;13(7):497-512.
219. Sekulic A, Migden MR, Oro AE, Dirix L, Lewis KD, Hainsworth JD, et al. Efficacy and safety of vismodegib in advanced basal-cell carcinoma. *The New England journal of medicine*. 2012;366(23):2171-9.
220. Gottesman MM, Fojo T, Bates SE. Multidrug resistance in cancer: role of ATP-dependent transporters. *Nature reviews Cancer*. 2002;2(1):48-58.
221. Wang J, Seebacher N, Shi H, Kan Q, Duan Z. Novel strategies to prevent the development of multidrug resistance (MDR) in cancer. *Oncotarget*. 2017;8(48):84559-71.
222. Trock BJ, Leonessa F, Clarke R. Multidrug Resistance in Breast Cancer: a Meta-analysis of MDR1/gp170 Expression and Its Possible Functional Significance. *JNCI: Journal of the National Cancer Institute*. 1997;89(13):917-31.
223. Wind NS, Holen I. Multidrug Resistance in Breast Cancer: From *In Vitro* Models to Clinical Studies. *International Journal of Breast Cancer*. 2011;2011:967419.
224. Januchowski R, Sterzyńska K, Zaorska K, Sosińska P, Klejewski A, Brązert M, et al. Analysis of MDR genes expression and cross-resistance in eight drug resistant ovarian cancer cell lines. *Journal of Ovarian Research*. 2016;9(1):65.
225. Paridaens R, Biganzoli L, Bruning P, Klijn JG, Gamucci T, Houston S, et al. Paclitaxel versus doxorubicin as first-line single-agent chemotherapy for metastatic breast cancer: a European Organization for Research and Treatment of Cancer Randomized Study with cross-over. *Journal of clinical oncology : official journal of the American Society of Clinical Oncology*. 2000;18(4):724-33.
226. Guo B, Villeneuve DJ, Hembruff SL, Kirwan AF, Blais DE, Bonin M, et al. Cross-resistance studies of isogenic drug-resistant breast tumor cell lines support recent clinical evidence suggesting that sensitivity to paclitaxel may be strongly compromised by prior doxorubicin exposure. *Breast cancer research and treatment*. 2004;85(1):31-51.
227. Aldonza MBD, Ku J, Hong J-Y, Kim D, Yu SJ, Lee M-S, et al. Prior acquired resistance to paclitaxel relays diverse EGFR-targeted therapy persistence mechanisms. *Science Advances*. 2020;6(6):eaav7416.
228. Liu R, Chen Y, Liu G, Li C, Song Y, Cao Z, et al. PI3K/AKT pathway as a key link modulates the multidrug resistance of cancers. *Cell death & disease*. 2020;11(9):797.
229. Abrams SL, Steelman LS, Shelton JG, Wong EW, Chappell WH, Basecke J, et al. The Raf/MEK/ERK pathway can govern drug resistance, apoptosis and sensitivity to targeted therapy. *Cell cycle*. 2010;9(9):1781-91.
230. Davoudi Z, Akbarzadeh A, Rahmatiyamchi M, Movassaghpour AA, Alipour M, Nejati-Koshki K, et al. Molecular target therapy of AKT and NF- κ B signaling pathways and multidrug resistance by specific cell penetrating inhibitor peptides in HL-60 cells. *Asian Pacific journal of cancer prevention : APJCP*. 2014;15(10):4353-8.
231. Oh S, Kim H, Nam K, Shin I. Silencing of Glut1 induces chemoresistance via modulation of Akt/GSK-3 β /beta-catenin/survivin signaling pathway in breast cancer cells. *Archives of biochemistry and biophysics*. 2017;636:110-22.
232. Koh GS, Jiang N, Kham SKY, Chew FT, Yeoh AEJ. Abstract 822: Drug resistance towards vincristine in acute lymphoblastic leukemia is mediated by the PI3K-Akt pathway. *Cancer research*. 2012;72(8 Supplement):822-.
233. Salaroglio IC, Mungo E, Gazzano E, Kopecka J, Riganti C. ERK is a Pivotal Player of Chemo-Immune-Resistance in Cancer. *International journal of molecular sciences*. 2019;20(10).
234. Davis JM, Navolanic PM, Weinstein-Opppenheimer CR, Steelman LS, Hu W, Konopleva M, et al. Raf-1 and Bcl-2 induce distinct and common pathways that contribute to breast cancer drug

resistance. *Clinical cancer research : an official journal of the American Association for Cancer Research*. 2003;9(3):1161-70.

235. Yan F, Wang XM, Pan C, Ma QM. Down-regulation of extracellular signal-regulated kinase 1/2 activity in P-glycoprotein-mediated multidrug resistant hepatocellular carcinoma cells. *World journal of gastroenterology*. 2009;15(12):1443-51.

236. Xiao Z, Ding N, Xiao G, Wang S, Wu Y, Tang L. Reversal of Multidrug Resistance by Gefitinib Via RAF1/ERK Pathway in Pancreatic Cancer Cell Line. *The Anatomical Record*. 2012;295(12):2122-8.

237. Pritchard JR, Lauffenburger DA, Hemann MT. Understanding resistance to combination chemotherapy. *Drug resistance updates : reviews and commentaries in antimicrobial and anticancer chemotherapy*. 2012;15(5-6):249-57.

238. Ferlay J, Colombet M, Soerjomataram I, Mathers C, Parkin DM, Pineros M, et al. Estimating the global cancer incidence and mortality in 2018: GLOBOCAN sources and methods. *International journal of cancer*. 2019;144(8):1941-53.

239. Bray F, Ferlay J, Soerjomataram I, Siegel RL, Torre LA, Jemal A. Global cancer statistics 2018: GLOBOCAN estimates of incidence and mortality worldwide for 36 cancers in 185 countries. *CA: a cancer journal for clinicians*. 2018;68(6):394-424.

240. Karst AM, Drapkin R. Ovarian Cancer Pathogenesis: A Model in Evolution. *Journal of Oncology*. 2010;2010:932371.

241. Torre LA, Trabert B, DeSantis CE, Miller KD, Samimi G, Runowicz CD, et al. Ovarian cancer statistics, 2018. *CA: a cancer journal for clinicians*. 2018;68(4):284-96.

242. Chen VW, Ruiz B, Killeen JL, Coté TR, Wu XC, Correa CN, et al. Pathology and classification of ovarian tumors. *Cancer*. 2003;97(S10):2631-42.

243. Kurman RJ, Shih Ie M. The origin and pathogenesis of epithelial ovarian cancer: a proposed unifying theory. *The American journal of surgical pathology*. 2010;34(3):433-43.

244. Vang R, Shih Ie M, Kurman RJ. Ovarian low-grade and high-grade serous carcinoma: pathogenesis, clinicopathologic and molecular biologic features, and diagnostic problems. *Advances in anatomic pathology*. 2009;16(5):267-82.

245. Orr B, Edwards RP. Diagnosis and Treatment of Ovarian Cancer. *Hematology/oncology clinics of North America*. 2018;32(6):943-64.

246. Hoskins WJ. Surgical staging and cytoreductive surgery of epithelial ovarian cancer. *Cancer*. 1993;71(4 Suppl):1534-40.

247. Bristow RE, Tomacruz RS, Armstrong DK, Trimble EL, Montz FJ. Survival effect of maximal cytoreductive surgery for advanced ovarian carcinoma during the platinum era: a meta-analysis. *Journal of clinical oncology : official journal of the American Society of Clinical Oncology*. 2002;20(5):1248-59.

248. Riggs MJ, Pandalai PK, Kim J, Dietrich CS. Hyperthermic Intraperitoneal Chemotherapy in Ovarian Cancer. *Diagnostics*. 2020;10(1).

249. Tomao F, Marchetti C, Romito A, Di Pinto A, Di Donato V, Capri O, et al. Overcoming platinum resistance in ovarian cancer treatment: from clinical practice to emerging chemical therapies. *Expert opinion on pharmacotherapy*. 2017;18(14):1443-55.

250. Ledermann JA. PARP inhibitors in ovarian cancer. *Annals of oncology : official journal of the European Society for Medical Oncology*. 2016;27 Suppl 1:i40-i4.

251. du Bois A, Floquet A, Kim JW, Rau J, del Campo JM, Friedlander M, et al. Incorporation of pazopanib in maintenance therapy of ovarian cancer. *Journal of clinical oncology : official journal of the American Society of Clinical Oncology*. 2014;32(30):3374-82.

252. Ricciardelli C, Ween MP, Lokman NA, Tan IA, Pyragius CE, Oehler MK. Chemotherapy-induced hyaluronan production: a novel chemoresistance mechanism in ovarian cancer. *BMC Cancer*. 2013;13(1):476.

253. Chen Y, Bieber MM, Teng NN. Hedgehog signaling regulates drug sensitivity by targeting ABC transporters ABCB1 and ABCG2 in epithelial ovarian cancer. *Molecular carcinogenesis*. 2014;53(8):625-34.

254. Ediriweera MK, Tennekoon KH, Samarakoon SR. Role of the PI3K/AKT/mTOR signaling pathway in ovarian cancer: Biological and therapeutic significance. *Seminars in cancer biology*. 2019;59:147-60.
255. Yoshida H, Teramae M, Yamauchi M, Fukuda T, Yasui T, Sumi T, et al. Association of copper transporter expression with platinum resistance in epithelial ovarian cancer. *Anticancer research*. 2013;33(4):1409-14.
256. Williams J, Lucas PC, Griffith KA, Choi M, Fogoros S, Hu YY, et al. Expression of Bcl-xL in ovarian carcinoma is associated with chemoresistance and recurrent disease. *Gynecologic oncology*. 2005;96(2):287-95.
257. Goncharenko-Khaider N, Matte I, Lane D, Rancourt C, Piche A. Ovarian cancer ascites increase Mcl-1 expression in tumor cells through ERK1/2-Elk-1 signaling to attenuate TRAIL-induced apoptosis. *Molecular cancer*. 2012;11:84.
258. Zhang Y, Huang F, Luo Q, Wu X, Liu Z, Chen H, et al. Inhibition of XIAP increases carboplatin sensitivity in ovarian cancer. *OncoTargets and therapy*. 2018;11:8751-9.
259. Tang N, Lyu D, Zhang Y, Liu H. Association between the ERCC1 polymorphism and platinum-based chemotherapy effectiveness in ovarian cancer: a meta-analysis. *BMC women's health*. 2017;17(1):43.
260. Thakur B, Ray P. Cisplatin triggers cancer stem cell enrichment in platinum-resistant cells through NF- κ B-TNF α -PIK3CA loop. *Journal of Experimental & Clinical Cancer Research*. 2017;36(1):164.
261. Westfall SD, Skinner MK. Inhibition of phosphatidylinositol 3-kinase sensitizes ovarian cancer cells to carboplatin and allows adjunct chemotherapy treatment. *Molecular Cancer Therapeutics*. 2005;4(11):1764-71.
262. Mansouri A, Ridgway LD, Korapati AL, Zhang Q, Tian L, Wang Y, et al. Sustained activation of JNK/p38 MAPK pathways in response to cisplatin leads to Fas ligand induction and cell death in ovarian carcinoma cells. *The Journal of biological chemistry*. 2003;278(21):19245-56.
263. Cancer Genome Atlas Research N. Integrated genomic analyses of ovarian carcinoma. *Nature*. 2011;474(7353):609-15.
264. Wu YH, Huang YF, Chen CC, Chou CY. Akt inhibitor SC66 promotes cell sensitivity to cisplatin in chemoresistant ovarian cancer cells through inhibition of COL11A1 expression. *Cell death & disease*. 2019;10(4):322.
265. Wu Y-H, Huang Y-F, Chen C-C, Huang C-Y, Chou C-Y. Comparing PI3K/Akt Inhibitors Used in Ovarian Cancer Treatment. *Frontiers in Pharmacology*. 2020;11(206).
266. Liu W, Wang Q, Li F, Zhang S, Cao L. [Correlations between the p-Akt-mTOR-p70S6K pathway and clinicopathological features or chemoresistance of ovarian cancer]. *Zhong nan da xue xue bao Yi xue ban = Journal of Central South University Medical sciences*. 2017;42(8):882-8.
267. Xu W, Yang Z, Lu N. A new role for the PI3K/Akt signaling pathway in the epithelial-mesenchymal transition. *Cell adhesion & migration*. 2015;9(4):317-24.
268. Chesnokov M, Khan I, Park Y, Ezel J, Mehta G, Yousif A, et al. The MEK1/2 pathway as a therapeutic target in high-grade serous ovarian carcinoma. *bioRxiv*. 2019:772061.
269. Hew KE, Miller PC, El-Ashry D, Sun J, Besser AH, Ince TA, et al. MAPK Activation Predicts Poor Outcome and the MEK Inhibitor, Selumetinib, Reverses Antiestrogen Resistance in ER-Positive High-Grade Serous Ovarian Cancer. *Clinical cancer research : an official journal of the American Association for Cancer Research*. 2016;22(4):935-47.
270. Iavarone C, Zervantonakis IK, Selfors LM, Palakurthi S, Liu JF, Drapkin R, et al. Combined MEK and BCL-2/X_L Inhibition Is Effective in High-Grade Serous Ovarian Cancer Patient-Derived Xenograft Models and BIM Levels Are Predictive of Responsiveness. *Molecular Cancer Therapeutics*. 2019;18(3):642-55.
271. Liu S, Zha J, Lei M. Inhibiting ERK/Mnk/eIF4E broadly sensitizes ovarian cancer response to chemotherapy. *Clinical & translational oncology : official publication of the Federation of Spanish Oncology Societies and of the National Cancer Institute of Mexico*. 2018;20(3):374-81.

272. Liu L, Wang X, Li X, Wu X, Tang M, Wang X. Upregulation of IGF1 by tumor-associated macrophages promotes the proliferation and migration of epithelial ovarian cancer cells. *Oncology reports*. 2018;39(2):818-26.
273. Liu Y, Tang J, Liu D, Zhang L, He Y, Li J, et al. Increased autophagy in EOC re-ascites cells can inhibit cell death and promote drug resistance. *Cell death & disease*. 2018;9(4):419.
274. Li X, Zhou Y, Li Y, Yang L, Ma Y, Peng X, et al. Autophagy: A novel mechanism of chemoresistance in cancers. *Biomedicine & Pharmacotherapy*. 2019;119:109415.
275. Xiao L, Shi XY, Zhang Y, Zhu Y, Zhu L, Tian W, et al. YAP induces cisplatin resistance through activation of autophagy in human ovarian carcinoma cells. *OncoTargets and therapy*. 2016;9:1105-14.
276. Zhang SF, Wang XY, Fu ZQ, Peng QH, Zhang JY, Ye F, et al. TXNDC17 promotes paclitaxel resistance via inducing autophagy in ovarian cancer. *Autophagy*. 2015;11(2):225-38.
277. He J, Yu JJ, Xu Q, Wang L, Zheng JZ, Liu LZ, et al. Downregulation of ATG14 by EGR1-MIR152 sensitizes ovarian cancer cells to cisplatin-induced apoptosis by inhibiting cyto-protective autophagy. *Autophagy*. 2015;11(2):373-84.
278. Xia M, Yu H, Gu S, Xu Y, Su J, Li H, et al. p62/SQSTM1 is involved in cisplatin resistance in human ovarian cancer cells via the Keap1-Nrf2-ARE system. *International journal of oncology*. 2014;45(6):2341-8.
279. Yu H, Su J, Xu Y, Kang J, Li H, Zhang L, et al. p62/SQSTM1 involved in cisplatin resistance in human ovarian cancer cells by clearing ubiquitinated proteins. *European journal of cancer*. 2011;47(10):1585-94.
280. Zhou F, Li YH, Wang JJ, Pan J, Lu H. Endoplasmic reticulum stress could induce autophagy and apoptosis and enhance chemotherapy sensitivity in human esophageal cancer EC9706 cells by mediating PI3K/Akt/mTOR signaling pathway. *Tumour biology : the journal of the International Society for Oncodevelopmental Biology and Medicine*. 2017;39(6):1010428317705748.
281. Pei L, Kong Y, Shao C, Yue X, Wang Z, Zhang N. Heme oxygenase-1 induction mediates chemoresistance of breast cancer cells to pharmorubicin by promoting autophagy via PI3K/Akt pathway. *Journal of cellular and molecular medicine*. 2018;22(11):5311-21.
282. Qi HY, Qu XJ, Liu J, Hou KZ, Fan YB, Che XF, et al. Bufalin induces protective autophagy by Cbl-b regulating mTOR and ERK signaling pathways in gastric cancer cells. *Cell biology international*. 2019;43(1):33-43.
283. Pyo JO, Nah J, Jung YK. Molecules and their functions in autophagy. *Experimental & molecular medicine*. 2012;44(2):73-80.
284. Levine B, Klionsky DJ. Development by self-digestion: molecular mechanisms and biological functions of autophagy. *Developmental cell*. 2004;6(4):463-77.
285. Mizushima N, Yoshimori T, Levine B. Methods in mammalian autophagy research. *Cell*. 2010;140(3):313-26.
286. Kabeya Y, Mizushima N, Ueno T, Yamamoto A, Kirisako T, Noda T, et al. LC3, a mammalian homologue of yeast Apg8p, is localized in autophagosome membranes after processing. *The EMBO journal*. 2000;19(21):5720-8.
287. Gaikwad SM, Gunjal L, Junutula AR, Astanehe A, Gambhir SS, Ray P. Non-invasive imaging of phosphoinositide-3-kinase-catalytic-subunit-alpha (PIK3CA) promoter modulation in small animal models. *PloS one*. 2013;8(2):e55971.
288. Ray P, Wu AM, Gambhir SS. Optical Bioluminescence and Positron Emission Tomography Imaging of a Novel Fusion Reporter Gene in Tumor Xenografts of Living Mice. *Cancer Research*. 2003;63(6):1160-5.
289. Heras-Sandoval D, Perez-Rojas JM, Hernandez-Damian J, Pedraza-Chaverri J. The role of PI3K/AKT/mTOR pathway in the modulation of autophagy and the clearance of protein aggregates in neurodegeneration. *Cellular signalling*. 2014;26(12):2694-701.
290. Levine B, Kroemer G. Autophagy in the pathogenesis of disease. *Cell*. 2008;132(1):27-42.

291. Liang C, Lee JS, Inn KS, Gack MU, Li Q, Roberts EA, et al. Beclin1-binding UVRAG targets the class C Vps complex to coordinate autophagosome maturation and endocytic trafficking. *Nature cell biology*. 2008;10(7):776-87.
292. Wirth M, Joachim J, Tooze SA. Autophagosome formation--the role of ULK1 and Beclin1-PI3KC3 complexes in setting the stage. *Seminars in cancer biology*. 2013;23(5):301-9.
293. Larsen KB, Lamark T, Overvatn A, Harneshaug I, Johansen T, Bjorkoy G. A reporter cell system to monitor autophagy based on p62/SQSTM1. *Autophagy*. 2010;6(6):784-93.
294. Chandra A, Pius C, Nabeel M, Nair M, Vishwanatha JK, Ahmad S, et al. Ovarian cancer: Current status and strategies for improving therapeutic outcomes. *Cancer medicine*. 2019;8(16):7018-31.
295. McDermott JE, Arshad OA, Petyuk VA, Fu Y, Gritsenko MA, Clauss TR, et al. Proteogenomic Characterization of Ovarian HGSC Implicates Mitotic Kinases, Replication Stress in Observed Chromosomal Instability. *Cell Reports Medicine*. 2020;1(1):100004.
296. O'Donovan TR, O'Sullivan GC, McKenna SL. Induction of autophagy by drug-resistant esophageal cancer cells promotes their survival and recovery following treatment with chemotherapeutics. *Autophagy*. 2011;7(5):509-24.
297. Han W, Pan H, Chen Y, Sun J, Wang Y, Li J, et al. EGFR tyrosine kinase inhibitors activate autophagy as a cytoprotective response in human lung cancer cells. *PLoS one*. 2011;6(6):e18691.
298. Wang RC, Wei Y, An Z, Zou Z, Xiao G, Bhagat G, et al. Akt-mediated regulation of autophagy and tumorigenesis through Beclin 1 phosphorylation. *Science*. 2012;338(6109):956-9.
299. Butler DE, Marlein C, Walker HF, Frame FM, Mann VM, Simms MS, et al. Inhibition of the PI3K/AKT/mTOR pathway activates autophagy and compensatory Ras/Raf/MEK/ERK signalling in prostate cancer. *Oncotarget*. 2017;8(34).
300. Klionsky DJ, Abdelmohsen K, Abe A, Abedin MJ, Abeliovich H, Acevedo Arozena A, et al. Guidelines for the use and interpretation of assays for monitoring autophagy (3rd edition). *Autophagy*. 2016;12(1):1-222.
301. Chauhan S, Goodwin JG, Chauhan S, Manyam G, Wang J, Kamat AM, et al. ZKSCAN3 is a master transcriptional repressor of autophagy. *Molecular cell*. 2013;50(1):16-28.
302. Lin JF, Lin YC, Tsai TF, Chen HE, Chou KY, Hwang TI. Cisplatin induces protective autophagy through activation of BECN1 in human bladder cancer cells. *Drug design, development and therapy*. 2017;11:1517-33.
303. Zhang Y, Xu M, Xia M, Li X, Boini KM, Wang M, et al. Defective autophagosome trafficking contributes to impaired autophagic flux in coronary arterial myocytes lacking CD38 gene. *Cardiovascular research*. 2014;102(1):68-78.
304. Yin H, Yang X, Gu W, Liu Y, Li X, Huang X, et al. HMGB1-mediated autophagy attenuates gemcitabine-induced apoptosis in bladder cancer cells involving JNK and ERK activation. *Oncotarget*. 2017;8(42):71642-56.
305. Tong Y, Huang H, Pan H. Inhibition of MEK/ERK activation attenuates autophagy and potentiates pemetrexed-induced activity against HepG2 hepatocellular carcinoma cells. *Biochemical and biophysical research communications*. 2015;456(1):86-91.
306. Yu L, Gu C, Zhong D, Shi L, Kong Y, Zhou Z, et al. Induction of autophagy counteracts the anticancer effect of cisplatin in human esophageal cancer cells with acquired drug resistance. *Cancer letters*. 2014;355(1):34-45.
307. Corcelle E, Nebout M, Bekri S, Gauthier N, Hofman P, Poujeol P, et al. Disruption of Autophagy at the Maturation Step by the Carcinogen Lindane Is Associated with the Sustained Mitogen-Activated Protein Kinase/Extracellular Signal-Regulated Kinase Activity. *Cancer Research*. 2006;66(13):6861-70.
308. Ghosh K, De S, Mukherjee S, Das S, Ghosh AN, Sengupta SB. Withaferin A induced impaired autophagy and unfolded protein response in human breast cancer cell-lines MCF-7 and MDA-MB-231. *Toxicology in vitro : an international journal published in association with BIBRA*. 2017;44:330-8.
309. Lin Z, Zhang Z, Jiang X, Kou X, Bao Y, Liu H, et al. Mevastatin blockade of autolysosome maturation stimulates LBH589-induced cell death in triple-negative breast cancer cells. *Oncotarget*. 2017;8(11):17833-48.

310. Ranieri R, Ciaglia E, Amodio G, Picardi P, Proto MC, Gazzero P, et al. N6-isopentenyladenosine dual targeting of AMPK and Rab7 prenylation inhibits melanoma growth through the impairment of autophagic flux. *Cell death and differentiation*. 2018;25(2):353-67.
311. Zhou F, Yang X, Zhao H, Liu Y, Feng Y, An R, et al. Down-regulation of OGT promotes cisplatin resistance by inducing autophagy in ovarian cancer. *Theranostics*. 2018;8(19):5200-12.
312. Xiang XY, Yang XC, Su J, Kang JS, Wu Y, Xue YN, et al. Inhibition of autophagic flux by ROS promotes apoptosis during DTT-induced ER/oxidative stress in HeLa cells. *Oncology reports*. 2016;35(6):3471-9.
313. Munafó DB, Colombo MI. A novel assay to study autophagy: regulation of autophagosome vacuole size by amino acid deprivation. *Journal of Cell Science*. 2001;114(20):3619-29.
314. Song Z, An L, Ye Y, Wu J, Zou Y, He L, et al. Essential role for UVRAG in autophagy and maintenance of cardiac function. *Cardiovascular research*. 2013;101(1):48-56.
315. Kim YM, Jung CH, Seo M, Kim EK, Park JM, Bae SS, et al. mTORC1 phosphorylates UVRAG to negatively regulate autophagosome and endosome maturation. *Molecular cell*. 2015;57(2):207-18.
316. Jäger S, Bucci C, Tanida I, Ueno T, Kominami E, Saftig P, et al. Role for Rab7 in maturation of late autophagic vacuoles. *Journal of Cell Science*. 2004;117(20):4837-48.
317. Gutierrez MG, Munafó DB, Berón W, Colombo MI. Rab7 is required for the normal progression of the autophagic pathway in mammalian cells. *Journal of Cell Science*. 2004;117(13):2687-97.
318. Wright CJM, McCormack PL. Trametinib: First Global Approval. *Drugs*. 2013;73(11):1245-54.
319. Ascierto PA, McArthur GA, Dreno B, Atkinson V, Liskay G, Di Giacomo AM, et al. Cobimetinib combined with vemurafenib in advanced BRAF(V600)-mutant melanoma (coBRIM): updated efficacy results from a randomised, double-blind, phase 3 trial. *The Lancet Oncology*. 2016;17(9):1248-60.
320. Duan G, Tang Q, Yan H, Xie L, Wang Y, Zheng XE, et al. A Strategy to Delay the Development of Cisplatin Resistance by Maintaining a Certain Amount of Cisplatin-Sensitive Cells. *Scientific reports*. 2017;7(1):432.
321. Caffrey PB, Zhu M, Zhang Y, Chinen N, Frenkel GD. Rapid development of glutathione-S-transferase-dependent drug resistance in vitro and its prevention by ethacrynic acid. *Cancer letters*. 1999;136(1):47-52.
322. Caffrey PB, Zhu M, Frenkel GD. Prevention of the development of melphalan resistance in vitro by selenite. *Biological trace element research*. 1998;65(3):187-95.
323. Yang X, Shen J, Gao Y, Feng Y, Guan Y, Zhang Z, et al. Nsc23925 prevents the development of paclitaxel resistance by inhibiting the introduction of P-glycoprotein and enhancing apoptosis. *International journal of cancer*. 2015;137(8):2029-39.
324. Gasch C, Ffrench B, O'Leary JJ, Gallagher MF. Catching moving targets: cancer stem cell hierarchies, therapy-resistance & considerations for clinical intervention. *Molecular cancer*. 2017;16(1):43.
325. Shibue T, Weinberg RA. EMT, CSCs, and drug resistance: the mechanistic link and clinical implications. *Nature reviews Clinical oncology*. 2017;14(10):611-29.
326. Liao J, Qian F, Tchabo N, Mhawech-Fauceglia P, Beck A, Qian Z, et al. Ovarian cancer spheroid cells with stem cell-like properties contribute to tumor generation, metastasis and chemotherapy resistance through hypoxia-resistant metabolism. *PloS one*. 2014;9(1):e84941.
327. Varum S, Rodrigues AS, Moura MB, Momcilovic O, Easley CA, Ramalho-Santos J, et al. Energy metabolism in human pluripotent stem cells and their differentiated counterparts. *PloS one*. 2011;6(6):e20914.
328. Lu Q, Zhang Y, Elisseeff JH. Carnitine and acetylcarnitine modulate mesenchymal differentiation of adult stem cells. *Journal of tissue engineering and regenerative medicine*. 2015;9(12):1352-62.
329. Shiraki N, Shiraki Y, Tsuyama T, Obata F, Miura M, Nagae G, et al. Methionine metabolism regulates maintenance and differentiation of human pluripotent stem cells. *Cell metabolism*. 2014;19(5):780-94.

330. Hirsch HA, Iliopoulos D, Tsiachlis PN, Struhl K. Metformin selectively targets cancer stem cells, and acts together with chemotherapy to block tumor growth and prolong remission. *Cancer research*. 2009;69(19):7507-11.
331. Shafiee MN, Khan G, Ariffin R, Abu J, Chapman C, Deen S, et al. Preventing endometrial cancer risk in polycystic ovarian syndrome (PCOS) women: could metformin help? *Gynecologic oncology*. 2014;132(1):248-53.
332. Shackelford DB, Abt E, Gerken L, Vasquez DS, Seki A, Leblanc M, et al. LKB1 inactivation dictates therapeutic response of non-small cell lung cancer to the metabolism drug phenformin. *Cancer cell*. 2013;23(2):143-58.
333. Patil S. Metformin treatment decreases the expression of cancer stem cell marker CD44 and stemness related gene expression in primary oral cancer cells. *Archives of oral biology*. 2020;113:104710.
334. Kim JH, Lee KJ, Seo Y, Kwon J-H, Yoon JP, Kang JY, et al. Effects of metformin on colorectal cancer stem cells depend on alterations in glutamine metabolism. *Scientific reports*. 2018;8(1):409.
335. Kim TH, Suh DH, Kim M-K, Song YS. Metformin against Cancer Stem Cells through the Modulation of Energy Metabolism: Special Considerations on Ovarian Cancer. *BioMed Research International*. 2014;2014:132702.
336. Evans JM, Donnelly LA, Emslie-Smith AM, Alessi DR, Morris AD. Metformin and reduced risk of cancer in diabetic patients. *Bmj*. 2005;330(7503):1304-5.
337. Birsoy K, Possemato R, Lorbeer FK, Bayraktar EC, Thiru P, Yucel B, et al. Metabolic determinants of cancer cell sensitivity to glucose limitation and biguanides. *Nature*. 2014;508(7494):108-12.
338. Fendt SM, Bell EL, Keibler MA, Olenchock BA, Mayers JR, Wasylenko TM, et al. Reductive glutamine metabolism is a function of the alpha-ketoglutarate to citrate ratio in cells. *Nature communications*. 2013;4:2236.
339. Hodeib M, Ogrodzinski MP, Vergnes L, Reue K, Karlan BY, Lunt SY, et al. Metformin induces distinct bioenergetic and metabolic profiles in sensitive versus resistant high grade serous ovarian cancer and normal fallopian tube secretory epithelial cells. *Oncotarget*. 2018;9(3):4044-60.
340. Abubaker K, Latifi A, Luwor R, Nazaretian S, Zhu H, Quinn MA, et al. Short-term single treatment of chemotherapy results in the enrichment of ovarian cancer stem cell-like cells leading to an increased tumor burden. *Molecular cancer*. 2013;12:24.
341. Ahmed N, Abubaker K, Findlay J, Quinn M. Cancerous ovarian stem cells: obscure targets for therapy but relevant to chemoresistance. *Journal of cellular biochemistry*. 2013;114(1):21-34.
342. Chen C, Liu Y, Liu R, Ikenoue T, Guan KL, Liu Y, et al. TSC-mTOR maintains quiescence and function of hematopoietic stem cells by repressing mitochondrial biogenesis and reactive oxygen species. *The Journal of experimental medicine*. 2008;205(10):2397-408.
343. Kobayashi CI, Suda T. Regulation of reactive oxygen species in stem cells and cancer stem cells. *Journal of cellular physiology*. 2012;227(2):421-30.
344. Xu S, Yang Z, Jin P, Yang X, Li X, Wei X, et al. Metformin Suppresses Tumor Progression by Inactivating Stromal Fibroblasts in Ovarian Cancer. *Molecular cancer therapeutics*. 2018;17(6):1291-302.
345. Zordoky BN, Bark D, Soltys CL, Sung MM, Dyck JR. The anti-proliferative effect of metformin in triple-negative MDA-MB-231 breast cancer cells is highly dependent on glucose concentration: implications for cancer therapy and prevention. *Biochimica et biophysica acta*. 2014;1840(6):1943-57.
346. Iliopoulos D, Hirsch HA, Struhl K. Metformin Decreases the Dose of Chemotherapy for Prolonging Tumor Remission in Mouse Xenografts Involving Multiple Cancer Cell Types. *Cancer research*. 2011;71(9):3196-201.
347. Dos Santos Guimaraes I, Ladislau-Magescky T, Tessarollo NG, Dos Santos DZ, Gimba ERP, Sternberg C, et al. Chemosensitizing effects of metformin on cisplatin- and paclitaxel-resistant ovarian cancer cell lines. *Pharmacological reports : PR*. 2018;70(3):409-17.

348. Yamamoto T, Ebisuya M, Ashida F, Okamoto K, Yonehara S, Nishida E. Continuous ERK activation downregulates antiproliferative genes throughout G1 phase to allow cell-cycle progression. *Current biology : CB*. 2006;16(12):1171-82.
349. Touil Y, Zuliani T, Wolowczuk I, Kuranda K, Prochazkova J, Andrieux J, et al. The PI3K/AKT signaling pathway controls the quiescence of the low-Rhodamine123-retention cell compartment enriched for melanoma stem cell activity. *Stem Cells*. 2013;31(4):641-51.
350. Huai L, Wang C, Zhang C, Li Q, Chen Y, Jia Y, et al. Metformin induces differentiation in acute promyelocytic leukemia by activating the MEK/ERK signaling pathway. *Biochemical and biophysical research communications*. 2012;422(3):398-404.
351. Shank JJ, Yang K, Ghannam J, Cabrera L, Johnston CJ, Reynolds RK, et al. Metformin targets ovarian cancer stem cells in vitro and in vivo. *Gynecologic oncology*. 2012;127(2):390-7.
352. Agathocleous M, Harris WA. Metabolism in physiological cell proliferation and differentiation. *Trends in cell biology*. 2013;23(10):484-92.
353. Owen MR, Doran E, Halestrap AP. Evidence that metformin exerts its anti-diabetic effects through inhibition of complex 1 of the mitochondrial respiratory chain. *The Biochemical journal*. 2000;348 Pt 3:607-14.
354. Janzer A, German NJ, Gonzalez-Herrera KN, Asara JM, Haigis MC, Struhl K. Metformin and phenformin deplete tricarboxylic acid cycle and glycolytic intermediates during cell transformation and NTPs in cancer stem cells. *Proceedings of the National Academy of Sciences of the United States of America*. 2014;111(29):10574-9.
355. Griss T, Vincent EE, Egnatchik R, Chen J, Ma EH, Faubert B, et al. Metformin Antagonizes Cancer Cell Proliferation by Suppressing Mitochondrial-Dependent Biosynthesis. *PLoS biology*. 2015;13(12):e1002309.
356. Liu X, Romero IL, Litchfield LM, Lengyel E, Locasale JW. Metformin Targets Central Carbon Metabolism and Reveals Mitochondrial Requirements in Human Cancers. *Cell metabolism*. 2016;24(5):728-39.
357. Bouckenooghe T, Remacle C, Reusens B. Is taurine a functional nutrient? Current opinion in clinical nutrition and metabolic care. 2006;9(6):728-33.
358. Lambert IH, Kristensen DM, Holm JB, Mortensen OH. Physiological role of taurine – from organism to organelle. *Acta Physiologica*. 2015;213(1):191-212.
359. Zhang X, Tu S, Wang Y, Xu B, Wan F. Mechanism of taurine-induced apoptosis in human colon cancer cells. *Acta biochimica et biophysica Sinica*. 2014;46(4):261-72.
360. Tu S, Zhang XL, Wan HF, Xia YQ, Liu ZQ, Yang XH, et al. Effect of taurine on cell proliferation and apoptosis human lung cancer A549 cells. *Oncology letters*. 2018;15(4):5473-80.
361. Bishnu A, Sakpal A, Ghosh N, Choudhury P, Chaudhury K, Ray P. Long term treatment of metformin impedes development of chemoresistance by regulating cancer stem cell differentiation through taurine generation in ovarian cancer cells. *The international journal of biochemistry & cell biology*. 2019;107:116-27.
362. Bishnu A, Phadte P, Dhadve A, Sakpal A, Rekhi B, Ray P. Molecular imaging of the kinetics of hyperactivated ERK1/2-mediated autophagy during acquirement of chemoresistance. *Cell death & disease*. 2021;12(2):161.
363. Davis A, Tinker AV, Friedlander M. "Platinum resistant" ovarian cancer: what is it, who to treat and how to measure benefit? *Gynecologic oncology*. 2014;133(3):624-31.
364. Burger RA, Sill MW, Monk BJ, Greer BE, Sorosky JI. Phase II trial of bevacizumab in persistent or recurrent epithelial ovarian cancer or primary peritoneal cancer: a Gynecologic Oncology Group Study. *Journal of clinical oncology : official journal of the American Society of Clinical Oncology*. 2007;25(33):5165-71.
365. Pujade-Lauraine E, Hilpert F, Weber B, Reuss A, Poveda A, Kristensen G, et al. AURELIA: A randomized phase III trial evaluating bevacizumab (BEV) plus chemotherapy (CT) for platinum (PT)-resistant recurrent ovarian cancer (OC). *Journal of Clinical Oncology*. 2012;30(18_suppl):LBA5002-LBA.

366. Kucukoner M, Isikdogan A, Yaman S, Gumusay O, Unal O, Ulas A, et al. Oral etoposide for platinum-resistant and recurrent epithelial ovarian cancer: a study by the Anatolian Society of Medical Oncology. *Asian Pacific journal of cancer prevention : APJCP*. 2012;13(8):3973-6.
367. Gordon AN, Fleagle JT, Guthrie D, Parkin DE, Gore ME, Lacave AJ. Recurrent epithelial ovarian carcinoma: a randomized phase III study of pegylated liposomal doxorubicin versus topotecan. *Journal of clinical oncology : official journal of the American Society of Clinical Oncology*. 2001;19(14):3312-22.
368. Unger FT, Witte I, David KA. Prediction of individual response to anticancer therapy: historical and future perspectives. *Cellular and molecular life sciences : CMLS*. 2015;72(4):729-57.
369. Andreotti PE, Cree IA, Kurbacher CM, Hartmann DM, Linder D, Harel G, et al. Chemosensitivity testing of human tumors using a microplate adenosine triphosphate luminescence assay: clinical correlation for cisplatin resistance of ovarian carcinoma. *Cancer research*. 1995;55(22):5276-82.
370. Konecny G, Crohns C, Pegram M, Felber M, Lude S, Kurbacher C, et al. Correlation of drug response with the ATP tumorchemosensitivity assay in primary FIGO stage III ovarian cancer. *Gynecologic oncology*. 2000;77(2):258-63.
371. Angers S, Salahpour A, Joly E, Hilaiet S, Chelsky D, Dennis M, et al. Detection of beta 2-adrenergic receptor dimerization in living cells using bioluminescence resonance energy transfer (BRET). *Proceedings of the National Academy of Sciences of the United States of America*. 2000;97(7):3684-9.
372. Dimri S, Malhotra R, Shet T, Mokal S, Gupta S, De A. Noncanonical pS727 post translational modification dictates major STAT3 activation and downstream functions in breast cancer. *Experimental Cell Research*. 2020;396(2):112313.
373. Chalhoub N, Baker SJ. PTEN and the PI3-kinase pathway in cancer. *Annual review of pathology*. 2009;4:127-50.
374. Issad T, Blanquart C, Gonzalez-Yanes C. The use of bioluminescence resonance energy transfer for the study of therapeutic targets: application to tyrosine kinase receptors. *Expert opinion on therapeutic targets*. 2007;11(4):541-56.
375. Aniketh Bishnu PP, Ajit Dhadve, Asmita Sakpal, Bharat Rekhi and Pritha Ray. Molecular Imaging of the kinetics of hyperactivated ERK1/2 mediated autophagy during acquirement of chemoresistance. *Cell Death and Disease* (In Press). 2021.
376. Januchowski R, Sterzynska K, Zaorska K, Sosinska P, Klejewski A, Brazert M, et al. Analysis of MDR genes expression and cross-resistance in eight drug resistant ovarian cancer cell lines. *Journal of ovarian research*. 2016;9(1):65.
377. Wu B, Zhu JS, Zhang Y, Shen WM, Zhang Q. Predictive value of MTT assay as an in vitro chemosensitivity testing for gastric cancer: one institution's experience. *World journal of gastroenterology*. 2008;14(19):3064-8.
378. Chen T, Wang C, Liu Q, Meng Q, Sun H, Huo X, et al. Dasatinib reverses the multidrug resistance of breast cancer MCF-7 cells to doxorubicin by downregulating P-gp expression via inhibiting the activation of ERK signaling pathway. *Cancer biology & therapy*. 2015;16(1):106-14.
379. Xiao Z, Ding N, Xiao G, Wang S, Wu Y, Tang L. Reversal of multidrug resistance by gefitinib via RAF1/ERK pathway in pancreatic cancer cell line. *Anatomical record*. 2012;295(12):2122-8.